Modulation of Ultrafast Excited State Dynamics in SDS Micelle

A Thesis
Submitted in Partial Fulfillment of the Requirements
for the Degree of

DOCTOR OF PHILOSOPHY

by

PUSPAL MUKHERJEE

to the

Department of Chemistry
Indian Institute of Technology Kanpur
Kanpur, India

March, 2018

STATEMENT

I hereby declare that the work presented in the thesis entitled "**Modulation of Ultrafast Excited State Dynamics in SDS Micelle**" is the result of original work carried out by me in the Department of Chemistry, Indian Institute of Technology Kanpur under the supervision of **Dr. Pratik Sen**.

In keeping with general practice of reporting scientific observations, due acknowledgements have been made wherever the work described is based on the findings of other investigators.

'18

Puspal Mukherjee. 12/3/18

March, 2018
IIT Kanpur

(Puspal Mukherjee)
12107080

CERTIFICATE

It is certified that the work reported in the thesis entitled "**Modulation of Ultrafast Excited State Dynamics in SDS Micelle**" has been carried out by **Mr. Pugal Mukherjee** under my supervision and has not been submitted elsewhere for a degree.

Pratik Sen.
12-03-2018

March, 2018
IIT Kanpur

(Dr. Pratik Sen)
Thesis Supervisor
Department of Chemistry
Indian Institute of Technology Kanpur
Kanpur, U.P. India- 208016

डा० प्रतीक सेन / Dr. Pratik Sen
सह–प्राध्यापक, रसायन विभाग
Associate Professor
Department of Chemistry
भारतीय प्रौद्योगिकी संस्थान कानपुर
Indian Institute of Technology Kanpur
Kanpur-208 016, INDIA

Department of Chemistry
Indian Institute of Technology Kanpur

Certificate of course work

This is to certify that **Mr. Puspal Mukherjee** has satisfactorily completed all the courses required for the Ph.D degree. The courses include:

CHM 614	Organic Photochemistry
CHM 629	Principles of Physical Chemistry
CHM 664	Modern Physical Methods in Chemistry
CHM 679	Molecular Reaction Dynamics
AE 698	Intro to Virtual Instrumentation
CHM 695	Molecular Modelling in Chemistry
CHM 799	Research
CHM 800	General Seminar
CHM 801	Graduate Seminar

Mr. **Puspal Mukherjee** was admitted to the candidacy of the Ph.D degree in August, 2013 after he successfully completed the written and oral qualifying examinations.

Head
Department of Chemistry
Indian Institute of Technology Kanpur
Kanpur – 208016, India

Sandeep Verma
Professor & Head
Department of Chemistry
I.I.T. Kanpur-208016 (India)

Convenor, DPGC
Department of Chemistry
Indian Institute of Technology Kanpur
Kanpur – 208016, India

Dedicated to

Ma and Baba

(my parents)

Acknowledgements

First of all, I want to express my sincere gratitude to my supervisor Dr. Pratik Sen whose teaching, mentoring, motivation and support made this thesis possible. Under his guidance I have learned what it takes to be researcher. He showed me the power of the technique called "spectroscopy" in chemistry. There were times when I was impatient, disoriented and delusional about my work but every single time he patiently turned me towards the right path. He also provided a healthy work environment in the lab where I had the freedom to enjoy my work. In fact, as time passed by, I understood more and more the process and representation of scientific work under his supervision. I will always remember the analysis sessions during which he helped me a lot to understand how to gain information and knowledge from the seemingly large datasets. I know, this is just the start and it is long way to go but my training in his lab will always be the treasure. I wish him and his family a very bright future ahead.

I want to take this opportunity to thank Prof. S. Manogaran, Prof. K. Srihari, Prof. J.N. Moorthy, Prof. A. Chandra, Prof. K. Poddar for their insightful teachings during coursework. I also want to thank Prof. D. Goswami and Dr. M. Chandra for helpful discussions. A special thank goes to Prof. K. Srihari for asking very insightful questions which lead me to learn fundamentals science more deeply. Prof. D. Goswami, Dr. M. Chandra and Dr. T.G. Gopakumar were very encouraging and helpful during my tenure as their teaching assistant. Prof. R. N. Mukherjee and Prof. J.K. Bera are duly acknowledged for letting me use their lab facilities. Dr. N.N. Nair and Dr. M. Ranganathan also helped me many times by their encouraging words and discussions. I was very fortunate to work as with Prof. P.K. Bharadwaj, Prof. A. Subramaniam and Dr. K. Biswas.

I want acknowledge Department of Chemistry, IIT Kanpur for making me a part of it. Thanks are also due to our respected head of the departments Prof. P.K. Bharadwaj (former) and Prof. S. Verma (current). Chemistry departmental staff

especially Sudha mam and Geeta mam's help and cooperation are also acknowledged.

I want to take this opportunity to express my gratitude to Prof. Hrishikesh Chatterjee of Ramakrishna Mission Residential College, Narendrapur who taught me what is meant by physical chemistry. All the teachers of my previous institutions Hooghly Branch Govt. School, Scottish Church College and IIT Guwahati are also acknowledged.

A very special thanks goes to my seniors Dr. Shahnawaz Rafiq Rather, Dr. Rajeev Yadav and Dr. Shradhey Gupta for their all their lessons and help regarding the work. Bhaswati and Vaisakh were two of my very close friends in lab and I shared very enjoyable moments with them. Somnath joined as a M.Sc. project student in our lab, we worked together and at the end we learnt from each other and became best friends. My junior Aritra helped me in my experiments and analysis and he has been a very effective person during it. I also want to thank my other labmates Faizi Da, Vijaykant Da, Vipin, Navin, Nilimesh, Shovon and Sukanta. I would like mention all the M.Sc. students who worked during my PhD tenure; Barun, Shubrangshu, Sayani, Indrani, Kuntal, Arusha, Apala, Nishith, Sakil. I want to thank Arunava Sengupta for cyclic voltammetry measurements and Dr. Suraj K. for very important discussion about DFT calculations. I want to acknowledge Sumit, Manolata Di and Suboohi for their collaborations. My batchmates Firoz, Avinash, Anup, Gopal, Chandan, Paramita, Khusboo, Susanta, Saikat, Soumyadeb were very friendly and supportive in this journey.

A traveler becomes tired during the journey and before reaching the destination rests at inn where he has never been and never will be. Similarly, in life some of the people around us whom we have never met before provide the similar comfort. I refuse to call them friends because I call them family. For me it was Siladitya, Pritam Da, Shubhadeep, Mainak, Amit, Tarak, Shubhabrata, Aviru, Abhigyan, Sutanu, Tarak Kangsabanik, Chirajyoti, Suman Da, Manik, Sohom, Arnab, Joydeb, Saikat, Indranil Da, Arunava, Arindam, Bappa Da, Surajit Da,

Paromita, Madhushree, Sanchari Di, Nabanita Di, Sayantani Di, Krishnendu Da, Debjit Da, Bishu Da, Mithun Da, Subanta, Sayan, and many more. Although they have been previously acknowledged but I want to include Bhaswati and Shovon to the list. Sumit and Suboohi were my collaborators but ended up being much more than just that. I would also like to remember Yeasin, Biswajit, Joga, Joydeep, Sudipta, Pradipta, Shweta for helping me through difficult times.

I am grateful to University Grants Commission for providing fellowship, IIT Kanpur for providing research facilities. Chemistry HPC, HPC 2010 and HPC 2013 are duly acknowledged for computational facilities.

My father, Tapan Kumar Mukherjee, battled his best for his family through ups and downs, gave me valuable lessons for life and was always there for me. Lastly, I want to mention my mother, Lipika Mukherjee, who would give up everything in her life to put a smile on my face. It was her constant support and never give up attitude that made this thesis writing possible.

Puspal Mukherjee

Synopsis

Name of the Student	Puspal Mukherjee
Roll Number:	12107080
Degree for which Thesis is Submitted:	Ph. D.
Department:	Chemistry
Supervisor:	Dr. Pratik Sen
Thesis Title:	Modulation of Ultrafast Excited State Dynamics in SDS Micelle
Month and Year of Submission:	February, 2018

This thesis primarily describes my work on four ultrafast processes in the electronically excited state viz. electron transfer, large amplitude motion, intramolecular proton transfer and solvation dynamics. All four of them are well-known in literature, but experimentally still not comprehended amply. For example, establishment of Marcus inverted region in case of bimolecular photoinduced electron transfer (PET) using fluorescence quenching experiment is a matter of debate due to the participation of diffusion in the reaction. The argument on the barrierless or with barrier potential energy surface for the large amplitude motion in the excited state is under debate. In case of solvation dynamics, the heterogeneity of the water molecules present in a micellar surface was predicted by simulations but experimentally the total solvent response was not observed to establish the situation. I tried to extend these insights further using femtosecond time resolved experiments and kinetic modeling. The processes (except for solvation dynamics) were first studied in common bulk solvents and then extended specially to sodium dodecyl sulfate micelle, which modulated their dynamics. While establishing Marcus inverted region in bimolecular electron transfer, I needed to partially incarcerate the donor and acceptor. The acceptors, a group of viologen molecules, being positively charged were held at the Stern layer of SDS

micelle by the negatively charged surfactant head groups. The donor coumarins were also distributed inside the micelle and thus SDS micelle helped in achieving the necessary condition. The negatively charged head groups of SDS were also used to put molecular rotor Thioflavin-T in a position where its amplitude motion is hindered compared to bulk solvents. The synthesized excited state proton transfer probe was insoluble in water. Therefore to study its photophysics in presence of water molecules, SDS micelle was used. Thus the change of dynamics of bulk solvents to SDS micelle was also observed and all these studies were performed in the water layer of the SDS micelle. Lastly the solvation dynamics in the same was also checked looking for multiple components of the solvent response.

Summary of the Work Done

(a) Absolute Rate of Ultrafast Photoinduced Bimolecular Electron Transfer Reactions

Fluorescence quenching studies through steady state and time-resolved measurements are inadequate to quantify the bimolecular electron transfer rate in bulk homogeneous solution due to constraints from diffusion. To nullify the effect of diffusion, direct evaluation of the rate of formation of a transient intermediate produced upon the electron transfer is essential. Methyl viologen, a well-known electron acceptor, produces a radical cation after accepting an electron, which has a characteristic strong and broad absorption band centered at 600 nm. Hence it is a good choice to evaluate the rate of photoinduced electron transfer reaction employing femtosecond broadband transient absorption spectroscopy. The time constant of the aforementioned process between pyrene and methyl viologen in methanol has been estimated to be 2.5 ± 0.4 ps using the same technique. The time constant for the backward reaction was found to be 14 ± 1 ps. These values did not change with variation of concentration of quencher, i.e., methyl viologen. Hence, it was inferred that diffusion has no contribution in the estimation of rate constants. However, on changing the solvent from methanol to ethanol, the time constant of

the electron transfer reaction has been found to increase and has accounted for the change in solvent reorganization energy.

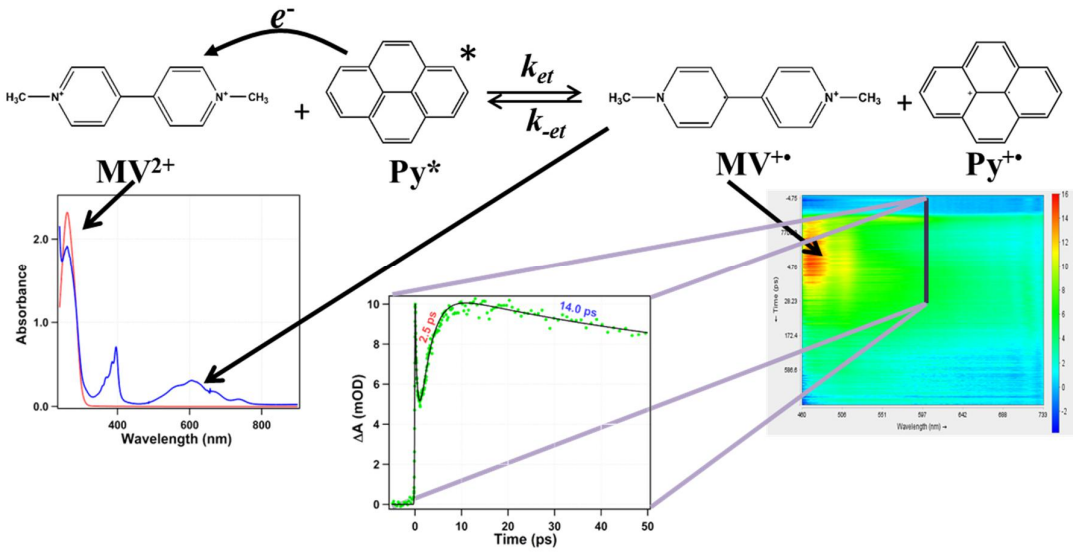

Next, I have studied the bimolecular photoinduced electron transfer (PET) reaction between benzophenone (Bp) and DABCO using femtosecond broadband transient absorption spectroscopy in different compositions of acetonitrile/1-butanol binary solvent mixtures. With the increase in the 1-butanol percentage in the mixture, I have observed an increase in the onset delay time for the detectable signal to appear for the $Bp^{\bullet-}$which is the product of the reaction. As 1-butanol is more viscous than acetonitrile, the onset time was related to the change in medium viscosity. Moreover, a complete kinetic analysis of the bimolecular PET reaction under different conditions was undertaken to show that from transient absorption spectroscopy, one can get the exact rate of electron transfer free from involvement of any other rate constants. This kind of kinetic analysis along with the experimental data is the first of its kind to prove that transient absorption spectroscopy is probably the most useful tool in studying PET reaction.

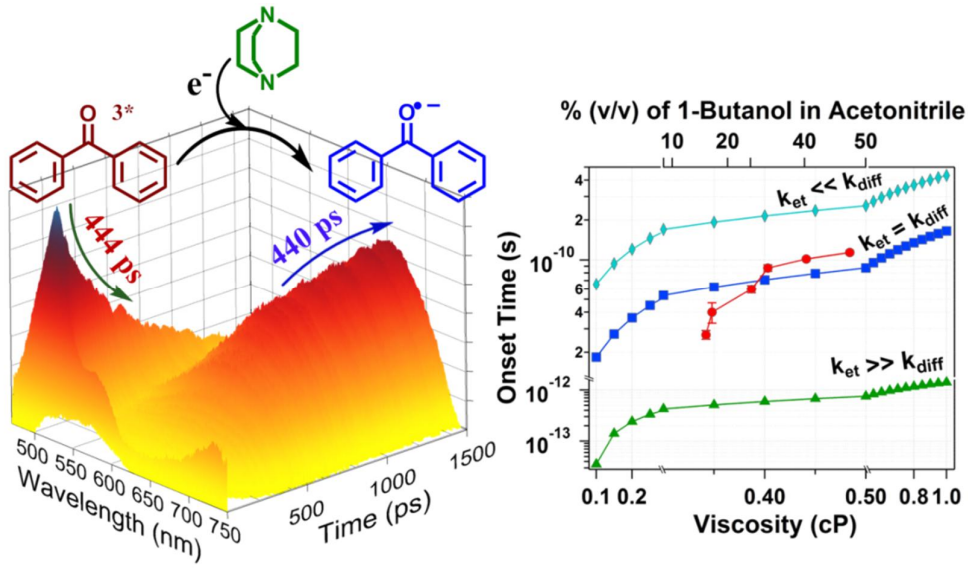

To explore Marcus inversion, ultrafast bimolecular photoinduced electron transfer (PET) between six coumarin dyes and four viologen molecules in the stern layer of sodium dodecyl sulfate micelle have been studied using femtosecond broadband transient absorption spectroscopy and femtosecond fluorescence up-conversion spectroscopy over a broad reaction exergonicity (ΔG^0). Emanating the formation of radical cation intermediates of viologen molecules using the transient absorption and the fast decay component of coumarins using the up-conversion studies the forward bi-molecular electron transfer rate (k_{et}) have been measured with high accuracy. The relationship of k_{et} with ΔG^0 found to follow a Marcus type bell-shaped dependence with an inversion at -1.10 eV. In this work, I have studied PET reaction using ultrafast spectroscopy at the quencher concentration where static quenching regime prevails. Moreover, the incompetency of Stern-Volmer experiments in studying ultrafast PET has been revealed. In contrary to previous claims, here it was found that the k_{et} is lower for lower lifetime coumarins, indicating that static, non-stationary and stationary regime of quenching have the minimal role to play to in the bi-molecular electron transfer process. By far, this study is believed to be the most efficient and immaculate way of approaching Marcus inverted region problem in the case of bimolecular PET and settles the long-lasting debate of whether the same can be observed in micellar systems.

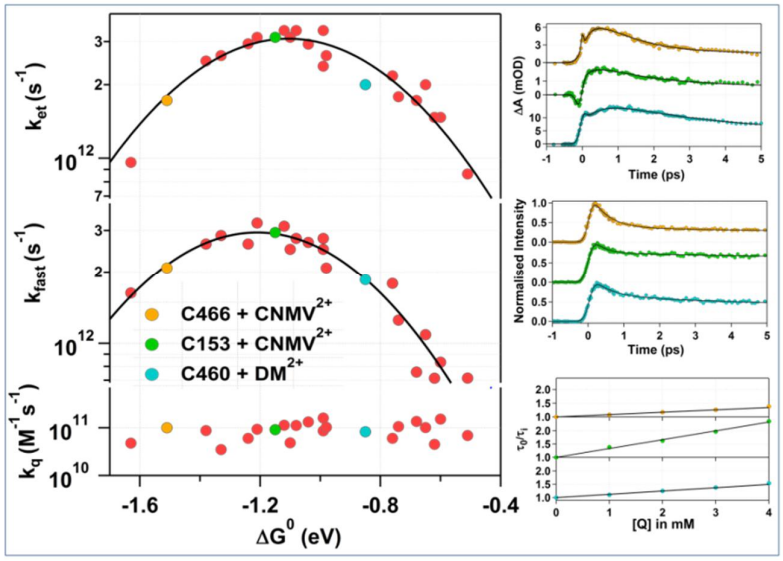

(b) Ultrafast Excited State Dynamics of Molecular Rotor Dye Thioflavin T

In the first part of this work, the ultrafast excited state dynamics of thioflavin T (ThT) has been investigated in methanol and chloroform. The first hand data of 30 times higher fluorescence quantum yield and observation of slow rise time in fluorescence intensity of ThT in chloroform compared to methanol indicate the complicated photophysics of the molecule. Time resolved fluorescence data along with temperature dependence on fluorescence quantum yield, TD-DFT calculations and femtosecond transient absorption study vividly suggest the involvement of one more twisted intramolecular charge transfer state (TICT-2) along with the TICT-1 state, in the excited state manifold of ThT, which was not identified earlier. Upon excitation to the LE state, ThT undergoes two different amplitude motions leading to either TICT-1 state or TICT-2 state along the dimethylanilino and dimethylamino torsional coordinate respectively. It was also established that the depletion of the molecule from the locally excited state to the TICT-1 state probably barrierless in nature, however, an inherent activation energy barrier is present between LE and TICT-2 states. This activation energy barrier in methanol (0.59 kcal mol^{-1}) was found to be exactly same as that available at room temperature, whereas the same in chloroform is found to be quite high (1.58 kcal

mol^{-1}). This barrier is proposed to be responsible for the high quantum yield of ThT in chlorinated solvents.

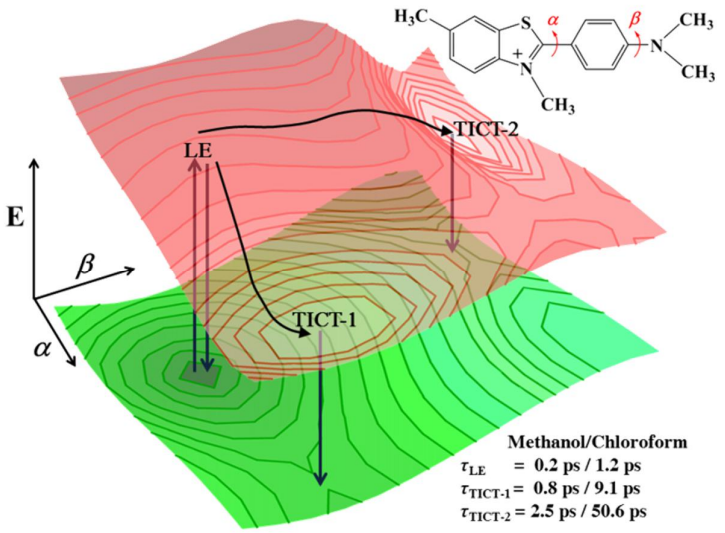

Extending the previous work, I have studied the dynamics of molecular rotor dye thioflavin T (ThT) in Stern layer of sodium dodecyl sulfate (SDS) micelle using femtosecond fluorescence up-conversion and broadband transient absorption spectroscopy. ThT being a positively charged molecule is expected to remain in the Stern layer of micelle due to columbic attraction with the negatively charged surfactant head groups. The restriction imposed by the environment slows down the rotation of molecular fragments, which increases its quantum yield ~8 times compared to pure water. The dual relaxation channel of ThT (LE → TICT1 and LE → TICT2) was confirmed and it was found that the lifetime of the three states namely LE, TICT1 and TICT2 are 0.5, 3.1 and 15.7 ps respectively in 40 mM SDS.

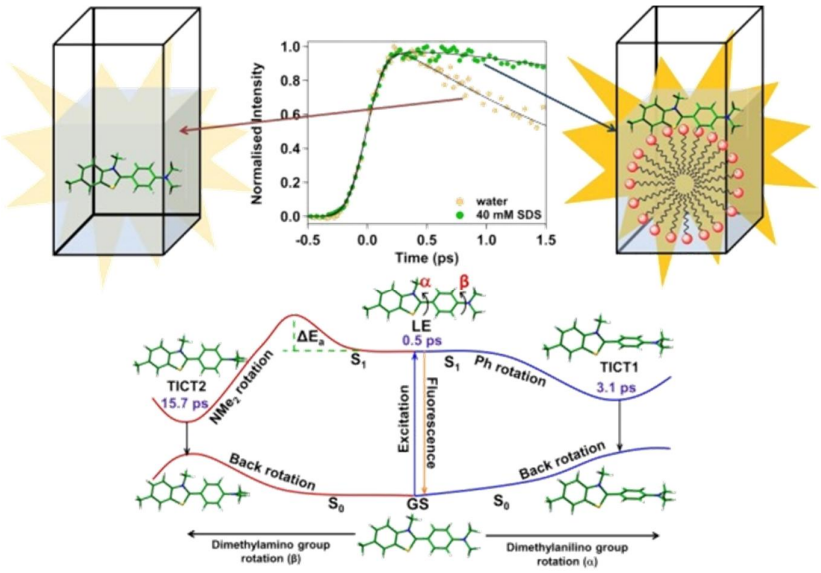

(c) Solvent Relaxation Accompanied Ultrafast Excited State Proton Transfer Dynamics Revealed in a Salicylideneaniline Derivative

In this study, I have investigated the excited state intramolecular proton transfer (ESIPT) and subsequent dielectric relaxation of a newly synthesized Schiff base molecule in cyclohexane, methanol and SDS micelle through femtosecond fluorescence up-conversion and broadband transient absorption spectroscopy. In methanol and SDS micelle the molecule exhibited a 0.6 ps rise component in fluorescence transients, which is larger than in cyclohexane and lead to the conclusion that a significant dielectric relaxation is operational for the keto tautomer. DFT calculations hint towards the existence of a small barrier (~0.07 eV) in the excited state. It was found that the molecule showed ultrafast proton transfer with a timescale about 0.2 ps followed by solvent relaxation of the keto tautomer in methanol and SDS medium. In non-polar cyclohexane, the solvation part was completely absent as expected. Computational study suggested the existence of a transition state in the proton transfer surface. Quantification of the system was done with two step model assigning the first rate constant to the relaxation of the excited state enol form and the second to the barrier crossing from the enol to keto form.

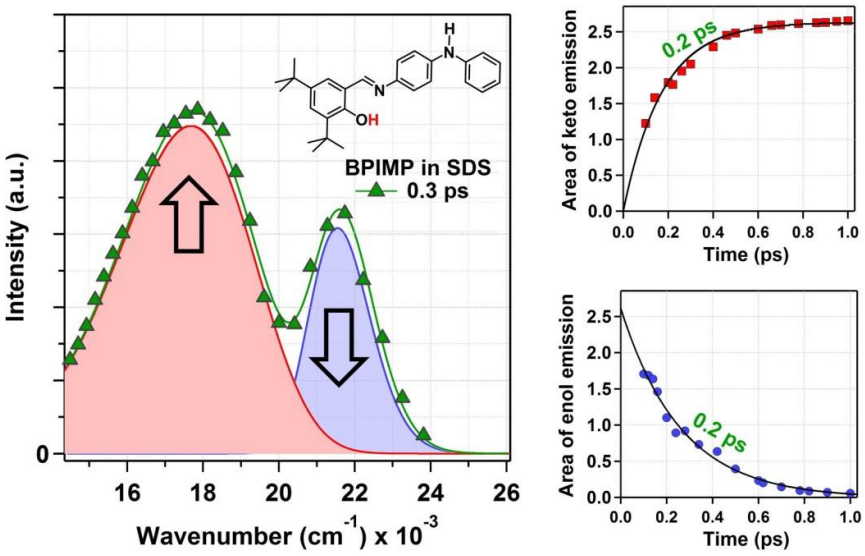

(d) Solvation Dynamics in SDS Micelle Revisited with Femtosecond Time Resolution to Reveal the Probe and Concentration Dependence

This last work is devoted to understand the probe and surfactant concentration dependence of solvation dynamics in SDS micelle. Here the solvation dynamics of four solvatochromic probes in SDS micelle in femtosecond-nanosecond time domain has been studied. Among them, DCM showed the largest average solvation time (180 ps) followed by C153 (145 ps), C480 (132 ps) and C460 (46 ps). The average solvation times are found follow the hydrophobicity of the probe and it was concluded that the location of probe inside SDS micelle determines the solvation time. The solvation dynamics of C480 in 10, 20, 40 and 200 mM SDS in water was also studied and a small but definite increasing trend in solvation time was found. Explanation of this behavior was found in the variation of aggregation number of SDS micelle as a function of its concentration. The analysis of solvent response function in all the cases revealed the existence of a ultrashort (~100fs) time component due to the libration motion of water molecules which means all the possible parts of solvation dynamics in SDS micelle was extracted.

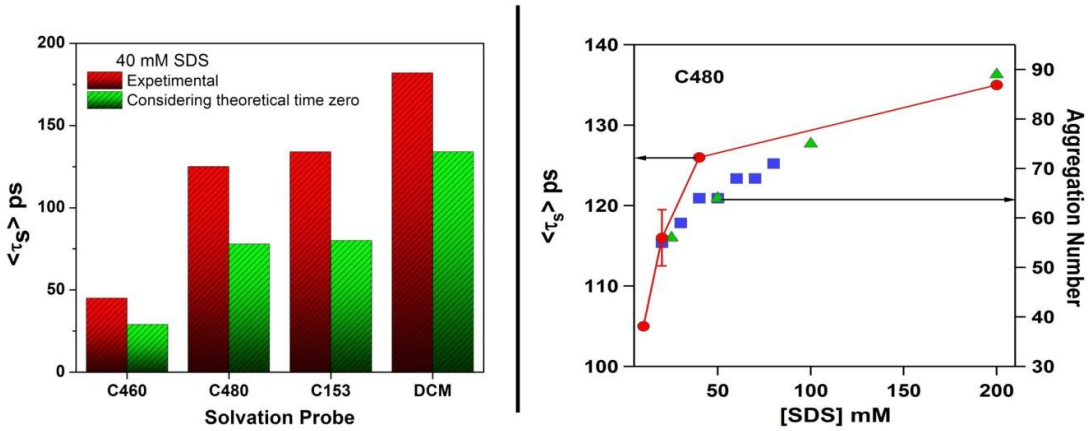
40 mM SDS
Expetimental
Considering theoretical time zero
<τs> ps
Solvation Probe
C460
C480
C153
DCM
C480
<τs> ps
Aggregation Number
[SDS] mM

Table of Contents

Chapter 1

Introduction

In this chapter, I have discussed the basics of four photophysical process viz. photoinduced electron transfer, ultrafast twisting motion in the excited state, excited state intramolecular proton transfer and solvation dynamics. These four processes have been explored throughout this thesis in bulk solvents and SDS micelle medium.

1.1. Ultrafast Excited State Dynamics

The definition of the term "ultrafast" for experimental physical chemists has changed over time with the development of short pulse lasers. The word “ultrafast” once meant picosecond to nanosecond time domain but with the introduction of “femtosecond” lasers, now we can study excited state phenomenon with sub-picosecond time resolution. Two of the most popular optical spectroscopic techniques in this field are transient absorption spectroscopy and fluorescence up-conversion spectroscopy. These two techniques have enabled us to explore the dynamics of various ultrafast photophysical processes. Four such fundamental processes studied in this thesis are photoinduced electron transfer, excited state twisting dynamics, excited state intramolecular proton transfer and solvation dynamics. In the following sections, overviews of these processes are discussed.

1.2. Photoinduced Electron Transfer

In the eighteenth century, Joseph Pristley first reported light induced conversions and production of “*dephlogisticated air”* in water by light in presence of a “*green substance”* from the plants.[1] This discovery of photosynthesis was probably the dawn of photochemical electron transfer reactions.[1] In the nineteenth century, studies by Seekamp, Fay and Döbereiner commenced chemical actinometry which is the example of another photochemical electron transfer.[1] Today photoinduced electron transfer is used to decipher some of the greatest challenges on earth like harvesting energy and mimicking photosynthesis.[2-9] Supramolecular assemblies are being developed which undergoes photoinduced electron transfer and artificially splits water.[10-14] Development in the field of nanomaterials and graphene promises more efficient materials for solar cell applications.[15-20]Dye sensitized solar cells are shown to revolutionize the field of solar energy harvesting by the group of Micheal Gratzel.[21-25] In all these cases photoinduced electron transfer is playing the pivotal role. Therefore the study of

kinetics and energetics of the process is necessary for advancement of applications in many fields.

1.2.1. Energetics of Photoinduced Electron Transfer

In case of photoinduced electron transfer, either the donor and acceptor can be excited or in other words the excited state can act as an electron donor or acceptor. As depicted in figure 1.1, when the donor is photoexcited, the electron from donors LUMO is transferred to the LUMO of acceptor.[26,27] When the acceptor is excited, one electron from the HOMO of the donor is transferred to the HOMO of acceptor.[26,27]From basic thermodynamics, its intuitive that exothermic reactions will be favored.

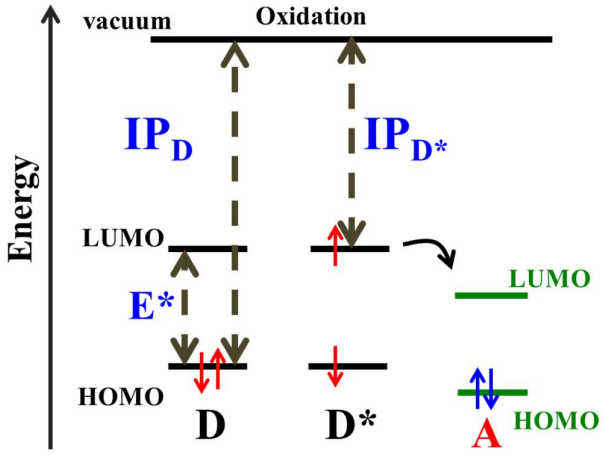

Figure 1.1. Schematic molecular orbital description of photoinduced electron transfer

Now the ionization potential of an excited molecule (IP*) will always be less compared to same in ground state (IP) as it requires less amount of energy to remove an unpaired electron from LUMO than a paired electron from HOMO.[27-29] In the same way, the electron affinity of excited molecule will be higher as more energy will be released when an electron will be put in the HOMO compared to LUMO.[28,29] Therefore, almost all of the PET reactions are exothermic in nature as the thermodynamics is controlled by the IP* and EA* of the donor and acceptor respectively. But the actual relation of energy and rate of PET reaction is not so

straightforward. For a gas-phase ground state bimolecular PET reaction the free energy change (ΔG) can be written as[28,29]

$$\Delta G = IP_D - EA_A \tag{1.1}$$

In the above equation, $IP_D$is the ionization potential of the donor and EA_A is the electron affinity of the acceptor. If we consider that the donor molecule was photo-excited then the ionization potential of the donor in the excited state (IP_D^*) will be less from the same in the ground state by the amount of energy of photon absorbed energy gap between the ground and excited state (E^*).[28,29]

$$IP_D^* = IP_D - E^* \tag{1.2}$$

So, for PET equation 1.1 will be written as [28,29]

$$\Delta G = IP_D - EA_A - E^* \tag{1.3}$$

In generally, most of the PET reactions are studied in some solvent. Therefore equation 1.3 needs to be modified to calculate the free energy in solvent media. First of all if both donor and acceptor are neutral molecules in the ground state then PET will generate radical cation and anion pair in the excited state. So a Columbic attraction term needs to be incorporated in equation 1.3. The radical ion pairs will also be solvated by the solvent especially by the polar solvent. So a solvation term is also incorporated. So equation 1.3 takes the form [28,29]

$$\Delta G = IP_D - EA_A - E^* - \frac{e^2}{2}\left[\frac{1}{r_D} + \frac{1}{r_A}\right]\left(1 - \frac{1}{\varepsilon}\right) - \frac{e^2}{\varepsilon \cdot d} \tag{1.4}$$

In the above equation, e is the charge of an electron, ε is the dielectric constant of the medium, d is the distance between the donor and acceptor radical ion of radii r_D and r_A respectively formed upon electron transfer. In solution, IP_D and EA_A can be measured from the oxidation-reduction potential of the molecule corrected with individual solvation energy.

$$IP_D = E(D^{\cdot+}/D) + \frac{e^2}{2r_D}\left(1 - \frac{1}{\varepsilon}\right) \tag{1.5}$$

$$EA_A = E(A/A^{\cdot -}) - \frac{e^2}{2r_A}\left(1 - \frac{1}{\varepsilon}\right) \quad (1.6)$$

Incorporating equation 1.5 and 1.6 in equation 1.4, we get

$$\Delta G^0 = E(D^{\cdot +}/D) - E(A/A^{\cdot -}) - E^* - \frac{e^2}{\varepsilon \cdot d} \quad (1.7)$$

Here, ΔG^0 is the standerd free energy change of PET reaction in solution or reaction exergonicity. Equation 1.7 is famously known as the Rehm-Weller equation.[28-30] Equation 1.7 is specific for neutral molecules undergoing one electron transfer. It has to be modified when the reactants are charged in the ground state which has been done in subsequent chapters.

1.2.2. Marcus Theory of Outer Sphere Electron Transfer

Outer and inner sphere electron transfer is classified based on the ligand participation in the reaction. In outer sphere electron transfer no bond is broken or formed however in inner sphere electron transfer the electron is transferred via a bridging ligand and the ligand can be exchanged after the reaction.[28,29,31] One of the classes of outer sphere electron transfer reactions is the isotopic exchange reaction and during Second World War several isotopic exchange reactions were studied labeling one of the reactant with a radio isotope. The reactants and products of these reactions have thermodynamically same energy as they are basically same. Self-exchange reactions involving smaller cations are relatively slow compared to the same involving larger cations. Libby tried to justify this based on the Franck-Condon principle which was primarily developed for photon excitations. In this theory, the electron jump is an instantaneous process and in the ultrafast timescale of this process the solvent molecules cannot reorient themselves and therefore remain in orientation to the reactant state.[29,31-36] Moreover the nuclear configuration does not match the product state and still remains the same as the reactant state. Thus a high energy state is produced which can be thought to act as a barrier to electron transfer. Now as smaller ions remains more solvated than the bigger ones, the solvent barrier is higher for smaller ions which in turn slows down

the rate. The problem with this theory is that it violates the second law of thermodynamics.[29,31-36]As there is no external excitation source available for ground state electron transfer reactions, the production of the high energy state is impossible and thereby the whole idea shatters down.[29,31-36]

The theory developed by Rudolph Marcus solved this problem and gave the first proper theoretical description of electron transfer reactions. [29,31-36] Broadly, the ET reactions are classified into two categories i.e. diabatic and adiabatic depending on the mixing of the two reactant and product states.[29,31-36] The system Hamiltonian is a sum of unperturbed Hamiltonian and a perturbation term which give rise to ET. If the motion on the potential energy surface does not change the electronic state of the system then it is termed as diabatic.[29,31-36] In the diabatic state the extent of interaction in weak-coupling regime which is also termed as non-adiabatic ET is given by

$$H = \langle 1 | H_{per} | 2 \rangle \tag{1.8}$$

If the coupling is large then it is known as adiabatic ET which is constructed from the linear combination of non-adiabatic states. In case of a strong coupling the electron moves smoothly over changes in nuclear coordinates. Now, as electrons occupy orbitals in a molecule, ET reactions are influenced by the interaction of the molecular orbitals. The strength of this interaction (H_{12}) decreases exponentially with distance as given by the following equation[29,31-36]

$$H_{12} = H_{12}^{0} \exp\left[\frac{-\beta(r-r_0)}{2}\right] \tag{1.9}$$

In the above equation, H_{12}^{0} is the value of H_{12} at $r = r_0$ and β is the orbital parameter. Many of the Marcus type ET reactions are in the weakly adiabatic domain. [29,31-36]

To conserve the second law of thermodynamics, ET must occur without any sudden change in energy or structure. Therefore a transition state must be reached and this transition state was characterized by Marcus having two iso-energetic

structures. These two structures differ only in their electronic configuration. One matches that of the reactants and the other of the products. Again, the solvent structure surrounding the transition state must preserve the total energy of the system i.e. the total energy of the solvent plus any one configuration of the transition state is same. This concept can be visualized by Franck-Condon principle also. The electron jump between the two structures in the transition state is so rapid that the surrounding solvent molecules along with the nuclear geometry of the reactant state cannot move during this. Therefore the two configurations in the transition state must be similar in energy. The approach of the reactants to the transition state and the separation of the transition state into products depend on the reaction co-ordinate of the reaction. Marcus successfully identified the coordinate of ET reactions to be the collective solvent polarization changes. In ET reactions the charge of the molecules changes and they are strongly coupled to the solvent structure. The solvent stabilization is maximum for the reactant and product but least for the transition state. When two reactant molecules approach each other at a certain probablilty, the thermal fluctuation of the surrounding solvent molecules takes the overall system to the transition state where the atomic configuration matches that of the reactants but the solvent cage is at a non-equlibrium geometry. After the ET, the product can just separate or they can be taken to the minima of product parabola again by the fluctuation of the solvent molecules. Now, as stated before ET are affected by the mutual orientation of the donor and acceptor molecules with the reactant precursor complex. So when the two molecules involved in ET reaction approach each other in the starting of the reaction, the ascent to the transition state is associated with a nuclear reorientation which means the equilibrium bond length, orientation and symmetry can change. Another important aspect of the transition state in ET reaction as pointed out by Marcus was that in case of activated complexes with large electronic overlap, the solvent molecules will be in equilibrium with the ionic charge of the activated complex which is actually the strongly adiabatic approximation.[29,31-36] In Marcus type ET model, the solvent molecules are in non-equilibrium with the activated complex

where the electronic overlap is weak in nature. Marcus assumed a harmonic potential energy surface for both the reactant and product with same curvature as a function of the reaction coordinate.[29,31-36] The reaction coordinate was defined according to the dielectric continuum model which describes the orientation of solvent molecules around the system using orientational polarization function.[29,31-36] Following this model and free energy minimization along the potential energy surface the reorganization parameters were obtained.[29,31-36] Solvent reorganization parameter indicates the reorientation of the solvent molecule dipoles during ET. There are several non-equilibrium orientations possible for the solvent molecules at the transition state and out of them the one which stabilizes the activated complex most decides the solvent reorganization energy which is given by the following equation.[29,31-36]

$$\lambda_s = e^2 \left(\frac{1}{2r_D} + \frac{1}{2r_A} - \frac{1}{r_{DA}}\right)\left(\frac{1}{\varepsilon_{op}} - \frac{1}{\varepsilon_s}\right) \tag{1.10}$$

In the above equation, e is electronic charge, r_D and r_A are the ionic radii of donor and acceptor and r_{DA} is the sum of them. The optical and static dielectric constants are given by ε_{op} and ε_s respectively.[29,31-36] Thus the dielectric constant of the solvent i.e. the polarity determines the stability of the transition state or the solvent barrier.[29,31-36] Similarly, the bond length changes from the equilibrium are taken into account by the nuclear reorganization. Classical harmonic oscillator expression was used to derive the nuclear reorganization energy over all the intramolecular vibrational modes.[29,31-36]

$$\lambda_i = \sum \left(\frac{f_i^{D\cdots A} f_i^{D^{\cdot+}\cdots A^{\cdot-}}}{f_i^{D\cdots A} + f_i^{D^{\cdot+}\cdots A^{\cdot-}}}\right) \Delta q_i^2 \tag{1.11}$$

Δq_i is the change in interatomic distance and f_i is the force constant of vibration.

Except for isotopic substitution reactions where the reactant and product potential energy parabola have exactly same minima, almost all other ET reactions are have some energy difference between them.[29,31-36] In other words, the reactions

are either endothermic or exothermic which implies they have a standard free energy change of the reaction and as discussed in the previous section the PET reactions are almost always exothermic in nature.[29,31-36] To calculate the rate of ET reactions, the relation between the free energy of activation and the standard free energy change of the reaction was derived by Marcus using the transition state theory where the probability of reactants crossing a barrier of certain height is calculated.[29,31-36] The whole proof is impossible to discuss here but a geometric proof considering the crossing of two parabolic functions can be shown.

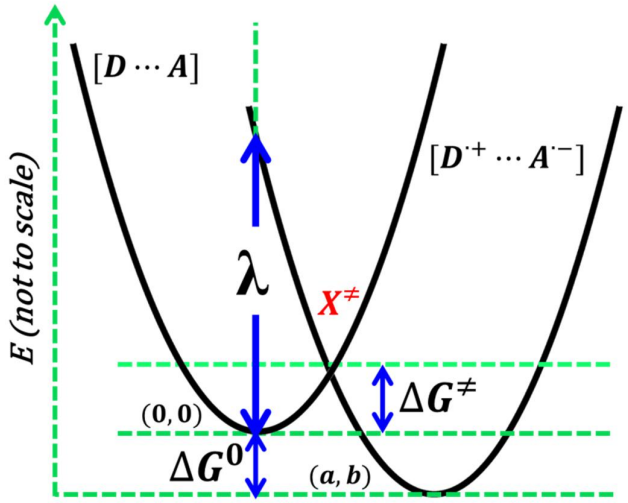

Figure 1.2. Potential energy surface description of photoinduced electron transfer

Let's assume the reactant complex and the product ion pair is represented by two parabolas marked $[D \cdots A]$ and $[D^{\cdot+} \cdots A^{\cdot-}]$ in an energy landscape as represented by figure 1.2. This two parabolas cross at a point marked $X^{\neq}$ which is the transition state of the ET reaction. Let's also assume the bottom of the reactant parabola I located at $(0,0)$ position and the same for the product parabola is located at point (a, b). So the equations for the reactant and product parabola are

$$y = x^2 \tag{1.12}$$

$$y = x^2 - 2ax + a^2 + b \tag{1.13}$$

The product parabola intercepts the y-axis at $a^2 + b$. Now, to find the activation energy of the reaction we need to find the crossing point of the two parabolas and setting the y values as equal, we find

$$x = \frac{a^2+b}{2a} \tag{1.14}$$

Substituting this value of x in equation 1.13, we find

$$y = \frac{(a^2+b)^2}{4a^2} \tag{1.15}$$

Now the y value at intersection is the activation energy $\Delta G^{\neq}$. So equation 1.15 can be written as

$$\Delta G^{\neq} = \frac{(a^2+b)^2}{4a^2} \tag{1.16}$$

The value of b is the displacement between the two parabolas along the y-axis which is nothing but the standard free energy of the reaction ΔG^0. Now the intersection of the product parabola is given by $\Delta G^0 + \lambda$ where λ is the total reorganisation energy which is nothing but the sum of solvent (λ_s)and nuclear reorganisation energy (λ_i)[29,31-36]

$$\lambda = \lambda_i + \lambda_s \tag{1.17}$$

So we can write

$$\Delta G^0 + \lambda = a^2 + b \tag{1.18}$$

Putting $b = \Delta G^0$, we get $\lambda = a^2$. Thus equation 1.18, transforms to

$$\Delta G^{\neq} = \frac{(\Delta G^0+\lambda)^2}{4\lambda} \tag{1.19}$$

Now, the rate of the reaction can be calculated using the Arrhenius equation as given below[29,31-36]

$$k_{et} = \frac{4\pi^2}{h}\frac{V_{el}^2}{\sqrt{4\pi\lambda_s k_B T}}\, exp\left\{-\frac{(\Delta G^0+\lambda)^2}{4\lambda k_B T}\right\} \quad (1.20)$$

The pre-exponential factor was derived by Marcus where V_{el} is electronic coupling matrix element.[29,31-36]

Now equation 1.19 proposes a unique problem. According to this equation, $\Delta G^{\neq}$ and ΔG^0 have a parabolic relation considering λ is fixed. Figure 1.3, depicts the variation of $\Delta G^{\neq}$ with change in reaction exergonicity ΔG^0.

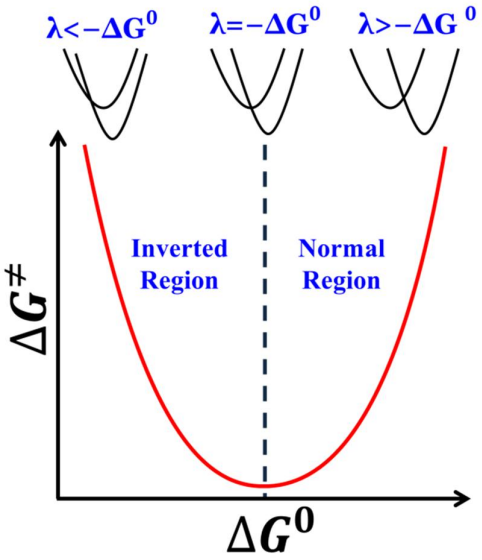

Figure 1.3. Relationship between $\Delta G^{\neq}$ and ΔG^0 as predicted by Marcus theory

Figure 1.3 implies that with increasing exothermicity of the reaction, the activation energy first decreases, then it reaches a minima and then it again rises. Generally, for other reactions, activation energy decreases with increase in exothermicity of the reaction which is the normal behavior. However the increase in $\Delta G^{\neq}$ with ΔG^0 was unprecedented before Marcus theory of ET reaction came to be and therefore this region was termed as the Marcus Inverted Region. Since rate of the reaction is related to ΔG^0 via equation 1.20, it will show a similar behavior but the dependence is mathematically not a parabola. So if, $\Delta G^0 > -\lambda$, then k_{et} increases with reaction exergonicity, which is the normal behavior. When $\Delta G^0 = -\lambda$, k_{et} reaches a maximum and with further increase in reaction exergonicity $(\Delta G^0 < -\lambda)$

a reduction in the rate of electron transfer reaction should occur which is the Marcus Inverted Region (MIR).[29,31-36]

1.2.3. Photoinduced Electron Transfer and Diffusion

The most routine method of studying PET is fluorescence quenching.[28,29] In this method, the rate of decrease of fluorescence intensity and lifetime of a fluorophore is monitored. Then a Stern-Volmer analysis is applied which gives us the dynamic quenching rate constant k_q. Many times this rate constant is directly assigned to the rate of PET. However, this analysis takes into account all the quenching mechanism along with PET.[28,29]

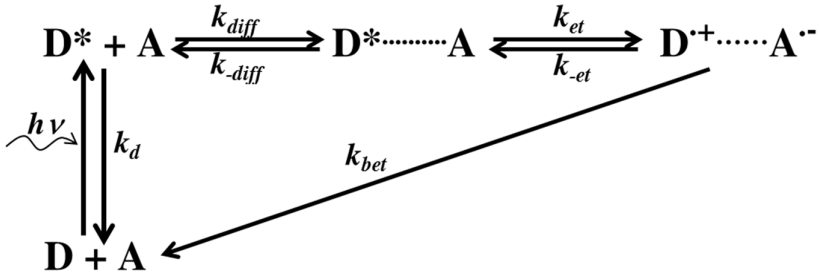

Figure 1.4. Schematic representation of bimolecular fluorescence quenching through PET

Now if we discard any other quenching mechanism in the excited state along with any type of product formation then the overall kinetics of PET can be represented according to figure 1.4. In figure 1.4, k_d is radiative rate of deactivation of donor, k_{diff} and k_{-diff} are the diffusional rate constants, k_{et} is the unimolecular rate of electron transfer, k_{-et} is the rate of reversible electron transfer and k_{bet} incorporates the entire possible phenomenon by which the ion pair can return to ground state configurations. The interesting part of the problem is the formation of encounter complex between the donor and the acceptor. In a solution, the donor and acceptor molecules are freely diffusing. However, electron transfer requires orbital overlap between the two molecules.[28-36] In classical theory, an encounter complex is a molecular ensemble between the excited donor molecules and ground state acceptor molecules separated at a certain distance (~7Å) and surrounded by

solvent. Formation of and encounter complex has been hypothesized by "random walk" problem.[28-36] The molecules move in solution in a random manner and they undergo several collisions.[29,31-36] These collisions or encounters have a certain lifetime and if electron transfer occurs within this lifetime then the ion-pair generated is known as contact ion pair (CIP).[29,31-36] The nuclear and electronic changes are required to occur within this lifetime. CIP can separate to form solvent separated ion-pairs (SSIP) if the solvent is polar or simple free radical ions.[29,31-36] However, if the interaction between the excited and ground state molecules is very strong, then the encounter complex can lead to exiplex formation which may have red shifted emission.[29,31-36] However, in the further discussion I will not consider any exciplex formation as no such signature was detected in the PET system that I studied. Now, the kinetics of the encounter complex formation is controlled by the rate of diffusion which is a second order process as well as fluorescence quenching. However the electron transfer step is a first order process. The relation between these three rate constants can be established following the kinetic scheme in figure 1.4.

The rate equations for $[D^*]$ is

$$\frac{d[D^*]}{dt} = -k_d[D^*] - k_{diff}[D^*][A] + k_{-diff}[D^* \cdots A] \quad (1.21)$$

We can also get the kinetics $[D^*]$ from Stern-Volmer equation

$$\frac{d[D^*]}{dt} = -\big(k_d + k_q[A]\big)[D^*] = -(\frac{1}{\tau_0} + k_q[A])[D^*] \quad (1.22)$$

The rate equations for encounter complex $[D^{*\cdots\cdots}A]$ and ionpair $[D^{\cdot+\cdots\cdots}A^{\cdot-}]$ are given by

$$\frac{d[D^*\cdots A]}{dt} = k_{diff}[D^*][A] - k_{-diff}[D^* \cdots A] - k_{et}[D^* \cdots A] + k_{-et}[D^{\cdot+} \cdots A^{\cdot-}] \quad (1.23)$$

$$\frac{d[D^{\cdot+}\cdots A^{\cdot-}]}{dt} = k_{et}[D^* \cdots A] - k_{-et}[D^{\cdot+} \cdots A^{\cdot-}] - k_{bet}[D^{\cdot+} \cdots A^{\cdot-}] \quad (1.24)$$

Invoking the steady state approximation for the intermediate ion pair and encounter complex and solving resulting expression for [$D^{\cdot+}\cdots A^{\cdot-}$] and [$D^{*}\cdots A$] we get equation the following expression

$$[D^{\cdot+}\cdots A^{\cdot-}] = \frac{k_{et}[D^{*}\cdots A]}{k_{-et}+k_{bet}} \tag{1.25}$$

$$[D^{*}\cdots A] = \frac{k_{diff}\left(1+\frac{k_{bet}}{k_{-et}}\right)}{k_{-diff}\left(1+\frac{k_{bet}}{k_{-et}}\right)+\frac{k_{et}k_{bet}}{k_{-et}}}[D^{*}][A] \tag{1.26}$$

Substituting results from equation 1.26 in equation 1.21 and using equation 1.22 we obtain

$$k_q = k_{diff} - \frac{k_{-diff}k_{diff}\left(1+\frac{k_{bet}}{k_{-et}}\right)}{k_{-diff}\left(1+\frac{k_{bet}}{k_{-et}}\right)+\frac{k_{et}k_{bet}}{k_{-et}}} \tag{1.27}$$

Simplifying equation 1.27 mathematically k_q can be obtained as

$$k_q = \frac{k_{diff}}{1+\frac{k_{-diff}}{k_{et}}+\frac{k_{-diff}k_{-et}}{k_{et}k_{bet}}} \tag{1.28}$$

Now for an exothermic photoinduced electron transfer reaction we can assume $k_{et} \gg k_{-et}$ and thus equation 1.28 can be modified to

$$k_q = \frac{k_{diff}}{1+\frac{k_{-diff}}{k_{et}}} \tag{1.29}$$

$$\frac{1}{k_q} = \frac{1}{k_{diff}} + \frac{1}{Kk_{et}} \tag{1.30}$$

In equation 1.30, $K = \frac{k_{diff}\,(M^{-1}s^{-1})}{k_{-diff}\,(M^{-1})}$ and is known as diffusional equilibrium constant for encounter complex formation and the expression for K is[1,29,37,38]

$$K = 4\pi N_A r^2 \delta r \exp(-\frac{\omega(r)}{RT}) \tag{1.31}$$

Where, N_A is Avogadro's number, r is distance between donor and acceptor in the encounter complex and $\omega(r)$ is the work required to bring the donor and acceptor

at a distance r, R is universal gas constant and T is absolute temperature. Electron transfer can effectively take place over a distance of r to $r+ \delta r$. If either or both the reactants are neutral species then the value of work function becomes zero.[1,29,37,38] In general a value of 2 Å is assumed for δr. Thus the value of K becomes approximately to 1 M^{-1}.[1,29,37,38] Therefore finally equation 1.30 takes the form

$$\frac{1}{k_q} = \frac{1}{k_{diff}} + \frac{1}{k_{et}} \tag{1.32}$$

From the above equation we can conclude that, if the ET process is the rate determining step ($k_{et} \ll k_{diff}$) then the measured quenching rate constant (k_q) would provide the value of k_{et}, but for the diffusion controlled reaction where diffusion process is the rate determining step ($k_{et} \gg k_{diff}$) k_q is unable to quantify k_{et}. In other words, for the diffusion limited bi-molecular PET reaction, the indirect quantification of k_{et} (by measuring k_q i.e. the steady-state or time-resolved quenching experiments) is impertinent. This problem was first elucidated by Rehm- Weller in their fluorescence quenching experiments.[30] They studied several donor-acceptor pairs in acetonitrile and found that with increase in free energy of the reaction the k_q values first increased but then attained a plateau region which is known as the diffusion limit.[30,39] This diffusion limit is put by the solvent where k_{et} becomes faster than k_{diff}.

1.2.4. Evidence of MIR: PET Experiments

The diffusion limit imposed an unprecedented problem on experimental observation of MIR. This problem was first solved by Miller et. al. in 1988 who used a steroidal spacer to incarcerate the donor and acceptor molecule.[40] In their pioneering work, the spacer molecule inhibited diffusion between the donor and acceptor molecules but allowed ET to happen in fluid medium.[40] By changing the donor acceptor pairs they were able to show the existence of MIR.[40] Following this work, several more observations were published in the next few years.[41-43] Several other techniques like scanning tunneling microscopy, dynamic nuclear polarization

other than fluorescence quenching were used in subsequent years to observe PET.[44,45] Establishment of MIR in still remains an interesting problem especially in case of bimolecular reactions. Over the years, another approach became very popular. Using different kinds of confined medium like micelle, reverse micelle, cyclodextrin etc several PET studies were performed.[46-53] The donor and acceptor molecules do not remain attached by a chemical spacer in these cases.[46-53] Instead confinement acts like a partially frozen medium. In bulk solution, the reaction exergonicity needed to observe MIR is very high and it is very hard to find suitable donor acceptor pairs which can achieve such high level of exothermicity. However, in confined medium the motions of the solvent molecules are retarded compared to the bulk medium and therefore the role of solvent reorganization energy is less pronounced.[46-59] In other words, less solvent reoraganisation energy is needed to achieve ET and because of this MIR can be observed at much less reaction exergonicity which is suitable for a many donor acceptor pair molecules.[46-59] Here it should be pointed out that in all these discussion it has been assumed that nuclear reorganization energy do not change with change in donor and acceptor molecules which is impossible. However, for a series of molecules sharing similar chemical structures and differing only in their substitution, the nuclear reorganization can practically be assumed to be a constant. Observation of MIR in confined medium using fluorescence quenching methods became very popular and this idea was later extended to ionic liquids where high viscosity of the medium was assumed to exert similar effect.[60,61] However, it was pointed out that time resolved fluorescence quenching experiments have an intrinsic problem. Diffusional encounter theory predicts that the quenching constant is a time dependent quantity.[62-64] Thus fluorescence intensity at a certain time $I(t)$ was described by the following equation.[62-64]

$$I(t) = I(0)exp\left[-\frac{t}{\tau_f} - c\int_0^t k(t')dt'\right] \quad (1.33)$$

In the above equation, $I(0)$ is the fluorescence intensity at time $t = 0$, $\tau_f$is the intrinsic fluorescence lifetime of the fluorophore, c is a constant. The most important part is the variation of quenching constant $k(t')$ with time which has been described by the following equation.[62-64]

$$k(t') = 4\pi \int_{r=r_0}^{\infty} w(r)n(r,t)r^2 dr \quad (1.34)$$

Here, $w(r)$ is the reaction probability which is a function of the distance between the reactant pair r and $n(r,t)$ is the reactant pair distribution function.[62-64] These formalism leads to an unprecedented behavior. Whenever, a fluorophore is excited it will always find some quencher molecule at its vicinity and therefore it will immediately undergo electron transfer.[62-64] This is the static quenching regime and called quenching sphere of action.[26,2762-64] As time progresses, quenching occur between molecules further and further apart. But electron transfer can only occur at a certain distance which means the time taken for the reactant pair to form the encounter complex through diffusion will also control the quenching rate and therefore the quenching rate constant keep on changing via a non-stationary phase until it reaches an equilibrium value which is known as the stationary phase of quenching.[62-64] The problem is the quenching need to take place within the intrinsic fluorescence lifetime of the probe and so for different fluorophores quenching will finish at different time regimes. That in turn shall determine the observed value of quenching rate constant. For long lifetime fluorophores the stationary regime will be reached and this portion is totally controlled by diffusion or in other words the viscosity of the mixture.[62-64] Separation of these three parts of quenching process is necessary to clearly establish the MIR and analysis by the group of Eric Vauthey put the previous experimental observations in questions through this type of analysis.[62-64] Therefore a remedial method is required by which MIR observations in case of bimolecular quenching can be justified or rejected and quenching experiments are certainly not going to help. In this thesis, the goal is to establish the appropriate experimental methods for PET studies.

1.3. Molecular Rotor Thioflavin-T (ThT): A Brief Overview

1.3.1. Twisted Intramolecular Charge Transfer and Molecular Rotors

When a fluorophore is excited, electron is transferred from its HOMO to LUMO which results in rapid change of dipole moment of the molecule. This state created due to absorption of light can be called a Locally Excited (LE) state of the molecule.[26,27] Technically, vertical excitation generates a Franck-Condon state in the molecule which undergoes ultrafast vibrational relaxation to form the LE state or the FC state can itself be the LE state.[26,27] If the molecule has electron donating group substitution, then the change in dipole moment will be bigger and if both electron donating and accepting substituents are present then a large change of dipole moment is expected.[26,27,65] Now, if the solvent surrounding the molecule is sufficiently polar then it can accommodate this change in dipole moment and assist the charge transfer in the molecule. Thus a solvent relaxed intramolecular charge transfer state (ICT) is formed from the LE state.[26,27,65] In general, the molecules containing aromatic moieties remain coplanar with the electron donating/accepting groups in the ground state which allows maximum amount of conjugation. Excitation to LE state does not permit nuclear motion according to Born-Oppenheimer approximation and therefore the same co-planer geometry is retained.[26,27,65,66] Now when the molecule undergoes charge transfer it can be assisted/associated with the rotation of molecular fragment or substitution resulting in loss of conjugation within the molecule and completes electron transfer from one fragment to the other.[26,27,65,66] This type of phenomenon is known as twisted intramolecular charge transfer (TICT) which was first discovered by Lippart in DMABN molecule.[65,67] TICT process is assisted by the polar solvent and occurs within the same potential energy surface of the excited state and therefore compounds undergoing TICT like DMABN shows dual fluorescence in polar solvents.[65-67] The shorter wavelength emission band appears from the LE state while the longer one originates from the TICT state.[26,27,65-67] Naturally, in non-polar solvents, only the LE state survives and only one fluorescence peak is

observed.[26,27,65-67] The photophysics of these types of molecules have been modelled using intramolecular electron transfer from donor part of the molecule to the acceptor fragment using Marcus theory.[65,66,68]

In my research I have worked with Thioflavin-T (ThT) which is classified as a molecular rotor. Molecular rotors like ThT, auramin-O (AuO), malachite green (MG) exhibit TICT but they are unique from other dual emitting TICT probes in one particular aspect. In case of molecular rotors, the TICT state is almost non-fluorescent making the LE state as the only fluorescent state.[66,68-71] Therefore unlike DMABN, molecular rotors shows only one fluorescent band in polar solvents and their fluorescence quantum yield is very low.[66,68-71] The torsional motion which takes the molecule from LE to TICT state is very fast and as the TICT acts as a very effective non-radiative channel in case of molecular rotors, the quantum yield of the molecule remains low in common bulk solvents.[66,68-72] However, the same property makes this particular class of dyes very effective in biological sample detection. The fast twisting motion depends heavily on the restrictions imposed by the surrounding such as medium viscosity.[66,68-71] Thus increase in medium viscosity or binding of the dye to a certain structure effectively restricts the amplitude motion and therefore increases its quantum yield. In fact, the quantum yield of such dyes can be tunable with viscosity and therefore molecular rotors are very effective microviscosity sensors.[68-76] Changes in viscosity in can cause several diseases in human body such as diabetes, hypercholesterolemia, cell malignancy etc.[77-81] Therefore microviscosity sensors can be very effective in detection of such diseases. In fact, ThT was introduced in 1965 for the detection of amyloid fibril formation. Many infamous diseases like Alzheimer's, Parkinson's and type-II diabetes and at least 20 more diseases are associated with amyloid fibril formation and curative treatments for them are hard to find.[82,83] Amyloid fibril formation is characterized by increased β-sheet formation in the protein and there is a notion that ThT binds to multistranded β-sheet in protein but the proper binding mechanism still has some controversy.[82-85]

The effectiveness of ThT in detection of fibrils is the dramatic change in quantum yield of about 2 orders of magnitude from unbound to bound state accompanied by shift in the emission maxima from ~450nm to ~480nm.[86] These visible changes in ThT fluorescence colour and intensity made it a popular amyloid sensor and several in-vivo and in-vitro studies were performed with it.[86] However, the exploration of its photophysics began much later.

1.3.2. Excited State Deactivation Models

The increase of fluorescence quantum yield of ThT in amyloid fibrils used to be explained by a model called eximer model.[82] In this model, the increment of fluorescence emission was attributed to formation of highly fluorescent eximers of ThT in the small cavities of fibrils.[82] Later optical microscopy revealed that ThT binds to amyloid fibril in monomeric form.[82] ThT was put into the molecular rotor domain by Stsiapura et.al. in 2007.[87,88] The photophysics of its predecessor AuO has been explored for long time and when ThT came into discussion it was modeled following the existing deactivation schemes of AuO.[86,87,88] For both the dyes, the excited state relaxation dynamics is based on the idea of a two state barrierless potential energy surface along the torsional coordinate of the molecule. Bagchi, Fleming and Oxtoby in 1983 described a model for non radiative transition in molecules.[89] In this model, the initial population created by excitation move towards a non-radiative curve crossing point on a barrierless potential energy surface.[89] This curve crossing point between the ground and excited state is the only place where internal conversion which was described mathematically by a delta function, can occur.[89] The problem with this model is at low viscosity limit it predicted an initial delay in the fluorescence decay but experimentally no such intimal delay was present in fluorescence transients of ThT.[86] Moreover, at high viscosity limit, the population cannot diffuse towards the crossing point and no crossing would occur.[86] A second more extensive model was proposed by Agmon et.al. for describing time resolved fluorescence behavior of p-HBDI, a green fluorescence protein chromophore which undergoes twisting motion along its two

substituted aromatic rings.[90] In this model, a non-local sink term was considered.[90] Unlike BFO model, this non-local sink term allows the internal conversion process to happen over all the possible molecular configurations; not only at the conical intersection.[90] Therefore the non-radiative decay rate becomes a function of twisting angle and at a particular molecular geometry the rate is maximum which in their case perpendicular geometry between the two aromatic fragments.[86,90] Once the non-radiative decay rate becomes a function of twisting angle it becomes inhomogenous i.e. a multiexponential decay is observed.[86,90] This model was termed inhomogeneous frozen model as it worked well for molecules in frozen solvents.[86,90-94] An extension was proposed by Agmon and Hopfield which incorporated population diffusion along the potential energy surface with influence from diffusion. This model incorporates random diffusion with propagation in an external potential and a process that decreases population.[86,90-94]

The last model to describe is the Glasbeek model which was proposed for the dynamics of AuO but can be applied for ThT as well.[92-96] In this model, a normalized twist coordinate (z) was defined as a function of time dependent twisting angle and the ground state, emissive state (F) and the dark TICT (D) state were all defined as a function of this coordinate.[92-96] Initial δ-function excitation populates the emissive state which then diffuses towards the TICT state via twisting motion.[92-96] The actual lowest excited state potential (S_1) has been considered as a mixture of the states along the twisting coordinate.[92-96]

$$S_1(z) = \frac{1}{2}[F(z) + D(z)] - \frac{1}{2}\sqrt{[F(z) - D(z)]^2 + 4C^2} \tag{1.35}$$

In the above equation, C is coupling parameter. At any given position the S_1 state is a mixture of an emissive state and a dark state which makes the transition to ground state, at any time, a z dependent quantity which is given by the following equation.[92-96]

$$M(z) = cos^2\left(\frac{1}{2}arctan\left(\frac{2c}{F(z)-D(z)}\right)\right) \tag{1.36}$$

Once the sample is irradiated, the excited state population generated shall no longer remain in equilibrium with the solvent. Glasbeek assumed this population to be a asymmetric log-normal function of z.[92-96] Then the time evolution of this population was modeled using the Debye-Smoulchowskii theory using a diffusion coefficient for the rotational coefficient of the molecular fragments and a frictional parameter.[92-96] With these information the time dependent fluorescence intensity was modelled and the equation was fitted numerically to the time dependent fluorescence spectra.[92-96] This model was applied to AuO experimental data by Meech to explain the dynamic Stokes shift and the fast loss of fluorescence intensity at shorter times.[97] In case of ThT, Erez et al. to calculate the time resolved emission spectra and a comparison with the experimental data revealed a short time mismatch for ThT in 1-propanol.[93,94] Now, as this model and previous ones involve diffusion coefficient for rotation and friction with solvent, the overall dynamics over a barrierless potential energy surface becomes viscosity controlled. Moreover assumption of inhomogeneous population in the excited state and coordinate dependent decay can explain the multiexponential nature of fluorescence intensity decays. All this models can be summarized as follows. When excited, ThT molecules populate the LE state which is an emissive state. Then twisting of dimethylanilino moiety with respect to benzothiazole moiety of ThT brings the population towards the TICT state while constantly decaying back to ground state. This LE→TICT transition is barrierless in nature and is controlled by viscous drag imposed by the medium on the rotation fragments. Any external effect like viscous drag or binding to fibril hinders the twisting motion of the molecule and thus leads to decrease in the rate of LE→TICT transition and therefore the quantum yield increases.

1.3.3. Study of ThT Photophysics

The time resolved experiments performed previously on ThT also corroborated with the two state nature of the excited state. Stsiapura et.al. established ThT as a molecular rotor in 2008 performing time resolved

fluorescence spectroscopy in 99% glycerol at different temperature.[98] They observed that with increase in temperature, the average lifetime as well as the quantum yield of ThT decreases.[98] They also modeled the temperature dependent rate using Debye-Smolchowskii theory.[98] The non-exponential nature of fluorescence intensity decay was assigned to the inhomogeneous distribution of population in the excited state because of twisting motion.[98] One important aspect covered in this report was recording of emission spectra of ThT ar 77K and discarding the idea of triplet formation.[98] In their next study, they used femtosecond transient absorption to study ThT in four low-viscosity solvents which were water, ethanol, 2-propanol, and butanol.[99] Viscosity of butanol is about three times of that of water but quantum yield increased about 14 times.[99] A sum of two exponential functions were used to fit the data and both the time components increased with increase in solvent viscosity.[99] However the order of increment neither was same nor was it at par with increase in viscosity. For example, from water to butanol the first component increased about 9 times whereas the second component increased about 100 times.[99] These parameters were obtained from the global fitting of the data and the two time components were assigned as the lifetime of LE and TICT state of ThT.[99] They explained all the data in terms of the barrierless rotor model based on the mutual rotation of benzothiazole part with respect to dimethylanilino part.[99] However, the authors themselves commented comparing the ethanol and butanol data that viscosity is not the only factor determining the photophysics of ThT. Moreover they found a long lived lifetime component in their fitting which fictitiously assigned to a metastable state. [99] Now the deactivation scheme proposed which was featured in later articles about ThT showed a conical intersection between the TICT state and the ground state.[99] Deactivation through a conical intersection does not depend upon one stretching component but the bending of the molecule plays a role too.[99] In fact, the authors associated the bending motion with the TICT to ground state deactivation.[99] The notion although accepted the viscosity controlled pathway but could not fully satisfies all the experimental observations. In a very recent paper, Stsiapura et.al.

studied ThT with several solvent by transient absorption spectroscopy focusing on the dielectric and hydrogen bonding properties of the solvents.[100] ThT is capable of forming hydrogen bond with polar solvents. The authors justified increase of TICT lifetime over ~3 times of diffusional limit with intermolecular hydrogen bond formation of the dimethyl amino group.[100] In this case, the static and dynamic solvent effect was modeled based on Marcus type electron transfer like DMABN and they established correspondence between dielectric constant of the solvent and rate of non-radiative decay.[100] However, in alcohols with longer alkyl chain (butanol, pentanol etc.) this analogy fails and the non-radiative process becomes diffusion limited.[100] Now, ThT is not exactly planer in the ground state. Several computational studies showed that the benzothiazole ring and the dimethylanilino moiety makes 37° angle when optimized in the ground state.[101,102] The rotation around the C-C single bond joining the two molecular fragments has been considered in the excited state and rigid a potential energy surface scan revealed that the TICT state reached upon this rotation is at 90° geometry between the two groups.[86,101-103] Thus a complete charge transfer and loss of conjugation happens in ThT. All these calculations used different level of computation but they more or less produced the same result along this coordinate. Now the choice of twisting coordinate is based on the deactivation models described above. [86,101-103]However, in ThT one more amplitude motion is possible i.e. the rotation of dimethylamino group in the excited state. The NMe_2 group is much smaller in size compared to the benzothiazole or dimethylanilino moiety and so the effect of medium hindrance was expected to be less promominent on this coordinate. [86,101-103] This particular twisting cocordinate was in fact considered by Singh et.al. in their computation but they discarded this channel as an effective quenching pathway for ThT based on the fact that it contains a very small potential energy barrier.[102] Although they incorporated a conductor like polarizable continuum model in their calculation but they only calculated for water and this type of computations do not incorporate any specific solvation.[102] So variation of the barrier height with dielectric properties of the solvents was not considered. An interesting fact can be highlighted here.

Although water has about twice the viscosity compared to methanol, the quantum yield of ThT reported in these two solvents till date has been same or ThT in water has less quantum yield than in methanol.[86,88] Now, in the computation data a proper conical intersection between the TICT and ground state of ThT was not found and therefore it was concluded that the TICT state may be very weakly emissive.[86,102,103] Ghosh supported this idea with experiments but Stsiapura discarded it by proposing reversible ring opening of the benzothiazole moiety.[99,104] Density functional theory calculations coupled with Glasbeek model has been used by Erez et. al. to mock the fluorescence spectra of ThT. To estimate the evolution of excited state population of ThT with time they used spherically symmetric diffusion problem software developed by Krissinel and Agmon.[93] Interestingly they observed that two processes are contributing to the excited state dynamics of ThT and although they considered the rotation of dimethylamino group briefly, but ultimately settled on the solvation dynamics to be responsible.[93] However, all this modelling and discussion does not explain the unusual quantum yield of ThT in chlorinated solvents. As a matter of fact, in one of the early papers on ThT reported this phenomenon but it did not come into discussion in later works.[105] This seemingly unusual quantum yield was an starting point to question the barrierless photophysics of ThT and as recent developments in the Auramin-O dynamics suggested the existence of a barrier in its excited state manifold, in this thesis I focused on studying ThT deactivation including the chlorinated solvents.

1.4. Excited State Intramolecular Proton Transfer

In chemistry and biology intra and intermolecular proton transfer reactions are frequent and important.[26,27,106-109] While the ground state reactions are most common, there are plenty of examples for the same in the excited state.[26,27,110-114] In the electronic excited state of a molecule, two types of proton transfer reactions can take place i.e. intra and intermolecular. When a proton transfer probe is excited, its acidity/basicity changes and it can transfer its labile proton to solvent which is known as the intermolecular proton transfer reaction. On the other hand, if

the probe contains heteroatoms as a part of its aromatic backbone or as a substitution, then the labile H can transfer to that heteroatom which is then termed as the excited state intramolecular proton transfer(ESIPT). Generally, in proton transfer probes the H remains attached to an electronegative atom like O or N. Electronic excitation brings about changes in the distribution of local electron density around the O-H or N-H bond and thus changes in acidity/basicity intialise ESIPT.[26,27,115] In most of the cases, O-H act as the donor and O or N acts as an acceptor but some cases are known where N-H can act as a donor.[116-119] An intramolecular hydrogen bond between the donor and acceptor fragments facilitates these processes but it is not necessary. In fact according to Kasha's description ESIPT can happen through a mediator when the H atom is far away from the acceptor.[110,120,121] The involvement of the mediator can be thought to violate the definition of ESIPT but in many such cases it is hard to distinguish from a direct process.[122,123] ESIPT processes are ultrafast in nature and occur on femtosecond time scales especially for direct ESIPT reactions.

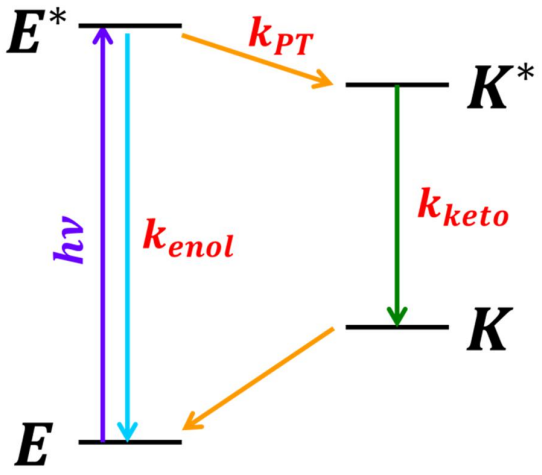

Figure 1.5. Schematic representation of four level ESIPT process

If the probe contains a phenolic OH group and in the excited state that proton is transferred to another atom then ESIPT can be represented as enol-keto tautomerisation in the excited state.[107,115,124] Thus, when the enol-form in the ground state is irradiated, it undergoes ESIPT and fluorescence emission comes

from the keto tautomer.[125,126] Therefore, ESIPT processes are associated with large amount of Stokes shift and this is one of the ways to identify its occurrence.[125,126] However the emission from the excited enol for can also be observed but in most cases intensity of enol emission is very weak compared to the keto-emission.[110-126] The simplistic four level ESIPT model for the process is shown in figure 1.5.The reverse proton transfer step is nothing but isomerization in the ground state. ESIPT is studied using time resolved fluorescence spectroscopy. The nature of fluorescence intensity decay collected at enol and keto emission maxima can be predicted through kinetic analysis of figure 1.5.[125] The kinetic equations for concentration of enol and keto form at a certain time after δ-function excitation can be written as[125-128]

$$\frac{d[E^*]}{dt} = -(k_{enol} + k_{PT})[E^*] \tag{1.37}$$

$$\frac{dK^*}{dt} = k_{PT}[E^*] - k_{keto}[K^*] \tag{1.38}$$

In the above equations, k_{enol} and k_{keto} are the rate of decay for enol and keto isomers and k_{PT} is the rate of proton transfer. Applying the condition $[E^*] = [E^*]_0$ at $t = 0$, we can solve equation 1.37 and 1.38 yielding the following result.

$$[E^*] = [E^*]_0 e^{-(k_{enol}+k_{PT})t} \tag{1.40}$$

$$[K^*] = \frac{k_{PT}[E^*]_0}{k_{enol}+k_{PT}-k_{keto}} \left(e^{-k_{keto}t} - e^{-(k_{enol}+k_{PT})t}\right) \tag{1.41}$$

So, the kinetics of enol is a single exponential decay with time but the kinetics of keto has a rise and a decay component. Consequently, the fluorescence transient recorded at enol emission wavelength shows only one decay component whereas the same recorded at keto emission wavelength shows a rise and decay part. This prediction is supported by numerous studies of ESIPT in the past.[125-128] But the time component corresponding to the rise part will not directly give the rate of proton transfer which is evident from equation 1.41. However, as the rate of direct proton transfer is generally much greater than the intrinsic decay of the enol

isomer i.e. $k_{PT} > k_{enol}$, a good estimation of proton transfer timescale can be obtained from decay rate of enol emission or growth of keto emission. In many instances, the effect of surrounding medium and other photophysical processes can interfere and influence the ESIPT process and the process become more complicated than the one showed in figure 1.5. The first and most common example of such influence can come from the surrounding solvent especially if the solvent is capable of forming hydrogen bonding.[128-131] In non-polar solvents, almost always the keto emission is too strong to observe any enol emission. In polar solvents, however, ESIPT can give rise to dual emission.[125,128-131] Previously it was mentioned that intramolecular hydrogen bonding in the proton transfer probe increase the efficiency of the ESIPT reaction because the reaction coordinate follows the same path.[125,128-131]When a hydrogen bond donating or accepting solvent is present, the solute shall form intermolecular hydrogen bond with the solvent which works as a perturbation to the system.[125,128-131] Polar solvents solvates the excited enol form and solvation increases the emission intensity of the enol. So a strong dual emission can be observed and one of the example of such phenomenon is the emission of 3-hydroxyflavon in methanol.[125,128-131] Based on the ratio of enol and keto emission in such molecules, many applications have been developed such as polarity sensing, biological structure and micelle structure sensing etc.[132-135]Another phenomenon which occur in polar solvent is formation of rotamers.[135-137]Benzoxazole derivatives can undergo twisting to form two different rotamers of enol in polar solvents.[135-137] Between the two forms, one has much higher chance of undergoing ESIPT as the intramolecular hydrogen bond can form in it. In the another conformation, the phenolic OH group and the acceptor do not face each other and ESIPT in hindered.[135-137] Thus photochemical cis trans isomerization assisted ESIPT can give rise to dual emission behavior depending on the medium.[135-137] Although, the pH of the solution has more prominent effect on intermolecular proton transfer reaction but it can affect the ESIPT too.[125,138,139] In basic solution the ESIPT process can be completely hindered due to deprotonation. In acidic solution the acceptor become protonated and it may seem that protonation

will increase the efficiency of ESIPT but this may not be the case because of the competition between the intra and intermolecular proton transfer.[125,138,139] ESIPT brings about changes in the charge distribution in the molecule and if an electron donating or withdrawing group is present within the molecule, an intramolecular charge transfer state can be easily formed.[125] This ICT state can form prior or after the ESIPT. ICT formation is always accompanied by solvatochromism as dielectric stabilization is a major driving force behind ICT.[140-141] So certain ESIPT probes can show solvatochromic shifts with change in the polarity of the medium.[140-141]

ESIPT processes are ultrafast in nature and the exploration of their dynamics still continues.[142-145] A complete kinetic modeling of ultrafast ESIPT process is not straightforward and in this thesis I have tried to come up with one by studying a new ESIPT probe both experimentally and computationally.

1.5. Solvation Dynamics: A Basic Outline

Solvation dynamics is basically the response of a dielectric medium to an externally applied electric field.[26,27,146-158] In fluorescence spectroscopy, probe molecules are excited by UV-Visible light which takes them to an excited electronic state by promoting electrons from HOMO to LUMO.[26,27,146-158] This process imposes a dipole moment in the molecule which acts as an external electric field to solvent.[26,27,146-158] The creation of the solute dipole by light is an instantaneous process. Now the solvent molecules remain in equilibrium with the probe in the ground state and they cannot reorient themselves with instantaneous alteration of charge distribution of the probe molecule.[26,27,146-158] So a high energy non-equilibrium state is created by irradiation which is known as the Franck-Condon state. With progress of time, solvent molecules reorient themselves to accommodate the new dipole moment in the excited state and thus the FC state is stabilized and a red-shift in the fluorescence spectrum is observed.[26,27,146-158] Obviously, the steady state fluorescence spectrum is an average over all the phenomenon in the excited state and so the said shift can only be observed with time resolved fluorescence spectroscopy. So when a fluorescent probe is excited by

a pulsed laser light, its emission spectra shifts to longer wavelengths with progress of time. The phenomenon has been shown in figure 1.6 and the change in the emission maxima with time is known as dynamic Stokes shift. [26,27,146-158] However, time resolved emission spectra (TRES) are not usually recorded directly. Instead they are constructed from the time dependent fluorescence intensity decays which is discussed in the next chapter. Solvation dynamics is evaluated using the solvent response function $C(t)$ which is defined as follows[26,27,146-158]

$$C(t) = \frac{\nu(t)-\nu(\infty)}{\nu(0)-\nu(\infty)} \tag{1.42}$$

In the above equation $\nu(t)$, $\nu(0)$ and $\nu(\infty)$ are the peak frequencies of time resolved emission spectra (TRES) of the solvatochromic molecule at time t, 0 and ∞, respectively. For a molecule with high excited state dipole moment compared to the ground state, the $\nu(\infty)$ is appeared at the lower energy than $\nu(0)$.[26,27,146-158] In the time of solvent relaxation the solute can evolve from one polar state to another. So the underlying assumption in equation 1.42 is solvent is minimally perturbed and solute is present in low concentration to avoid any solute correlation. The $C(t)$ function often has a simple exponential relation with the longitudinal relaxation time $(\tau_L)$of the solvent.[146-158]

$$C(t) = aexp\left(-\frac{t}{\tau_L}\right) \tag{1.43}$$

In most of the cases, the decay of $C(t)$ with time is non-exponential. The prediction of mono exponential is given by simple continnum dielectric model of solvation and linear response theory.[146-158] However, solvation dynamics depends heavily on nature of solute-solvent interaction. Primarily the deviation originates from translation, rotation and orientation of solvent molecules and the timescale of these motions are not similar.[146-158] Frictionless libration and vibrational motion takes the dominant role in the initial time of the solvent relaxation.[26,27,146-158] These motions are influenced by hydrogen bonding ability of the solvents but very weakly and relaxation happens on a femtosecond time scale. At picosecond and

longer timescale, diffusive translation and orientation takes the driving seat. In this part the motions of molecules in the first solvation shell determines the time component of relaxation.[146-158] All these motions are influenced by temperature and therefore temperature change can severely affect the solvation time. Pressure has also been shown to affect solvation time.[159,160]

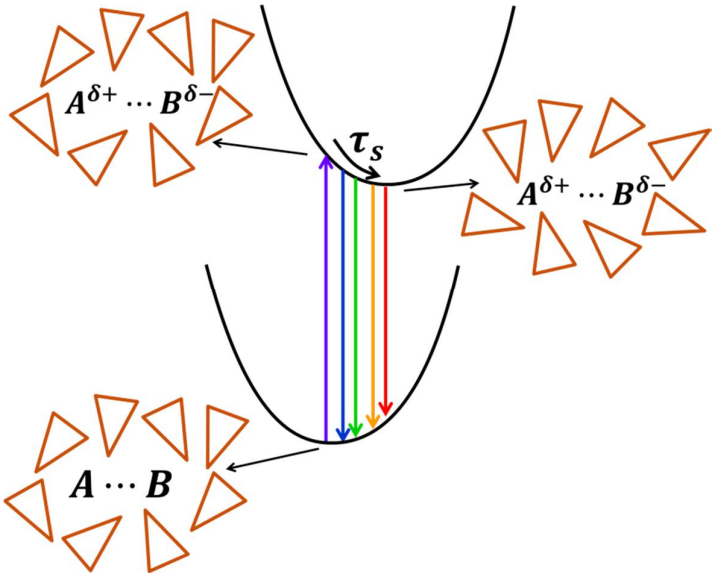

Figure 1.6. Schematic representation of the solvation dynamics process

Time resolved fluorescence spectroscopy is not the only way of observing solvent relaxation. Photon Echo spectroscopy has been used extensively to study solute solvent interaction and relationship between optical dynamics and solvation.[146-158] Both these spectroscopic methods studies solvents from a solutes perspective i.e. they follow a certain character of a probe molecule considering it as a small perturbation within the domain of linear response theory.[146-158] However, solvation dynamics is also studied from the perspective of solvents too. Ultrafast terahertz and vibrational (IR) spectroscopy has been employed to explore the changes inter and intra molecular vibrational modes.[161-163] Optical Kerr effect spectroscopy has been successfully used to explore the low-frequency vibrational modes of solvents and their time dependence.[164-166] However, fluorescence spectroscopic techniques still remain the most frequently used method.

Solvation dynamics influences excited state reactions such as electron transfer, proton transfer etc. and it can influence ultrafast torsional motion i.e. all the photophysical processes studied in this thesis. The first studies on solvation dynamics studies were performed with picosecond lasers in normal bulk solvents where a large unresolved sub-picosecond component was detected and it was found that solvation dynamics depend on the nature of the solvent strongly.[146-158] However, no specific probe dependences were found. With the advancement of ultrafast laser systems, femtosecond fluorescence up-conversion experiments provided new details about the sub-picosecond time component of solvation.[146-158] Even the existence of a sub 100 fs time component of solvation was revealed and it was assumed to be Gaussian in character.[146-158] With the progress of experiments, the techniques were applied to more complex chemical systems such as water in a confined system and in biological media such as proteins and DNA etc.[146-158] Solvation dynamics turned out to be useful tool in those systems as the water dynamics in constrained spaces are different than the bulk water. Solvent response of water in cyclodextrin media revealed a long component of solvation which was further discovered in micelle and reverse micelles. Many theoretical and computational studies were performed to understand this slow component of solvation.[146-158] Especially in proteins, the experiments and computations suggested a retardation of translational motion of the first hydration layer compared to bulk which may be origin of the long component. In case of DNA, the structure and conformation largely depend on hydration and interconversion of structure is shown to be possible due to change in hydration.[146-158] Solvation dynamics studies in lipid vesicles which mimic a cell revealead the presence of two kinds of water molecules, entrapped and bulk like. Polymer, hydrogel and zeolites were also studied to understand the nature of water present within them.[154,167] In recent years, these studies have been extended in the room temperature ionic liquids and a fast and slow component of solvation was found.[167-170]

The effect of solvation dynamics on the processes happening in condensed phase is immense. The movement of small sized ions in water depends on the ion-dipole interaction between the ions and the solvent.[146-158] The exploration of ultrafast solvation time enlightened the reduction of friction on the ions and brought the experiments and theory in agreement. In case of electron transfer reactions, solvation dynamics affects adiabatic ET but found to have little to no effect on non-adiabatic ET.[146-158] In the weakly adiabatic limit, the rate of ET is very fast and in the timescale of ultrafast component of solvation. This part of solvation is dominated by libration and intermolecular vibrational modes of solvent and they are not coupled to the longitudinal modes. Therefore, solvation does not significantly affect the rate of ET in weak adiabatic cases but it has been found in some cases the rate is enhanced by libration modes.[146-158] However, solvation plays a vital role in other chemical reactions where charge transfer contributes to the reaction. In case of reactions such as proton transfer, isomerization the timescale matches that of solvation time and therefore solvation dynamics control the rate of transition state crossing.[146-158] Since solvation dynamics can affect all the three photophysical processes explored in this thesis, it became a requirement to study in SDS micellar environment.

References

1. *Photoinduced Electron Transfer I*; Mattay, J., Ed.; Topics in Current Chemistry; Springer Berlin Heidelberg: Berlin, Heidelberg, 1990; Vol. 156.
2. Scholes, G. D. *Chem. Rev.* **2017**, *117*, 247–248.
3. Kundu, S.; Patra, A. *Chem. Rev.* **2017**, *117*, 712–757.
4. Li, Z.; Liu, C.; Zhang, Z.; Zhang, X.; Guo, W.; Ruan, S.; Zhang, L.; Long, Y. *J. Phys. Chem. C* **2017**, *121*, 8722–8730.
5. Eskandarloo, H.; Kierulf, A.; Abbaspourrad, A. *Nanoscale* **2017**, *9*, 12218–12230.
6. Hedley, G. J.; Ruseckas, A.; Samuel, I. D. W. *Chem. Rev.* **2017**, *117*, 796–837.
7. Fujitsuka, M.; Majima, T. Photoinduced Electron Transfer Processes in Biological and Artificial Supramolecules. In *Supramolecular Chemistry*; John Wiley & Sons, Ltd: Chichester, UK, 2012.
8. Wasielewski, M. R. *Chem. Rev.* **1992**, *92*, 435–461.
9. Morseth, Z. A.; Pho, T. V.; Gilligan, A. T.; Dillon, R. J.; Schanze, K. S.; Reynolds, J. R.; Papanikolas, J. M. *J. Phys. Chem. B* **2016**, *120*, 7937–7948.
10. Imahori, H.; Sakata, Y. *Adv. Mater.* **1997**, *9*, 537–546.
11. Tachibana, Y.; Vayssieres, L.; Durrant, J. R. *Nat. Photonics* **2012**, *6*, 511–518.
12. Bard, A. J.; Fox, M. A. *Acc. Chem. Res.* **1995**, *28*, 141–145.
13. Joya, K. S.; Joya, Y. F.; Ocakoglu, K.; van de Krol, R. *Angew. Chemie Int. Ed.* **2013**, *52*, 10426–10437.
14. Andreiadis, E. S.; Chavarot-Kerlidou, M.; Fontecave, M.; Artero, V. *Photochem. Photobiol.* **2011**, *87*, 946–964.
15. Sun, S.; Gao, L.; Liu, Y. *Appl. Phys. Lett.* **2010**, *96*, 83113(1-3).
16. Miao, X.; Tongay, S.; Petterson, M. K.; Berke, K.; Rinzler, A. G.; Appleton, B. R.; Hebard, A. F. *Nano Lett.* **2012**, *12*, 2745–2750.
17. Yin, Z.; Zhu, J.; He, Q.; Cao, X.; Tan, C.; Chen, H.; Yan, Q.; Zhang, H. *Adv. Energy Mater.* **2014**, *4*, 1300574.
18. Lin, T.; Huang, F.; Liang, J.; Wang, Y. *Energy Environ. Sci.* **2011**, *4*, 862–865.
19. Yang, H.; Guai, G. H.; Guo, C.; Song, Q.; Jiang, S. P.; Wang, Y.; Zhang, W.; Li, C. M. *J. Phys. Chem. C* **2011**, *115*, 12209–12215.
20. Dutta, M.; Sarkar, S.; Ghosh, T.; Basak, D. *J. Phys. Chem. C* **2012**, *116*, 20127–20131.
21. Grätzel, M. *Nature* **2001**, *414*, 338–344.
22. O'Regan, B.; Grätzel, M. A Low-Cost, *Nature* **1991**, *353*, 737–740.

23. Grätzel, M. *J. Photochem. Photobiol. C Photochem. Rev*. **2003**, *4*, 145–153.
24. Grätzel, M. *Inorg. Chem.* **2005**, *44*, 6841–6851.
25. Gratzel, M., (Ed.) Energy Resources through Photochemistry and Catalysis*;* Academic Press: New York, 1983.
26. Lakowicz, J. R. *Principles of Fluorescence Spectroscopy*; Springer US: Boston, MA, 2006.
27. Valeur, B.; Berberan-Santos, M. N. *Molecular Fluorescence*; Wiley-VCH Verlag GmbH & Co. KGaA: Weinheim, Germany, 2012
28. Turro, N. J.; Ramamurthy, V.; Scaiano, J.C. *Modern Molecular Photochemistry of Organic Molecules*, University Science Books, Sausalito, California, 2010.
29. Kavarnos, G. J.; Turro, N. J. *Chem. Rev.* **1986**, *86*, 401-449.
30. Rehm, D.; Weller, A. *Isr. J. Chem.* **1970**, *8*, 259-271.
31. Bagchi, B. *Molecular Relaxation in Liquids*, Oxford University Press, New York, USA, 2012.
32. Marcus, R.A. *J. Chem. Phys.* **1956**, *24*, 966-978.
33. Marcus, R.A. *J. Chem. Phys.* **1957**, *26*,867-871.
34. Marcus, R.A. *J. Chem. Phys.* **1957**, *26*, 872-877.
35. Marcus, R.A. *J. Electroanal. Chem.* **2000**, *483*, 2-6.
36. Marcus, R.A. *Discuss. Faraday Soc.*, **1960**, *29*, 21-31.
37. Nad, S.; Pal, H. *J. Phys. Chem. A.* **2000**, *104*, 673-680.
38. Sutin, N. *Acc. Chem. Res.* **1982**, *15* (9), 275–282.
39. Rosspeintner, A.; Koch, M.; Angulo, G.; Vauthey, E. *J. Am. Chem. Soc.* **2012**, *134*, 11396−11399
40. Miller, J. R.; Calcaterra, L. T.; Closs, G. L. *J. Am. Chem. Soc*. **1984**, *106*, 3047-3049
41. Miller, J. R.; Beitz, J. V.; Huddleston, R. K. *J. Am. Chem. Soc*.**1984**, *106*, 5057-5068.
42. Turró, C.; Zaleski, J. M.; Karabatsos, Y. M.; Nocera, D. G. *J. Am. Chem. Soc*.**1996**, *118*, 6060-6067.
43. Rau, H.; Frank, R.; Greiner, G. *J. Phys. Chem.***1986**, *90*, 2476-2481.
44. Schmickler, W.; Tao, N. *Electrochim. Acta* **1997**, *42*, 2809.
45. Becker, H. G.; Pfeifer, D.; Urban, K. *J. Chem. Soc., Faraday Trans. 2* **1989**, *85*, 1765.
46. Ghosh, S.; Sahu, K.; Mondal, S. K.; Sen, P.; Bhattacharyya, K. A *J. Chem. Phys*. **2006**, *125*, 054509-1-7.
47. Ghosh, S.; Mondal, S. K.; Sahu, K.; Bhattacharyya, K. *J. Chem. Phys.* **2007**,*126*, 204708(1-11)

48. Ghosh, S.; Mondal, S. K.; Sahu, K.; Bhattacharyya, K. *J. Phys. Chem. A* **2006**, *110* , 13139-13144
49. Mandal, U.; Ghosh, S.; Dey, S.; Adhikari, A.; Bhattacharyya, K. *J. Chem. Phys*. **2008** , *128* , 164505(1-10)
50. Kumbhakar, M.; Nath, S.; Mukherjee, T.; Pal, H. *J. Chem. Phys*. **2004**, *120*, 2824-2834
51. Kumbhakar, M.; Singh, P. K.; Satpati, S. K.; Nath, S.; Pal, H. *J. Phys. Chem. B*, **2010**, *114*, 10057-10065
52. Satpati, S. K.; Kumbhakar, M.; Nath, S.; Pal, H. *J. Photochem. Photobiol. A* **2008**, *200*, 270-276.
53. Kumbhakar, M.; Singh, P. K.; Nath, S.; Bhasikuttan, A. C.; Pal, H. *J. Phys. Chem. B*, **2008**, *112* , 6646-6652.
54. Bhattacharyya, K. *Acc. Chem. Res*. **2003**, *36*, 95-101.
55. Bhattacharyya, K.; Bagchi, B. *J. Phys. Chem. A.* **2000**, *104*, 10603-10613.
56. Nandi, N.; Bhattacharyya, K.; Bagchi, B. *Chem. Rev*. **2000**, *100*, 2013-2046.
57. Riter, R. E.; Willard, D. M.; Levinger, N. E. *J. Phys. Chem. B* **1998**, *102*, 2705-2714.
58. Piletic, I. R.; Moilanen, D. E.; Spry, D. B.; Levinger, N. E.; Fayer, M. D. *J. Phys. Chem. A* **2006**, *110*, 4985-4999.
59. Senapati, S.; Chandra, A. *J. Phys. Chem. B,* **2001**, *105*, 5106-5109.
60. Paul, A.; Samanta, A. *J. Phys. Chem. B* **2007**, *111*, 1957-1962.
61. Santhosh, K.; Samanta, A. *J. Phys. Chem. B* **2010**, *114*, 9195–9200.
62. Rosspeintner, A.; Koch, M.; Angulo, G.; Vauthey, E. *J. Am. Chem. Soc.* **2012**, *134*, 11396−11399.
63. Koch, M.; Rosspeintner, A.; Angulo, G.; Vauthey, E. *J. Am. Chem. Soc.* **2012**, *134*, 3729-3736.
64. Rosspeintner, A.; Vauthey, E. *Phys. Chem. Chem. Phys.* **2014**, *16*, 25741-25754.
65. Rettig, W. *Top. Curr. Chem.* **1994**, *169*, 253–299.
66. Haidekker, M. A.; Theodorakis, E. A. *Org. Biomol. Chem.* **2007**, *5*, 1669–1678.
67. Lippert E, Liider W, Boos H (1962) in: *Advances in molecular spectroscopy* Mangini A (ed), Pergamon, Oxford.
68. Grabowski, Z. R. *Pure Appl. Chem* **1983**, *55*, 245–252.
69. Haidekker, M. A.; Theodorakis, E. A. *J. Biol. Eng*. **2010**, *4*, 1–14.
70. Kottas, G. S.; Clarke, L. I.; Horinek, D.; Michl, J. *Chem. Rev*. **2005**, *105*, 1281–1376.
71. Grabowski, Z. R.; Rotkiewicz, K.; Rettig, W. *Chem. Rev*. **2003**, *103*, 3899–4032.

72. Haidekker, M. A.; Theodorakis, E. A. *J. Biol. Eng.* **2010**, *4*, 11(1-14).
73. Sutharsan, J.; Lichlyter, D.; Wright, N. E.; Dakanali, M.; Haidekker, M. A.; Theodorakis, E. A. *Tetrahedron* **2010**, *66*, 2582–2588.
74. Zhou, F.; Shao, J.; Yang, Y.; Zhao, J.; Guo, H.; Li, X.; Ji, S.; Zhang, Z. *European J. Org. Chem.* **2011**,. *25*, 4773–4787.
75. Lee, S.-C.; Heo, J.; Ryu, J.-W.; Lee, C.-L.; Kim, S.; Tae, J.-S.; Rhee, B.-O.; Kim, S.-W.; Kwon, O.-P. *Chem. Commun.* **2016**, *52*, 13695–13698.
76. Kuimova, M. K.; Yahioglu, G.; Levitt, J. A.; Suhling, K. *J. Am. Chem. Soc.* **2008**, *130*, 6672–6673.
77. Shinitzky, M.in *Physiology of membrane fluidity*, ed. M. Shinitzky, CRC Press, Boca Raton, 1984.
78. Singer, S. J.; Nicolson, G. L. *Science* **1972**, *175* (4023), 720–731.
79. Deliconstantinos, G.; Villiotou, V.; Stavrides, J. C. *Biochem. Pharmacol.* **1995**, *49*, 1589–1600.
80. Nadiv, O.; Shinitzky, M.; Manu, H.; Hecht, D.; Roberts, C. T.; LeRoith, D.; Zick, Y. *Biochem. J.* **1994**, *298*, 443–450.
81. Klaver, J. H.; Greve, E. L.; Goslinga, H.; Geijssen, H. C.; Heuvelmans, J. H. *Br J Ophthalmol* **1985**, *69*, 765–770.
82. Groenning, M. *J. Chem. Biol.* **2010**, *3*, 1–18.
83. Biancalana, M.; Koide, S. Molecular *Biochim. Biophys. Acta - Proteins Proteomics* **2010**, *1804*, 1405–1412.
84. Babenko, V.; Dzwolak, W. *Chem. Commun.* **2011**, *47*, 10686–10688.
85. Nelson, R.; Eisenberg, D. *Curr. Opin. Struct. Biol.* **2006**, *16*, 260–265.
86. Amdursky, N.; Erez, Y.; Huppert, D. *Acc. Chem. Res.* **2012**, *45*, 1548–1557.
87. Stsiapura, V. I.; Maskevich, A. A.; Kuzmitsky, V. A.; Turoverov, K. K.; Kuznetsova, I. M. *J. Phys. Chem. A* **2007**, *111*, 4829–4835.
88. Maskevich, A.A.; Stsiapura, V.I.; Kuzmitsky, V.A.; Kuznetsova, I.M.; Povarova, O.I.; Uversky, V.N. et al., *J. Proteome Res.* **2007**, *6*, 1392–1401.
89. Bagchi, B.; Fleming, G. R.; Oxtoby, D. W. *J. Chem. Phys.* **1983**, *78*, 7375–7385.
90. Gepshtein, R.; Huppert, D.; Agmon, N. *J. Phys. Chem. B* **2006**, *110*, 4434–4442.
91. Agmon, N.; Hopfield, J. J. *J. Chem. Phys.* **1983**, *78*, 6947–6959.
92. Simkovitch, R.; Gepshtein, R.; Huppert, D. *J. Phys. Chem. A* **2015**, *119*, 1797–1812.
93. Erez, Y.; Liu, Y.-H.; Amdursky, N.; Huppert, D. *J. Phys. Chem. A* **2011**, *115*, 8479–8487.
94. Amdursky, N.; Gepshtein, R.; Erez, Y.; Huppert, D. *J. Phys. Chem. A* **2011**, *115*, 2540–2548.

95. Glasbeek, M.; Zhang, H. *Chem. Rev*. **2004**, *104*, 1929–1954.
96. Van Der Meer, M.J.; Zhang, H.; Glasbeek, M. *J. Chem. Phys*. **2000**, *112*, 2878–2887.
97. Kondo, M.; Heisler, I. A.; Meech, S. R. *J. Phys. Chem. B* **2010**, *114*, 12859–12865.
98. Stsiapura, V. I.; Maskevich, A. A.; Kuzmitsky, V. A.; Uversky, V. N.; Kuznetsova, I. M.; Turoverov, K. K. *J. Phys. Chem. B* **2008**, *112*, 15893–15902.
99. Stsiapura, V. I.; Maskevich, A. A.; Tikhomirov, S. A.; Buganov, O. V. *J. Phys. Chem. A* **2010**, *114*, 8345–8350.
100. Stsiapura, V. I.; Kurhuzenkau, S. A.; Kuzmitsky, V. A.; Bouganov, O. V.; Tikhomirov, S. A. *J. Phys. Chem. A* **2016**, *120*, 5481–5496.
101. Singh, P.K.; Kumbhakar, M.; Pal, H.; Nath, S. *J. Phys. Chem. B.* **2010,** *114*, 5920–5927
102. Singh, P.K.; Kumbhakar, M.; Pal, H.; Nath, S. *J. Phys. Chem. B.* **2010**, *114*, 2541-2546.
103. Stsiapura, V. I.; Maskevich, A. A.; Kuzmitsky, V. A.; Turoverov, K. K.; Kuznetsova, I. M. Computational Study of Thioflavin T Torsional Relaxation in the Excited State. *J. Phys. Chem. A* **2007**, *111* (22), 4829–4835.
104. Ghosh, R.; Palit, D. K. *ChemPhysChem* **2014**, *15*, 4126–4131.
105. Voropai, E. S.; Samtsov, M. P.; Maskevich, A. A.; Stepuro, V. I.; Povarova, O. I.; Kuznetsova, I. M.; Turoverov, K. K.; Fink, A. L. *J. Appl. Spectrosc.* **2003**, *70*, 868–874.
106. Mulkidjanian, A. Y.; Cherepanov, D. A. *Photochem. Photobiol. Sci.* **2006**, *5*, 577.
107. Douhal, A.; Lahmani, F.; Zewail, A. H. *Chem. Phys.* **1996**, *207*, 477–498.
108. Chou, P.-T.; Solntsev, K. M. *J. Phys. Chem. B* **2015**, *119*, 2089–2089.
109. Gensch, T.; Heberle, J.; Viappiani, C. *Photochem. Photobiol. Sci*. **2006**, *5*, 529.
110. Sengupta, P. K.; Kasha, M. *Chem. Phys. Lett.* **1979**, *68*, 382–385.
111. Tolbert, L. M.; Solntsev, K. M. *Acc. Chem. Res*. **2002**, *35*, 19–27.
112. Leiderman, P.; Genosar, L.; Huppert, D. *J. Phys. Chem. A* **2005**, *109*, 5965–5977.
113. Brand, L.; Laws, W. R. in *Time-Resolved Fluorescence Spectroscopy in Biochemistry and Biology*; Springer US: Boston, MA, 1983.
114. Shizuka, H. *Acc. Chem. Res.* **1985**, *18*, 141–147.
115. Zhao, J.; Ji, S.; Chen, Y.; Guo, H.; Yang, P. *Phys. Chem. Chem. Phys.* **2012**, *14*, 8803–8817.

116. Huang, L.; Gu, B.; Su, W.; Yin, P.; Li, H. *RSC Adv*. **2015**, *5*, 76296–76301.
117. Suzuki, N.; Fukazawa, A.; Nagura, K.; Saito, S.; Kitoh-Nishioka, H.; Yokogawa, D.; Irle, S.; Yamaguchi, S. *Angew. Chemie Int. Ed.* **2014**, *53*, 8231–8235.
118. Han, G. R.; Hwang, D.; Lee, S.; Lee, J. W.; Lim, E.; Heo, J.; Kim, S. K. *Sci. Rep.* **2017**, *7*, 3863.
119. Henary, M. M.; Wu; Cody, J.; Sumalekshmy, S.; Li, J.; Mandal, S.; Fahrni, C. J. *J. Org. Chem.* **2007**, *72*, 4784–4797.
120. Kasha, M. *J. Chem. Soc. Faraday Trans. 2* **1986**, *82*, 2379.
121. Chou, P.; McMorrow, D.; Aartsma, T. J.; Kasha, M. *J. Phys. Chem.* **1984**, *88*, 4596–4599.
122. Arnaut, L. G.; Formosinho, S. J. *J. Photochem. Photobiol. A Chem.* **1993**, *75*, 1–20.
123. Formosinho, S. J.; Arnaut, L. G. *J. Photochem. Photobiol. A Chem.* **1993**, *75*, 21–48.
124. Kimura, Y.; Fukuda, M.; Suda, K.; Terazima, M *J. Phys. Chem. B* **2010**, *114*, 11847–11858.
125. Kwon, J. E.; Park, S. Y. *Adv. Mater*. **2011**, *23*, 3615–3642.
126. Goodman, J.; Brus, L. E. *J. Am. Chem. Soc*. **1978**, *100*, 7472–7474.
127. Smith, N. A.; Meech, S. R. *Int. Rev. Phys. Chem.* **2002**, *21* (1), 75–100.
128. Woolfe, G. J.; Thistlethwaite, P. J. *J. Am. Chem. Soc.* **1981**, *103*, 6916–6923.
129. Van Benthem, M. H.; Gillispie, G. D. *J. Phys. Chem.* **1984**, *88*, 2954–2960.
130. McMorrow, D.; Kasha, M. *J. Am. Chem. Soc.* **1983**, *105* (15), 5133–5134.
131. Strandjord, A. J. G.; Barbara, P. F. *J. Phys. Chem.* **1985**, *89*, 2355–2361.
132. Ercelen, S.; Klymchenko, A. S.; Demchenko, A. P. *FEBS Lett.* **2003**, *538*, 25–28.
133. Klymchenko, A. S.; Demchenko, A. P. *Phys. Chem. Chem. Phys.* **2003**, *5*, 461–468.
134. Klymchenko, A. S.; Demchenko, A. P. *J. Am. Chem. Soc.* **2002**, *124*, 12372–12379.
135. Das, K.; Sarkar, N.; Ghosh, A. K.; Majumdar, D.; Nath, D. N.; Bhattacharyya, K. *J. Phys. Chem.* **1994**, *98*, 9126–9132.
136. Iijima, T.; Momotake, A.; Shinohara, Y.; Sato, T.; Nishimura, Y.; Arai, T. *J. Phys. Chem. A* **2010**, *114*, 1603–1609.
137. Stephan, J. S.; Grellmann, K. H. *J. Phys. Chem.* **1995**, *99*, 10066–10068.
138. Rodriguez Prieto, F.; Rios Rodriguez, M. C.; Mosquera Gonzalez, M.; Rios Fernandez, M. A. *J. Phys. Chem.* **1994**, *98*, 8666–8672.

139. Shaikh, M.; Dutta Choudhury, S.; Mohanty, J.; Bhasikuttan, A. C.; Nau, W. M.; Pal, H. *Chem. - A Eur. J.* **2009**, *15*, 12362–12370.
140. Hsieh, C.-C.; Jiang, C.-M.; Chou, P.-T. *Acc. Chem. Res.* **2010**, *43*, 1364–1374.
141. C.-C. Hsieh , M.-L. Ho , P.-T. Chou , in Advanced Fluorescence Reporters in Chemistry and Biology I , Vol. 8 (Eds. A. P. Demchenko),Springer Berlin Heidelberg , 2010 , pp. 225-266
142. Wang, H.; Zhang, H.; Abou-Zied, O. .; Yu, C.; Romesberg, F. .; Glasbeek, M. *Chem. Phys. Lett.* **2003**, *367*, 599–608.
143. Ziółek, M.; Kubicki, J.; Maciejewski, A.; Naskręcki, R.; Grabowska, A. *Phys. Chem. Chem. Phys.* **2004**, *6*, 4682–4689.
144. Simkovitch, R.; Huppert, D. *J. Phys. Chem. B* **2015**, *119*, 10244–10251.
145. Lee, J.; Kim, C. H.; Joo, T. *J. Phys. Chem. A* **2013**, *117*, 1400–1405.
146. Nandi, N.; Bhattacharyya, K.; Bagchi, B. *Chem. Rev.* **2000**, *100* (6), 2013–2046.
147. Chandra, A.; Bagchi, B. *J. Chem. Phys.* **1991**, *94* (12), 8367–8377.
148. Zhong, D.; Pal, S. K.; Zewail, A. H. *Chem. Phys. Lett.* **2011**, *503*, 1–11.
149. Bagchi, B.; Jana, B. *Chem. Soc. Rev.* **2010**, *39*, 1936.
150. Nagarajan, V.; Brearley, A. M.; Kang, T.; Barbara, P. F. *J. Chem. Phys.* **1987**, *86*, 3183–3196.
151. Nome, R. A *J. Braz. Chem. Soc.* **2010**, *21*, 2189–2204.
152. Loring, R. F.; Yan, Y. Y.; Mukamel, S. *Chem. Phys. Lett.* **1987**, *135*, 23–29.
153. Yan, Y. J.; Sparpaglione, M.; Mukamel, S. *J. Phys. Chem.* **1988**, *92*, 4842–4853.
154. Pal, S. K.; Zewail, A. H. Dynamics of Water in Biological Recognition. *Chem. Rev.* **2004**, *104* (4), 2099–2124.
155. Stratt, R. M.; Maroncelli, M. *J. Phys. Chem.* **1996**, *100*, 12981–12996.
156. Sen, P.; Ghosh, S.; Sahu, K.; Mondal, S. K.; Roy, D.; Bhattacharyya, K. *J. Chem. Phys.* **2006**, *124* (20), 204905.
157. Sen, P.; Pal, S.; Bhattacharyya, K.; Bagchi, B. *J. Chinese Chem. Soc.* **2006**, *53*, 169–180.
158. Sen, P.; Mukherjee, S.; Halder, A.; Bhattacharyya, K. *Chem. Phys. Lett.* **2004**, *385*, 357–361.
159. Molotsky, T.; Koifman, N.; Huppert, D. *J. Phys. Chem. A* **2002**, *106*, 12185–12190.
160. Hara, K.; Baden, N.; Kajimoto, O. *J. Phys. Condens. Matter* **2004**, *16*, S1207–S1214.
161. Heyden, M.; Sun, J.; Funkner, S.; Mathias, G.; Forbert, H.; Havenith, M.; Marx, D. *Proc. Natl. Acad. Sci.* **2010**, *107*, 12068–12073.

162. Leitner, D. M.; Gruebele, M.; Havenith, M. *HFSP J.* **2008**, *2*, 314–323.
163. Xu, J.; Plaxco, K. W.; Allen, S. J. *Protein Sci.* **2006**, *15*, 1175–1181.
164. Smith, N. A.; Lin, S.; Meech, S. R.; Yoshihara, K. *J. Phys. Chem. A* **1997**, *101*, 3641–3645.
165. Jaye, A.; Hunt, N. T.; Meech, S. R. *J. Chem. Phys.* **2006**, *124*, 24506.
166. Zolotov, B.; Gan, A.; Fainberg, B. D.; Huppert, D. *Chem. Phys. Lett.* **1997**, *265*, 418–426.
167. Wang, H.; Holmberg, B. A.; Yan, Y. *J. Am. Chem. Soc*. **2003**, *125*, 9928–9929.
168. Zhang, X.-X.; Liang, M.; Ernsting, N. P.; Maroncelli, M. *J. Phys. Chem. Lett.* **2013**, *4*, 1205–1210.
169. Samanta, A. *J. Phys. Chem. Lett.* **2010**, *1*, 1557–1562.
170. Shim, Y.; Kim, H. J. *J. Phys. Chem. B* **2013**, *117*, 11743–11752.

Chapter 2

Experimental Methods

In this chapter, the details of the experimental methods have been described. I have described the instrumentation and data analysis procedure for time correlated single photon counting, femtosecond transient absorption spectroscopy and fluorescence up-conversion spectroscopy in my research. Besides a brief description of density functional theory has also been provided.

2.1. Steady State Measurements

Steady state absorption spectra were recorded in Shimadzu UV-2450 and JASCO V-670 spectrophotometer. Both the instruments are equipped with deuterium and halogen lamp as light source and photomultiplier tube as detector. Steady state emission spectra were recorded in Fluoromax-4, Horiba Jobin-Yvon spectrofluorimeter equipped with a 150W xenon arc lamp as excitation source and a photomultiplier tube (190nm-850nm) as detector.

2.2. Time Correlated Single Photon Counting (TCSPC) Method

2.2.1. Basic Principle

The basic idea behind measurement of fluorescence lifetime is to excite the sample using a delta function pulse and measure the time taken for fluorescence intensity to fall to minimum or a certain value. However, there are some basic problems associated with the measurements. First of all the time scale of fluorescence decays of most organic samples are very small i.e. in nanosecond time domain. So to measure fluorescence lifetime directly we need a detector with very fast response which is difficult. Secondly, to characterize a sample, we not only need to measure its fluorescence lifetime but also the complete shape of the decay i.e. the familiar exponential waveform of fluorescence lifetime to resolve any multi exponential decays present in the sample. Now the response of the detector is the measurement of a single photon. So in order to resolve a nanosecond order lifetime component, we would need a picosecond order response from the detector. Even with a very fast photodiode and GHz oscilloscope this is impossible to achieve and the weak emission from the sample after passing through all the optics may fail to create an electric signal. So an analog measurement can never be able to achieve a complete waveform of fluorescence decay of a sample. The solution is provided by time correlated single photon counting method (TCSPC), first introduced by Bollinger and Thomas in 1961, where time of arrival of photon at the detector is measured with respect to the reference signal i.e. the excitation pulse.[1,2] This process is repeated for several cycles until a histogram of the waveform is born.

TCSPC can detect a very low level of signal because of its statistical method. In TCSPC measurements a high repetition rate laser source is used and the principle is that detection of a single photon within the pulse period is an unlikely event and detection of two photons is extremely unlikely. So only the first photon detected within two consecutive excitation of the sample is considered. The excitation pulse acts as the start signal and the first detected photon acts as the stop signal. The time difference between the start and stop signal is measure and stored. If the single photon detection criterion is followed, then there can be several cycles where no photon will be detected which is fine because the occurrence of no photon per cycle or single photon per cycle is completely random and measurement over many repeating cycles would statistically always generate the distribution. Whenever a photon is detected in a cycle, a count 1 is recorded in the memory and the time of its arrival is noted. The essential part of this type of data recording is the time to amplitude converter (TAC). The excitation pulse sends a synchronization signal (the “start” signal) to the TAC and the capacitor within it starts charging. When the emission photon or the “stop” signal is acquired, the charging of the capacitor stops. The voltage within the capacitor increases linearly in this time window and thus a voltage ramp is generated. An analog to digital converter named multichannel analyser (MCA) stores the magnitude of this voltage in a designated channel according to the time. Over many repetitions, the complete histogram is stored in MCA. Adhering to the one photon detection per cycle principle, the experimental stop rate should be kept below 2% of the start rate. This ratio is important when the “dead time” of the electronics is considered. Dead time is the minimum time taken by the electronics to detect two successive photons. So if the “stop” rate is high, then chances are multiple photons can come in a pulse cycle and the first emitted photon will not be the first detected photon as it may fall within the dead time of electronics. This will results in a situation called “pulse pile-up” which is actually over-representation of certain points in the histogram.[2,3]

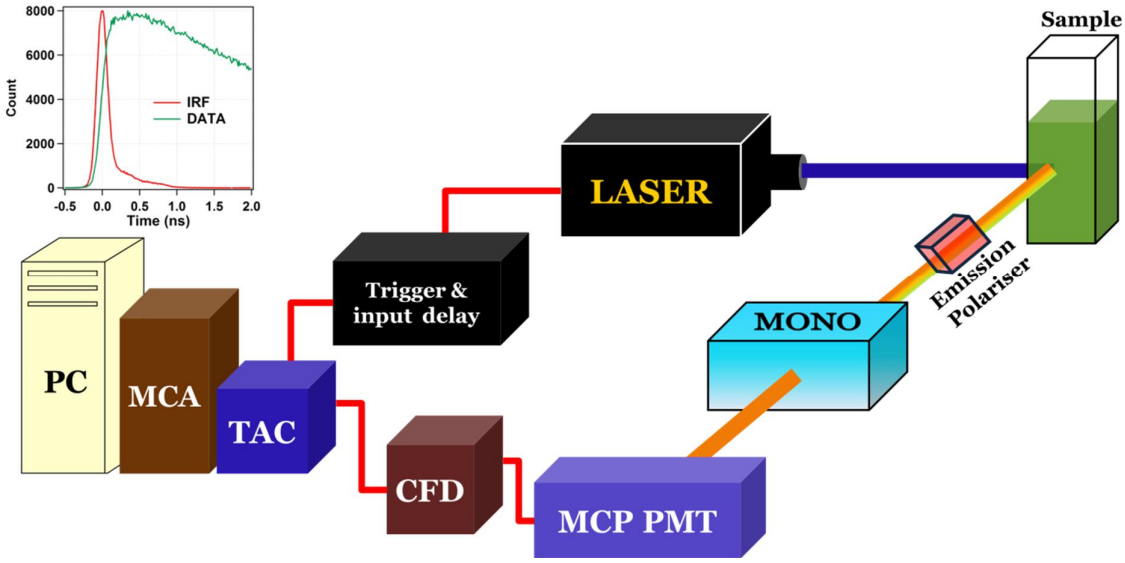

Figure 2.1:- Schematic diagram of a standard TCSPC setup along with typical IRF and data

The detector used in modern TCSPC setup is multichannel plate photomultipliertubes (MCP PMT). The advantage of using MCP PMT over single electron response detectors or simple PMT lies in the transit time spread (TTS) of the detector which seriously affects the time resolution of the instrument. Once a photoelectron is generated at the cathode of a PMT, it is amplified in the dynodes. As this process of multiplication generates a group of electrons having a range of velocities and individually they can take different paths to reach the anode, a distribution of transit times are generated which is the TTS. TTS is less for MCP PMT compared to PMT and as TTS determines the instrument response, the use of MCP PMT is preferred. The rise and fall time of the electronics used in the TCSPC setup causes a time jitter in the measurement. Moreover random amplification optical signal by detector can cause a amplitude jitter in the electric signal. If a simple discriminator is used to send signal at TAC, then it can be triggered if the leading edge of the electric pulse crosses a certain threshold value. Therefore a constant fraction discriminator (CFD) is used in TCSPC. Basically, a CFD sends a signal at TAC at constant fraction of a pulse and therefore the height difference induced time jitters are avoided. The instrument response function (IRF) of a TCSPC instrument recorded by measuring the signal from a scattering process is

influenced by laser pulse width, TTS and any other time jitters in the instrument. A schematic diagram depicting all the components of a TCSPC setup has been shown in figure 2.1.

In my experiments, I have used two different TCSPC instruments. The first one is LifeSpec II from Edinburgh Instruments, U.K. This instrument is equipped with thermoelectrically cooled Hamamatsu R3809-50 MCP PMT with intrinsic detector response <25 ps. The excitation sources are picosecond pulse diode lasers (EPL-series) from the same company. For my experiments, I have used 375nm and 445 nm diode lasers with 80 ps pulse width. The IRF of this instrument measured by scattering from Ludox suspension was 120 ps. The second instrument is Fluorolog-3 from Horiba Jobin Yvon. The excitation sources in this equipment is pulsed nano-LED with <1 ns pulse width. The IRF measured in this instrument was 1.4 ns. All the data were acquired at Magic Angle polarization to avoid any contribution from the rotational diffusion of the molecules. The data obtained from the two instruments were analysed in FAST and DAS software respectively. Here a brief overview of the fitting procedure has been presented.

2.2.2. Data Analysis Procedure

The data analysis procedure is not straight forward because the excitation pulse is not a delta function i.e. it has a finite width in time domain and the IRF of the instrument has a finite width. These factors affect the data and the measured fluorescence decay actually becomes a convolution of the IRF and the actual fluorescence intensity decay.

$$I(t) = \int_0^t P(t)F(t - t')dt' \qquad (2.1)$$

Now using this convolution to fit the data is not straightforward as the problem itself is ill-posed. The convolutions requires exact form of IRF or prompt to be known, the theoretical model for fluorescence to be known and experimental random noise to be minimized. Therefore most of the commercial software like

FAST or DAS uses iterative method or specifically non-linear least square method to extract fluorescence lifetime. First of all, the pure fluorescence intensity decay is estimated by a sum of lifetime components multiplied by their weighted amplitudes as follows.[3-7]

$$F(t) = \sum_{i=1}^{n} a_i e^{-\frac{t}{\tau_i}} \quad (2.2)$$

$$\sum_{i=1}^{n} a_i = 1 \quad (2.3)$$

Here, τ_i are the lifetime components and a_i are the amplitudes. The IRF profile is recorded using a scatter as stated before but it is measure at the excitation wavelength not at the emission wavelength which is intrinsically wrong. Nevertheless, measurement of IRF using the same number of channels is required for the reconvolution. As this reconvolution is done in a quantized manner i.e. per channel basis, a sum is used instead of integration in equation 2.1. The IRF is assumed to be a series of δ-functions with different amplitudes in different channels. The measured data is expressed as[3-7]

$$I(t) = \sum_{t_i=0}^{t} P(t)F(t - t_i)\Delta t \quad (2.4)$$

In the above equation, Δt is the time/channel. Two more parameters are needed in the final fitting equation. There can slight mismatch of time zero position of IRF and intensity decay data which is accommodated by a shift parameter(Δ). A noise factor (A) is needed to for the fitting. So all together the final form is

$$D(t) = A + I(t + \Delta) \quad (2.5)$$

The consistency of the assumed model is tested by the "goodness of the fit".[3-7]

$$\chi^2 = \sum_{j=1}^{n} \frac{[Y(j) - D(j)]^2}{\sigma_j^2} \quad (2.6)$$

In the above equation, $Y(j)$ is the fitted data,$D(j)$ is the experimental data and σ_j^2 is the standerd deviation. However, χ^2 is not the best choice for large number of datapoints. Instead, a quantity $\chi^2{}_R$ is defined as

$$\chi_R^2 = \frac{\chi^2}{n-p} \tag{2.7}$$

Here, n is the number of data points and p is the number of parameters. For TCSPC measurements, n is much larger than p. The value of χ^2 is estimated with different choice of fitting parameters and multiexponential model and the fitting is accepted comapring the value of χ^2 for different sets. However, this iterative method suffers from an intrinsic problem of choice of model based on intuition and as many different models can satisfy the fitting criteria, prior knowledge of the system is extremely important for TCSPC fitting.

2. 3. Femtosecond Fluorescence up-conversion spectroscopy

2.3.1. Basic Principle

Fluorescence up-conversion spectroscopy is based on the principle of cross-correlation between the emission from an electronically excited molecule and a gate beam. Such optical gating of fluorescence was first described by Hallidy and Topp in 1977.[8] The employment of femtosecond lasers has enabled this technique to measure fluorescence intensity decays from sub-picosecond to nanosecond time domain.[9-12] In this technique, the second harmonic of a femtosecond oscillator (a mode-locked Ti:Sapphire laser operating at frequency (ω_1) in this case) is used to excite the sample electronically.

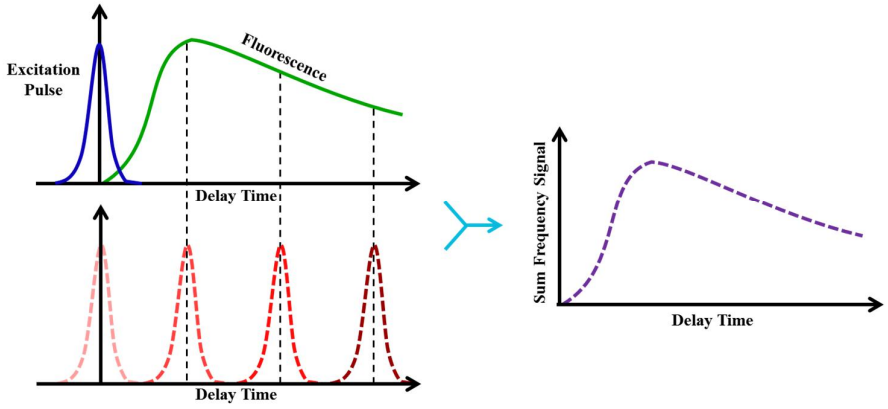

Figure 2.2 Schematic principle of fluorescence up-conversion spectroscopy

As depicted in figure 2.2, the arrival of the excitation pulse at the sample marks time zero (t=0) and results in the emission of incoherent fluorescent light (ω_2) from the excited molecules. It is mixed with the gate pulse which is basically the residual fundamental gate light arriving at time t = τ in a non-linear crystal (β-barium borate crystal, potassium dideuterium phosphate crystal etc) and thus the sum frequency (ω_3) of those two signals is generated.

$$\omega_3 = \omega_1 + \omega_2 \qquad (2.8)$$

The time of arrival of gate pulse is controlled by a mechanical delay stage. It can be shown that at any time, the intensity of the sum frequency light (I_{sum}) is proportional to the cross correlation function of that of the fluorescence (I_{fl}) and gate beam (I_G).[9]

$$I_{sum} \propto \int_{-\infty}^{+\infty} I_{fl}(t) I_G(t-\tau) dt \quad (2.9)$$

The sum frequency light is only generated when the gate pulse is present in the crystal and thus we can achieve time resolution comparable to laser pulse width.

2.3.2. Instrumental setup

Schematic optical layout of the instrument (FOG 100, CDP systems, Moscow, Russia) along with the external laser source has been shown in figure 2.3. The output of a mode-locked Ti:Sapphire laser (Mai-Tai HP, Spectra Physics, USA) operating at a repetition rate of 80 MHz with average power ~2.5 W and ~ 100 fs pulse width was used as the fundamental frequency radiation (ω_1). The light was focused onto a β-barium borate crystal (BBO, 0.2 mm thickness) to generate the second harmonic ($2\omega_1$) of the fundamental light which was used for sample excitation. The second harmonic mixed with fundamental light was collimated using lens L_2 onto the dichroic mirror/dichroic beamsplitter (DM_1) which splits the input beam into excitation and gate beams. The reflected excitation beams passed through a Berek polarizer (B) which was used to adjust the polarization of the excitation light. I have used neutral density filters (ND filters, F) before the polarizer to control the intensity of the excitation light and cut-off filters to remove residual fundamental light. Then the light is reflected from another beam splitter (BS_1) and focused on the rotating sample cell S using lens L_3. The fluorescence emission from the sample (ω_2) was collected by lens L_4 and passed through a cut-off filter F_2 to remove excitation ($2\omega_1$) light. The gate beam was directed with mirrors M_3 and M_4 to a gold coated retro-reflector (RR) mounted on a mechanical delay line controlled by the software. Both the emission and the gate pulse were collected by lens L_5 and focused on a second non-linear BBO crystal (0.2mm or 0.5mm thick) where the sum frequency of the two incident beams are generated i.e. $\omega_3 = \omega_1 + \omega_2$. For the experiments described in this thesis, the fluorescence are in visible region and the gate pulse in near IR region and therefore the sum frequency obtained was in the UV region. The emission and the gate beam were prevented to reach the detector by means of iris and by using appropriate cut-off filters (F_3).

Lens L_7 was used to focus the sum frequency light to the input slit of the monochromator. The sum frequency signal was selected by the monochromator and detected by a photomultiplier tube (PMT) coupled with a photon counting device. Data acquisition, monochromator and optical delay line is controlled by LUMEX software (CDP Corp).

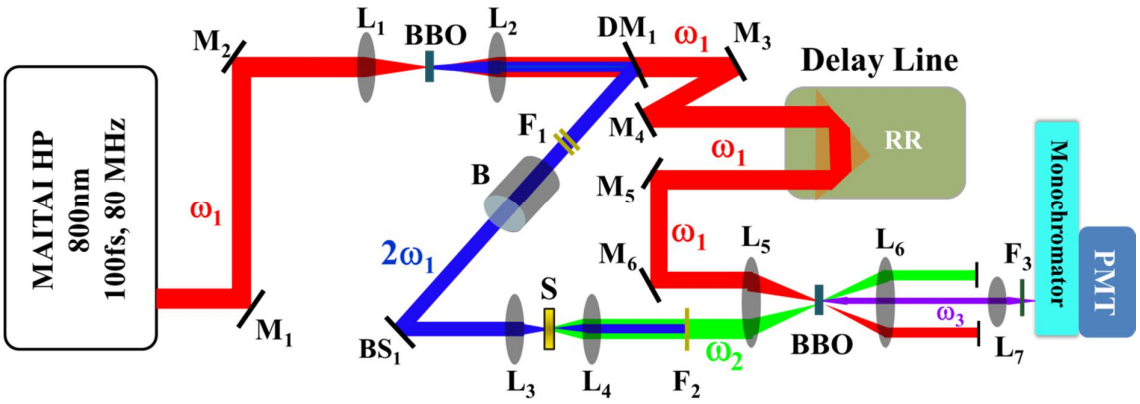

Figure 2.3 Schematic optical diagram of femtosecond fluorescence up-conversion setup

2.3.3. Principle of Second Harmonic and Sum Frequency Generation

Fluorescence up-conversion spectroscopy involves generation of sum frequency of fluorescence from sample and the gate beam. It also involves generation of second harmonic light of the fundamental beam for excitation purpose. Both the phenomena are a part of non-linear optical phenomenon which is discussed in this section. At normal condition i.e. in presence of low intensity light, the response of the medium of propagation to the light is linear. This is to say that the optical phenomenon in this situation can be explained with a linear refractive index of the medium. However, when an intense high power laser light is present the response of the medium deviates from linearity. The electric field associated with high intensity radiation can alter the refractive index of medium which is the origin of non-linear effect.[13-15] The response of a medium to the electric field of propagating electromagnetic radiation can be described as the Taylor expansion of the dielectric polarization density (dipole moment per unit volume) or simply induced polarization (P_k) as a function of electric field (E_i) at time t.

$$P_k(t) = \epsilon_0\left(\chi_{ik}^{(1)}E_i(t) + \chi_{ijk}^{(2)}E_i(t)E_j(t) + \chi_{ijlk}^{(3)}E_i(t)E_j(t)E_l(t) + \cdots\right) \quad (2.10)$$

In the above equation, ϵ_0 is the permittivity of vacuum and $\chi^{(n)}$ is the n-th order optical susceptibility of the medium and it is a $(n+1)$ order tensor. In right hand side of equation 2.10, the first term corresponds to linear response whereas the higher order terms correspond to higher order (nonlinear) response of the medium. For simplicity, P_k and E_i are considered to be scaler quantities for a non-linear optical process occurring in a specific direction. Both second harmonic and sum frequency generation is a second order non-linear phenomenon and so, I will refer only the second order polarization as [13-15]

$$P^{(2)}(t) = \epsilon_0\chi^{(2)}E^2(t) \quad (2.11)$$

Now let us consider the second order response to a monochromatic input field of frequency ω is given by

$$E(t) = \mathcal{E}exp(-i\omega t) + \mathcal{E}^*exp(i\omega t) \quad (2.12)$$

In the above equation, $\mathcal{E}$ is the field amplitude. Plugging equation 2.12 to equation 2.11 we get the second order response of the medium as

$$P^{(2)}(t) = 2\epsilon_0\mathcal{E}\mathcal{E}^* + \left(\epsilon_0\chi^{(2)}\mathcal{E}^2exp(-i2\omega t) + \epsilon_0\chi^{(2)}\mathcal{E}^{*2}exp(i2\omega t)\right) \quad (2.13)$$

The first term in equation 2.13 defines a constant static field which is known as optical rectification and the second term defines an output of frequency twice of the input field which is the second harmonic generation.[13-15] It is important to point out that the even order terms in equation 2.10 will vanish if the crystal has inversion symmetry and therefore second harmonic generation can occurs only in specific non-linear optical (NLO) crystals. One more important thing in non-linear processes such as frequency doubling is phase matching among the interacting waves to ensure that amplitude contribution of the output wave from different part of the NLO crystal are in phase at the end of crystal. In second harmonic generation, we are creating light of twice frequency whose wave vector $k_{2\omega}$ is given by

$$k_{2\omega} = \frac{2\omega}{c}n_{2\omega} \quad (2.14)$$

In the above equation, c is the speed of light and $n_{2\omega}$ is the refractive index for the second harmonic light. Similarly, the wave vector for input light is given by

$$k_\omega = \frac{\omega}{c} n_\omega \tag{2.15}$$

In frequency doubling in crystal, phase matching satisfies when $k_{2\omega} = k_\omega$ i.e. $n_{2\omega} = n_\omega$ but dispersion inhibits this from occurring. So birefringent crystals are used where the refractive index for light of different polarization are different and phase matching condition is satisfied by using extraordinary polarization for ω and ordinary polarization for 2ω so that $n_o(2\omega) = n_e(\omega)$. Moreover, the intensity of the sum frequency signal generated in a NLO crystal of thickness is given by

$$I_{sig}(\lambda) \propto \left(\frac{L}{\lambda}\right)^2 sinc^2\left(\frac{\Delta kL}{2}\right) \tag{2.16}$$

$$\Delta k(\lambda) = \frac{4\pi}{\lambda}\left(n_\lambda - n_{\frac{\lambda}{2}}\right) \tag{2.17}$$

Therefore, phase matching only works for a light of particular wavelength. However femtosecond laser pulses consists of large bandwidth and the frequency doubling of the signal will be regulated by the FWHM of the $sinc^2\left(\frac{\Delta kL}{2}\right)$ function. In our case, as described in previous section we use a BBO crystal of thickness ~0.2 mm and as BBO is a negative birefringent crystal, the phase matching condition will be satisfied only when the input radiation is ordinary polarized and second harmonic light is extraordinary polarized.

Now, BBO crystal was also used in the setup I used to generate the sum frequency signal of sample emitted fluorescence and gate light. In case of sum frequency generation (SFG) the two incident radiation have two different colours of light or two different frequencies.[13-15]

$$E(t) = \mathcal{E}_1 exp(-i\omega_1 t) + \mathcal{E}_2 exp(-i\omega_2 t) + c.c. \tag{2.18}$$

Here, $c.c.$ denotes complex conjugate. Replacing equation 2.18 into equation 2.11 gives us

$$P^{(2)}(t) = 2\epsilon_0(\mathcal{E}_1\mathcal{E}_1^* + \mathcal{E}_2\mathcal{E}_2^*) + \epsilon_0\chi^{(2)}[\mathcal{E}_1^2 exp(-2i\omega_1 t) + \mathcal{E}_2^2 exp(-2i\omega_2 t) + 2\mathcal{E}_1\mathcal{E}_2 exp(-2i(\omega_1 + \omega_2)t) + 2\mathcal{E}_1\mathcal{E}_2^* exp(-2i(\omega_1 - \omega_2)t) + c.c.] \tag{2.19}$$

So in this case we will generate the sum frequency $(\omega_1 + \omega_2)$, the difference frequency $(\omega_1 - \omega_2)$ and the optical rectification. Phase matching also applies to this case and based on the phase matching condition either the sum frequency light or the difference frequency light will be emitted with significantly more intensity than the other. For SFG, the phase matching condition is[10-15]

$$k_3 = k_1 + k_2 \tag{2.20}$$

In the above equation, k_3 represents the wave vector of the sum frequency light and k_1 and k_2 represents the same for input beams. Now, in a crystal the refractive index seen by one polarization of light can be adjusted by changing the angle. For simplicity, if I consider an uniaxial crystal i.e. $n_x = n_y = n_o$ and $n_z = n_e$ considering z-axis as the optical axis, we can write the phase matching condition as given below.[10-15]

$$\frac{1}{n_e^2(\theta)} = \frac{cos^2\theta}{n_o^2(\theta)} + \frac{sin^2\theta}{n_o^2(\theta)} \tag{2.21}$$

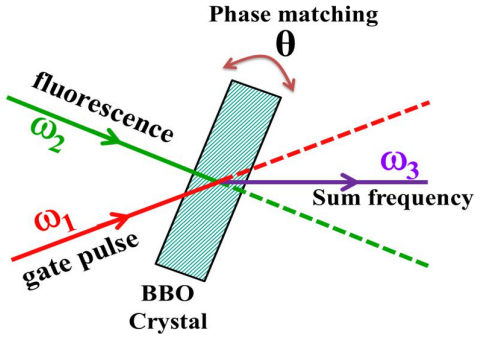

Figure 2.4 Schematic diagram depicting sum frequency generation in a BBO crystal

It should be pointed out that there are broadly two kinds of phase matching e.g. Type 1 where the output wave has different polarization than the input waves and Type 2 where one of the input waves has different polarization that the other two. In the setup I used, the fluorescence from the sample was collected from the sample using a lens and leaking excitation light was cut-off through filter. Then the gate beam and the fluorescence beam were focused onto the BBO crystal through another lens. As I collected fluorescence intensity decay of various samples at various wavelengths, data acquisition at a particular wavelength required rotating

the BBO crystal at the suitable phase matching angle where intensity of the sum frequency signal generated from the gate light and that specific wavelength of fluorescence light was maximum. However it should be mentioned that in most of the fluorescence up-conversion systems only type 1 phase matching is used. To collect the fluorescence intensity decays at magic angle polarization, the pump beam was rotated with respect to the gate beam at a certain angle with the help of a Berek compensator. Berek compensator consists of a uniaxial crystal which when tilted at a certain angle makes the axis in the plane of incidence extraordinary and depending on the tilting, a light of certain wavelength can be rotated at any angle.

2.3.4. Data Analysis Procedure

When we measure the fluorescence intensity decay of a fluorophore having a long lifetime, we can assume that the excitation pulse is an δ-function i.e. it has no width in time domain. However, in femtosecond fluorescence up-conversion spectroscopy we deal with lifetime components is sub-picosecond time domain and the above assumption become invalid as no optical pulse have zero width. Moreover, the laser pulse passes through several dispersive optics which inherently broadens the pulse. NLO crystals also impose dispersion and therefore the overall instrument response function has a finite non-negligible width. In my case, I measured the instrument response function (IRF) before each experiment using the Raman signal of water which is shifted about 3300 cm^{-1} compared to the excitation light.[10-12,16] Raman scattering process is known to have zero-time delays and so when the sum frequency of water Raman and gate beam was generated the temporal profile of the pulses were preserved. The intensity of the water Raman signal at different time delays will be in accordance with the cross-correlation function described by equation 2.9. Thus replacing the sample cell with a water cell and measuring the decay at specific wavelength, I ended up with an IRF which can be perfectly modelled by a Gaussian function having a FWHM of about 250 fs.

$$G(x) = \frac{1}{\sigma\sqrt{2\pi}} e^{-(x-\mu)^2/2\sigma^2} \quad (2.22)$$

In the above equation, σ is the width parameter of the Gaussian and μ is the x-axis position of the function. The FWHM (H) of the above function is given by

$$H = 2\sigma\sqrt{2\ln 2} \approx 2.3548\sigma \quad (2.23)$$

For all practical purposes, we consider the excitation occurring at zero time. So, for data analysis, I have used the Gaussian function with$\mu = 0$. Now, in any time dependent fluorescence lifetime measurement using a pulsed light, the decay curve is altered by the finite width of the pulse. Especially, when we want to extract very short lifetime components, it is absolutely necessary to extract the exact intensity decay from the acquired data. The procedure to filter the data from any undesired signal is known as deconvolution. Fluorescence intensity decays obtained from femtosecond fluorescence up-conversion measurements were a convolution of IRF and actual intensity decay of the sample. To extract the lifetime components, I fitted individual decays using a convolution function of IRF and a sum of exponential functions. Briefly, I am presenting the convolution of a Gaussian (IRF) given and a single exponential function which can be extended to multiple exponentials. Setting $\mu = 0$ in equation 2.22

$$G(x) = \frac{1}{\sigma\sqrt{2\pi}} e^{-x^2/2\sigma^2} \quad (2.24)$$

$$S(x) = exp(-\frac{x}{\tau}) \quad (2.25)$$

In equation 2.25, τ is the lifetime. Now the convolution is defined as

$$I(t) = G(x) * S(x) = \frac{1}{\sigma\sqrt{2\pi}} \int_0^\infty exp\left(-\frac{x}{\tau}\right) exp\left(-(t-x)^2/2\sigma^2\right) dx =$$

$$\frac{1}{\sigma\sqrt{2\pi}} \int_0^\infty exp\left(-\frac{\left(x^2+t^2+\frac{2\sigma^2 x}{\tau}-2tx\right)}{2\sigma^2}\right) dx \quad (2.26)$$

Now using the transformation,

$$z = \frac{\left(x - \left(t - \frac{\sigma^2}{\tau}\right)\right)}{\sigma\sqrt{2}} \tag{2.27}$$

$$\frac{\left(x^2 + t^2 + \frac{2\sigma^2 x}{\tau} - 2tx\right)}{2\sigma^2} = z^2 + \frac{1}{\tau}\left[t - \frac{\sigma^2}{2\tau}\right] \tag{2.28}$$

Using equation 2.27 and 2.28 in equation 2.26 we get,

$$I(t) = \frac{1}{\sqrt{\pi}} exp\left(-\frac{1}{\tau}\left(t - \frac{\sigma^2}{2\tau}\right)\right) \int_{-\left(\frac{t - \frac{\sigma^2}{\tau}}{\sigma\sqrt{2}}\right)}^{\infty} exp(-z^2) dz \tag{2.29}$$

Now the error function are introduced as

$$erf(x) = \frac{2}{\sqrt{\pi}} \int_0^x exp(-z^2)\, dz \tag{2.30}$$

Here, it should be noted that error function is an odd function which means $erf(x) = erf(-x)$. Now introducing the error function in equation 2.30 gives

$$I(t) = \frac{1}{\sqrt{\pi}} exp\left(\frac{\sigma^2}{2\tau^2} - \frac{t}{\tau}\right)\left(1 - erf\left(\frac{\sigma^2 - t\tau}{\sqrt{2}\sigma t}\right)\right) \tag{2.31}$$

The above equation has been used to fit the fluorescence intensity decay data. Equation 2.31 depicts only the convolution of single exponential with Gaussian. However, while fitting the data, in most of the cases I needed more than one exponential function to fit the data. Convolution is a linear operation which follows distributive and additive property. So in case of multiexponential fitting, equation 2.31 was expanded as a summation of several lifetime exponential convoluted with same Gaussian having proper weightage coefficients. Therefore, in this thesis, when fitting with multiexponential function is mentioned it actually means the convoluted function. All the fitting of the up-conversion data were done using IGOR Pro (WaveMetrics, Inc.) software.

2.4. Time Resolved Emission Spectra

Fluorescence intensity decay with time at particular wavelength recorded from TCSPC or fluorescence up-conversion spectroscopy provides information about the excited state processes. However, another powerful tool to observe fate of photoexcited molecule is to study its time resolve emission spectra (TRES). Basically the steady state emission spectra of a molecule is a time average of all the TRES and investigation of TRES can provide very valuable important information about the excited state processes such as charge transfer, excited state reactions etc.[6,17-21] Moreover it can also elucidate the interaction of excited state molecules with surrounding solvents.[6] Recording of TRES at different times was done in the past but they were distorted by the instrument response.[17-21]Besides recording of TRES directly requires detection of a large number of wavelengths simultaneously. Fortunately, TRES can be prepared from the time resolved fluorescence decays recorded at various wavelengths over the entire range of emission spectra.[6,17-21] The intensity of TRES $\left(I(\lambda,t)\right)$ is a function of both wavelength and time but can be separated into the product of time and wavelength dependent function as given below.

$$I(\lambda,t) = A(\lambda)B(t) \tag{2.32}$$

The time dependent function $B(t)$ is actually the sum of exponentials used to express time resolved fluorescence decay. So $B(t)$ is given by

$$B(t) = \sum_{i=0}^{n} a_i e^{-t/\tau_i} \tag{2.33}$$

Here, a_i represents normalized fitting coefficients of lifetime component τ_i. The estimation of $A(\lambda)$ is difficult because the intensity with wavelength do not follow any well-defined law. So, it is obtained in the following way. As previously stated, the steady state emission spectra is a time average of the TRES which can be expressed mathematically as

$$I_{ss}(\lambda) = \int_0^\infty A(\lambda)B(t) = A(\lambda)\int_0^\infty B(t) \tag{2.34}$$

From equation 2.33 and 2.34 we can obtain $A(\lambda)$.

$$A(\lambda) = \frac{I_{ss}(\lambda)}{\sum_i a_i \tau_i} \tag{2.35}$$

Therefore, equation 2.32 becomes

$$I(\lambda, t) = \frac{I_{ss}(\lambda)}{\sum_i a_i \tau_i} \sum_{i=0}^{n} a_i e^{-t/\tau_i} \tag{2.36}$$

According to equation 2.36, we can record fluorescence intensity decay at a particular wavelength and knowing its steady state intensity can construct the time dependent intensity behavior. This procedure was applied to several wavelengths to obtain multiple points and then each of the TRES was fitted by a lognormal function described by Maroncelli and Fleming.[18,19]

$$L(\nu) = g_0 exp\left\{ -\ln 2 \left(\frac{\ln\left(1 + \frac{2b(\nu - \nu_p)}{\Delta}\right)}{b} \right)^2 \right\} \tag{2.37}$$

In the above equation, g_0, b, ν_p, Δ are peak height, asymmetry parameter, peak frequency, width parameter. The width parameter is related to full width half maxima (Γ) as follows[18,19]

$$\Gamma = \Delta \left(\frac{\sinh(b)}{b} \right) \tag{2.38}$$

The fitting has been done IGOR Pro software and different fitting parameters obtained were used to understand different excited state processes which will be discussed in their appropriate sections.

2.5. Femtosecond Broadband Transient Absorption Spectroscopy

2.5.1. Basic Principle

Femtosecond molecular dynamics is studied by several techniques out of which pump-probe techniques are very popular and broadband transient absorption spectroscopy is one of them. Generally, in pump probe experiments, a non-stationary molecular state is prepared by an ultrashort laser pulse which is called the pump and the time evolution of that newly prepared state is monitored using another suitable time delayed laser pulse known as the probe.[22-25] In transient absorption spectroscopy, we use resonant excitation i.e. the excited electronic state population is prepared by the pump pulse and the population decay is not instantaneous unlike Raman spectra.[22-25]The study of the dynamics of the excited state will depend on the choice of the probe pulse. The probe can be monochromatic or broadband in UV-Visible or IR region and they can be used to explore different photophysical properties of the molecule.[22-25]Moreover, observation of the action of pump depends on either the change in characteristic (like intensity) of the probe or the events created by the probe itself after the action of the pump.[22-25] We observe the first case in transient absorption spectroscopy.

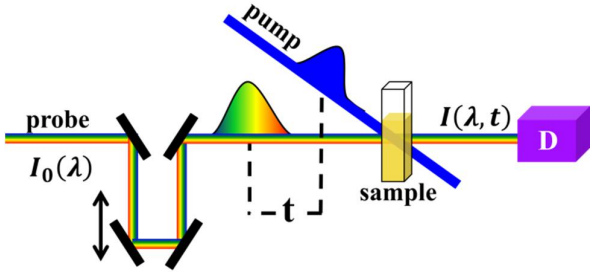

Figure 2.5 Schematic representation of transient absorption spectroscopy experiment

In our lab setup, I used either 400nm or 266 nm light as pump light which excites a fraction of molecules in the electronic excited state. A visible (450nm-750nm) white light continuum (WLC) probe is passed through the sample at various delay times controlled by a mechanical delay stage and the change in intensity of the probe light is monitored by the detector while the pump is dumped. In figure 2.5 a schematic diagram is shown to explain the operation. The intensity of the probe is

kept very low compared to the pump to avoid any multistep or multiphoton processes exerted by the probe itself. The detection is done simultaneously over the range of probe spectrum at a particular time and the process is repeated over multiple time delays which is basically the time gated detection.[22-25] Since this is an absorption spectroscopy, Lambert-Beer law can be applied on the probe light.

$$I(\lambda,t) = I_0(\lambda) \times 10^{-\varepsilon(\lambda)N(t)l} \quad (2.39)$$

In equation 2.39, $I_0(\lambda)$ and $I(\lambda,t)$ are the intensity of the probe light before and after passing the sample at delay time t respectively as illustrated in figure 2.5. It should be specified that the time zero is labeled to the particular position of the delay where pump and probe pulses reach the sample simultaneously. $\varepsilon(\lambda)$ is the molar extinction coefficient at wavelength λ, $N(t)$ is the population of a state after t time of the pump excitation and l is the path length of the sample. So according to figure 2.5 and equation 2.39, the absorbance $A(\lambda,t)$ is given by

$$A(\lambda,t) = log\frac{I_0(\lambda)}{I(\lambda,t)} = \varepsilon(\lambda)N(t)l \quad (2.40)$$

Now the quantity that is observed in transient absorption technique is the change in absorbance with and without the action of pump which is mathematically expressed as follows.

$$\Delta A(\lambda,t) = A(\lambda,t) - A(\lambda) \quad (2.41)$$

$$\Delta A(\lambda,t) = log\frac{I_0(\lambda)}{I(\lambda,t)} - log\frac{I_0(\lambda)}{I(\lambda)} = log\frac{I(\lambda)}{I(\lambda,t)} \quad (2.42)$$

Equation 2.42 implies a situation where the measurement of probe intensity with and without illumination of the sample by pump will give us the observable quantity. So we can simply write

$$\Delta A(\lambda,t) = log\frac{I^{probe}}{I^{probe}_{pump}} \quad (2.43)$$

It should be pointed out that in equation 2.43; the quantity I^{probe} is actually measured blocking the pump light completely with the use of a chopper. The population created or depleted by pump light will decay or grow with time i.e. as $N(t)$ changes with time, $\Delta A(\lambda,t)$ also changes with time and that provides us the photophysical dynamics of the system. Furthermore, as the observable $\Delta A(\lambda,t)$

does not contain any $I_0(\lambda)$ term, the intensity of probe before the sample need not to be measured which means a single beam spectrophotometer will work just fine. However, to subtract the noise in the probe light, a dual beam spectrophotometer is often used. Now this particular pump probe technique being an absorption spectroscopy can track both radiative and non-radiative processes depending on the spectrum of the probe.[22-25] Four major processes can be observed in transient absorption spectroscopy which are depicted in figure 2.6 and described below.

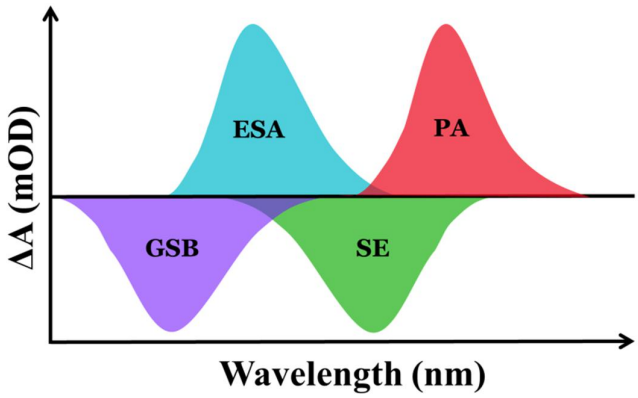

Figure 2.6 Contribution of different photophysical processes in transient absorption spectra

Ground state bleaching - The pump pulse excites a portion of molecules from ground state to excited state and the population in ground state decreases. Therefore, the amount of probe light absorbed by the ground state molecule become less after the pump excitation compared to the absorption without pump excitation i.e. $I^{probe} < I^{probe}_{pump}$. So a negative ΔA spectrum is observed which reduces with increment in time delay between the pump and the probe due to deactivation of molecules from excited to ground electronic state. This particular signal is known as ground state bleaching (GSB).

Stimulated Emission:- Electronically excited molecules undergoes spontaneous emission (fluorescence) and deactivate to ground state. However, if a resonating photon from external radiation passes through the excitation volume, it can stimulate the emission process from excited to ground state which is known as stimulated emission. The stimulated emitted photon has the same direction as the

stimulating radiation photon. So if some or all frequencies present in the probe pulse resonate with the excited and ground state of the sample (including vibrational levels), probe can stimulate emission from the sample excited by the pump. Moreover, the emitted photons will travel with the probe and reach the detector which in turn will see an increase in intensity of the probe at certain wavelengths after the action of pump. Therefore $I^{probe} < I^{probe}_{pump}$ will be satisfied and a negative spectrum will be observed in transient absorption. This is known as stimulated emission (SE) signal which resembles the spontaneous emission spectra of the molecule. SE signal remains Stokes shifted compared the GSB signal but there can be significant overlap at early times. SE also deceases with time exactly as the excited state population decreases due to different radiative and non-radiative molecular processes under the assumption that the intensity of the probe light is so small that it does not change the population of the excited state significantly.

Excited State Absorption:- The applicability of transient absorption signal lies in the distinction of recognizing transitions which are not possible to observe using fluorescence techniques. One of them is the observation of excited state absorption (ESA) signal. The pump beam creates a particular electronic excited state in the sample. Now, some of the wavelengths of light present in probe light can be in resonance with the energy gap between the populated excited state and other higher energy states and thus is absorbed by the excited state molecules. This particular transition is not possible without the pump and therefore, in this case, $I^{probe} > I^{probe}_{pump}$ and we can observe a positive signal in the spectra.

Product Absorption:- Product absorption (PA) signal is another feature in transient absorption spectroscopy which is difficult to observe using fluorescence techniques. Once excited, the molecule can undergo several transformations and excited state reactions like photoinduced electron and proton transfer etc. and the new transient species thus generated can absorb the probe light which results in a

positive spectral signature in the transient absorption spectroscopy as $I^{probe} > I^{probe}_{pump}$.

The observation of these four phenomena makes transient absorption spectroscopy an immensely powerful technique but the limitations are put by several factor and among them the spectral spread of the probe and instrument response can restrict observation of one or more processes described above.

2.5.2. Instrumental Setup

The femtosecond broadband transient absorption spectrometer in our lab is a commercially one (Femto-Frame-II, IB Photonics, Bulgaria) which I have used for all my studies. The optical layout of the system has been shown in figure 2.7. The 800 nm output of a Ti:Sapphire regenerative amplifier (SpitfirePro XP, Spectra-Physics, USA) pumped by a 20-W Q-switched Nd:YLF laser (Empower, Spectra-Physics, USA) and seeded by a Ti-Sapphire femtosecond oscillator (MaiTai SP, Spectra- Physics, USA) was used as the fundamental light for transient absorption experiments. The repetition rate and the pulse width of the output was 1kHz and ~80 fs measured using a commercial autocorrelator. This fundamental beam was split into two parts at beamsplitter BS_1. One part was used to generate the pump light and the other was used for the probe. The pump light was generated inside a JANOS tripler supplied by the same company. The 800 nm light was focused onto a BBO crystal where the second harmonic 400nm light was produced. The second harmonic and the residual 800 nm light passed through a waveplate and collinearly fell onto a second BBO crystal where the third harmonic 266 nm light was generated according to the principles described in section 2.3.3. These three lights were separated using a set of dichroic mirrors and the 400 nm or the 266nm light was used for excitation light by using mirror M_6 or M_7. The other part of the fundamental beam after reflecting through mirror M_5 was passed through a retroreflector (RR) mounted on a mechanical delay stage using mirrors M_{B1}, M_{B2} & M_{B3}. This delay stage was used to generate maximum 2ns time delay between the pump and the probe. A very small part of the 800 nm light was split in BS_2 and allowed to fall on a photodidode PD which controlled the chopper. The rest of the

fundamental beam passed through a linear neutral density filter (ND_1), an iris and focused on a 0.3 mm sapphire crystal by lens L_4.

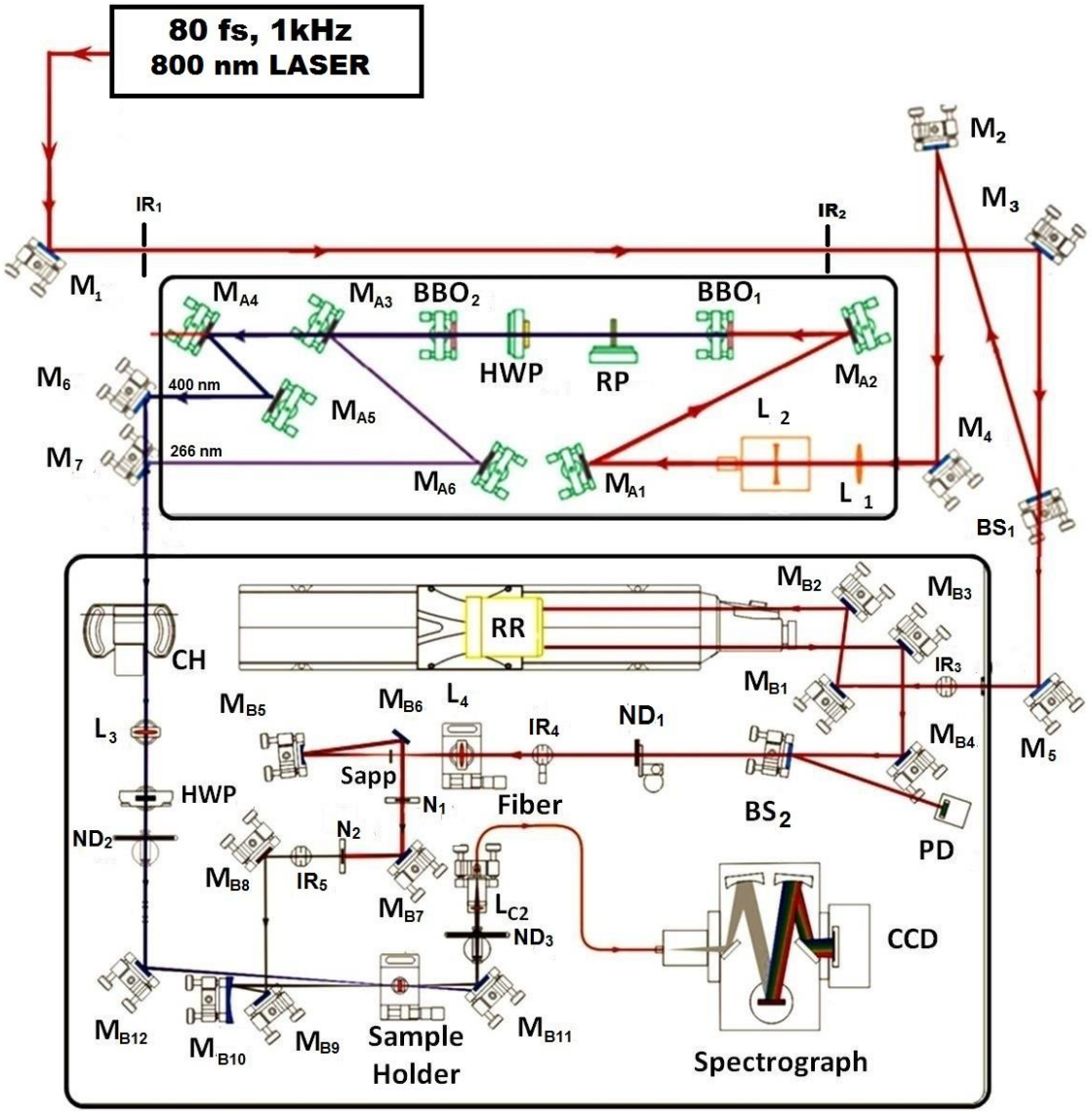

Figure 2.7 Optical layout of the femtosecond broadband transient absorption spectrometer

Thus the white light continuum (WLC) probe spanning across 450nm-750nm was generated in the sapphire crystal (Sapp). However, the character/shape of the probe light largely depends on the power and beam shape controlled by the ND filter and the iris. The WLC then collected by a parabolic mirror M_{B5} and directed through the two Notch filters (N_1 and N_2) to cutoff residual fundamental radiation of 800nm using mirror M_{B6} and M_{B7}. Then the probe light is focused on the sample

using another parabolic mirror M_{B10}. Meanwhile the pump light is directed through chopper and its polarization is adjusted compared to the probe using a half wave plate. A rotating ND filter (ND_2) controls the power of the pump and using lens L_3 and mirror M_{B12} the pump beam is focused into the same spot in the sample cuvette as the probe beam. A typical focal spot size is 100-200μm. The function of the chopper is to cut-off the pump light for certain time to allow measurement without pump as explained in the previous section. The polarization control is required to record data without interference from anisotropy of the system. The probe beam after passing through the sample is focused on the 200μm optical fiber cable by means of mirror M_{B11}. Another ND filter (ND_3) controls the amount of probe light that reaches the detector. The detector is a CCD spectrograph which detects the probe light scattered by a pair of diffraction gratings. The pump beam have slight inclination compared to the probe beam and therefore cannot reach the detector. The zero time is adjusted by observing the signal of a known sample (C152 in ethanol in my case) varying the delay time. The whole setup is controlled by software based on LABVIEW platform. The pump power is kept ~10-15 μW during measurements. Steady state absorption spectra were taken before and after the measurements to ensure no photo degradation of the sample.

2.5.3. Instrument Response Function (IRF) and Chirp

In broadband transient absorption spectroscopy, the instrument response function (IRF) is given by the cross correlation of the pump and the probe light.[26-28] Generally pulses travelling through transmitting optics broadens them but in this pump probe technique several other factors like presence of instantaneous signals or artifacts, group velocity dispersion etc. do affect the data and IRF acquisition. The use of high power pulses in transient absorption spectroscopy gives rise to several kinds of artifacts in the data and two photon absorption (TPA) is one of them. The sample under study can absorb two photons from the pump and spectrally broad probe pulse simultaneously which will result in the change in absorbance of the probe light resulting in an unwanted signal.[24,27,28] Stimulated

Raman amplification can also occur if the pump and the probe are very close in frequency.[27,28] However, in my case the spectral separation of the excitation from the probe let this effect diminish. Moreover, the timescale of SRA is in the range of instrument response i.e. very short lived. Cross-phase modulation occurs when the intense pump light modifies the refractive index of the medium which in turn changes the spectra of the probe light. Cross phase modulation affects the spectra at time zero mostly.[27,28] All three artifacts have a linear correspondence with the intensity of the pump pulse. So using less intense pump pulse, higher optical density of the sample and less chirped WLC probe light, these artifacts can be avoided in the acquired data. However, the IRF measurement can get seriously affected by them. The IRF of the transient absorption setup was measured by replacing the sample solution in the cuvette with pure solvents. The femtosecond pump pulse induces instantaneous effects in solvents which can be applied to measure the IRF. For instance, pump pulse can induce non-resonant coherent signal from pure solvent like stimulated Raman scattering, impulsive Raman scattering or off-resonant transient birefringence etc. which give the pump-probe cross correlation of the system.[25,27-30] Two factors are to be considered for IRF and data analysis. The first one is the group velocity dispersion and subsequent chirp present in the data. Group velocity dispersion (GVD) is a well-known optical process where light of different frequencies travel at different velocity in a medium other than vacuum. The probe light has a broad spectrum. Naturally, the red end of the probe light travels faster than the blue end and as the probe light passes through transmitting optics, the light gets spread in time. Moreover, inside sample solution, the probe light travels faster than the pump light as the pump has a shorter wavelength than the probe. GVD in optics and sample cell induces chirp in the measured data i.e. the overlap of the pump and probe at different wavelengths happens at different times. In other words the time zero is shifted along the probe spectrum which does not affect the actual dynamics of the sample but it needs to be known to compare the sample dynamics at different wavelengths or to fit the data globally. However, the chirp can be easily estimated from the time zero position of

the pure solvent response at different wavelengths.[25,27-30] Along with GVD, cross phase modulation induced by the pump light on a linearly chirped probe light modulates the Gaussian shaped IRF and distorts it.[27-30] Therefore, once the solvent response is measured, it is fitted at different wavelengths with a Gaussian and its first and second derivative to account for the shape. The time position obtained from such fitting at several wavelengths are then used to estimate the chirp in the data. The chirp is usually corrected by fitting with a polynomial and designating a position in the spectrum where time zero is to be set. In figure 2.8, I have shown the IRF obtained at multiple wavelengths in acetonitrile, methanol and chloroform along with the fitting. The width of the Gaussian fit obtained was 50-60 fs depending on the wavelength. Using the relation between the width parameter and the FWHM of Gaussian given in equation 2.23, the estimated IRF is 120-140 fs. From the figure, it is quite clear that the center of IRF is shifted to longer times at longer wavelengths of the probe.

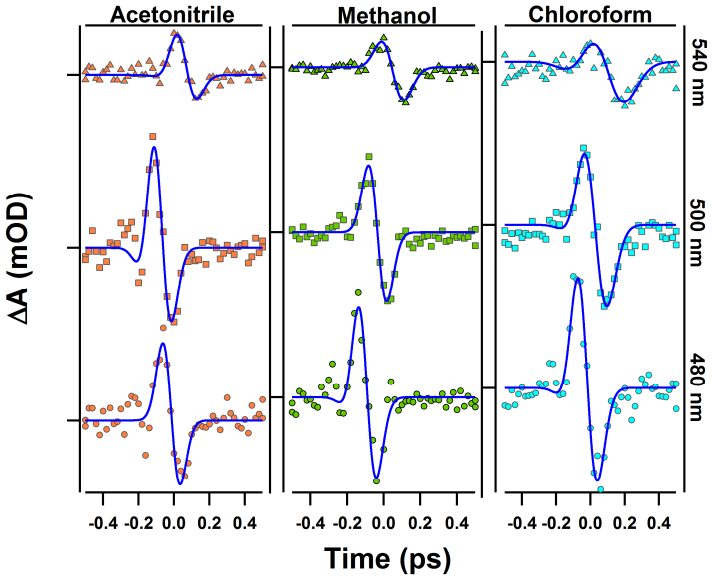

Figure 2.8 The IRF of transient absorption setup recorded in acetonitrile, methanol and chloroform using 400nm pump. The solid blue lines indicate fitting.

2.5.4. Data Analysis

Broadband transient absorption spectroscopy generates a massive amount of data which is simultaneously or "globally" analysed. The dataset itself is a two

way data or in other words it contains two independent experimental variable; time and wavelength. So a model based global analysis procedure is necessary. I have used an open source java-based software GLOTARAN for analysis of transient absorption data. The operational details of this software have been discussed in ref 31 and 32. A very brief idea of the procedure employed is discussed here. First of all, while analyzing transient absorption data it is assumed that the data has homogeneity i.e. a set of parameters can describe the data and the overall dynamics can be assigned to individual member or reaction pair of the system. The data has contribution from all the photophysical processes described in previous section at different times and wavelengths. The experiment essentially an absorption spectroscopy and therefore Beer-Lambert's law can be applied. It is also considered that the whole dataset is the superposition of spectral properties weighted by their concentration.

$$\psi(t,\lambda) = \sum_{l=1}^{n_{comp}} c_l(t)\varepsilon_l(\lambda) \qquad (2.44)$$

In the above formalism, $c_l(t)$ is the concentration of the l-th component at time t and $\varepsilon_l(\lambda)$ is the extinction coefficient of the same component at wavelength λ. A typical global analysis procedure can resolve upto 10 such components. Prior knowledge of the system is used to assume the minimum number of components necessary to fit the data. Now the overall data can be fitted by two methods. Either we can fit the data with knowledge of $c_l(t)$ which is known as the kinetic model or we can fit the data using the knowledge of $\varepsilon_l(\lambda)$ which is known as the spectral model. In our case we have a prior understanding of the concentration profiles which are exponentially variable with time. Therefore the idea is to fit $\psi(t,\lambda)$ with sufficient number of exponential components convoluted with the IRF function. IRF is modeled with Gaussian function and the convolution of exponential with Gaussian has already been described in section 2.3.4. Now the experimental data is in the form of a m × n matrix where measurements are done over m wavelengths for n times. One of the ways to extract the number of independent components in such kind of data is singular value decomposition (SVD) which is defined as [31,32]

$$\psi(t,\lambda) = \sum_{n=1}^{n_{max}} u_n(t) w_n(\lambda) SV_n \quad (2.45)$$

So the minimum number of parameters needed for fitting was first estimated from SVD, then the sum of exponentials convoluted with Gaussian IRF was fitted into the whole dataset simultaneously. The dispersion was modeled with a polynomial function while fitting.

2.6. Density Functional Theory (DFT) Calculations

Prediction of photophysical behavior of a molecule requires knowledge of it electronic structure in ground and electronic excited state, energy gap between different levels, electron density in molecular orbitals etc. Additionally, the changes in electronic state energies brought about by distortions in molecular geometry often help photo-chemists understand molecular properties.[33-37] For these purposes and many more, computational chemistry is essential. I have explicitly used density functional theory calculations for works done in this thesis. All the calculations were performed in Gaussian 09 software and results were viewed using Gaussview 05 software.[38] Density functional theory (DFT) is probably the most powerful tool for calculating electronic structure of a molecule.[33-37] DFT was introduced in two groundbreaking papers in 1964 and 1965 and Walter Kohn received the Nobel Prize in chemistry in 1998.[39-40] Ground state geometry and electronic structure calculations were all calculated using DFT but for excited state calculations time dependent potentials are needed which are incorporated in time dependent density functional theory (TDDFT). Here I am going to discuss their basic idea based on which the computations were performed without going into details.

For any quantum chemical calculation in ground state, the goal is to solve the time independent Schrödinger equation which under Born-Oppenheimer approximation can be written as

$$\widehat{H}_{el}\psi_{el} = E_{el}\psi_{el} \tag{2.46}$$

In an N-electron M-nuclei system the electronic Hamiltonian is given by

$$\widehat{H}_{el} = -\frac{1}{2}\sum_{i=1}^{N}\nabla_i^2 - \sum_{i=1}^{N}\sum_{A=1}^{M}\frac{Z_A}{r_{iA}} + \sum_{i=1}^{N}\sum_{j>i}^{N}\frac{1}{r_{ij}} \tag{2.47}$$

The problem is equation 2.47 cannot be solved without proper approximations and even then the wavefunction being a non-observable quantity cannot be truly measured. So it becomes increasingly difficult to construct increasingly accurate wavefunctions with so many degrees of freedom.[33-37]In DFT, the state is defined by the density of the interacting electrons; not by their individual interaction which

is valid for any fermions for that matter.[33-37]Contrary to wavefunction, electron density is an observable and the information of all the coordinates are not required to calculate expectation value.[33-37]Now, first Hohenberg-Kohn theorem stated that the electron density determines all ground state properties of the system. [33-37] So total energy ($E[\rho]$) is a functional of electron density(ρ) in presence of an external potential ($v_{ext}(r)$) like electric field from nuclei.[33-37]

$$E[\rho] = F[\rho] + \int v_{ext}(r)\rho(r)dr \quad (2.48)$$

The second Hohenberg-Kohn theorem states that variational principle applies to $E[\rho]$ and it will reach minimum when ρ will be equilibrium electron density. Here $F[\rho]$ is universal functional i.e. it does not depend on external potential.[33-37] The recipe for calculating the functional came from Kohn-Sham theorem which gave the ground state electronic energy as

$$E[\rho] = -\frac{1}{2}\sum_{i=1}^{N}\langle\psi_i|\nabla_i^2|\psi_i\rangle - \int\sum_{A=1}^{M}\frac{Z_A}{r_{Ai}}\rho(r)dr + \frac{1}{2}\int\int\frac{\rho(r_1)\rho(r_2)}{r_{12}}dr_1dr_2 + E_{xc} \quad (2.49)$$

In the above equation, the first term is the kinetic energy of electrons, second term is electron nucleus attraction term, the third term is the electron-electron repulsion term and E_{xc} is exchange correlation energy which is unknown. So several approximated functional are used. The ground state electron density is defined by one orbital Kohn Sham wavefunctions. [33-37]

$$\rho(r) = \sum_{i=1}^{N}|\psi_i(r)|^2 \quad (2.50)$$

One of the approximations for exchange correlation is the local density functional (LDA). It assumes the inhomogenous density of solid or liquid can be calculated using homogenous electron gas. More sophisticated approximations are hybrid functional and among them the Becke, 3-parameter, Lee-Yang-Parr (B3LYP) is probably the most popular in chemistry. Hybrid functional like B3LYP combines orbital dependent Hatree-Fock and an explicit density functional like LDA and generalized gradient approximation.[33-37]

Another important point for computations is the use of basis set which is a mathematical description of orbitals. In Gaussian calculations I have used split-

valence basis sets like 6-31G, 6-311G etc. The idea proposed by Boys and explicitly developed by Pople is to replace Slater type orbitals with Gaussian orbitals.[33-37,41,42] However, calculations with Gaussian orbitals do not match that of Slater type orbitals specially at shorter distance.[33-37,41,42] One way out is to use a sum of multiple Gaussian orbitals and each of those Gaussian are called primitive Gaussian.[33-37,41,42] Now the most used are the split-valence basis sets where a sum of Gaussian functions (6 in case of 6-31G) known as contracted Gaussian function is used to represent the inner shell atomic orbitals, and a larger number of contracted Gaussian to represent valence orbitals. Like in 6-31G, the compact valence orbital is represented by a contraction of 3 Gaussian and the extended valence orbital is represented by one Gaussian. The – indicates split-valence and G indicates Gaussian.[41,42]

In photochemistry, we often need to calculate the vertical excitation energy to match the absorption spectra and to study the dynamics of a molecule in the excited state by performing a geometry scan. DFT does not include a way to calculate the excited state properties and therefore time dependent density functional theory (TDDFT) has been developed. In TDDFT, we calculate the response of system to an external perturbation like polarizability which is system response to an external electric field. The basic idea is to solve the time dependent many particle Schrodinger equation.

$$i\frac{\partial}{\partial t}\psi(r_1, r_2 \cdots\cdots r_N, t) = \widehat{H}(t)\psi(r_1, r_2 \cdots\cdots r_N, t) \quad (2.51)$$

The problem is in time independent Schrodinger equation we solve for an eigenstate whereas in time dependent Schrodinger equation, we observe the time evolution of a state. The time dependent Hamiltonian $\widehat{H}(t)$ consist of kinetic energy and electron electron interaction term with the external potential term $(\hat{V}_{ext}(\{r\}, t))$which is expressed as a sum of one body potentials.[43-47]

$$\hat{V}_{ext}(\{r\}, t) = \sum_{i=1}^{N} v_{ext}(r_i, t) \quad (2.52)$$

Now, the time evolution of the system is controlled by the external potential like illumination with light/radiation. Runge and Gross established that there is an one

to correspondence between the time dependent potentials and densities i.e. if two different time dependent potentials act on same initial state of a system then they will generate two different time dependent densities.[43-47]Another problem with TDDFT is variational principle cannot be applied to it as energy is not conserved here.[43-47]So instead a quantity called quantum mechanical action (A_{xc}) is defined which can be used in place of energy. Runge and Gross also modified the Kohn-Sham equation to show that the exchange correlation functional (ν_{xc})is a derivative of action functional.[43-47]

$$\nu_{xc}(\rho) = \frac{\partial A_{xc}}{\partial \rho} \tag{2.53}$$

As the correct form of the functional in the ground state is not known, adiabatic local density approximation (ALDA) is applied and then the same functional which is applied in the ground state is used in the excited state. Next the problem of causality exists in TDDFT which states that the response functions must be zero before a certain time or before the time at which the external perturbation was turned on. The causality problem along with the boundary conditions were solved by van Leeuwen in 1998.[43-47]In TDDFT, adiabatic approximations are made to the exchange correlations which works satisfactorily if the excited state does not differ much from the ground state. Now, photoabsorption cross section is related to imaginary part of dynamic polarizability which is estimated from the linear density response function of the system perturbed by a small external potential. Lastly, specific photoabsorption phenomenon such as double excitation, excitation to higher states or charge transfer states were calculated using TDDFT by several modifications made by researchers in the last decade.[43-47]

Solvent effects in DFT and TDDFT computation performed with Gaussian software can be incorporated through self-consistence reaction field method which places the solute in a cavity of reaction field.[33-37,48] The most commonly used method and the one I have used in all the solvent dependent calculations is Polarisable Continuum Model (PCM). PCM model calculate the free energy of a molecule as a sum of electrostatic energy, dispersion-repulsion free energy and

cavitation energy. The cavity is an Onsagar cavity defined by van der Waals radius of atoms.[48] PCM model does not take into account any specific solvation like hydrogen bonding interaction. It only applies a dielectric continuum which behaves like the polarity of the solvent.

2.7. Cyclic Voltammetry Measurements

In my experiments, I have used two different instruments for measurement of cyclic voltammetry (CV) data. One set of experiments were performed using CH instruments, Electrochemical Analyzer/Workstation model 600B series. The cell contains a Beckman M-39273 platinum-inlay working electrode, a Pt wire auxiliary electrode, and a saturated calomel electrode (SCE) as reference electrode. For coulometry, a platinum wire-gauze was used as the working electrode. The solutions were ~1.0 mM sample and 0.1 M supporting electrolyte, tetrabutylammonium perchlorate or lithium chloride, as needed. Spectroelectrochemical measurements were performed using a custom-made cell (Model EF-1350) from Bioanalytical Systems Inc. The measured redox potentials at 298 K were converted to the ferrocenium/ferrocene (Fc+/Fc) reference. Under our experimental conditions, the $E_{1/2}$ and peak-to-peak separation ΔEp values (CH_2Cl_2) for couple Fc+/Fc were 0.49 V and 120 mV versus SCE, respectively.

The other set of cyclic voltammetry experiments were performed using BAS Epsilon electrochemical workstation. A standard three electrode cell was selected with a BAS MF 2012 glassy carbon electrode as working electrode, a platinum wire as an auxiliary electrode and Ag/AgCl electrode as a reference electrode. The details of the cell configuration are previously reported.[49] No correction was made for liquid junction potential. Potentials were measured at 298 K. To reduce the uncompensated solution resistance in the cell configuration the reference electrode tip was placed close to the working electrode. All the potentials are here reported vs SCE by converting the values obtained vs Ag/AgCl using a factor of −0.045 V.

2.8. Nuclear Magnetic Resonance Spectroscopy

^{1}H and ^{13}C NMR spectra were recorded in deuterated solvents in a 400 MHz/500MHz NMR spectrometer (JEOL, Japan).

2.9. Materials

Pyrene, methyl viologen, benzophenone, 1,4-diazabicyclo[2.2.2]octane (DABCO), benzyl viologen dichloride, sodium dodecyl sulfate, thioflavin-T were

purchased from Sigma-Aldrich. Laser grade coumarin dyes were purchased from Exciton. High performance liquid chromatography grade methanol, acetonitrile, chloroform, dimethylsulphoxide, cyclohexane were purchased from MERCK, India, Fisher Scientific and Spectrochem, India. Double distilled water was used in all the studies. Thioflavin-t has been recystallised twice from methanol before using.

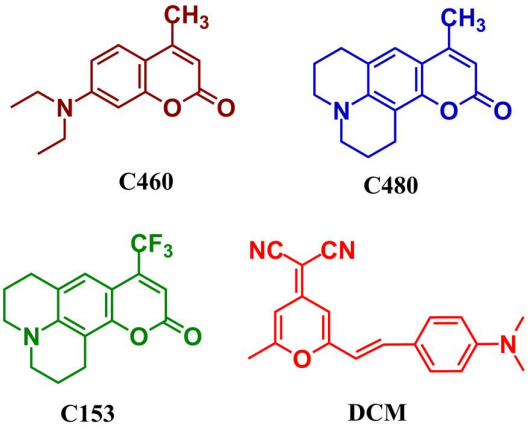

Figure 2.9 Structure of fluorophores used in solvation dynamics study

2.10. Synthetic Procedures

2.10.1. Synthesis procedure for 1,1'-bis(cyanomethyl)-4,4'-bipyridine-1,1'-diium bromide ($CNMV^{2+}$)

1,1'-bis(cyanomethyl)-4,4'-bipyridine-1,1'-diium bromide ($CNMV^{2+}$) was synthesized according to previous report.[50] Briefly, 4,4' bipyridine (0.781g, 0.05mol) was heated in 50 ml dimethyl formamide solvent with 2-bromoactonitrile (1.8g, 0.015mol) at 60˚C for 16 hrs. It was then cooled to room temperature and 200 ml acetone was added and it was allowed to stand overnight. The yellow precipitate thus obtained was filtered, washed with acetone and dried under vacuum. ~1.3 g product was obtained which was characterized by the ^{1}H-NMR spectra (400MHz, D6-DMSO): δ 9.5 ppm (doublet, J= 7Hz, 4H) ; δ 8.87 ppm (doublet, J= 5.5Hz, 4H), δ 6.12 ppm (singlet, 4H) along with δ 3.35 ppm and δ 2.46 ppm for residual water present in D6-DMSO and deuterium peak of D6-DMSO respectively

2.10.2 Synthesis procedure for 1,1'-dimethyl-2,2'-bipyridine-1,1'-diium iodide (DM^{2+})

1,1'-dimethyl-2,2'-bipyridine-1,1'-diium iodide (DM^{2+}) was also synthesized following the procedure described in reference 50. 2,2' bipyridine (0.53 mg; 3.35 mmol) and methyl iodide (1.5ml, 24.1 mmol) was dissolved in 6 ml acetonitrile and heated in a microwave for 1 hr at 120˚C. A yellow precipitate was obtained which was washed with acetonitrile and dried under vacuum. The compound was characterized by ^{1}H-NMR spectra (400MHz) in D6-DMSO solvent: ^{1}H-NMR peaks: δ 9.36 ppm (doublet, J= 8Hz, 2H) ; δ 8.83 ppm (doublet, J= 6.8Hz, 2H), δ 8.44 ppm and 8.42 ppm (these two peaks are very close and hard to resolve; corresponds to 4H), δ 4.1 ppm (singlet, 6H) along with δ 3.33 ppm and δ 2.46 ppm for residual water present in D6-DMSO and deuterium peak of D6-DMSO respectively.

References

1. Bollinger, L. M.; Thomas, G. E. *Rev. Sci. Instrum.* **1961**, *32* (9), 1044–1050.
2. O'Connor, D. V. and Phillips, D. *Time-Correlated Single Photon Counting*; Academic Press, London, 1984.
3. *Techniques;* Lakowicz, J. R., Ed.*; Topics in Fluorescence Spectroscopy;* Springer US: Boston, **2002***; Vol. 1*.
4. Becker, W. *Advanced Time-Correlated Single Photon Counting Techniques*; Castleman, A. W., Toennies, J. P., Zinth, W., Eds.; Springer Series in Chemical Physics; Springer Berlin Heidelberg: Berlin, Heidelberg, 2005; Vol. 81.
5. Becker, W. Introduction to Multi-Dimensional Tcspc. In *Springer Series in Chemical Physics*; 2015; Vol. 111, pp 1–63.
6. Lakowicz, J. R. *Principles of Fluorescence Spectroscopy;* Springer US: Boston, MA, 2006.
7. Smith, D. A.; McKenzie, G.; Jones, A. C.; Smith, T. A. *Methods Appl. Fluoresc.* **2017**, *5* (4), 42001.
8. Hallidy, L. A.; Topp, M. R. *Chem. Phys. Lett.* **1977**, *46* (1), 8–14.
9. Kahlow, M. A.; Jarzęba, W.; DuBruil, T. P.; Barbara, P. F. *Rev. Sci. Instrum.* **1988**, *59* (7), 1098–1109.
10. Shah, J. *IEEE J.* **1988**, *24* (2), 276–288.
11. Wirth, M. J. *Anal. Chem.* **1990**, *62* (4), 270A–277A.
12. Xu, J.; Knutson, J. R. Chapter 8 Ultrafast Fluorescence Spectroscopy via Upconversion. Applications to Biophysics. In *Methods in Enzymology*; 2008; Vol. 450, pp 159–183.
13. Boyd, R. *Nonlinear Optics*, 3rd ed.; Academic Press, 2008.
14. Y.R. Shen, The principles of nonlinear optics (John Wiley, New York, 1984)
15. Zernike, Frits ; Midwinter, J. E. *Applied Nonlinear Optics*; John Wiley & Sons, Ltd., 1973.
16. *Encyclopedia of Chemical Physics and Physical Chemistry*; Spencer, N.D.; Moore, J. H., Ed.; CRC Press, 2001.
17. Easter, J. H.; DeToma, R. P.; Brand, L. *Biophys. J.* **1976**, *16* (6), 571–583.
18. Maroncelli, M.; Fleming, G. R. *J. Chem. Phys.* **1987**, *86* (11), 6221–6239.
19. Horng, M. L.; Gardecki, J. A.; Papazyan, A.; Maroncelli, M. *J. Phys. Chem.* **1995**, *99* (48), 17311–17337.
20. Fleming, G. R.; Gijzeman, O. L. J.; Freed, K. F.; Lin, S. H. *J. Chem. Soc. Faraday Trans. 2* **1975**, *71*, 773.

21. Brearley, A. M.; Strandjord, A. J. G.; Flom, S. R.; Barbara, P. F. *Chem. Phys. Lett.* **1985**, *113* (1), 43–48.
22. *Femtosecond Laser Pulses*; Rullière, C., Ed.; Advanced Texts in Physics; Springer New York: New York, NY, 2005.
23. *The Exploration of Supramolecular Systems and Nanostructures by Photochemical Techniques*; Ceroni, P., Ed.; Lecture Notes in Chemistry; Springer Netherlands: Dordrecht, 2012; Vol. 78.
24. Ruckebusch, C.; Sliwa, M.; Pernot, P.; de Juan, A.; Tauler, R. *J. Photochem. Photobiol. C Photochem. Rev.* **2012**, *13* (1), 1–27.
25. Berera, R.; van Grondelle, R.; Kennis, J. T. M. *Photosynth. Res.* **2009**, *101* (2–3), 105–118.
26. Mouton, N.; Sliwa, M.; Buntinx, G.; Ruckebusch, C. *J. Chemom.* **2010**, *24* (7–8), 424–433.
27. Ziólek, M.; Lorenc, M.; Naskrecki, R. *Appl. Phys. B* **2001**, *72* (7), 843–847.
28. Lorenc, M.; Ziolek, M.; Naskrecki, R.; Karolczak, J.; Kubicki, J.; Maciejewski, A. *Appl. Phys. B Lasers Opt.* **2002**, *74* (1), 19–27.
29. Cho, M.; Du, M.; Scherer, N. F.; Fleming, G. R.; Mukamel, S. *J. Chem. Phys.* **1993**, *99* (4), 2410–2428.
30. Kovalenko, S. A.; Ernsting, N. P.; Ruthmann, J. *Chem. Phys. Lett.* **1996**, *258* (3–4), 445–454.
31. Van Stokkum, I. H. M.; Larsen, D. S.; Van Grondelle, R. *Biochim. Biophys. Acta - Bioenerg.* **2004**, *1657* (2–3), 82–104.
32. Snellenburg, J. J.; Laptenok, S. P.; Seger, R.; Mullen, K. M.; vanStokkum, I. H. M. *J. Stat. Softw.***2012**, *49*, 1-22.
33. Burke, K. Perspective on Density Functional Theory. *J. Chem. Phys.* **2012**, *136* (15), 150901.
34. Kohn, W. *Rev. Mod. Phys.* **1999**, *71* (5), 1253–1266.
35. Jones, R. O.; Gunnarsson, O. *Rev. Mod. Phys.* **1989**, *61* (3), 689–746.
36. Parr, R. G. Density Functional Theory of Atoms and Molecules. In *Horizons of Quantum Chemistry*; Springer Netherlands: Dordrecht, 1980; pp 5–15.
37. Koch, W.; Holthausen, M. C. *A Chemist's Guide to Density Functional Theory*; Wiley-VCH Verlag GmbH: Weinheim, FRG, 2001.
38. Gaussian 09, Revision E.01, Frisch, M. J. *et. al*. Gaussian, Inc., Wallingford CT, 2009.
39. Hohenberg, P.; Kohn, W. *Phys. Rev.* **1964**, *136* (3B), B864–B871.
40. Kohn, W.; Sham, L. J. *Phys. Rev.* **1965**, *140* (4A), A1133–A1138.
41. Davidson, E. R.; Feller, D. *Chem. Rev.* **1986**, *86* (4), 681–696.
42. McQuarrie, D. A.; Simon, J.D. *Physical Chemistry: A Molecular Approach* University Science Books, 2011.

43. *Recent Advances in Density Functional Methods*; Chong, D. P., Ed.; Recent Advances in Computational Chemistry; World Scientific Publishing Co. Pte. Ltd., 1995.
44. Ullrich, C. A. *Time-Dependent Density-Functional Theory*; Oxford University Press, 2011.
45. Casida, M. E. *J. Mol. Struct. THEOCHEM* **2009**, *914* (1–3), 3–18.
46. Runge, E.; Gross, E. K. U. *Phys. Rev. Lett.* **1984**, *52* (12), 997–1000.
47. P.W., A.; Friedman, R. S. *Molecular Quantum Mechanics*, 5th ed.; Oxford University Press, 1997.
48. Tomasi, J.; Mennucci, B.; Cammi, R. *Chem. Rev.* **2005**, *105* (8), 2999–3093.
49. Dutta, I.; Sarbajna, A.; Pandey, P.; Rahaman, S. M. W.; Singh, K.; Bera, J. K. *Organometallics* **2016**, *35* (10), 1505–1513.
50. Petersson, J.; Hammarström, L. *J. Phys. Chem. B* **2015**, *119*, 7531.

This page intentionally left blank

Chapter 3

Absolute Rate of Ultrafast Photoinduced Bimolecular Electron Transfer Reactions

This chapter deals with the problem of measurement of actual rate of photoinduced electron transfer in liquid phase separating the rate constant of diffusion and establishing the presence of Marcus inverted region in case of bimolecular PET reactions. First, it has been established that broadband transient absorption spectroscopy can be successfully used to detect the radical cation and measure the rate of its formation which directly correlates to the rate of PET. Next the manifestation of viscosity or diffusion on the transient absorption data of PET has been explored and a complete kinetic analysis was undertaken to show that the rate constant of PET obtained was free from diffusion. With this knowledge, the Marcus inversion was established for bimolecular PET reaction between coumarins and viologens on the Stern layer of SDS micelle which was extremely useful in partial restrain of reactants to make observations in static quenching regime. This chapter has been divided into three parts to discuss each step of the problem mentioned above.

Chapter 3

Part A

Real Time Quantification of Ultrafast Photo-induced Bi-molecular Electron Transfer Rate: Direct Probing of the Transient Intermediate

Puspal Mukherjee, Somnath Biswas and Pratik Sen *J. Phys. Chem. B*, **2015**, *119*, 11253–11261.

3.A.1. Introduction

Electron transfer (ET) reactions are omnipresent in nature. In many chemical and biological processes such as in photosynthesis and metabolism, ET reactions plays a pivotal role.[1-12] A very important category of ET reactions is photoinduced electron transfer (PET) reaction. PET has been used to concur some of the greatest challenges of human survival, like energy harvesting from sunlight and mimicking our sources for food.[13-14] As anticipated, during twenty and twenty-first century there has been extensive studies in the literature on PET due to its potentiality to meet the energy demand of the universe.[15-20] PET chemistry allows exploiting the energy stored in the excited state to be utilized chemically. So, it is indispensable to investigate the ultrafast excited state dynamics of PET to device model PET system for numerous practical applications.

From nineteenth century researchers have tried to explain the kinetics of PET.[10] Succeeding a prolonged study and discussion, Rudolph A. Marcus first acquainted the theory of ET in 1956.[21-23] He was the pioneer in successfully interpreting the relation between reaction exergonicity and activation energy of the reaction with the involvement of nuclear and solvent reorganisation.[21-26] Marcus inverted region has been discussed in chapter 1 and there have been several attempts to prove this captivating theoretical prediction.[27-35] But major studies failed to establish the theory as in bulk solution PET rate constant reach the diffusion controlled limit at moderately exergonic condition and remains same at higher exergonicity too. Unavailability of electron donor-acceptor pair with such high exergonicity put the limit on observation of MIR in low viscosity solvents. In recent years it has been shown that analysing the data with a quenching model accounting for both static and transient domain of the process can result into disappearance of MIR.[36] It was speculated by Vauthey and co-workers that the observation of MIR in confined systems is apparent and is an effect of viscosity of the solvent and the lifetime of the probe molecule.[37,38] Therefore it is necessary to measure the actual ET rate between a donor and an acceptor, which is free from the

effect of diffusion, and can be used to settle the controversy raised by Vauthey and co-workers. Understandably fluorescence quenching experiments cannot serve the purpose. Direct measurements of bi-molecular ET rate are rare in the literature as the distinction or elimination of the role of diffusion is extremely difficult. Nevertheless, the effect of diffusion in the bi-molecular PET reaction could be nullified if the rate of transient intermediate (i.e. the product of the ET reaction) could be probed directly.

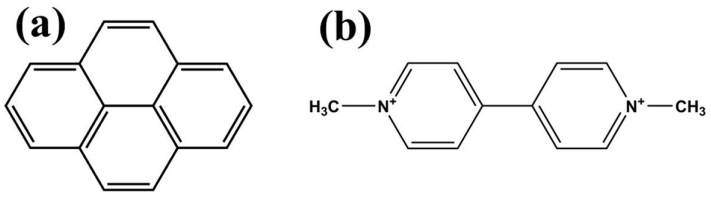

Scheme 3.A.1. Chemical structure of (a) pyrene (donor) and (b) methyl viologen

In this work, I have studied the bi-molecular PET rate between pyrene (Py) and methyl viologen (MV^{2+}) (scheme 3.A.1.), where the former is the donor and the latter is the acceptor, in low viscosity solvents like methanol (MeOH) and ethanol (EtOH) to directly measure the rate of bimolecular PET reaction without any constrain by diffusion. MV^{2+} is an well-known electron acceptor used in several ET reactions e.g. electron ejection from gold nano-particle,[39] modified Zn porphyrin,[40] tris (2,2-bipyridine)ruthenium(II),[41] etc. Upon accepting electron, MV^{2+} forms radical cation ($MV^{+\bullet}$) and that could be detected directly by the transient absorption spectroscopy. The rate of formation of the $MV^{+\bullet}$ would be exactly equal to the ET rate (k_{et}) as this being the product of the ET reaction and the kinetics of formation of $MV^{+\bullet}$ from the encounter complex is a first order and unimolecular process even if the overall kinetics is second order and bimolecular.[10,42-44] In this way, the contribution of the diffusion can be excluded fully from the calculated rate constant of bimolecular PET.

3.A.2. Results and Discussion

3.A.2.1. Quenching studies

Quenching of Py emission by MV^{2+} by means of bi-molecular PET process has been studied using steady state and time-resolved fluorescence spectroscopic measurements. As PET is a dynamic quenching process, one of the most familiar ways to study this is Stern-Volmer method. MV^{2+} has an overlapping absorption spectrum with Py in MeOH (Figure 3.A.1) but MV^{2+} does not show any emission even in very high concentration when excited around 340 nm.

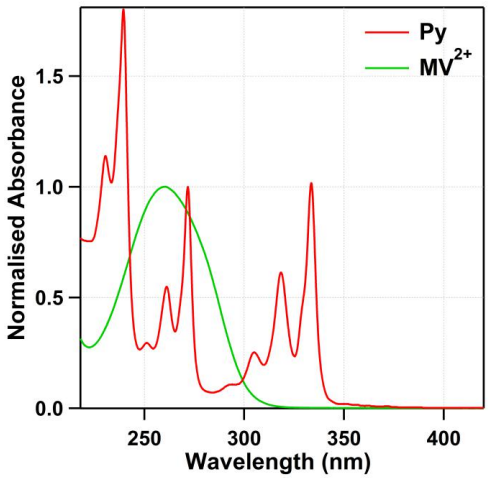

Figure 3.A.1. Absorption spectra of Py and MV^{2+} in methanol

Thus the emission spectra remained free of any contribution from MV^{2+} and quenching of Py could be measure without any hindrance. For the steady state and time resolved measurements the sample was excited at 340 nm. Py shows its characteristic emission spectra in methanol (Figure 3.A.2) and with the addition of MV^{2+} to the solution of Py in MeOH, a monotonous decrease in the emission intensity and fluorescence lifetime was observed (Figure 3.A.3).

To calculate the average lifetime of Py at each concentration of MV^{2+}, I have fitted the lifetime data using a sum of two exponential. The time components and their amplitudes obtained from the fitting were used to calculate the average lifetime using the following equation:

$$\tau_{avg} = \frac{a_1\tau_1 + a_2\tau_2}{a_1 + a_2} \quad (3.A.1)$$

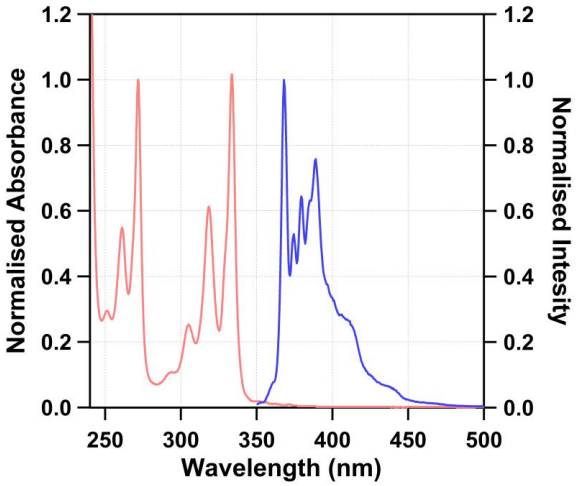

Figure 3.A.2. Absorption and emission spectra of Py in methanol

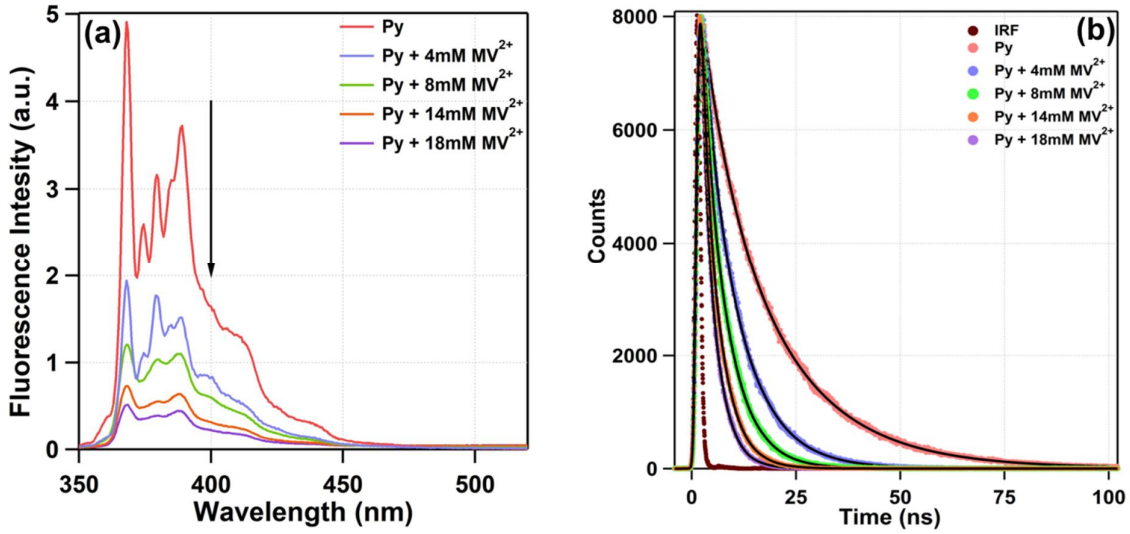

Figure 3.A.3. (a) Steady state (b) Time resolved data of fluorescence quenching of Py in MeOH by MV^{2+}

From both steady state and time resolved data I have plotted $\frac{I_0}{I}$ and $\frac{\tau_0}{\tau}$ as a function of methyl viologen concentration ($[Q]$), which follows the following equations.

$$\frac{I_0}{I} = 1 + K_{SV}\ [Q] \quad (3.A.2)$$

$$\frac{\tau_0}{\tau} = 1 + k_q \tau_0 [Q] \qquad (3.A.3)$$

Where I_0 is the emission intensity of Py in absence of quencher (MV^{2+}), I is the emission intensity of Py in presence of the quencher (MV^{2+}), τ_0 is the fluorescence lifetime of Py in absence of quencher (MV^{2+}) and τ is the fluorescence lifetime of Py in presence of quencher (MV^{2+}). For the entire range of concentration of the quencher used, the values of $\frac{I_0}{I}$ and $\frac{\tau_0}{\tau}$ did not deviate (Figure 3.A.4) from the linearity confirming the existence of only one type of quenching process i.e. dynamic quenching. From the slope of the linear plot the K_{SV} value is found to be 232 (± 7) M^{-1}. The fluorescence lifetime of Py in MeOH in absence of quencher was measured to be 15.4 ns. Using this lifetime value, the k_q value is estimated to be 1.5 x 10^{10} M^{-1} s^{-1}. The k_q value thus obtained accounts for the electron transfer as well as diffusion of the reactants in MeOH. It is actually an overall combination of all the kinetic processes contributing to electron transfer process. For a chemical reaction the slower step is the rate determining step. If the rate of diffusion is slower than the electron transfer then k_q would be dominated by diffusion. Typically diffusion rate constant in a low viscosity solvent like MeOH is in the order of 10^{11} s^{-1}. Comparing with k_q we can say that it is hard to estimate the rate of electron transfer as stated previously. That is the reason I turned our vision to a more direct approach of measuring the exact rate of electron transfer i.e. through femtosecond TA spectroscopy.

3.A.2.2. Cyclic voltammetry and spectroelectrochemistry of MV^{2+}

To determine the reduction potentials of MV^{2+} we have performed the cyclic voltammetry measurement in MeOH. The first and second reduction potential of MV^{2+} found out to be -0.43 V and -0.90 V respectively as shown in figure 3.A.5a, which is in agreement with the previously reported value.[41] It is evident that the first one corresponds to the formation of $MV^{+\bullet}$. Nevertheless, I have recorded the absorbance before the electrolysis and also after the first reduction of MV^{2+} to ensure the formation of the $MV^{+\bullet}$ by applying two different electrode potentials. MV^{2+} has an absorption peak around 260 nm in MeOH.

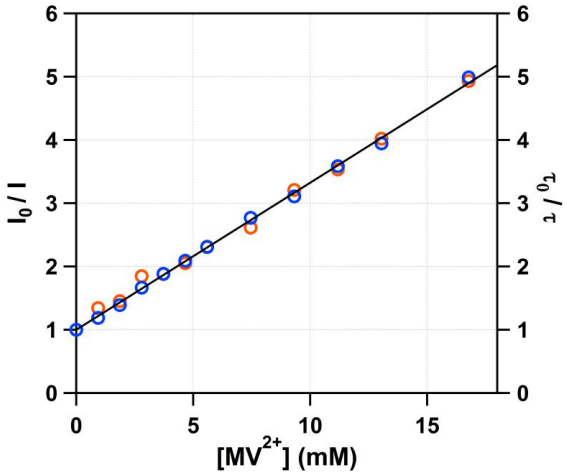

Figure 3.A.4. Stern-Volmer plot for quenching of Py by MV^{2+} in methanol

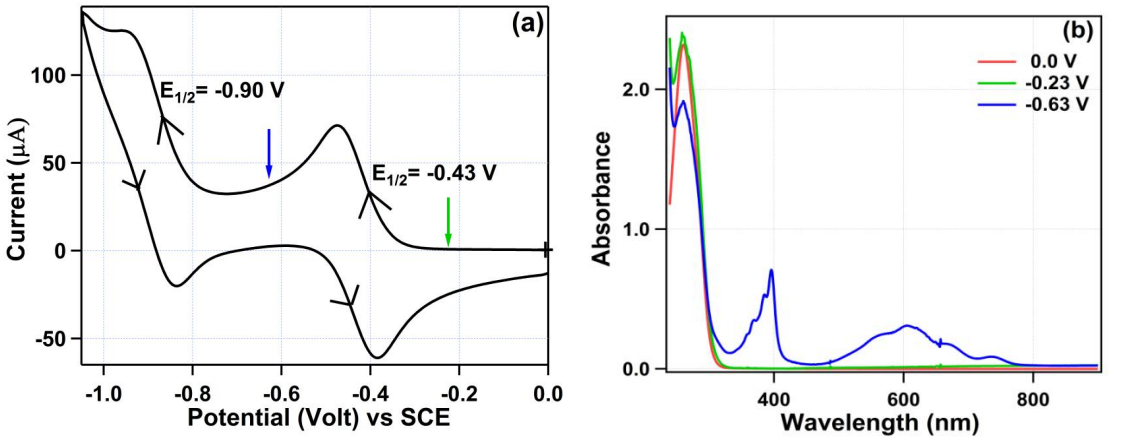

Figure 3.A.5. (a) Cyclic voltammetry of MV^{2+} in methanol (b) absorption spectra of MV^{2+} at different electrode potentials (the arrows indicate the potential at which spectra were taken)

The peak at 260 nm did not shift when -0.23 V which is less than the first reduction potential of MV^{2+} was applied (Figure 3 A.5b). But at a greater potential i.e. -0.63 V, a broad absorption band having maxima around 605 nm appeared along with another peak at 396 nm. These two peaks were a distinct characteristics of the $MV^{+\bullet}$ (Figure 3b).[45] The molar extinction coefficient of $MV^{+\bullet}$ reported in the previous study were 13,800 M^{-1} cm^{-1} (609 nm) and 42,700 M^{-1} cm^{-1} (396 nm).[45] As our broad band white light continuum in the TA setup perfectly overlaps with the 605 nm peak, I proceed to detect the rate of formation of $MV^{+\bullet}$ in real time.

3.A.2.3. Femtosecond TA measurements

I have recorded the TA spectra of Py in MeOH to compare it with the changes occur upon addition of MV^{2+} to it. The excited state dynamics of Py is well known and has been characterised by many spectroscopic methods including TA technique.[46,47]

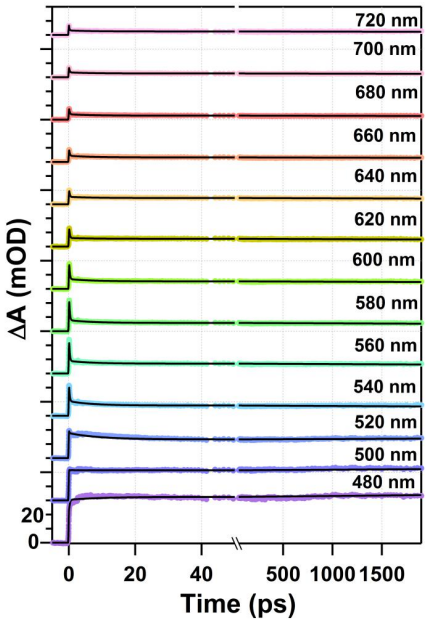

Figure 3.A.6. Stern-Volmer plot for quenching of Py by MV^{2+} in methanol

Table 3.A.1. Kinetic rate constants obtained from global fitting.

	Solvent	τ_1(ps) [a]	τ_2(ps) [b]	τ_3(ps) [c]	τ_4(ps) [d]	τ_5(ps)
Py	MeOH	0.20(d)	7.0(d)	-	-	20000 (fixed) (d)
MV^{2+}	MeOH	0.37(d)	32.8(d)	-		8200(d)
Py (200 µM) + MV^{2+} (10 mM)	MeOH	0.48(d)	2.5(r)	13.5(d)	77(d)	5040(d)
Py (200 µM) + MV^{2+} (20 mM)	MeOH	0.58(d)	2.4(r)	14.0(d)	118(d)	4300(d)
Py (200 µM) + MV^{2+} (30 mM)	MeOH	0.51(d)	2.5(r)	14.1(d)	141(d)	4300(d)
Py (200 µM) + MV^{2+} (40 mM)	MeOH	0.55(d)	2.2(r)	14.0(d)	190(d)	4400(d)
Py (200 µM) + MV^{2+} (20 mM)	EtOH	0.50(d)	5.1(r)	15.2(d)	160(d)	4430(d)

[a] ± 0.1 ps [b] ± 0.4 ps [c] ± 1 ps [d] ± 5 ps

The molecule is said to undergo a very fast internal conversion (IC) from S_n to S_1 state followed by a vibrational cooling of the S_1 state on exciting at 266 nm.[46] As Py has a very long fluorescence lifetime in MeOH, it is understandable that we cannot observe the complete deactivation of the S_1 state of Py with our present experimental setup. But I observed the early time dynamics as depicted in figure 3.A.6 and compared it with the previously observed values. Essentially I have obtained three time constants for Py in MeOH, which are tabulated in table 3.A.1. The pump beam (266 nm) excites Py molecules to S_6 or higher state. The first time constant of 200 fs in MeOH has been attributed to the IC of S_6-S_1 state and consequently a vibrationally hot S_1 state is generated. In the next few ps, the internal vibration relaxation occurred and I obtained a time constant of ~7 ps. These values are in good agreement with the previously reported one.[46,47] The third long time component of 20,000 ps remain fixed during the fitting of the data, which corresponds to the lifetime of S_1 state and has no relevance in the present discussion. All the peaks in the transient absorption spectrum of Py also have been assigned. In the time domain of the first few picoseconds I have observed changes in the spectrum; however beyond 60 ps no further change in the spectrum was observed. Following Miyasaka et al.[46] the absorption band around 470 nm and 510 nm in the TA spectrum of Py has been assigned to its excited state absorption S_1-S_{11} and S_1-S_{10} respectively. The chances of excimer formation have been discarded due to the low concentration used in our study and the choice of our solvent being MeOH.

From cyclic voltammetry and spectro-electrochemistry measurements it is clear that $MV^{+\bullet}$ has a strong and broad absorption centred around 600 nm. The spectrum of our probe light spreads over 460-750 nm gave us a perfect measurement condition to track the formation of $MV^{+\bullet}$ species. The bi-molecular PET reaction between Py and MV^{2+} was probed directly by monitoring the formation of the $MV^{+\bullet}$ during the course of the reaction using transient absorption spectroscopic technique for the direct measurement of the rate of this bi-molecular PET reaction. A mixture of Py (200 μM) and MV^{2+} (different concentration ca. 10

mM, 20 mM, 30 mM, 40 mM) was used for this measurement and were excited at 266 nm. Figure 3.A.7a depicts the kinetics and figure 3.A.7b depicts the spectra obtained from Py – 20 mM MV^{2+} in MeOH. The presence of a distinct rise component and its subsequent decay in the kinetic data around 600 nm region (absorption region of $MV^{+\cdot}$) signified the formation of $MV^{+\bullet}$ species by electron transfer from Py to MV^{2+} and subsequent back electron transfer process.

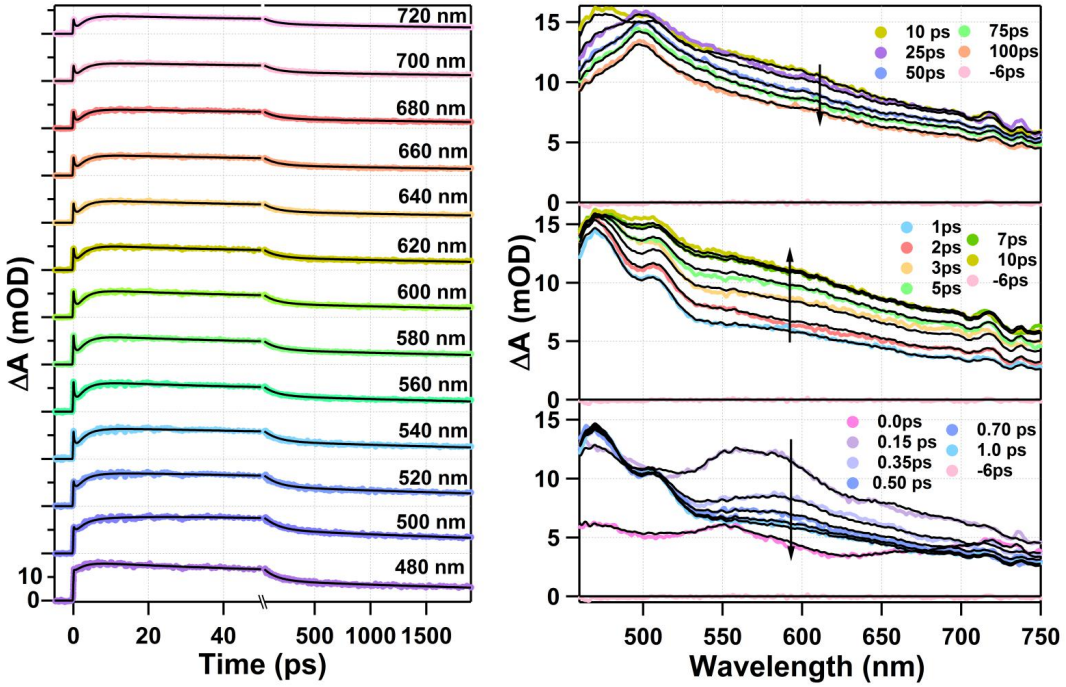

Figure 3.A.7. Plot of (a) kinetic traces at different wavelength (b) spectra at different times of Py + 20mM MV^{2+}in MeOH (the black lines indicate the fitting).

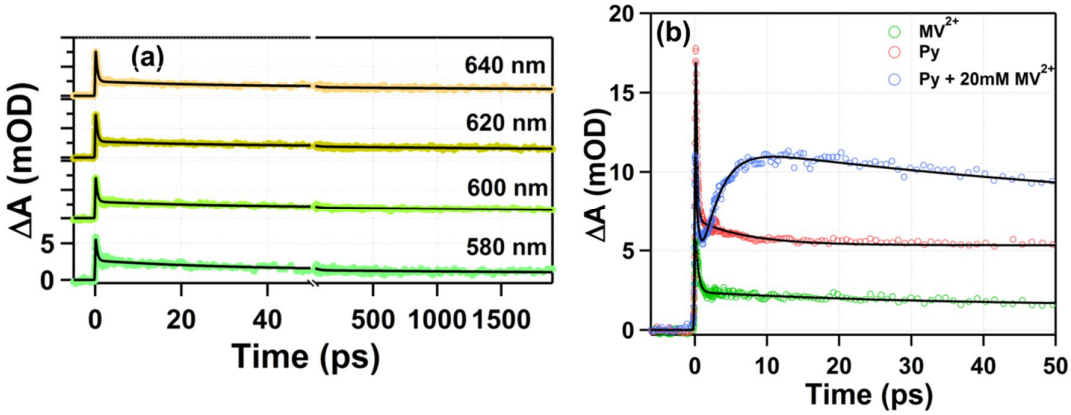

Figure 3.A.8. Plot of kinetic traces at (a) different wavelength of 20mM MV^{2+}in MeOH (b) 600 nm $MV^{2+,}$ Py and Py + 20mM MV^{2+} in MeOH (the black lines indicate the fitting)

This feature was absent in the kinetics of Py as discussed above, as well as in case of pure methyl viologen. This is to note that MV^{2+} also get excited by 266 nm pump pulse, however its excited state dynamics in 460-720 nm region does not reflect the formation of any new state (i.e. no rise time has been observed as can be seen in figure 3.A.8a), which has also been reported earlier.[48] A comparison between the kinetics of Py, MV^{2+} and a mixture of Py and 20 mM MV^{2+} at 600 nm (figure3.A.8b) clearly shows the existence of the growth in transient only for the last case. Thus the assignment of the rise component observed in the Py – MV^{2+} mixtures to the electron transfer process is further supported. It is worth mentioning that the growth part did not start immediately after the excitation. The small time delay in the start of the growth part indicate that the reactants need a finite time to diffuse before the electron transfer could take place in the encounter complex. The decay part immediately after the growth component assigned to the back electron transfer process and manifest that the species is indeed transient. The kinetic data were successfully fitted using global fitting procedure using a sum of five exponential functions. The time constants are listed in table 3.A.1. The τ_2, which is the rise time component, is found to be 2.5 ± 0.4 ps. The corresponding decay time (τ_3) is 14 ± 1 ps. The inverse of the τ_2 provide us the rate of electron transfer reaction between Py and MV^{2+}, which is 4 x 10^{11} s^{-1}. It is clear that this process is faster than the diffusion process. As diffusion has no role to play in the formation of $MV^{+\bullet}$ species in the encounter complex (which has been observed through TA measurement) the rate constant obtained are purely due to electron transfer. τ_4 and τ_5 are due to excited state dynamics of unreacted Py and MV^{2+} and it is not straight forward to isolate and comment on them. In the global fitting procedure, all the kinetics at different wavelengths were fitted using the same time constant and it accounts for the changes obtained in every wavelength. To prove this, I have performed the transient absorption measurement with definite Py concentration and different MV^{2+} concentration i.e. 10 mM, 20 mM, 30 mM and 40 mM. The plots of kinetic data are shown in figure 3.A.9a, 3.A.7a, 3.A.9b and 3.A.9c respectively. A comparison of the effect of MV^{2+} concentration is shown

also shown in figure 3.A.10a. It clearly showed similar kind of transient for all the different concentrations and were fitted by same method. The time constants obtained for all the different concentrations of MV^{2+} are listed in table 3.A.1. We can immediately see that neither the τ_2 nor the τ_3 vary with the concentration. As the variation of the concentration did not altered the process I could confirm that it is purely due to forward and backward electron transfer between Py and MV^{2+}. Thus it can be concluded that for the given donor acceptor pair (Py and MV^{2+}), the rate constant for electron transfer is 4 x 10^{11} s^{-1} and the same for back electron transfer is 7 x 10^{11} s^{-1} in MeOH.

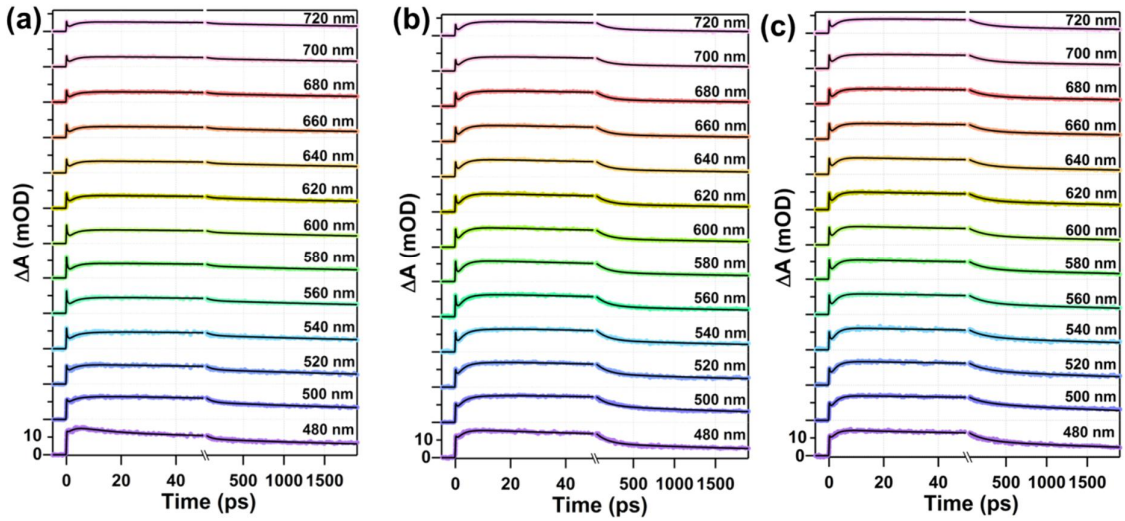

Figure 3.A.9. Plot of kinetic traces at different wavelength of (a) Py + 10mM MV^{2+} (b) Py + 30mM MV^{2+} (c) Py + 40mM MV^{2+} in MeOH (the black lines indicate the fitting)

3.A.2.4. Comparison of rate of bi-molecular PET between Py and MV^{2+} in MeOH and EtOH

In case of PET, k_{et} depends on solvent reorganization energy as evident from equation 1. Thus if I change the medium, the rate of electron transfer is bound to change. To explore this I have studied the PET between the same pair (200 µM Py and 20 mM MV^{2+}) in EtOH (Figure 3.A.11). The presence of rise and decay feature again signifies the effective electron transfer reaction. The time components obtained from the global fitting of the data have also been listed in table 1. The time constant for forward electron transfer obtained is 5 ps and the

same for the back electron transfer is 14 ps. The increasing in the rise time component in ethanol compared to methanol (see figure 3.A.10b) could be rationalize by higher solvent reorganization energy in ethanol. However, the backward electron transfer rate is almost similar in both the cases.

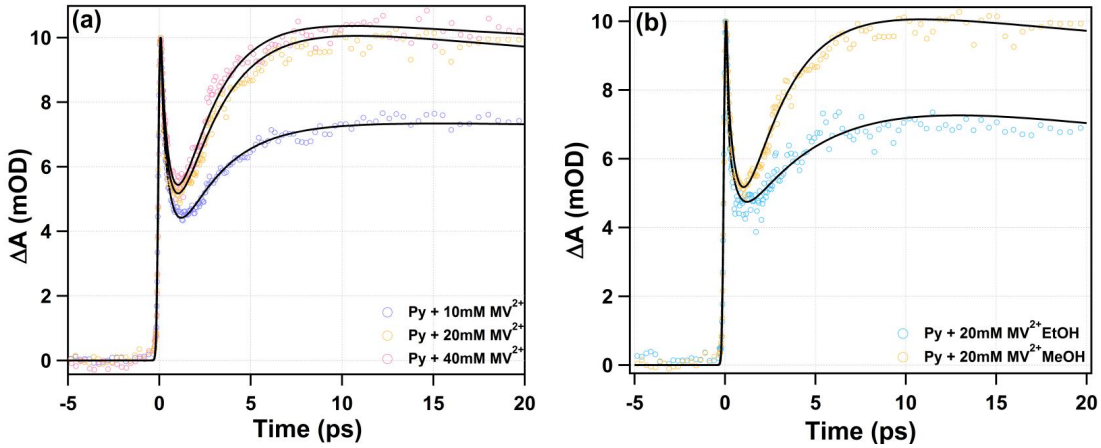

Figure 3.A.10. Plot of kinetic traces at 600 nm (a) Py + different concentration of MV^{2+} in MeOH (b) Py + 20mM MV^{2+} in different solvents (the black lines indicate the fitting).

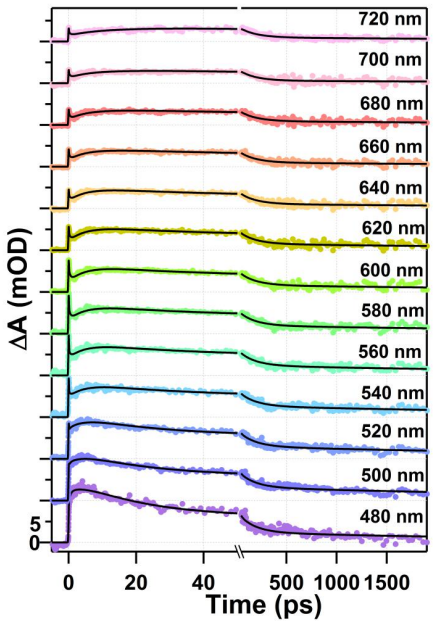

Figure 3.A.11. Plot of kinetic traces at different wavelength of Py + 20mM MV^{2+}in EtOH (the black lines indicate the fitting).

3.A.3. Conclusion

PET reaction between Py and MV^{2+} has been monitored in low viscosity solvent by using femtosecond transient absorption measurement and has been compared it with the conventional steady state quenching data. The measured time component of the bi-molecular PET reaction between Py and MV^{2+} in MeOH is 2.5 ± 0.5 ps. The forward as well as the backward ET rate did not vary with respect to the change in the acceptor concentration. As expected, the time component of the back ET rate (14 ± 1 ps) is higher than the forward one (2.5 ± 0.5 ps). The estimated value of k_{et} and k_q are respectively 4×10^{11} s^{-1} and 1.5×10^{10} $M^{-1}s^{-1}$. The rate of electron transfer remain unchanged on increasing the concentration of the acceptor, however a slower rate of electron transfer (2.5×10^{11} s^{-1}) was observed on changing the solvent from MeOH to EtOH. The higher reorganization energy in EtOH is attributed for this lower ET rate constant.

References:

1. Wang, H.; Lin, S.; Allen, J. P.; Williams, J.C.; Blankert, S.; Laser, C.; Woodbury, N.W. *Science* **2007**, *316*, 747-750
2. Whatley, F.R.; Tagawa, K.; Arnon, D.I. *Biochemistry* **1963**, *49*, 266-270
3. Nishitani, S.; Kurata, N.; Sakata, Y.; Misumi, S. *J. Am. Chem. Soc*. **1983**, *105*, 7771-7774
4. Fleming, G.R.; Martin, J. L.; Breton, J. *Nature* **1988**, *333*, 190-192
5. Martin, J.L.; Breton, J.; Hoff, A.J.; Migus, A.; Antonettl, A. *Proc. Nati. Acad. Sci. USA* **1986**, *83*, 957-961
6. Blazyk, J.L.; Gassner, G.T.; Lippard, S.J. *J. Am. Chem. Soc.* **2005**, *127*, 17364-17376
7. Gray, H.B.; Winkler, J.R. *Proc. Nati. Acad. Sci. USA* **2002**, *102*, 3534-3539
8. Gray, H.B.; Winkler, J.R. *Q. Rev. Biophys.* **2003**, *36*, 341-372
9. Bolton, J.R.; Mataga, N.; Mclendon G. Electron Transfer in Inorganic, Organic and Biological Systems, Advances in Chemistry Series, vol. 228, American Chemical Society, Washington, DC, **1991**.
10. Matty J. (Ed.), Photoinduced Electron Transfer, Topics in Current Chemistry, vol. 163, Springer Verlag, Berlin, **1992**.
11. Chanton, M.; Fox, M.A. Photoinduced Electron Transfer, vol. 1–4, Elsevier, New York, **1988**.
12. Jortner, J.; Bixon, M. (Eds.), Electron Transfer from Isolated Molecules to Biomolecules, Advances in Chemical Physics parts 1 & 2, vols. 106 & 107, Wiley, New York, **1999**.
13. Wasielewski, M.R. Photoinduced *Chem. Rev.* **1992**, *92*, 435-461
14. Karkas, M. D.; Johnston, E.V.; Akermark, B. *Acc. Chem. Res.* **2014**, *47*, 100-111
15. Noy, D.; Moser, C.C.; Dutton, P.L. *Biochim. Biophys. Acta*. **2006**, *1757*, 90-105
16. Chan, W.; Tritsch, J.R.; Zhu, X.Y. *J. Am. Chem. Soc.* **2012**, *134*, 18295−18302
17. Krishnamurthy, S.; Kamat, P.V.. *Chem. Phys. Chem.* **2014**, *15*, 2129–2135
18. Meyer, T.J *Acc. Chem. Res.* **1989**, *22*, 163-170
19. Gratzel, M., (Ed.) Energy Resources through Photochemistry and Catalysis; Academic Press: New York, **1983**.
20. Grätzel, M. *J. Photochem. Photobiol. C Photochem. Rev*. **2003**, *4*, 145–153.
21. Marcus, R.A. *J. Chem. Phys*. **1956**, *24*, 966-978
22. Marcus, R.A. *J. Chem. Phys*. **1957**, *26*, 867-871
23. Marcus, R.A. *J. Chem. Phys*. **1957**, *26*, 872-877

24. Marcus, R.A. *J. Electroanal. Chem.* **2000**, *483*, 2-6
25. Marcus, R.A. *Discuss. Faraday Soc.*, **1960**, *29*, 21-31
26. Ghosh, S.; Sahu, K.; Mondal, S. K.; Sen, P.; Bhattacharyya, K. A. *J. Chem. Phys.* **2006**, *125*, 054509-1-7
27. Rehm, D.; Weller, A. *Isr. J. Chem.* **1970**, *8*, 259-271
28. Bock, C. R.; Meyer, T. J.; Whitten, D. G. *J. Am. Chem. Soc.* **1975**, *97*, 2909-2911
29. Nagle, J. K.; Dresick, W. J.; Meyer, T. J. *J. Am. Chem. Soc.* **1979**, *101*, 3993-3995
30. Scheerer, R.; Graetzel, M. *J. Am. Chem. Soc.* **1977**, *99*, 865–871
31. Eriksen, J.; Foote, C.S. *J. Phys. Chem.* **1978**, *82*, 2659–2662
32. Ballardini, R.; Varani, G.; Indelli, M. T.; Scandola, F.; Balzani, V *J. Am. Chem. Soc*. **1978**, *100*, 7219–7223
33. Scandola, F.; Balzani, V. *J. Am. Chem. Soc*. **1979**, *101*, 6140–6142
34. Balzani, V.; Scandola, F.; Orlandi, G.; Sabbatini, N.; Indelli M. T. *J. Am. Chem. Soc*. **1981**, *103*, 3370–3378
35. Creutz,C.; Sutin, N. *J. Am. Chem. Soc.* **1977**, *99*, 241–243
36. Rosspeintner, A.; Koch, M.; Angulo, G.; Vauthey, E. *J. Am. Chem. Soc.* **2012**, *134*, 11396−11399
37. Koch, M.; Rosspeintner, A.; Angulo, G.; Vauthey, E. *J. Am. Chem. Soc.* **2012**, *134*, 3729-3736
38. Rosspeintner, A.; Vauthey, E. *Phys. Chem. Chem. Phys.* **2014**, *16*, 25741-25754
39. Navalon, S.; Miguel, M.; Martin, R.; Alvaro, M.; Garcia, H. *J. Am. Chem. Soc*. **2011,** *133*, 2218–2226
40. Hayashi, T.; Takimura, T.; Ogoshi, H. *J. Am. Chem. Soc*. **1995**, 117, 11606-11607
41. Nakato, T.; Watanabe, S.; Kamijo, Y.; Nono, Y. *J. Phys. Chem. C* **2012,** *116*, 8562−8570
42. Kavarnos, G. J.; Turro, N. J. *Chem. Rev.* **1986**, *86*, 401-449
43. Nad, S.; Pal, H. *J. Phys. Chem. A.* **2000**, *104*, 673-680
44. Marcus, R. A.; Sutin, N. *Biochimica. Biophysica. Acta* **1985**, *811*, 265-322
45. Watanabe, T.; Honda, K. *J. Phys. Chem.* **1982**, *86*, 2617-2619
46. Miyasaka, H.; Masuhara, H.; Mataga, N. *Laser. Chem.* **1983**, *1*, 357-386
47. Foggi, P.; Pettini, L.; Santa, I.; Righini, R.; Califano, S. *J. Phys. Chem.* **1995**, *99*, 7439-7445
48. Peon, J.; Tan, X.; Hoerner, J. D.; Xia, C.; Luk, Y. F.; Kohler, B. *J. Phys. Chem. A* **2001**, *105*, 5768-5777.

Chapter 3

Part B

Decoupling the Diffusion from Bimolecular Photoinduced Electron Transfer Reaction: A Combined Ultrafast Spectroscopic and Kinetic Analysis

Puspal Mukherjee and Pratik Sen *Phys. Chem. Chem. Phys.*, **2017**, *19*, 11220-11229.

3.B.1. Introduction

In chemical kinetics, fast reactions are one of the important topics of discussion, and among them, diffusion controlled reactions are of primary interest for their involvement in many important chemical, physiological and biological processes.[1-4] Diffusion, defined as the migration of neutral molecules and ions in the absence of any external electric field, is of profound concern for chemical reactions and processes happening in gaseous, condensed or biological medium.[1-7] In a biological system where macromolecules are always diffusing, the said process becomes an integral part of many mechanisms such as substrate binding in proteins, translocation of proteins in a nucleic acid, binding of oxygen in red blood cells, transport of substances through the cell wall, etc.[2,8,9] One of the well-studied reactions in chemistry is enzyme catalysis reaction which was the among the first few bimolecular reactions, which were successfully modeled using the theory of spherically symmetric diffusion process.[10-11] Perhaps the most prominent effect of diffusion on the overall kinetics of a reaction can be observed in the case of very rapid bimolecular events due to the small size of the molecule and short diffusional distance. This phenomenon is very common in the case of physical or chemical reactions stimulated by light (e.g. photoinduced electron transfer) or radiation (e.g. reactions of solvated electrons).[12-13]

Bimolecular fluorescence quenching through excited state energy transfer, charge transfer and electron transfer are overall diffusion controlled reactions in solutions.[12-15] Examples of such processes are singlet and triplet quenching by oxygen, quenching of tryptophan fluorescence by imidazole, charge transfer quenching of xanthenium and thioxanthenium carbocations, etc.[12-18] These are only a few examples of such processes studied earlier. In the present work, however, I am only interested in photoinduced electron transfer reactions in the low-viscous medium. These types of reactions are characterized by the formation of an encounter complex between a photoexcited donor and acceptor or vice-versa through diffusion.[19-20]

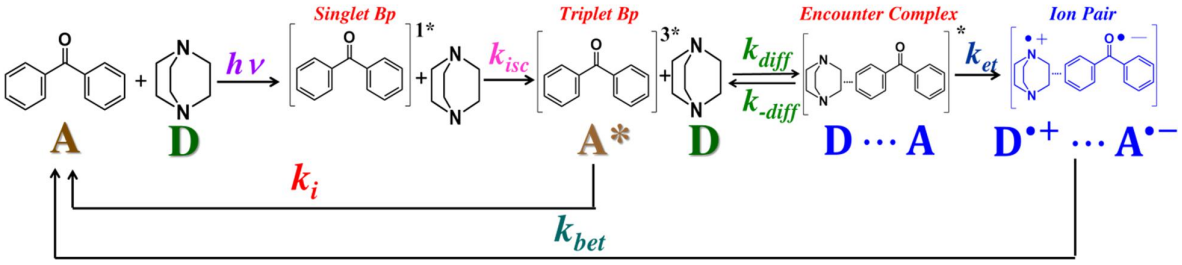

Scheme 3.B.1. Kinetic representation of bimolecular photoinduced electron transfer reaction between benzophenone (Bp, A) and 1,4-diazabicyclo[2.2.2]octane (DABCO, D).

After the formation of the encounter complex, electron transfer occurs between the donor and the acceptor molecule, generally at a rate faster than that of diffusion. The process has been represented schematically in a simplified form in Scheme 3.B.1.[19-21] In the scheme, [D·····A] represent the encounter complex and [$D^{\cdot+}$·····$A^{\cdot-}$] represent the ion pair generated in the reaction. Forward and backward rate constants are given by k_{diff} and k_{-diff}, rate of electron transfer is given by k_{et} and deactivation of the ion pair to the ground state is given by k_{bet}.[20-21] Though many other processes like dissociation, triplet recombination, excited state reaction, etc. may follow the electron transfer step, we have considered this simple scheme. The well-known relation between quenching rate constant (k_q), diffusional rate constant (k_{diff}) and electron transfer rate constant (k_{et}) can be derived from kinetics of scheme 3.B.1. after steady state approximation applied to the intermediates as shown in chapter 1 and is given by [20-22]

$$\frac{1}{k_q} = \frac{1}{k_{diff}} + \frac{1}{k_{et}} \qquad (3.B.1)$$

According to equation 3.B.1, if $k_{et} \gg k_{diff}$, then the rate determining step of the reaction will be diffusion and $k_q \cong k_{diff}$. Now, the rate constant for diffusion is given by

$$k_{diff} = 4\pi R^* D N_A \qquad (3.B.2)$$

In the above equation, D is the sum of diffusion coefficients of the two reactants in solution, N_A is the Avogadro's number and R^* is the maximum distance at which the reaction can occur. Now, if we assume that the hydrodynamic radius of both the species are same (which is of course an optimistic assumption)

and applying Stokes-Einstein relation then, we arrive at the relation between k_{diff} and viscosity coefficient (η) as follows[23]

$$D = \frac{kT}{6\pi\eta a} \quad (3.B.3)$$

$$k_{diff} = \frac{8RT}{3\eta} \quad (3.B.4)$$

Here, k is Boltzmann constant, a is hydrodynamic radii, R is the universal gas constant and T is temperature. In an electron transfer reaction, donor and acceptor molecules form encounter complex through diffusion and then electron transfer occurs within the encounter complex leading to the formation of ion-pair intermediates. The character of the ion-pair shall depend on the nature of the medium in which the reaction occurs. In scheme 3.B.1. I have shown the ion-pair as contact ion pair (CIP) which is the most common intermediate formed in almost every PET reaction. Now if the environment is a polar solvent, then the contact ion pair undergoes a separation to form the solvent separated ion pair (SSIP).[24-26] While CIP is more explored through studies of exciplex formation, SSIP is less investigated due to its dynamic nature. Identification of the ion-pair formed during such reaction has been done previously through flash photolysis experiments and in recent years through sub-picosecond transient absorption measurements.[22,24-27] In the previous chapter, I have characterized the ion-pair during the PET reaction between pyrene and methyl viologen and successfully predicted the rate of electron transfer from femtosecond transient absorption measurements.[22] However, the most used technique employed to study PET reactions is fluorescence up-conversion and TCSPC measurements. There are several reports published earlier, where the authors have used these two techniques to study the well-known Marcus inversion.[28-32]These measurements relied upon the non-exponential nature of the fluorescence transients of the excited fluorophore in presence of quencher. It has been discovered that the ultrashort component of the decay remains free from the effect of diffusion and can be used as the actual rate of electron transfer.[29] This is possible due to the fact that fluorescence quenching is a non-Markovian process.[33] Once the fluorophore is excited, it will always find some quencher in its vicinity

and the ultrafast component of the decay shall give k_{et}. However, concerns have been raised on the observed data about the effect of viscosity.[29] The important question remains is, how the nature of the signal shall change if we change the viscosity of the solution. Previously, Scully *et al.* have analyzed the apparent discrepancy in diffusion coefficient obtained from the Stern-Volmer experiment and Stokes-Einstein-Debye theory, and designated the mismatch to the nature of the exciplex.[34] Diffusional encounter theory has previously been employed to analyze fluorescence quenching experiment assuming quenching rate constant itself is a time-dependent quantity.[35] Ultrafast time-resolved infrared spectroscopy has also been used to identify and to measure the rate of ion-pair and exciplex formation.[36,37] Despite several efforts in the past, the decoupling of the role of diffusion from the measured rate of electron transfer is not trivial till date. In this report, we have tried to tackle this enormous challenge in a very simple way.

For this purpose, I have studied a common photoinduced electron transfer reaction between benzophenone (Bp) and 1,4-diazabicyclo[2.2.2]octane (DABCO) [scheme 3.B.2] in different compositions of acetonitrile and 1-butanol solvent mixtures. This solvent mixture gave a range of viscosity to study the viscosity effect. As predicted by the Marcus theory, changing the solvent shall change the solvent reorganization energy, and consequently k_{et} shall change. However, the change in the rate of diffusion due to change in viscosity should be seen even if k_{et} changes. Benzophenone is a well-known electron acceptor, which forms a radical anion upon accepting the electron.[38] The reason we chose DABCO is that the CT complex formed between Bp and DABCO is well characterized, and it is the only aliphatic amine whose CT complex with Bp is observable inside the time window of the setup (described later).[39]

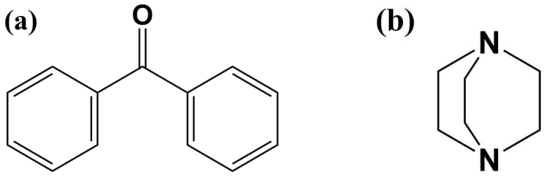

Scheme 3.B.2. Molecular structure of (a) benzophenone (Bp) and (b) 1,4-diazabicyclo[2.2.2]octane (DABCO).

3.B.2. Results

To check the viscosity dependence of photoinduced electron transfer reactions I have studied the PET between Bp and DABCO in acetonitrile — 1-butanol binary solvent mixture using femtosecond broadband transient absorption spectroscopy. In the previous transient absorption study of the PET reaction between pyrene and methyl viologen, I have proposed that with an increase in medium viscosity, the onset of the rise signal of the methyl viologen radical cation shifts to longer time regime.[22] The proposed reasoning was that it takes a finite time for the reactants to approach each other to form the encounter complex. It implies that for a low viscosity solvent, encounter complex formation takes shorter time and for high viscosity solvent it should take longer time. Once a perceptible amount of encounter complex is formed then the electron transfer reaction can be tracked through the formation of radical cation/anion. Therefore, depending on the solvent viscosity, there shall be a delay in the appearance of transient absorption signal of radical cation/anion intermediate. Thus, through femtosecond transient absorption spectroscopy we may observe the effect of viscosity in the obtained kinetics. However, the rapid PET reaction between pyrene and methyl viologen and the insolubility of methyl viologen in less polar solvents barred us from observing the viscosity effect in quantifiable range. These problems were minimized by taking the Bp-DABCO system. Bp is known to be an excellent electron acceptor with blue colored radical anion formation.[39]The PET mainly occurs to the triplet state of Bp, and it has been extensively studied with many electron donors such as dimethylaniline, diethylaniline, DABCO, etc.[39,41-43] For this work I have chosen Bp-DABCO pair because the PET between them can be easily monitored in our transient absorption setup without interference from other processes such as proton transfer, and both of the molecules are soluble in most of the organic solvents. The change of viscosity of acetonitrile and 1-butanol mixture composition has been previously reported by Nikam *et al*.[44] In figure 3.B.1a, the transient absorption spectra obtained at different time intervals for a mixture of 10 mM Bp with 300 mM DABCO in pure acetonitrile is given. We can clearly see the

formation of triplet benzophenone (^{3}Bp*) around 525 nm at early times of the dynamics.[39,42,43,45,46]

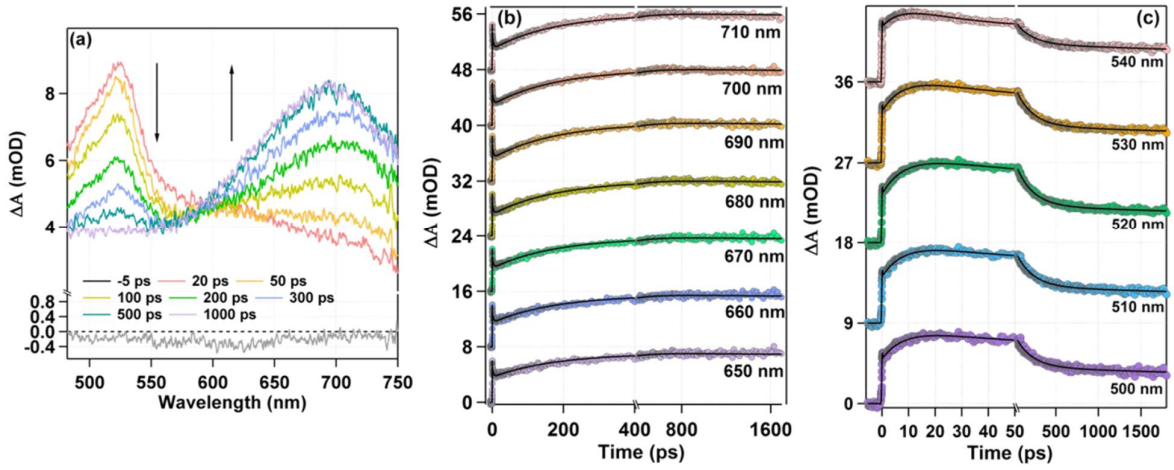

Figure 3.B.1. (a) Transient absorption spectra at different times (b) kinetics of Bp$^{\cdot-}$ (c) kinetics of ^{3}Bp* at different wavelengths for the 10 mM Bp / 300 mM DABCO in acetonitrile. The sample was excited at 266 nm. Black lines represent the global fitting of the experimental data.

With the progress of time, this peak diminishes, and a new peak around 700 nm grows, which we have assigned to the formation of Bp$^{\cdot-}$.[39,45,46] The assignment of these two peaks were discussed in great details for the exactly same system in many previous publications, and there was some controversy regarding the formation of contact ion-pair and solvent separated ion pair in protic and aprotic solvents.[39,45-48] Therefore I am not discussing here the origin of these peaks. However, I would like to point out that the existence of the isosbestic point in figure 3.B.1a around 595 nm. The existence of this isosbestic point indicates the electron transfer from the triplet state of Bp. Thus the time scales for the decay of ^{3}Bp* signal and the growth of Bp$^{\cdot-}$ signal should match closely. From the kinetics, at different wavelength as depicted in figure 3.B.1b, it can be seen that the increase of Bp$^{\cdot-}$ signal reaches almost a flat region after 1 ns, similar to the observation by Miyasaka *et al.*[45] The same can be said for the kinetics around 525 nm, i.e. kinetics of ^{3}Bp*, which attained a valley at the same time-scale as depicted in figure 3.B.1c. I have fitted the kinetics with a sum of a three exponential function using global

fitting method over the 660 – 720 nm wavelength range, i.e. the whole range of $Bp^{\cdot-}$ spectra, and listed them in table 3.B.1.

Table 3.B.1. Global fitting parameters obtained from the fitting of kinetic data for $Bp^{\cdot-}$ in acetonitrile/1-butanol binary solvent mixtures of varying proportions. The number in parenthesis is the reported value in the literature.

% 1-Butanol in Acetonitrile (v/v)	Viscosity [a] (cP)	Fitting Wavelength Range (nm)	τ_1 (ps) (decay)	τ_2 (ps) (rise)	τ_3 (ps) (decay)
0	0.342	650-720	2.1	244±20 (300 [b])	15000 (fixed)
10	0.348	650-720	2.2	336±25	25000 (fixed)
20	0.387	640-710	5.3	440±30	25000 (fixed)
30	0.403	620-700	13.6	705±40	25000 (fixed)
40	0.441	610-690	15.2	1000±40	25000 (fixed)
50	0.484	610-680	39.0	1130±30	-

[a] data taken from reference 44 [b] data taken from reference 45

The rise component has been assigned to the rate of forward electron transfer. We can see from the table 3.B.2 that the rate of decay of $^3Bp^*$ also matches with the growth of $Bp^{\cdot-}$. This is to emphasize that previously Devadoss *et al.* and Peters *et al.* concluded that the correspondence of these two rate processes is the proof that electron transfer between the triplet state of Bp and DABCO.[39,46] The same experiment has been performed in the acetonitrile/1-butanol binary solvent mixture of varying proportions, and the results are shown in figure 3.B.2. In every case, I have observed an isosbestic point, which confirmed electron transfer from triplet state of Bp. The correspondence of rate of decay of $^3Bp^*$ with the growth of $Bp^{\cdot-}$ have also been observed in every case and we have listed all of them in tables 3.B.1 and 3.B.2. However, the maximum delay of our setup barred me from observing the charge recombination process as it occurs on a longer time scale. I would like to point out that there is a change in rate constants and shifts in the maxima position of $Bp^{\cdot-}$ absorption band. The reason for such observation is sufficiently discussed in many previous publications, and therefore I am not discussing it here.[39,45,46]

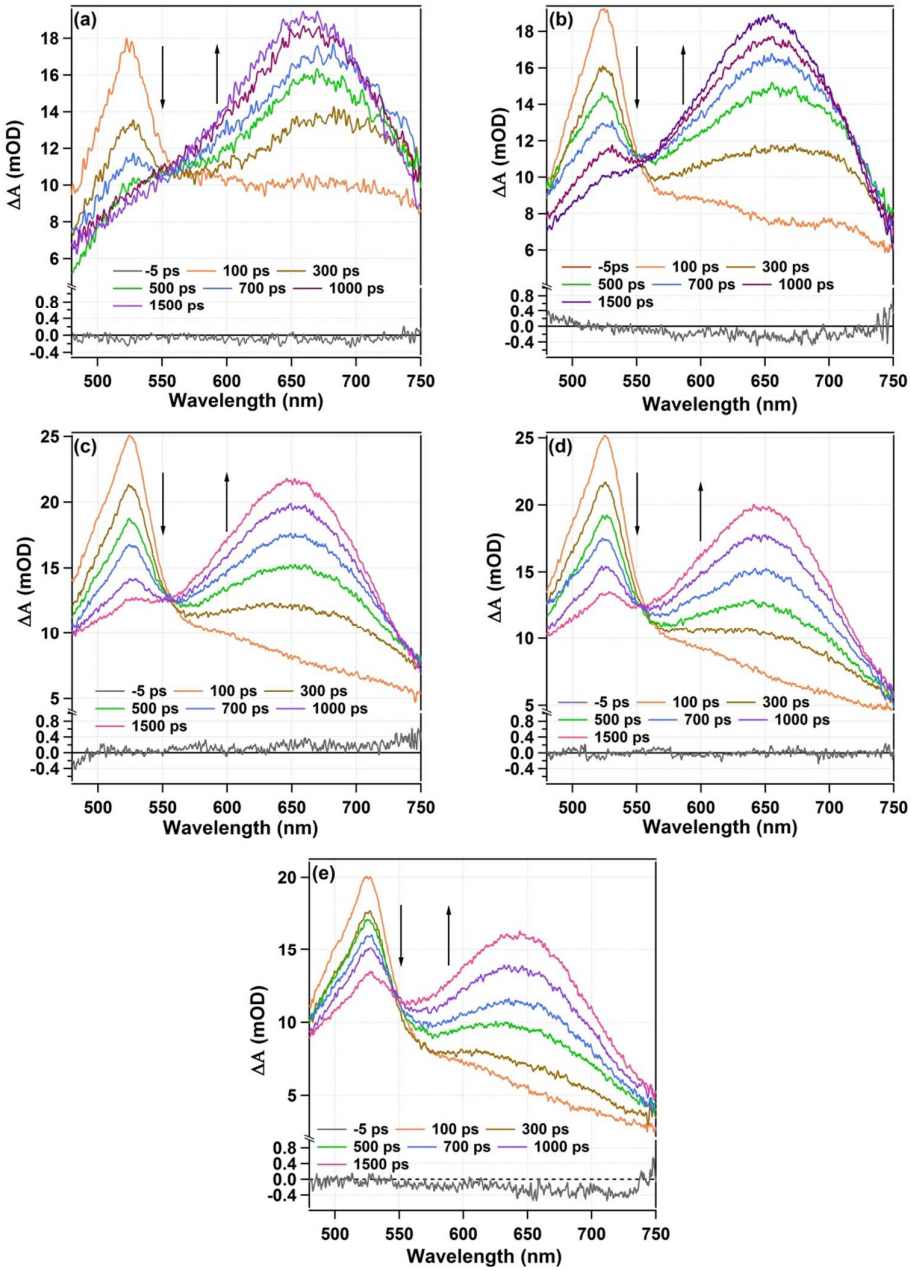

Figure 3.B.2. Transient absorption spectra at different times for 10 mM Bp / 300 mM DABCO in (a) 10%, (b) 20%, (c) 30%, (d) 40% and (e) 50% (v/v) of 1-Butanol in acetonitrile. The samples were excited at 266 nm.

With a change in the composition of acetonitrile/1-butanol mixture the viscosity of the mixture changes monotonically, which I also have listed in table 3.B.1.[44] When I have studied the PET reaction between Bp and DABCO in these mixtures through transient absorption spectroscopy, I saw an interesting feature, i.e. with the increase in viscosity of the solvent mixture the ^{3}Bp* became long-

lived and the onset of the $Bp^{\cdot-}$ rise signal shifted at a longer time. For elucidation of the point, I have presented the contour plots of the transient absorption data in figure 3.B.3. As can be seen here, the peak due to $^3Bp^*$ around 525 nm become long-lived and the peak due to $Bp^{\cdot-}$ around 690 nm appears at longer times, with increase in 1-butanol percentage in the mixture. A quick glance to figure 3.B.3 reveals that the $^3Bp^*$ signal diminishes in acetonitrile within 400 ps, but for 50% 1-butanol in acetonitrile, $^3Bp^*$ signal can be observed until 1800 ps. Similarly, the signal of $Bp^{\cdot-}$ can be seen from 60 ps in case of pure acetonitrile, which starts coming around 500 ps in case of 50% 1-butanol in acetonitrile.

Table 3.B.2. Global fitting parameters obtained by fitting the Bp^3* kinetics data over 500 – 540 nm in acetonitrile/1-butanol binary solvent mixtures of varying proportions. The number in parenthesis is the reported value in the literature.

% 1-Butanol in Acetonitrile (v/v)	Viscosity [a] (cP)	τ_1 (ps) (decay)	τ_2 (ps) (rise)	τ_3 (ps) (decay)	τ_4 (ps) (decay)
0	0.342	8.5	20.8 (20.0[b])	241±25 (270[c])	10000 (fixed)
10	0.348	7.4	22.6	310±30	50000 (fixed)
20	0.387	8.4	23.4	444±30	50000 (fixed)
30	0.403	7.8	29.5	690±40	50000 (fixed)
40	0.441	8.1	33.5	950±50	50000 (fixed)
50	0.484	8.2	25.2	1070±40	50000 (fixed)

[a] data taken from reference 44 [b] data taken from reference 39 [c] data taken from reference 45

Marcus theory signifies that with the change in solvent reorganization energy the rate of electron transfer changes. As acetonitrile and 1-butanol do not have same polarity or dielectric constant, it is expected that solvent reorganization energy will change in its binary solvent mixture, followed by $k_{et.}$ Moreover, the oxidation and reduction potential of donor and acceptor shall change with the change in the medium, which will also change the reaction exergonicity. Thus the rate of ion pair formation i.e. rise component in transient absorption signal of $Bp^{\cdot-}$, is expected to vary with increasing amount of 1-butanol in acetonitrile. On the other hand, the encounter complex formation in the excited state is expected to be affected by the viscosity of the medium, because this process is a bimolecular diffusion controlled reaction. With the increase in bulk viscosity of the medium, I

have observed a delayed formation of $Bp^{\cdot-}$ in my experiments. Assuming that electron transfer starts immediately after encounter complex formation and I can minimally detect a certain amount of $Bp^{\cdot-}$, a correspondence between the viscosity and delaying of signal can be made. When I excite the sample, the singlet state of Bp is populated, which goes to triplet Bp, followed by the formation of encounter complex between $^3Bp^*$ and DABCO, which got delayed with increase in solvent viscosity. Then the electron transfer took place within the encounter complex and the signal for $Bp^{\cdot-}$ can be detected. Therefore the step of encounter complex formation, which got delayed more and more with increase in 1-butanol proportion, accounts for the delayed observation of $Bp^{\cdot-}$ signal. Perhaps it can be more aptly justified if I can support through the kinetic analysis of scheme 3.B.1.

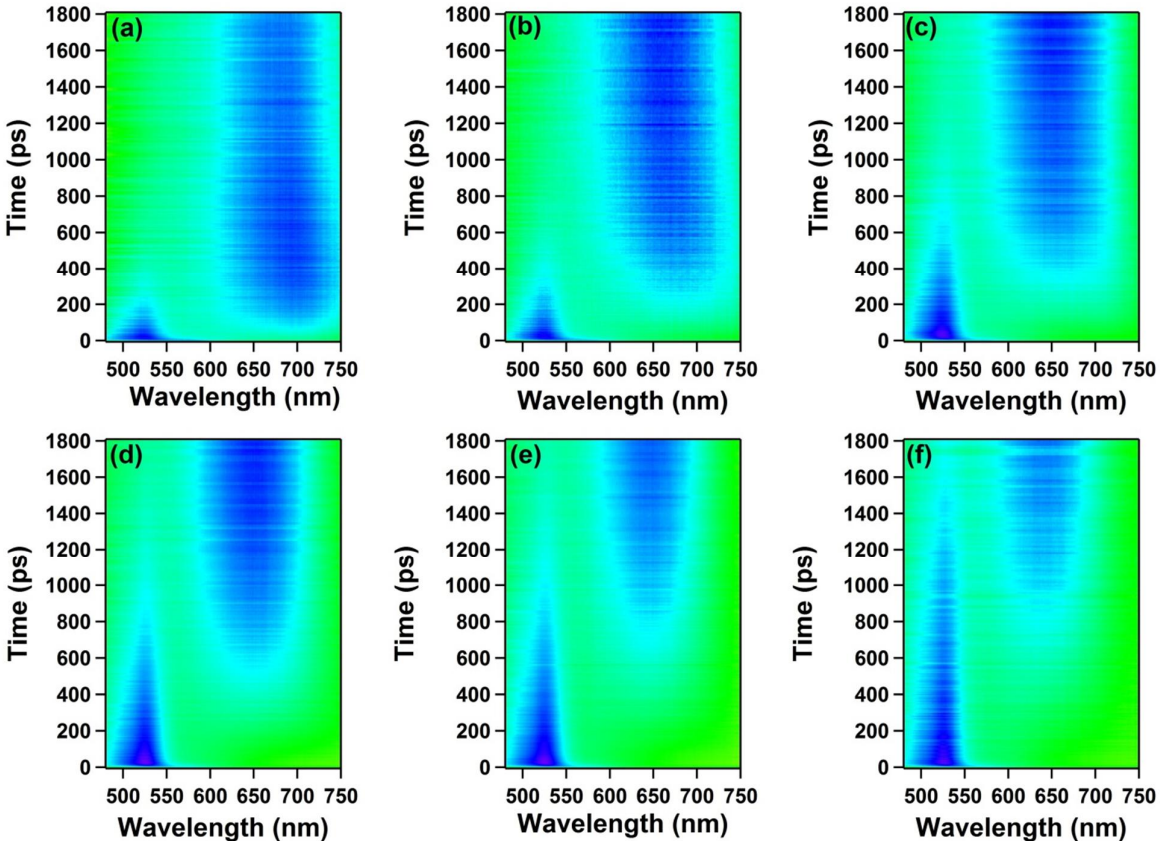

Figure 3.B.3. Evolution of transient absorption signal with time over 480 – 750 nm region for 10 mM Bp / 300 mM DABCO in (a) 0%, (b) 10%, (c) 20%, (d) 30% (e) 40% and (f) 50% (v/v) of 1-Butanol in acetonitrile. The samples were excited at 266 nm.

3.B.3. Discussion

Following the mechanism proposed in scheme 3.B.1, I have analyzed the time evolution of the species involved in the reaction in the following way.

$$\frac{d[A^*]}{dt} = -k_i[A^*] - k_{diff}[D][A^*] + k_{-diff}[D \cdots A]^* \quad (3.B.5)$$

$$\frac{d[D\cdots A]^*}{dt} = k_{diff}[D][A^*] - k_{-diff}[D \cdots A]^* - k_{et}[D \cdots A]^* \quad (3.B.6)$$

$$\frac{d[D^{\cdot+} \cdots A^{\cdot-}]}{dt} = k_{et}[D \cdots A]^* - k_{bet}[D^{\cdot+} \cdots A^{\cdot-}] \quad (3.B.7)$$

In this case, the concentration of donor, i.e. DABCO, was kept much higher than that of Bp and consequently even higher than the concentration of Bp*. Thus during the PET reaction we have assumed that $[D]$ remains constant. This assumption is also valid for other cases of PET, as the quencher concentration is always kept at much higher concentration than that of fluorophore. Laplace transformation of equation 3.B.5 gives

$$L([A^*]) = \frac{[A^*]_0 + k_{-diff}L([D\cdots A]^*)}{s + k_i + k_{diff}[D]} \quad (3.B.8)$$

Considering the initial concentration of the encounter complex is zero, the Laplace transformation of equation 3.B.6 yields

$$L([D \cdots A]^*) = \frac{k_{diff}L([A^*])[D]}{s + k_{-diff} + k_{et}} \quad (3.B.9)$$

In the above equations, "s" is the transform variable. Replacing the value of $L([A^*])$ from equation 3.B.8 in equation 3.B.9, we get

$$L([D \cdots A]^*) = \frac{k_{diff}[D][A^*]_0}{(s+\alpha)(s+\beta)} \quad (3.B.10)$$

where

$$\alpha + \beta = k_i + k_{diff}[D] + k_{-diff} + k_{et} \quad (3.B.11)$$

$$\alpha\beta = k_{-diff}k_i + k_{et}k_i + k_{et}k_{diff}[D] \quad (3.B.12)$$

The inverse Laplace transformation of equation 3.B.10 shall yield the kinetics of $[D \cdots A]^*$ as

$$[D \cdots A]^* = \frac{k_{diff}[D][A^*]_0}{(\beta-\alpha)}[e^{-\alpha t} - e^{-\beta t}] \quad (3.B.13)$$

Employing Laplace transformation on equation 3.B.7 and using equation 3.B.10 we get

$$L([D^{\cdot+} \cdots A^{\cdot-}]) = \frac{k_{diff}k_{et}[D][A^*]_0}{(s+\alpha)(s+\beta)(s+k_{bet})} \quad (3.B.14)$$

Inverse Laplace transformation of equation 3.B.14 produces kinetics of $[D^{\cdot+} \cdots A^{\cdot-}]$ as

$$[D^{\cdot+} \cdots A^{\cdot-}] = -k_{diff}k_{et}[D][A^*]_0\left[\frac{(k_{bet}-\beta)e^{-\alpha t}+(\alpha-k_{bet})e^{-\beta t}+(\beta-\alpha)e^{-k_{bet}t}}{(k_{bet}-\beta)(\alpha-k_{bet})(\beta-\alpha)}\right] \quad (3.B.15)$$

The values of α and β is given by (from equations 3.B.11 and 3.B.12)

$$\alpha, \beta = \frac{1}{2}\left[(k_i + k_{diff}[D] + k_{-diff} + k_{et}) \pm \sqrt{\left(k_i + k_{diff}[D] + k_{-diff} + k_{et}\right)^2 - 4\left(k_{-diff}k_i + k_{et}k_i + k_{et}k_{diff}[D]\right)}\right] \quad (3.B.16)$$

Now, to solve α, β one can use some simple assumptions. Firstly, for a PET reaction, the rate of intrinsic fluorescence decay (k_i) is much smaller compared to rate of diffusion (k_{diff}) and rate of forward electron transfer (k_{et}). In the present case the excited state lifetime of Bp in acetonitrile is ~14 μS, which is ~10^4 times higher compared to diffusion and electron transfer time scale. Thus as a valid reason, I can drop the terms involving k_i and rewrote the equation 3.B.16 as

$$\alpha, \beta = \frac{1}{2}\left[(k_{diff}[D] + k_{-diff} + k_{et}) \pm \sqrt{\left(k_{diff}[D] + k_{-diff} + k_{et}\right)^2 - 4\left(k_{et}k_{diff}[D]\right)}\right] \quad (3.B.17)$$

Next I can assume that $k_{diff}[D] \approx k_{-diff}$,[20,21] which will modify equation 3.B.17 to

$$\alpha,\beta = \frac{1}{2}\left[(2k_{diff}[D] + k_{et}) \pm \sqrt{\left(2k_{diff}[D] + k_{et}\right)^2 - 4\left(k_{et}k_{diff}[D]\right)}\right] \quad (3.B.18)$$

Now, three different situations can arise. First, $k_{et} \ll k_{diff}[D]$. Applying this condition we get, $\alpha = 2k_{diff}[D] + \frac{k_{et}}{2}$ and $\beta = \frac{k_{et}}{2}$.

Using these two roots we can write equation 3.B.15 as

$$[D^{\cdot+} \cdots A^{\cdot-}] = k_{diff}k_{et}[D][A^*]_0 \times \left[\frac{\left(k_{bet}-\frac{k_{et}}{2}\right)e^{-\left(2k_{diff}[D]+\frac{k_{et}}{2}\right)t}+\left(2k_{diff}[D]+\frac{k_{et}}{2}-k_{bet}\right)e^{-\frac{k_{et}}{2}t}-2k_{diff}[D]e^{-k_{bet}t}}{\left(k_{bet}-\frac{k_{et}}{2}\right)\left(2k_{diff}[D]+\frac{k_{et}}{2}-k_{bet}\right)2k_{diff}[D]}\right] \quad (3.B.19)$$

In equation 3.B.19, the coefficient of $e^{-\frac{k_{et}}{2}t}$ has negative sign as $k_{et}, k_{bet} \ll k_{diff}[D]$ and therefore signifies the formation of radical ion-pair.

The next condition is $k_{et} \approx k_{diff}[D]$, which leads us to $\alpha,\beta = \frac{(3\pm\sqrt{5})}{2}k_{et}$ or $\alpha,\beta = \frac{(3\pm\sqrt{5})}{2}k_{diff}[D]$.

$$[D^{\cdot+} \cdots A^{\cdot-}] = k_{diff}[D][A^*]_0 \left[\frac{\left(k_{bet}-\frac{(3-\sqrt{5})}{2}k_{diff}[D]\right)e^{-\frac{(3+\sqrt{5})}{2}k_{diff}[D]t}+\left(\frac{(3+\sqrt{5})}{2}k_{diff}[D]-k_{bet}\right)e^{-\frac{(3-\sqrt{5})}{2}k_{diff}[D]t}-\sqrt{5}k_{diff}[D]e^{-k_{bet}t}}{\sqrt{5}\left(k_{bet}-\frac{(3-\sqrt{5})}{2}k_{diff}[D]\right)\left(\frac{(3+\sqrt{5})}{2}k_{diff}[D]-k_{bet}\right)}\right] \quad (3.B.20)$$

In the above equation, I have replaced all the k_{et} terms with $k_{diff}[D]$. Although it is unlikely that they are exactly equal, however they can be of the same order as I have seen in Bp-DABCO system in acetonitrile/1-butanol binary solvent mixture. Equation 3.B.20 shows that the coefficient of one of the exponential term has negative sign if $k_{bet} < k_{diff}[D]$, and therefore signifies the formation of radical ion-pair.

The last situation, $k_{et} \gg k_{diff}[D]$, as well as, $k_{bet} > k_{diff}[D]$ is also extremely likely and important because it is the steady state condition on encounter complex. I have encountered a similar situation to this while studying PET

between pyrene and methyl viologen in methanol and between coumarins and viologens in micellar media.[22,28] Applying steady state approximation on equation 3.B.6 we get

$$[D \cdots A]^* = \frac{k_{diff}[D][A^*]}{k_{-diff}+k_{et}} \qquad (3.B.21)$$

Using equation 3.B.21 and under the assumption $k_{et} \gg k_{diff}[D], k_{-diff}, k_i$ we get the kinetics of ion pair as

$$[D^{\cdot+} \cdots A^{\cdot-}] = \frac{k_{et}k_{diff}[D][A^*]_0}{(k_{et}+k_{-diff})(k_{et}-k_{bet})}(-e^{-k_{et}t} + e^{-k_{bet}t}) \qquad (3.B.22)$$

In equation 3.B.22, the formation of encounter complex is given by $e^{-k_{et}t}$. Thus fitting the rise and decay part of the kinetics will give us k_{et} and k_{bet}.[21,23]

Using equations 3.B.15, I have computationally generated the plot of the change in concentration of ion pair with time and represented the same in figure 3.B.4. To achieve this plot I have assumed donor and acceptor concentration to be 0.3 and 0.01 M, which is same as in experimental condition. However, I would like to point out that these values are not relevant as the reaction is taking place in the electronic excited state of the molecule, where the concentrations are not same as that of the ground state. Except for the forward and backward diffusional rate constant all the other values are taken from the Bp-DABCO system in acetonitrile. Despite the qualitative nature of the plots, one can see from figure 3.B.4a that a decrease in the rate of forward diffusion by an order of magnitude delayed the growth of the ion-pair. This is the same feature that I obtained experimentally. It should be noted that the decrease in the forward rate constant of diffusion essentially means increase in the viscosity of the media, which leads to the delayed formation of the encounter complex. I have also varied the backward diffusion rate constant keeping all other rate constants fixed and plotted the formation of ion-pain in figure 3.B.4b. In this case, not much dependence has been observed for the kinetics of ion-pair. Perhaps the best way to understand the effect described above through some quantification. For this purpose, I have assumed that in my

experiment, I can detect the signal of $Bp^{\cdot-}$ at a certain minimum concentration, which I have approximated to be 5% of maximum ion pair formed. In case of 300 mM DABCO (donor) with 10 mM Bp (acceptor), considering a 10% excitation and k_i and k_{-diff} to be 0, I found the maximum concentration of the ion-pair would be ~0.9 mM. This sets my apparent detection limit to be 0.045 mM (5%).

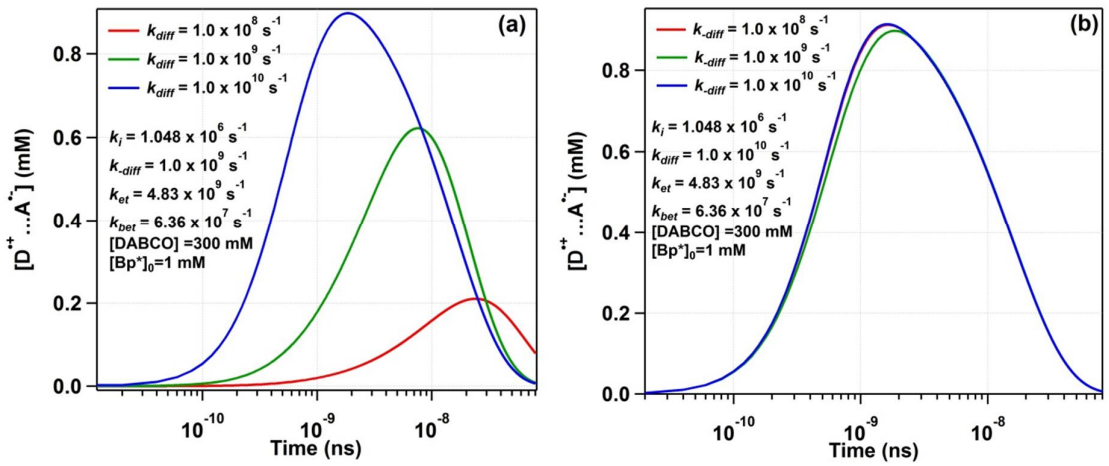

Figure 3.B.4. Time dependence of ion-pair concentration in a bimolecular photoinduced electron transfer reaction as obtained from equations 3.B.15 and 3.B.16.

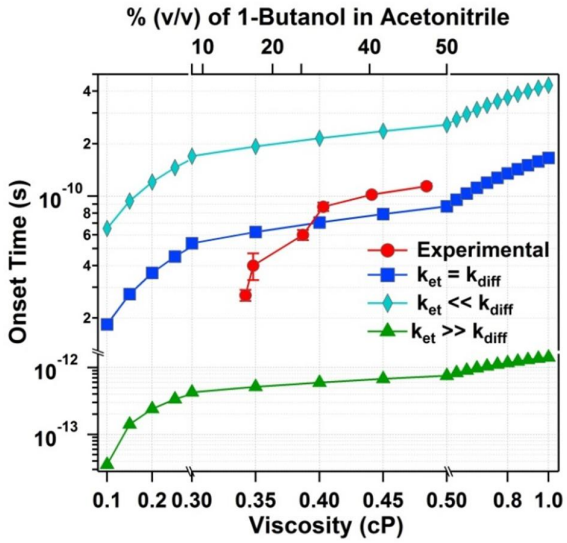

Figure 3.B.5. Onset delay time of ion-pair formation for three limits namely $k_{et} \ll k_{diff}[D]$ (♦, Cyan), $k_{et} = k_{diff}[D]$ (■, Blue) and $k_{et} \gg k_{diff}[D]$ (▲, Green) as calculated from equations 19, 20 and 22, respectively. The plot also contains the experimentally estimated onset delay time of $Bp^{\cdot-}$ (●, Red) for 10 mM Bp / 300 mM DABCO in 0%, 10%, 20%, 30%, 40% and 50% (v/v) of 1-Butanol in acetonitrile.

In table 3.B.3, I have tabulated the time when the said detection limit is reached in figure 3.B.4a and figure 3.B.4b. It is very clear that when I decrease the forward diffusional rate constant (commensurate with the increase in viscosity), keeping rest of the rate constants fixed, the overall time to achieve the observable concentration of the ion-pair increases monotonically. Thus with the increase in the viscosity of the medium we see a delay in the signal of ion-pair formation. On the other hand, when the backward diffusional rate constant is varied, no change in time to witness the observable concentration of the ion-pair has been noticed.

Table 3.B.3. Comparison of time taken to reach an apparent detectable limit of ion-pair in figures 3.B.4a and 3.B.4b.

Rate Constants		Time (ns)
k_{diff} (s^{-1})[a]	k_{-diff} (s^{-1})[a]	when $[D^{\cdot+} \cdots A^{\cdot-}]$ = 0.045 mM
1×10^8	1×10^9	2.16
1×10^9	1×10^9	0.34
1×10^{10}	1×10^9	0.10
1×10^{10}	1×10^8	0.10
1×10^{10}	1×10^9	0.10
1×10^{10}	1×10^{10}	0.10

[a] rest of the rate constants are fixed

The same procedure can be applied to my experimental data too. For each of the solvent mixtures, I have taken the change in ΔOD at wavelength maxima of $Bp^{\cdot-}$ signal and assumed that the least I can detect is 5% of that signal. Following, I have calculated the time taken to achieve the said signal in each solvent mixtures and plotted them against the viscosity of the solvent mixture. With the increase in the viscosity of the medium, the minimum detection time becomes longer. This observation is at par with the conclusion drawn from the kinetic analysis above. However, to take a step further I have calculated the same from equation 3.B.19, 3.B.20 and 3.B.22 under three conditions as stated previously. In figure 3.B.5, both the data obtained from experimental data and using kinetic equations are plotted. Here to note that for the first case, $k_{et} \ll k_{diff}[D]$, I have assumed $k_{diff}[D]$ is 10 times of k_{et} and for the third case, $k_{et} \gg k_{diff}[D]$, I have assumed $k_{diff}[D]$ is 0.1 times of k_{et}. From figure 3.B.5 I can see that maximum onset delay time is

observed for $k_{et} \ll k_{diff}[D]$, followed by $k_{et} \approx k_{diff}[D]$ and $k_{et} \gg k_{diff}[D]$. My experimental data showed that it varies from a condition where $k_{et} > k_{diff}[D]$ to $k_{et} < k_{diff}[D]$, which actually crosses the calculated line for $k_{et} = k_{diff}[D]$, which tells us if experimentally I can have $k_{et} = k_{diff}[D]$, I can get a match with kinetic calculations. Thus the onset delay time can be successfully associated with the change in solvent viscosity, which changes the diffusional rate constants.

3.B.4. Conclusion

Broadband transient absorption spectroscopy led me to quantify the forward rate of electron transfer in a bimolecular PET reaction by observing the formation of the product. This quantification is free from the involvement of any other rate constants, which I have established through the kinetic analysis of the reaction scheme. In this method, I have observed a certain onset delay time for the detectable signal to appear. I have also shown that the onset delay time of the signal arrives from the change diffusional rate constant, which is inversely proportional to solvent viscosity. Thus I conclude that femtosecond transient absorption spectroscopy can be the most useful tool for studying PET.

References

1. L. Cussler, *Diffusion: Mass Transfer in Fluid Systems*, Cambridge University Press, New York, 2009.
2. Mereghetti, P.; Kokh, D.; Mccammon, J. A.; Wade, R. C. *BMC Biophys.* **2011**, *4*, 2.
3. Lin, C. S.; Denton, E. B.; Gaskill, H. S.; Putnam, G. L. *Ind. Eng. Chem.* **1951**, *43* , 2136–2143.
4. Astarita G. and Ocone, R. in *Special Topics in Transport Phenomena*, eds. Astarita, G. and Ocone, R. Elsevier Science, Amsterdam, 2002,. 171–226.
5. Ye, S.; Chen, Z.; Ha, Y.-C.; Wiley, B. J. *Nano Lett.* **2014**, *14* , 4671–4676.
6. Schaeffer, H. A. *J. Non. Cryst. Solids* **1984**, *67*, 19–33.
7. Calef, D. F; Deutch, J. M. *Annu. Rev. Phys. Chem.* **1983**, 493–524.
8. Berg, O. G.; Winter, R. B.; von Hippel, P. H. *Biochemistry* **1981**, *20*, 6929–6948.
9. Shoup, D.; Lipari, G.; Szabo, A. *Biophys. J.* **1981**, *36*, 697–714.
10. Alberty, R.; Hammes, G. G. *J. Phys. Chem.* **1958**, *62*, 154–159.
11. Schurr, J. M. *Biophys. J.* **1970**, *10*, 717–727.
12. *Principles of Fluorescence Spectroscopy*; Lakowicz, J. R., Ed.; Springer US: Boston, MA, 2006.
13. Valeur, B.; Berberan-Santos, M. N. *Molecular Fluorescence*; Wiley-VCH Verlag GmbH & Co. KGaA: Weinheim, Germany, 2012.
14. Rice, S. A. Chapter 2 Diffusion-Controlled Reactions in Solution. In *Comprehensive Chemical Kinetics*; **1985**; Vol. 25, 3–46.
15. Lin, C. S.; Denton, E. B.; Gaskill, H. S.; Putnam, G. L. Diffusion-Controlled Electrode Reactions. *Ind. Eng. Chem.* **1951**, *43* 9, 2136–2143.
16. Patterson, L. K.; Porter, G.; Topp, M. R. *Chem. Phys. Lett.* 1970, *7*, 612–614.
17. Samanta, A.; Gopidas, K. R.; Das, P. K. *J. Phys. Chem.* **1993**, *97*, 1583–1588.
18. Willaert, K.; Engelborghs, Y. *Eur. Biophys. J.* **1991**, *20*, 177–182.
19. Sutin, N. Nuclear, *Acc. Chem. Res.* **1982**, *15*, 275–282.
20. Kavarnos, G. J.; Turro, N. J. *Chem. Rev.* **1986**, *86*, 401–449.
21. Photoinduced Electron Transfer. Topics in Current Chemistry; Matty, J., Ed.; Springer Verlag: Berlin, **1992**; Vol. 163.
22. Mukherjee, P.; Biswas, S.; Sen, P. *J. Phys. Chem. B* **2015**, *119*, 11253–11261.
23. P. W. Atkins, J. DePaula, *Atkins' Physical chemistry*, Oxford University Press, Oxford, 2006.
24. Gould, I. R.; Farid, S. *Acc. Chem. Res.* **1996**, *29*, 522–528.
25. Nad, S.; Pal, H. *J. Phys. Chem. A* **2000**, *104*, 673–680.

26. Rosspeintner A. and Vauthey, E. *Phys. Chem. Chem. Phys.*, **2014**, *16*, 25741–25754.
27. Vauthey, E. *J. Photochem. Photobiol. A Chem.*, **2006**, *179*, 1–12.
28. Mukherjee, P.; Das, A.; Sengupta, A.; Sen, P. *J. Phys. Chem. B*, **2017**, *121*, 1610–1622.
29. Kumbhakar, M.; Manna, A.; Sayed, M.; Kumar, A.; Pal, H. *J. Phys. Chem. B* **2014**, *118*, 10704–10715
30. Kumbhakar, M.; Singh, P. K.; Nath, S.; Bhasikuttan, A. C.; Pal, H. *J. Phys. Chem. B* **2008**, *112* , 6646–6652.
31. Waskasi, M. M.; Kodis, G.; Moore, A. L.; Moore, T. A.; Gust, D. ; Matyushov, D. V. *J. Am. Chem. Soc.*, **2016**, *138*, 9251–9257.
32. Petersson, J.; Hammarström, L. *J. Phys. Chem. B*, **2015**, *119*, 7531–7540.
33. Ghosh, S.; Sahu, K.; Mondal, S. K.; Sen, P.; Bhattacharyya, K. *J. Chem. Phys.*, **2006**, *125*, 54509.
34. Scully, A. D.; Ohtaka, H.; Takezaki, M.; Tominaga, T. *J. Phys. Chem. A*, **2015**, *119*, 2770–2779.
35. Rosspeintner, A.; Koch, M.; Angulo, G.; Vauthey, E. *J. Am. Chem. Soc*., **2012**, *134*, 11396–11399.
36. Koch, M.; Licari, G.; Vauthey, E. *J. Phys. Chem. B*, **2015**, *119*, 11846–11857.
37. .Letrun, R.; Vauthey, E. *J. Phys. Chem. Lett.*, **2014**, *5*, 1685–1690.
38. Peters, K. S.; Freilich, S. C.; Schaeffer, C. G *J. Am. Chem. Soc*., **1980**, *102*, 5701–5702.
39. Peters, K. S.; Lee, J. *J. Phys. Chem.*, **1993**, *97*, 3761–3764.
40. Snellenburg, J. J.; Laptenok, S. P.; Seger, R.; Mullen, K. M.; van Stokkum, I. H. M. *J. Stat. Softw.*, **2012**, *49*, 1-8.
41. Bhattacharyya, K.; Das, P. K. *J. Phys. Chem.*, **1986**, *90*, 3987–3993.
42. Simon, J. D.; Peters, K. S. *J. Am. Chem. Soc*., **1981**, *103*, 6403–6406.
43. Miyasaka, H.; Mataga, N. *Bull. Chem. Soc. Jpn.*, **1990**, *63*, 131–137.
44. Nikam, P. S.; Shirsat, L. N.; Hasan, M. *J. Chem. Eng. Data*, **1998**, *43*, 732–737.
45. Miyasaka, H.; Morita, K.; Kamada, K.; Mataga, N. *Chem. Phys. Lett.*, **1991**, *178*, 504–510.
46. Devadoss, C.; Fessenden, R. W. *J. Phys. Chem.*, **1990**, *94*, 4540–4549.
47. Miyasaka, H.; Morita, K.; Kamada, K.; Mataga, N. *Bull. Chem. Soc. Jpn.*, **1990**, *63*, 3385–3397.
48. Haselbach, E.; Jacques, P.; Pilloud, D.; Suppan, P.; Vauthey, E. *J. Phys. Chem.*, **1991**, *95*, 7115–7117.

Chapter 3

Part C

Bi-molecular Photo-induced Electron Transfer in Static Quenching Regime: Illustration of Marcus Inversion in Micelle

Puspal Mukherjee, Aritra Das, Arunava Sengupta and Pratik Sen *J. Phys. Chem. B*, **2017**, *121*, 1610–1622.

3.C.1. Introduction

Marcus theory for outer sphere electron transfer reactions is one of the most remarkable and paramount achievements in chemistry in the 20th century. The theory of electron transfer, for which Rudolph Marcus was awarded the Nobel Prize in Chemistry in 1992, has already discussed in details in chapter 1 of this thesis. So here, I will only highlight the observations made in confined systems. In this approach, which became popular over the years to obtain MIR is the use of constrained media such as micelle and reverse micelle.[1,2] The primary reason behind this is the slow solvent relaxation time in such confined media. Zusman *et al.* first raised this issue in a report, where they derived a modified pre-exponential factor for Marcus theory, which incorporated the strong solvent interaction in polar solvent by introducing a solvation term $\left(\frac{1}{\tau_L}\right)$ in the pre-exponential factor.[1,3] In cases of less viscous but highly polar solvents such as water and short chain alcohols, extremely fast solvation time influences and modifies the rates of electron transfer. Bagchi and co-workers included classical low-frequency vibrational modes along with solvent relaxation to predict that the ultrafast component of solvation dynamics contribute significantly to the enhancement of the rate of electron transfer in MIR.[4] Yet Yoshihara *et al.* suggested that in neat donor solvent the kinetics of electron transfer is faster than solvation.[5] In organized assemblies, the solvation time does show a ultrafast component as demonstrated by Mandal *et al.* in their femtosecond solvation dynamics study of DCM dye in neutral TX-100 and cationic CTAB micelle, but the overall sub-nanosecond solvation time in micelle are much slower (~100 times) compared to that in bulk solvents.[6] Recently Choudhury *et al.* studied the sub-picosecond solvation dynamics in SDS micelle using coumarin 500 as the probe molecule and got an ultrafast time component of 1.48 ps along with a slower time component 27 ps of solvation.[7] However, in a micellar media, the donor and acceptor molecules stay very close to each other and thus the rate of electron transfer is expected to be free from the effect of diffusion and as fast as in neat solvents as studied by Yoshihara

and co-workers.[8] There is another advantage of studying the PET reactions in micelles. The width of the Marcus parabola depends on the solvent reorganization energy and with retardation of solvent motion near the Stern-layer of a micelle or the water pool of a reverse micelle the steepness of the parabola increases. This is to imply that solvent reorganization becomes less effective and an inversion, as predicted by Marcus, can be achieved at a much lower reaction exergonicity compared to the bulk solvents.[9] Thus this approach became very popular among scientists, and we got a large number reports in the early part of this millennium depicting MIR in micelles, reverse micelles, cyclodextrins, etc.[10-14] Soon this idea is extended to other media such as ionic liquids.[15-18] All of these reports used fluorescence quenching method, both steady state and time resolved, to obtain the desired result.

However, speculation rose about the observation of MIR in the manner described above.[19] It was pointed out that all these reports made a fundamental mistake, which is the considering quenching rate constant to be a time independent quantity. Vauthey and co-workers employed diffusional encounter theory to the systems under study and claimed that all these observations are spurious.[19] In brief, fluorescence quenching rate can be considered in three different time regimes in any solvent, namely static, non-stationary and stationary.[19] The contribution of each of the quenching rate constants in various time domains to the overall quenching rate constant can be very different depending upon the solvent viscosity and the lifetime of the fluorophore. It was shown that if one can extract the information of individual rate constants from a steady state and time resolved quenching data; then we can observe that the static rate constant is free from the effect of diffusion whereas the stationary rate constant is not. This is because, at very early stage of quenching, some reactant pairs are situated in the optimum distance (quenching sphere of action) for electron transfer to occur and thus does not need to undergo diffusion to form the encounter complex. However, at longer times, the quenching process becomes diffusion controlled. Thus depending on the

extent of the lifetime of fluorophore used, the contribution from these 3 quenching rate constants vary considerably and in cases of short lifetime fluorophores, we see a significant contribution from static part making the quenching rate fast whereas in cases of fluorophores with longer lifetimes the stationary part prevails making the quenching rate slow. This way the examples of MIR observations mentioned earlier were discarded by commenting that they were merely the effect of viscosity and the intrinsic fluorescence lifetime.[19]

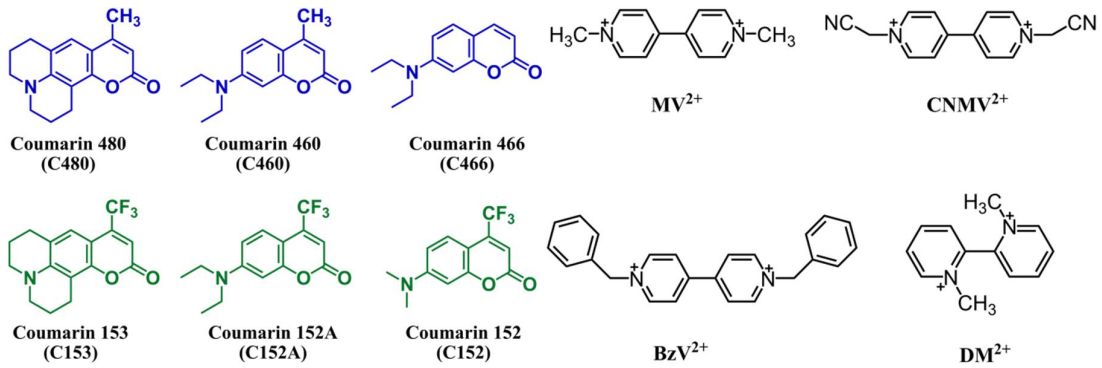

Scheme 3.C.1. Chemical Structure of coumarin dyes and viologen molecules used in the present study

I found that both the ends of the debate have very strong arguments and it is important to resolve it experimentally. In this chapter, I studied the electron transfer reaction between six different coumarin dyes and four viologen molecules (Scheme 3.C.1). Femtosecond transient absorption spectroscopic study was employed to observe the formation of radical cation intermediates of viologens and to calculate the actual rate of electron transfer as established in our previous study. The coumarin dyes have similarity in structure and have an average lifetime distribution from ~0.5 ns to ~6 ns. However, the major difference between this study and most of the previous studies is the fact that in this case coumarins act as electron donor whereas most of the previously mentioned studies employed coumarins as electron acceptors. This change gave me the opportunity to observe the short lifetime coumarins in the lower exergonic region and longer lifetime coumarins in the higher exergonic regions, unlike previous studies. Indeed, I observed a lowering of the rate in case of short lifetime coumarins and

enhancement of the rate of longer lifetime coumarins, contrary to the claim of Vauthey and co-workers.[19] Sodium dodecyl sulfate (Scheme 3.C.1) micelle was the choice of constrained media because of two reasons. First, dicationic viologen molecules at higher concentrations will be mostly present in the stern layer of the SDS micelle due to the Columbic attraction between the negatively charged head groups of the surfactants and the positively charged viologen molecules. Second, in the case of ionic micelles coumarin molecules are known to be present at the stern layer close to the head group of the surfactants.[6,9]Thus though I did not link the donor and acceptor, but somehow incarcerated them in a very specific region of a system. This situation allowed us to study the bimolecular PET reaction without the effect of diffusion. Indeed I observed a unique bell-shaped dependence of the rate of formation of radical cation intermediates with the reaction exergonicity, which is first of its kind. I also correlated this data with the ultrafast decay component of fluorescence decay of coumarins and showed that the same dependence could be observed but with a slight change in rate constants in some cases. Moreover, I have elucidated the inefficiency of time-resolved Stern-Volmer type experiments in observing the MIR.

3.C.2. Results

To obtain the rate of photoinduced electron transfer reaction between each of the pair I have chiefly employed transient absorption spectroscopy. In the purview of the studies mentioned in the introduction section, I also correlated the same with fluorescence up-conversion and Stern-Volmer type quenching experiments. To give a basic idea of our study, the detailed experimental results of PET reaction between C153 and MV^{2+} is discussed below.

In figure 3.C.1a and 3.C.1b, I have represented the steady-state fluorescence quenching experiments of C153 by MV^{2+} in 40 mM SDS solution. The same has been performed with time-correlated single photon counting method. Following Stern-Volmer (equation 3.C.1 and 3.C.2) we expect a linear relationship between $\frac{I_0}{I_i}$ and $[Q]$.

$$\frac{I_0}{I_i} = 1 + K_{SV}[Q] \quad (3.C.1)$$

$$\frac{\tau_0}{\tau_i} = 1 + k_q \tau_0 [Q] \quad (3.C.2)$$

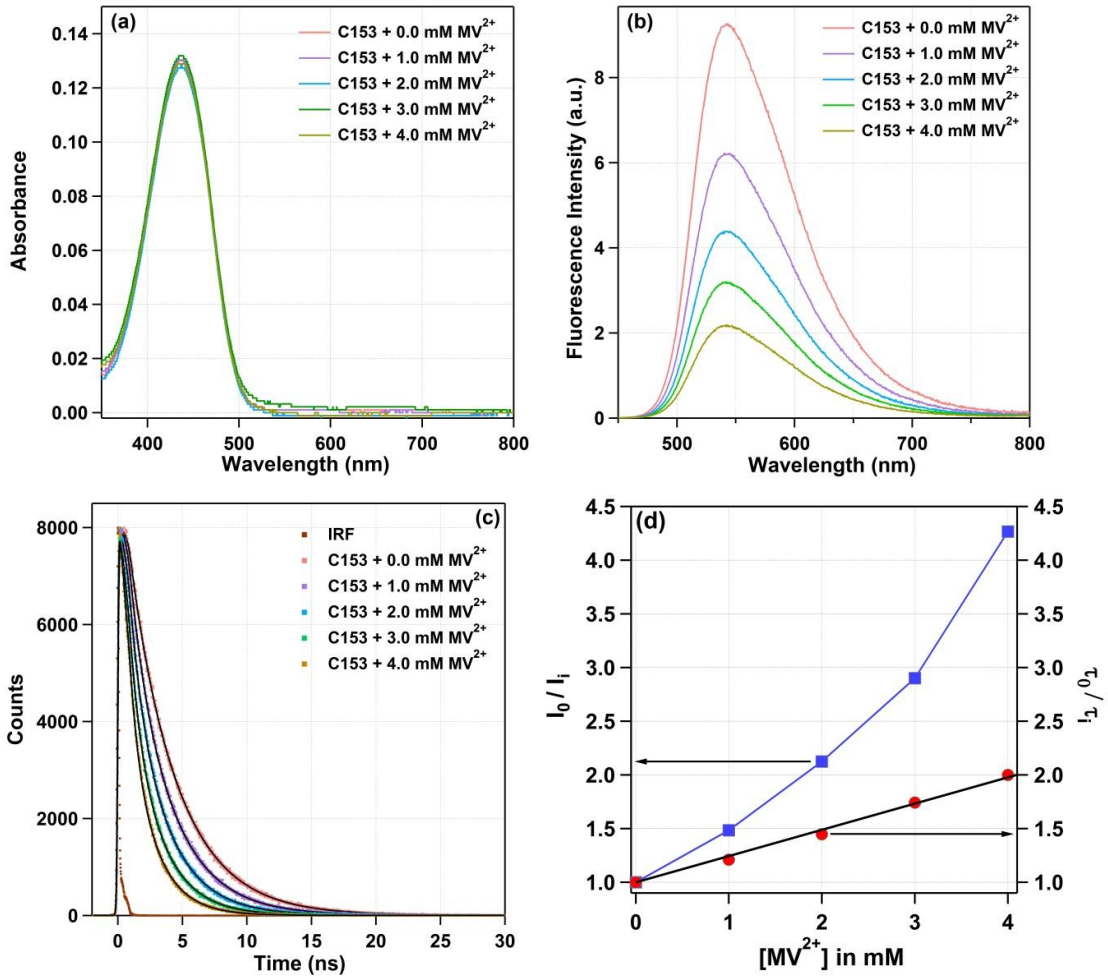

Figure 3.C.1. (a) UV-Visible (b) fluorescence spectra (c) time-resolved data at 542 nm (d) Stern- Volmer plot of fluorescence quenching of C153 by MV^{2+}

However, as can be seen from figure 3.C.1d, the plot of $\frac{I_0}{I_i}$ vs $[Q]$ completely deviates from linearity even at the lower concentration of quencher. This corresponds to the fact that in our case the quenching is of mixed type i.e. both dynamic and static quenching is happening at the same time even at a very low quencher concentration. This situation may arise when the two reactants are situated in a close proximity of one another with a less contribution of diffusion. In

our case, the coumarins and viologens are not connected by any chemical bond, but MV^{2+} is present in the Stern layer of the micelle due to the coulombic attraction with SDS headgroups, and C153 is distributed in the micelle. Thus we see the involvement of static quenching in the overall quenching process at a quencher concentration of ~1 mM and higher. Nonetheless, in this scenario, I can extract the dynamic information by using time-resolved fluorescence studies at a low to moderate quencher concentration, and, the same has been done for C153 and MV^{2+} (figure 3.C.1c and 3.C.1d).

Table 3.C.1. Quenching rate constants obtained from the Stern-Volmer analysis.

Reactant pair	k_q ($M^{-1}s^{-1}$) / 10^{10}	Reactant pair	k_q ($M^{-1}s^{-1}$) / 10^{10}
C480 + MV^{2+}	6.00	C152A + $CNMV^{2+}$	16.06
C466 + MV^{2+}	11.29	C480 + DM^{2+}	4.83
C460 + MV^{2+}	8.60	C466 + DM^{2+}	10.25
C153 + MV^{2+}	6.00	C460 + DM^{2+}	8.25
C152 + MV^{2+}	10.10	C153 + DM^{2+}	4.49
C152A + MV^{2+}	15.17	C152 + DM^{2+}	6.90
C480 + $CNMV^{2+}$	4.77	C480 + BzV^{2+}	3.50
C466 + $CNMV^{2+}$	10.00	C466 + BzV^{2+}	9.30
C460 + $CNMV^{2+}$	8.73	C460 + BzV^{2+}	11.21
C153 + $CNMV^{2+}$	9.15	C152 + BzV^{2+}	10.60
C152 + $CNMV^{2+}$	13.26	C152A + BzV^{2+}	13.58

All the fluorescence transients were fitted with a sum of two exponential functions and the average lifetime was used to get the Stern Volmer plot. In case of C153/MV^{2+} in SDS micelle the value of the quenching rate constant (k_q) was found to be 6.00×10^{10} M^{-1} s^{-1}. The striking feature of Stern-Volmer quenching

constant is being more than the diffusion rate constant may contributed from some long range interaction and excitation transfer mechanism.[20] I have performed the same Stern-Volmer experiment with all the 6 coumarin and 4 viologen molecules. In each case, I observed that the $\frac{I_0}{I_i}$ vs [Q] plot deviates from linearity over 1 mM quencher concentration. Thus I confirmed that both static and dynamic quenching is operational in all cases. The full set of measured k_q values are listed in table 3.C.1.

As argued in the introduction section and as it is clear from the Stern-Volmer plot that at lower quencher concentration dynamic quenching has a major role to play, thus the k_q obtained is very close to diffusional rate constant. Therefore it is very important to quantify k_{et}. I have argued in previous chapters that following the formation radical ion intermediate we can measure k_{et} and in this study also I have used the same technique. Moreover, in two recent publication depicting MIR, transient absorption spectroscopy has been employed in the same manner to track the formation and charge recombination of the radical ion intermediates.[21,22] MV^{2+} is a well-known quencher and forms a radical cation $MV^{+\cdot}$ accepting an electron from a donor and the species $MV^{+\cdot}$ is known for its characteristic absorption band in the visible region. Kaifer and Bard already studied the reduction of MV^{2+} in SDS micelle and they showed that the absorption spectra of $MV^{+\cdot}$ (first reduction of MV^{2+}) has a peak around 620 nm.[23] Thus it is expected that in the wavelength span of the probe light of our transient absorption spectroscopy setup I should be able to see the signature of $MV^{+\cdot}$ formed upon electron transfer from coumarin dyes. As a matter of fact, the radical cation formed from all these viologens have a peak around 600 to 620 nm and can be tracked using a visible probe light.[21,23] Using coumarins as electron donor also have some additional advantages. All the coumarins have a broad absorption band near 400 nm (see figure 3.C.2a), which is gave us the opportunity to use 400 nm as the pump. Moreover, at this wavelength, the viologens do not have any significant absorption (see figure 3.C.2b) even at a very high concentration, which ensured

that the transient absorption data would be free from the excited state dynamics of the viologens. SDS too does not have any absorption at 400 nm and thus the possibility of the surfactant being the excited state electron donor can be ruled out. Porel *et al.* have studied the electron transfer between C153 and MV^{2+} in 30% acetonitrile water mixture using femtosecond transient absorption and could not obtain any absorbance due to $MV^{+\cdot}$.[24] According to them, in such cases, the reaction is completely diffusion controlled and $MV^{+\cdot}$ fails to accumulate in sufficient amount to be observed in transient absorption setup. Thus in my case, if some coumarin is distributed outside the micelles in the bulk water phase, I should not observe any contribution from the PET in the bulk phase as in that phase the accumulation of $MV^{+\cdot}$ will be very less.

In figure 3.C.3a we have represented the transient absorption spectra at different times obtained by exciting a mixture of C153 and 10 mM MV^{2+} in 40 mM SDS solution. From 500 to 550 nm region we can observe the stimulated emission (SE) band of C153 but in 580 to 700 nm region we can observe the peak of $MV^{+\cdot}$, which gradually grows with time then diminishes at longer times. This absorption band of $MV^{+\cdot}$ does not have any special feature around 580 nm, and thus I exclude the possibility of dimerization of $MV^{+\cdot}$, which is expected given the time window of my observation at which PET cannot yield any intermediate with high enough concentration to form the dimer at a the sub-picosecond time-scale.[25] I have taken the kinetic data at a wavelength interval where the formation and decomposition of $MV^{+\cdot}$ can be clearly observed and free from the SE band of the coumarin i.e. 580 nm to 680 nm and fitted the kinetics at all the wavelengths using a global fitting with a sum of four exponential functions. This analysis ensures that all the changes happening at a stretch of wavelengths are taken care at the same time. Few representative kinetic data are plotted in figure 3.C.2b to show the excellence of our fitting procedure.

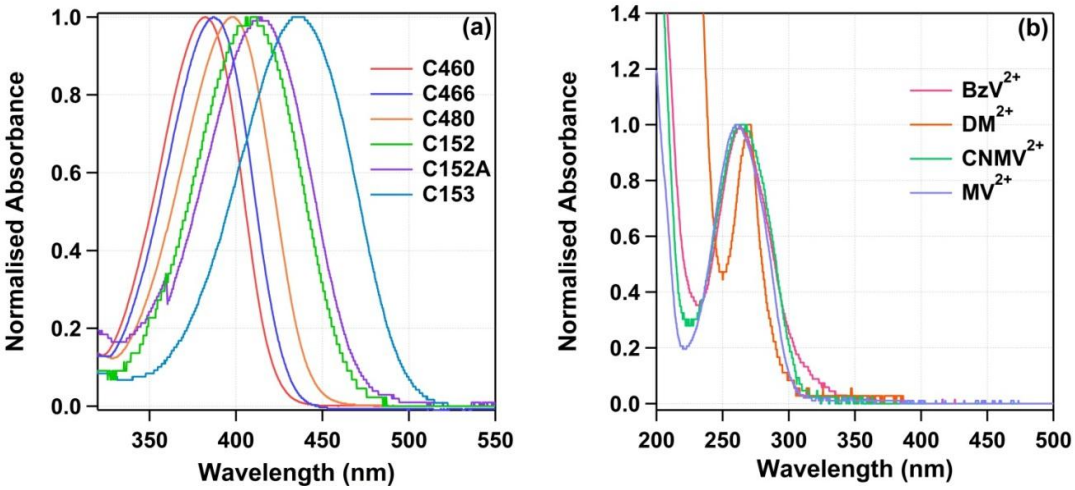

Figure 3.C.2. Normalised Absorption Spectra of (a) coumarins (b) viologens used in the study in 40 mM SDS solution

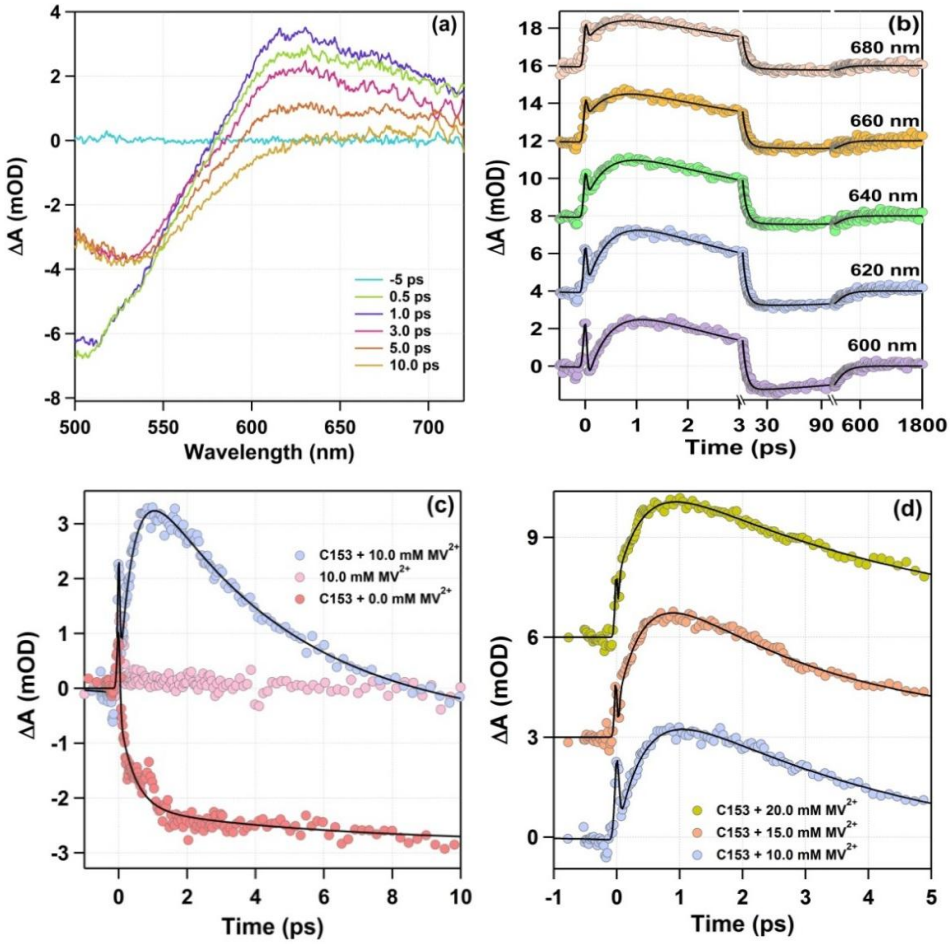

Figure 3.C.3. Plot of (a) transient absorption spectra at different times (b) kinetic traces at different wavelengths (c) comparison of kinetic traces for quenching of C153 by MV^{2+} in 40mM SDS (d) comparison of kinetic traces for quenching of C153 by different concentration of MV^{2+} in 40mM SDS

The global fitting time constants thus obtained for PET between C153 and MV^{2+} are 0.46, 4.3, 95.75 and 139 ps of which the first one is the rise component and thus assigned to forward electron transfer. The second time component of 4.3 ps signifies the charge recombination rate between the ion pair formed by the forward electron transfer. Along with this process, the reactants come back to the ground state, and I have previously demonstrated that it is independent of quencher concentration. Therefore I have assigned this decay component to the time constant of the back electron transfer process. The rest of the time components belong to the excited state dynamics of C153. The inverse of the forward and backward time components are 2.326×10^{12} s^{-1} and 2.33×10^{11} s^{-1} and designated as k_{et} and k_{bet} respectively. It is clear that the forward rate constant is much faster than diffusional rate constant. In figure 3.C.3c a comparison between the observed dynamics at 620 nm of the three systems i.e. C153 with no added electron acceptor, MV^{2+} with no added electron donor and C53 with MV^{2+} has been represented, where a clear evidence of rise and decay of $MV^{+\cdot}$ can be observed. To ensure that there is no initial quencher concentration dependence of the rise time of $MV^{+\cdot}$, we have also performed a MV^{2+} concentration dependent (10, 15 and 20 mM) transient absorption spectroscopic study and the time trace at 620 nm is depicted in figure 3.C.3d. The rise time components obtained from the global fitting are 0.46 ps, 0.44 ps and 0.43 ps for 10 mM, 15 mM and 20 mM MV^{2+} respectively. This experiment preserves the fact that I am indeed watching the first order electron transfer step and this time constants are not concentration dependent.

Perhaps another interesting observation is the fact that the rising part starts immediately after the pulse or the instrument response function. This signifies that the formation of $MV^{+\cdot}$ started almost immediately after the excitation and there was no lag period before it. In the previous chapter, I have reported a time lag before the start of the $MV^{+\cdot}$ signal due to the approach of the two reactants before electron transfer. In the present case, the immediate formation of the $MV^{+\cdot}$ signifies that both the donor (C153) and the acceptor (MV^{2+}) are present nearby the

Stern layer of the micelle. A similar feature has been observed in the transient absorption kinetics of all other donor-acceptor pairs and all the four time constants obtained from global analysis of the data, in the same manner, is reported in table 3.C.2.

Table 3.C.2. Time constants obtained from global fitting of transient absorption data.

Reactant pair	τ_1 (ps) (rise)	τ_2 (ps) (decay)	τ_3 (ps) (decay)	τ_4 (ps) (decay)
C480 + MV^{2+}	0.34	1.16	19.40	1800 (fixed)
C466 + MV^{2+}	0.30	2.96	80.75	1000 (fixed)
C460 + MV^{2+}	0.42	3.00	39.00	1000 (fixed)
C153 + MV^{2+}	0.46	4.30	95.75	139
C152 + MV^{2+}	0.50	3.10	10.20	367
C152A + MV^{2+}	0.68	4.50	18.05	303
C480 + $CNMV^{2+}$	1.04	4.54	38.20	1800 (fixed)
C466 + $CNMV^{2+}$	0.58	0.80	10.20	842
C460 + $CNMV^{2+}$	0.40	1.26	25.40	1000 (fixed)
C153 + $CNMV^{2+}$	0.32	1.58	23.00	1800 (fixed)
C152 + $CNMV^{2+}$	0.34	2.24	15.50	800
C152A + $CNMV^{2+}$	0.30	1.26	5.85	333
C480 + DM^{2+}	0.32	3.00	33.65	716
C466 + DM^{2+}	0.38	3.14	31.15	1000 (fixed)
C460 + DM^{2+}	0.50	2.76	23.60	620
C153 + DM^{2+}	0.68	1.34	17.85	1800 (fixed)
C152 + DM^{2+}	1.16	1.22	21.00	220
C480 + BzV^{2+}	0.38	1.80	45.8	1500
C466 + BzV^{2+}	0.32	3.34	33.76	1000 (fixed)
C460 + BzV^{2+}	0.30	2.96	19.80	1000 (fixed)
C152 + BzV^{2+}	0.56	0.88	7.18	243
C152A + BzV^{2+}	0.58	16.02	78.40	900

At least a wavelength range of 80-100 nm around the absorption maxima of the radical cation has been used to fit the data in each case. The concentration of MV^{2+} and $CNMV^{2+}$ is kept at 10 mM in each case while the concentration of DM^{2+} was 20 mM as at any lower concentration of DM^{2+} I was unable to achieve any clear signal. Experiments with BzV^{2+} had to be performed at a maximum of 8 mM as I found that it is close to the saturation of BzV^{2+} in SDS solution. The time constant of forward electron transfer obtained from the global fitting of the transient absorption data for all the 22 reaction pairs varies from 0.3 ps to 1.16 ps. Here one clarification needs to be given about the longest lifetime component of the fitting. As one can observe in some donor-acceptor pairs we got a shorter value of τ_4 but in some cases I got a much longer value, which is even greater than the normal fluorescence lifetime of the dye (table 3.C.3) following which I have to fix a certain value to obtain the fitting.

Table 3.C.3. Lifetime of coumarin dyes in SDS in absence of quencher measure at their emission maxima.

Sample Name	λ_{em}^{max}	τ_0 (ns)
C152 A	521 nm	0.50
C466	470 nm	0.94
C152	523.5 nm	0.95
C460	461 nm	1.50
C153	542.5 nm	3.65
C480	481 nm	6.21

The origin of the unusually long lifetime component can be explained in the following way. At this high quencher concentration, a large number of dicationic viologens are bound to SDS through Columbic force with a certain binding constant. Upon accepting an electron, they are converted to a monocationic form having lower binding constant than the dicationic form due to less charge. Thus there is a possibility of some displacement of these monocations at the micellar

interface following the change in the binding constant. For such events the back electron transfer process is not favorable and contributes to the residual signal in our observation.

As discussed till now, using transient absorption technique we can isolate and quantify k_{et} and clearly with change in the reactant pair, I obtained a variation in k_{et}. However, most of the previous studies employed time-resolved fluorescence technique to obtain the same data.[9-14] As shown in table 3.C.1, time-resolved Stern Volmer experiments yield nothing but the diffusional rate and later it will be shown that k_q basically is incorrect in this kind of studies, I had to turn my eyes towards femtosecond fluorescence up-conversion because of the following argument. When the fluorophore is excited in presence of quencher, it always have some quencher molecules within its vicinity or within the quenching sphere of action.[19] Thus some of the fluorophore decays back to the ground state in a very short time within which the reaction does not become diffusion controlled. Later solvation and diffusion takes over and controls the excited state deactivation process and thus we observe a slow k_q. However, there must exist a very short decay profile, which should be equal to k_{et}, and can be extracted using fluorescence up-conversion technique.[17] Since my systems showed an appreciable amount of static quenching at high quencher concentration, it was expected that the said analogy shall also apply in our system. Therefore I have studied the same systems using fluorescence up-conversion technique and measured the decay profiles at the wavelength maxima of the coumarin dyes. Figure 3.C.4 shows the same for the C153 MV^{2+} system measured at 542.5 nm which is the emission maxima for C153 in SDS. The data was fitted with a sum of four exponential functions and the time constants obtained were 0.56, 8.50, 112.0 and 644 ps. The first time component is faster than the fastest solvation time in SDS micelle which is 1.48 ps and very much comparable to the same obtained by transient absorption studies.[7] This signifies that we can assign this component to k_{et}. In figure 3.C.4 we have also showed the kinetics of C153 without the addition of quencher, which prominently shows a long growth part due to solvation.

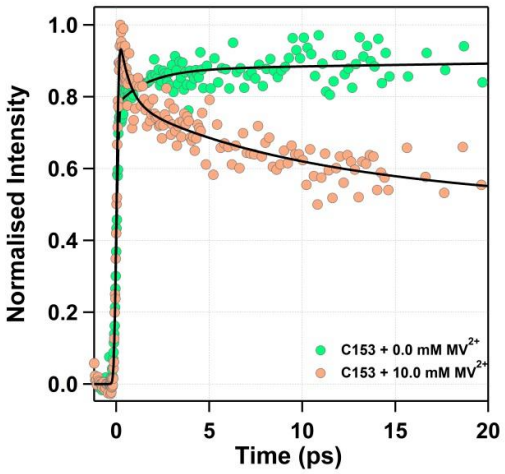

Figure 3.C.4. Plot of fluorescence transients at 542 nm for C153 and C153 + MV^{2+} in 40 mM SDS.

The same experiment has been performed with other reactant pairs at their accumulating to the decay at the emission maxima of each of the coumarin (see table 3.C.3) and the fastest time component obtained is reported in table 3.C.4. Except for a few cases the time constants matches well enough with the same obtained through transient absorption.

To calculate the ΔG^0 value for each pair of donor and acceptor, Rehm Weller equation has been used which is given in equation 3.C.3 with a slight modification.

$$\Delta G^0 = \boldsymbol{E_{D/D^+}} - \boldsymbol{E_{A^{2+}/A^+}} - \boldsymbol{E_{0,0}} + \frac{\boldsymbol{e^2}}{\boldsymbol{\varepsilon_s r_0}} \qquad (3.C.3)$$

The Columbic term in my case has to be taken as a positive term and not as a negative term because in the ion-pair formed upon electron transfer both the molecules have a positive charge. Thus instead of an attractive potential term, we used a repulsive potential term. The oxidation potentials of four coumarins used in this study which are C480, C153, C460 and C152A are already reported previously in acetonitrile solvent.[26] Rest of the oxidation and reduction potentials were needed to be measured and to do that cyclic voltammetry experiments were carried out on C152, C466, and all the four viologens.

Table 3.C.4. Time constants obtained from fitting of fluorescence up-conversion data.

Reactant pair	τ_1 (ps)	τ_2 (ps)	τ_3 (ps)	τ_4 (ps)
C480 + MV^{2+}	0.38	11.90	100.4	425.0
C466 + MV^{2+}	0.32	12.15	145.0	495.0
C460 + MV^{2+}	0.36	6.50	38.4	250.0
C153 + MV^{2+}	0.56	8.50	112.0	644.0
C152 + MV^{2+}	0.92	7.60	205.5	722.4
C152A + MV^{2+}	1.20	5.60	70.4	441.1
C480 + $CNMV^{2+}$	0.61	7.50	58.0	578.0
C466 + $CNMV^{2+}$	0.48	10.70	49.5	205.2
C460 + $CNMV^{2+}$	0.38	5.05	55.0	577.7
C153 + $CNMV^{2+}$	0.34	8.75	100.0	986.0
C152 + $CNMV^{2+}$	0.37	4.30	66.1	760.9
C152A + $CNMV^{2+}$	0.40	6.90	87.2	820.0
C480 + DM^{2+}	0.40	4.20	36.3	217.7
C466 + DM^{2+}	0.48	4.20	34.3	246.9
C460 + DM^{2+}	0.54	6.45	84.4	443.4
C153 + DM^{2+}	1.40	12.70	77.5	334.4
C152 + DM^{2+}	1.40	34.70	184.0	503.5
C480 + BzV^{2+}	0.36	13.70	113.3	807.3
C466 + BzV^{2+}	0.32	8.92	69.5	495.0
C460 + BzV^{2+}	0.36	2.60	37.2	451.4
C152 + BzV^{2+}	0.80	12.95	50.4	442.2
C152A + BzV^{2+}	1.32	8.70	91.0	515.3

The cyclic voltammetry of C152 and C466 in acetonitrile (figure 3.C.5) show one electron oxidation process at $E_{1/2}$ values 1.14 V (peak to peak separation, ΔE_p = 240 mV) and 0.915 V (peak to peak separation, ΔE_p = 170 mV) vs. SCE respectively.

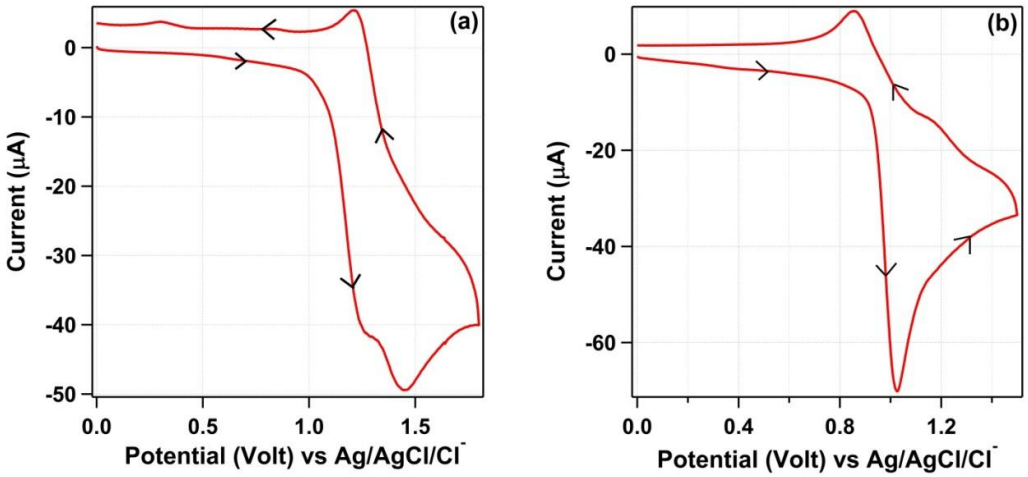

Figure 3.C.5. Cyclic voltammetry of (a) C152 and (b) C466 in acetonitrile

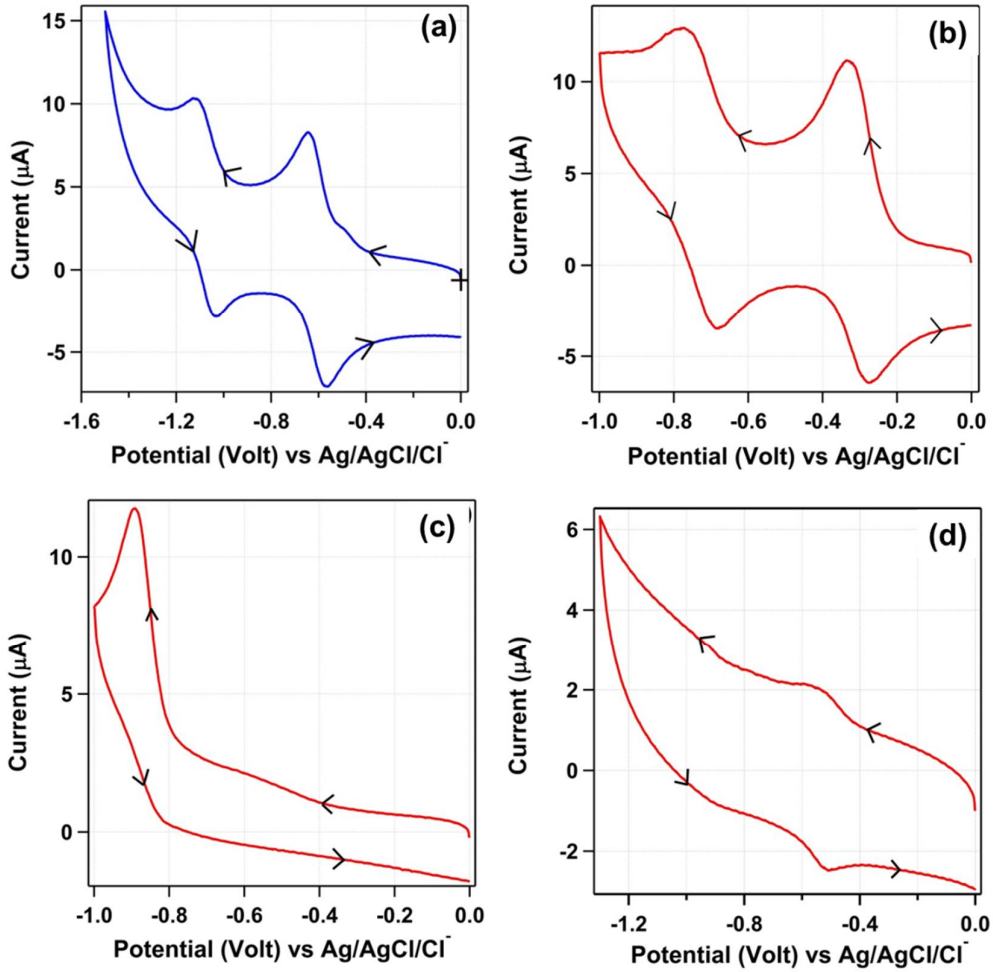

Figure 3.C.6. Cyclic voltammetry of (a) MV^{2+} (b) $CNMV^{2+}$ (c) DM^{2+} and (d) BzV^{2+} 70 mM SDS with 50 mM NaCl as supporting electrolyte.

The oxidations for both coumarins are chemically irreversible (ratio of cathodic and anodic peak current i_{pc}/i_{pa} ≈0.6 and 0.2 respectively) and electrochemically quasi-reversible electron transfer reactions. $E_{1/2}$ values were measured by the differential pulse voltammetry. A shift factor of +0.16 V has been used for SDS from acetonitrile based on previous literature.[27] The cyclic voltammetry of MV^{2+}, $CNMV^{2+}$, BzV^{2+} and DM^{2+} in 40 mM SDS solution (figure 3.C.6) show two reductions, however except MV^{2+} only first reduction potentials are reported here as required. The $E_{1/2}$ values for the first one electron reduction of MV^{2+}, $CNMV^{2+}$, BzV^{2+} and DM^{2+} are at -0.65 V (peak to peak separation, ΔE_p = 65 mV) ,-0.26 V (peak to peak separation, ΔE_p = 60 mV), ,-0.57 V (peak to peak separation, ΔE_p = 30 mV) and ,-0.79V (peak to peak separation, ΔE_p = 80 mV) vs SCE respectively, whereas for MV^{2+} $E_{1/2}$ value for second one-electron reduction potential is at -1.12 V (peak to peak separation, ΔE_p = 90 mV) vs SCE. The reduction potentials of MV^{2+} are comparable to the previously reported values.[23] The first reductions for MV^{2+} and BzV^{2+} are both chemically reversible (ratio of cathodic and anodic peak current i_{pc}/i_{pa} ≈0.9 for both) and the same for $CNMV^{2+}$ and DM^{2+} are chemically irreversible whereas all the reductions are electrochemically reversible electron transfer reactions. The $\boldsymbol{E_{0,0}}$ term has been calculated from the overlap of normalized absorption and emission spectra of coumarin. The last term which is columbic term is calculated taking a value of static dielectric constant of the SDS medium as 32.[11] The separation between donor and acceptor is taken as a sum of their radii estimated from the optimized structure.

All of the parameters thus required to calculate ΔG^0 and the same obtained for different pairs have been summarized in table 3.C.5 along with the rate constant of formation of radical cation intermediate from transient absorption studies and the fast decay component from the fluorescence up-conversion studies. To give an idea of how the rate of electron transfer is changing with changes in ΔG^0, I have plotted the kinetics at 620 nm obtained from transient absorption data for three representative pairs in figure 3.C.7.

Table 3.C.5. Electron transfer parameters for different coumarin and viologen pairs.

Reactant pair	E_{D/D^+} (V vs SCE) in acetonitrile	E_{D/D^+} (V vs SCE) in SDS micelle	E_{A^{2+}/A^+} (V vs SCE) in SDS micelle	$E_{0,0}$ (eV)	$\frac{e^2}{\varepsilon_s r_0}$ (eV)	ΔG^0 (eV)	[a]k_{rise}^{TA} (s^{-1}) / 10^{12}	[a]k_{fast}^{UC} (s^{-1}) / 10^{12}
C480 + MV^{2+}	0.72[a]	0.88	-0.65	2.8182	0.04674	-1.24	2.941	2.632
C466 + MV^{2+}	0.92[b]	1.08	-0.65	2.8972	0.0479	-1.12	3.333	3.125
C460 + MV^{2+}	1.09[a]	1.25	-0.65	2.9384	0.0465	-0.99	2.381	2.778
C153 + MV^{2+}	0.89[a]	1.05	-0.65	2.5051	0.0461	-0.76	2.174	1.786
C152 + MV^{2+}	1.14[b]	1.3	-0.65	2.6496	0.0468	-0.65	2.000	1.087
C152A + MV^{2+}	1.2[a]	1.36	-0.65	2.6552	0.0466	-0.60	1.470	0.833
C480 + $CNMV^{2+}$	0.72	0.88	-0.26	2.8182	0.0462	-1.63	0.962	1.627
C466 + $CNMV^{2+}$	0.92	1.08	-0.26	2.8972	0.0473	-1.51	1.724	2.083
C460 + $CNMV^{2+}$	1.09	1.25	-0.26	2.9384	0.0460	-1.38	2.500	2.632
C153 + $CNMV^{2+}$	0.89	1.05	-0.26	2.5051	0.0456	-1.15	3.125	2.941
C152 + $CNMV^{2+}$	1.14	1.3	-0.26	2.6496	0.0463	-1.04	2.933	2.673
C152A + $CNMV^{2+}$	1.2	1.36	-0.26	2.6552	0.0461	-0.99	3.333	2.500
C480 + DM^{2+}	0.72	0.88	-0.79	2.8182	0.0453	-1.10	3.125	2.500
C466 + DM^{2+}	0.92	1.08	-0.79	2.8972	0.0464	-0.98	2.632	2.083
C460 + DM^{2+}	1.09	1.25	-0.79	2.9384	0.0451	-0.85	2.000	1.852
C153 + DM^{2+}	0.89	1.05	-0.79	2.5051	0.0447	-0.62	1.471	0.714
C152 + DM^{2+}	1.14	1.3	-0.79	2.6496	0.0454	-0.51	0.862	0.714
C480 + BzV^{2+}	0.72	0.88	-0.57	2.8182	0.0409	-1.33	2.632	2.857
C466 + BzV^{2+}	0.92	1.08	-0.57	2.8972	0.04179	-1.21	3.125	3.226
C460 + BzV^{2+}	1.09	1.25	-0.57	2.9384	0.0407	-1.08	3.333	2.778
C152 + BzV^{2+}	1.14	1.3	-0.57	2.6496	0.0410	-0.74	1.786	1.250
C152A + BzV^{2+}	1.2	1.36	-0.57	2.6552	0.0408	-0.68	1.724	0.758

[a]TA and UC designate the transient absorption and upconversion studies respectively.

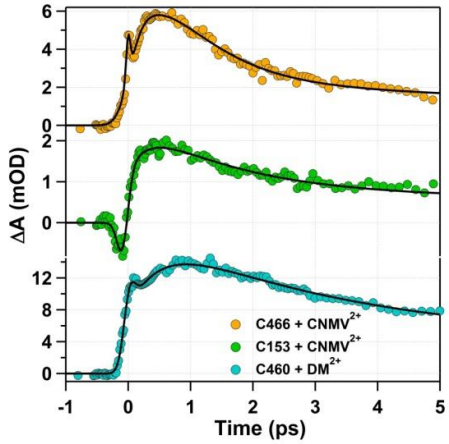

Figure 3.C.7. Comparison of transient absorption kinetics for different donor-acceptor pairs at 620 nm.

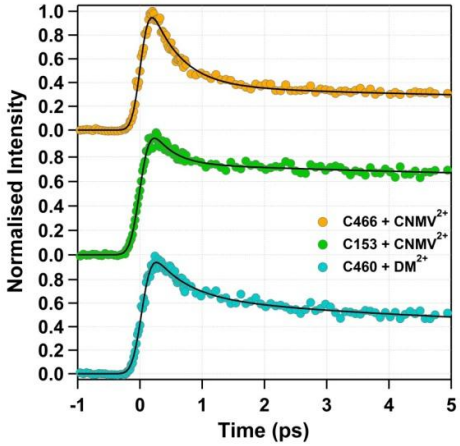

Figure 3.C.8. Comparison of fluorescence up-conversion kinetic traces for different donor-acceptor pairs at emission maxima of the donor.

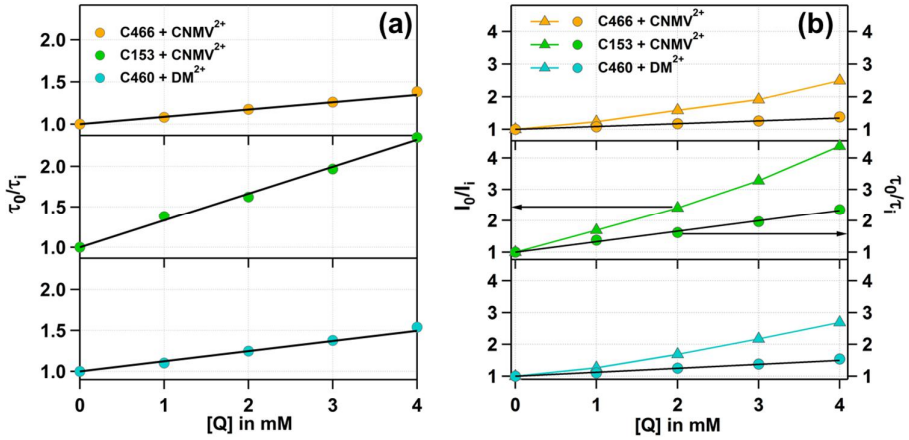

Figure 3.C.9. The Stern-Volmer plot for different donor-acceptor pairs at emission maxima of the donor.

For the same pair the up-conversion transients are plotted in figure 3.C.8 along with the Stern-Volmer plots for them in figure 3.C.9a. The plots of $\frac{I_0}{I_i}$ vs $[Q]$ for the three pairs are also given in figure 3.C.9b to show that the deviation from linearity arose early in all cases. Hence, static quenching mechanism is expected to be operational for all the coumarin-viologen pairs and at the concentration where femtosecond experiments were performed it was safe to assume that maximum contribution arose from the static quenching mechanism. The three pairs were chosen to represent three widely different values of ΔG^0 and it is clear from the plots that at an intermediate value of ΔG^0 the fastest rate of electron transfer is observed. Both increasing and decreasing in ΔG^0 leads to decrease in k_{et}. Thus I have plotted the measured k_{et} along with the k_q values for all the pairs as a function of ΔG^0 in figure 3.C.10. The variation of k_{et} with ΔG^0 clearly shows a bell-shaped dependence, which was predicted in Marcus theory. I have fitted the same with a function similar to equation 1.20. The point of inversion obtained at -1.10 eV where ΔG^0 is equals to reorganization energy. This observation is at par with previous studies done in micellar environment confirming the existence of MIR in present case.[9-13] The inverted region is designated by at least 7 points unlike previous studies, where a maximum of 1-2 points were achieved in this region. This is of course not within the error bar in this case (~10%). Considering that the change in nuclear reorganization energy is negligible for each pair as the structure of the coumarins used are very similar to each other as well as the viologens, I can claim that this is the definitive proof of existence of MIR in case of bimolecular PET in micelle. This is the first time such evidence has been obtained for donor acceptor pairs which are not linked by any chemical bond. When I have plotted the fast decay components obtained from fluorescence up-conversion studies vs ΔG^0 I also observed a similar bell shaped dependence as depicted in figure 3.C.11. Upon fitting the dependence a similar point of inversion has been observed considering the error associated with the measurements.

Hence I think that the ultrafast component of the fluorescence quenching can be used to obtain MIR but the exact estimation of the rate constants can only be acquired from transient absorption studies.

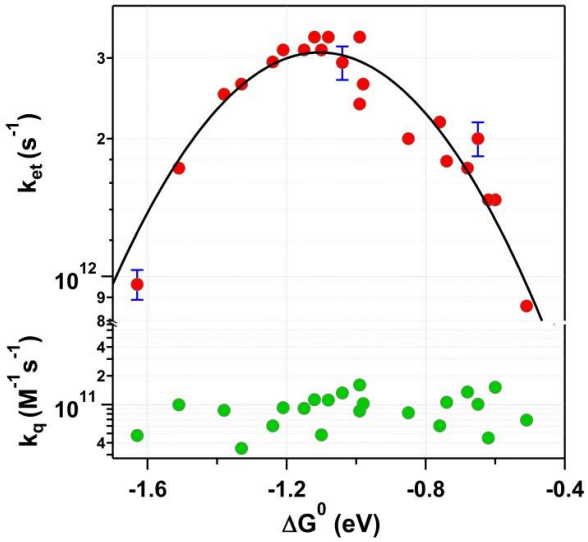

Figure 3.C.10. Plot of k_{et} vs ΔG^0 for different donor-acceptor pairs obtained from transient absorption spectroscopy along with k_q vs ΔG^0 for the same.

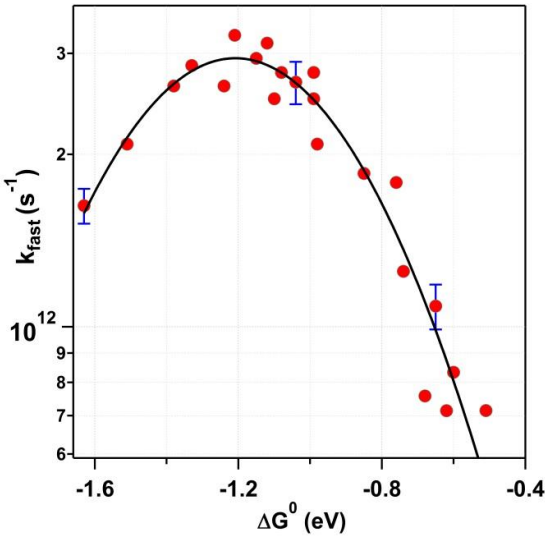

Figure 3.C.11. Plot of k_{fast} vs ΔG^0 for different donor-acceptor pairs obtained from fluorescence up-conversion studies.

3.C.3. Discussion

This study revealed the existence of MIR in a unique way. The rate of electron transfer estimated from measuring the rate constant of the formation of intermediate radical cation clearly gave evidence in support of it along with fluorescence up-conversion studies. However keeping in mind the arguments presented in the introduction part, favoring or disfavoring of the existence of MIR in constrained media such as micelles, few more points need to be discussed here.

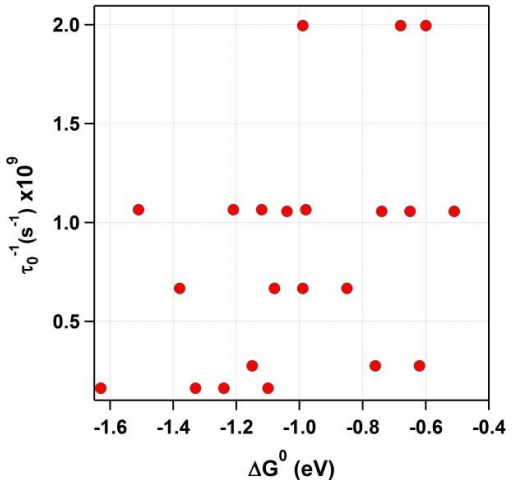

Figure 3.C.12. Plot of inverse of intrinsic lifetime of different coumarins with ΔG^0 of their respective reactions with viologens.

First of all, I agree with Vauthey and co-workers regarding the impossibility of observing MIR through dynamic Stern-Volmer experiments. All the measured k_q values plotted in figure 3.C.10 has no specific trend, which Vauthey and co-workers worked out using differential encounter theory. I present a plot of inverse of natural lifetime of the coumarin dyes in SDS micelle with ΔG^0 (Figure 3.C.12) and compare the trend with the same k_q vs ΔG^0 plot. One can easily see that the dynamic part of the quenching (low quencher concentration region) follows the same trend as the lifetime of the coumarin dyes. The longer lifetime coumarins i.e. C480 and C153 have the slowest k_q values and shorter lifetime coumarins like C152A and C152 has the faster k_q values. This happens because of the diffusion controlled nature of quenching. This probably is the cleanest evidence achieved till

date of the non-observation of MIR without applying any special treatment to the quenching data, which Vauthey and co-workers tried to establish so far using differential encounter theory.[19] But when I inspect the transient absorption data and the fluorescence up-conversion data we see that this lifetime trend is completely destroyed. For example, though C152A and C152 have the shortest lifetimes, k_{et} for PET between C152A and DM^{2+} , C152 and DM^{2+} , C152A and MV^{2+} , C152 and MV^{2+}, etc. are slow compared to others. The same is valid for pairs like C153 and $CNMV^{2+}$ and C480 and MV^{2+}, where the lifetime of the coumarin dyes are long but they show fast electron transfer as they are positioned close to the inversion point of the parabola. This shows the importance of my study and the techniques employed here. This also signifies that MIR does exist and can be observed in micellar environment contrary to the claim of Vauthey and co-workers. The effect from change in concentration of the quencher can also be neglected as all the quenchings have appreciable amount of static component. The only thing remains though is the effect of solvation in my study. The ultrafast solvation time estimated in SDS micelle is 1.48 ps as reported previously.[7] While doing transient absorption studies we did not agonize about solvation because of the following reasons. First of all the spectra of radical cations are observed at the red side of the emission band of the coumarins and the time constants obtained are also much faster than solvation time. Moreover, the quencher concentration used in the study ensured a more or less complete quenching of the emission band thus making the rise part of kinetic traces free from SE. In up-conversion studies, I also have observed faster electron transfer than solvation in most of the cases. However in some reactant pairs, where the electron transfer is considerably slower, solvation does affect the kinetic traces as they are taken in the emission maxima of the fluorophore. Therefore I observed a mismatch between k_{et} acquired from transient absorption and up-conversion studies for such pairs with slower electron transfer rate.

Though I have concluded mainly from the ion-pair formation process but it is a popular idea to follow the charge recombination process as well.[22] However,

when the electron transfer process occurs from the excited state there are two limitations. First is the estimation of ΔG^0 in the excited state is difficult and can only be estimated roughly from the Rehm-Weller equation. Second is the entropy factor has to be taken care. The back electron transfer originates from the ion-pair formed in the excited state, where the donor and acceptor are present in some kind of a molecular ensemble. This differentiates the back electron transfer from the forward electron transfer. I am sure that if these factors are taken care properly, from my charge recombination data one can obtain the MIR for back electron transfer process as well, which is beyond the scope of this work. May be in a further report I will elucidate on this analysis.

3.C.4. Conclusion

Marcus inverted region for bi-molecular photo-induced electron transfer reaction between coumarin and viologens has been successfully demonstrated in SDS micelle following the formation of radical cation intermediate of viologens and the ultrafast decay of coumarin fluorescence. In this work, I have studied the process in completely static quenching regime and therefore both the forward electron transfer rates obtained from femtosecond transient absorption measurements and fluorescence up-conversion measurements correlated to a bell-shaped dependence of k_{et} with ΔG^0. I have also demonstrated the inadequacy of dynamic Stern-Volmer measurements to predict Marcus inverted region in the same medium. Indeed we have assumed that because of similarities in structure of the coumarins and the same for viologens, electronic coupling and nuclear reorganization energy do not vary. I have not discussed the charge recombination process, the rate of which we obtained from our studies. But I am sure that a complete analysis taking into account the excited state oxidation reduction potential, the change in reaction entropy in the excited state etc. will also correlate the charge recombination rates to MIR. This work successfully demonstrates the usability of broadband transient absorption measurements to study PET reactions and in future can be used to study MIR in low viscous solvents and other medium.

References

1. Ghosh, S.; Sahu, K.; Mondal, S. K.; Sen, P.; Bhattacharyya, K. *J. Chem. Phys.* **2006**, *125*, 54509.
2. Singh, P. K.; Nath, S.; Bhasikuttan, A. C.; Kumbhakar, M.; Mohanty, J.; Sarkar, S. K.; Mukherjee, T.; Pal, H. *J. Chem. Phys.* **2008**, *129* (11), 114504.
3. Zusman, L. D. *Chem. Phys.* **1980**, *49* (2), 295–304.
4. Gayathri, N.; Bagchi, B. *J. Phys. Chem.* **1996**, *100*, 3056–3062.
5. Yoshihara, K.; Tominaga, K.; Nagasawa, Y. *Bull. Chem. Soc. Jpn.* **1995**, *68*, 696–712.
6. Mandal, D.; Sen, S.; Bhattacharyya, K.; Tahara, T. *Chem. Phys. Lett.* **2002**, *359* , 77–82.
7. Choudhury, S.; Mondal, P. K.; Sharma, V. K.; Mitra, S.; Sakai, V. G.; Mukhopadhyay, R.; Pal, S. K. *J. Phys. Chem. B* **2015**, *119* , 10849–10857.
8. Kobayashi, T.; Takagi, Y.; Kandori, H.; Kemnitz, K.; Yoshihara, K. *Chem. Phys. Lett.* **1991**, *180*, 416–422.
9. Kumbhakar, M.; Nath, S.; Mukherjee, T.; Pal, H. *J. Chem. Phys.* **2005**, *123*, 34705.
10. Kumbhakar, M.; Nath, S.; Mukherjee, T.; Pal, H. *J. Chem. Phys.* **2004**, *120*, 2824–2834.
11. Kumbhakar, M.; Nath, S.; Mukherjee, T.; Pal, H. *J. Chem. Phys.* **2005**, *122* , 84512.
12. Kumbhakar, M.; Nath, S.; Pal, H.; Sapre, A. V.; Mukherjee, T. *J. Chem. Phys.* **2003**, *119*, 388–399.
13. Ghosh, S.; Mondal, S. K.; Sahu, K.; Bhattacharyya, K. *J. Phys. Chem. A* **2006**, *110*, 13139–13144.
14. Chakraborty, A.; Seth, D.; Chakrabarty, D.; Hazra, P.; Sarkar, N. *Chem. Phys. Lett.* **2005**, *405*, 18–25.
15. Das, A. K.; Mondal, T.; Sen Mojumdar, S.; Bhattacharyya, K. Marcus-like *J. Phys. Chem. B* **2011**, *115*, 4680–4688.
16. Santhosh, K.; Samanta, A. *J. Phys. Chem. B* **2010**, *114* , 9195–9200.
17. Kumbhakar, M.; Manna, A.; Sayed, M.; Kumar, A.; Pal, H. *J. Phys. Chem. B* **2014**, *118* , 10704–10715.
18. Santhosh, K.; Samanta, A. *ChemPhysChem* **2012**, *13*, 1956–1961.
19. Rosspeintner, A.; Koch, M.; Angulo, G.; Vauthey, E. *J. Am. Chem. Soc.* **2012**, *134* , 11396–11399.
20. Ray, R.; Mukherjee, S. *Proc. Ind. Nat. Sci. Acad.* **1992**, *58*, 173-180.
21. Petersson, J.; Hammarström, L. *J. Phys. Chem. B* **2015**, *119*, 7531.

22. Waskasi, M. M.; Kodis, G.; Moore, A. L.; Moore, T. A.; Gust, D.; Matyushov, D. V. *J. Am. Chem. Soc*.**2016**, *138*, 9251.
23. Kaifer, A. E.; Bard, A. J. *J. Phys. Chem.* **1985**, *89*, 4876–4880.
24. Porel, M.; Chuang, C. H.; Burda, C.; Ramamurthy, V. *J. Am. Chem. Soc*. **2012**, *134*, 14718–14721.
25. Bird, C. L.; Kuhn, a. T. *Chem. Soc. Rev*. **1981**, *10*, 49.
26. Jones, G.; Griffin, S. F.; Choi, C. Y.; Bergmark, W. R. *J. Org. Chem.* **1984**, *49* , 2705–2708.
27. Ghosh, S.; Mondal, S. K.; Sahu, K.; Bhattacharyya, K. *J. Chem. Phys*. **2007**, *126*, 204708.

This page intentionally left blank

Chapter 4

Ultrafast Excited State Dynamics of Molecular Rotor Dye Thioflavin-T

Thioflavin-T is a common amyloid fibril sensor dye. The exceptionally high fluorescence quantum yield of thioflavin-T in the amyloid bound form compared to the same in water made it a viable sensor. Thioflavin-T undergoes ultrafast twisting dynamics in its excited state which makes the dye almost non-fluorescent in solution but in fibrils, this twisting is hindered severely which increases the quantum yield. For the same reason, it can be used as a viscosity sensor. The established deactivation models assign a barrierless potential energy surface for the large amplitude motion with formation of a dark twisted intramolecular charge transfer (TICT) state. However, it cannot justify the unusually high quantum yield of the dye in chlorinated solvents. In this chapter, which has been divided into two parts, I have experimentally and computationally explored the possibility of existence of two TICT state and a potential energy barrier in the excited state manifold of thioflavin-T by studying it first in chloroform and methanol and then adsorbed on SDS micelle.

Chapter 4

Part A

Dual Relaxation Channel in Thioflavin-T: An Ultrafast Spectroscopic Study

Puspal Mukherjee, Shahnawaz Rafiq and Pratik Sen *J. Photochem. Photobiol. A Chem.* **2016**, *328*, 136–147.

4.A.1. Introduction

Thioflavin-T (ThT, Scheme 4.A.1) is a widely known amyloid fibril sensor and has been thoroughly used to detect fibril formation.[1] The widespread use of ThT has been noticed in the past for diagnosis of diseases like Alzheimer's, Parkinson's, type-II diabaties, etc.[1] These diseases are characterized by increased *β*-sheet rich protein structures and the fluorescence property of ThT abruptly enhanced in such structures.[2] Both spectroscopic and computational methods have been employed to understand the underlying mechanism of the fluorescence enhancement of ThT in amyloid fibrils.[3-9] The widespread application of ThT is not only restricted for structural characterization of amyloid fibrils, but few reports have also showed that it has an affinity to bind with α-helical poly-L-glutamic acid and G-quadruplex DNA.[10,11]

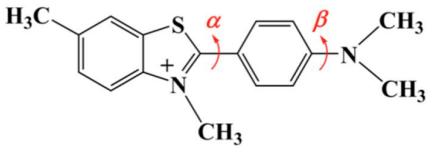

Scheme 4.A.1. Structure of Thioflavin T (ThT)

The use of ThT to sense the formation of amyloid fibrils has been proposed to be based on its property of being a barrierless molecular rotor.[12-14] As widely proposed, ThT undergoes an internal conformational change along the C-C single bond in the excited state, which causes a drift of electronic density from the locally excited (LE) state to an intra-molecular charge transfer state in the same potential energy surface.[12] Since this process is facilitated by twisting motion of the molecular segments, the charge transfer state thus formed has been postulated to be a twisted intra-molecular charge transfer (TICT) state. This twisting motion acts as a strong non-radiative channel and essentially renders the TICT state highly non-fluorescent.[12-14] During the binding of ThT to the amyloid fibrils, the intra-molecular twisting motion is restricted due to the steric hindrance with the surrounding protein side chains leading to highly inefficient non-radiative pathways, causing an enhancement of the fluorescence quantum yield. This

property makes ThT a viable sensor for sterically restricted environments.[12-19] The models describing the deactivation dynamics of ThT has been discussed in chapter 1. As evident from that discussion, all the different models proposed that the dynamics of ThT is mainly controlled by viscosity of the medium over a barrierless potential energy surface along the torsional coordinate of dimethylanilino moiety relative to benzothiazole ring. No delay in the initial decay of the fluorescence has been observed before and hence enunciates the rapid depletion of the excited state in low viscous alcoholic solvents and this behavior is expected to be extendible to other solvents of similar viscosity. However, the value of fluorescence quantum yield of ThT in chloroform seems to pose a threat to the already established excited state relaxation models. In the present work, I have tried to throw light on such anomalous observation of photophysical properties from the perspectives of ultrafast time resolved studies.

4.A.2. Results

4.A.2.1. Steady state absorption and emission studies

Absorption spectra of ThT in methanol and chloroform show a single band with maxima at 415 nm and 425 nm, respectively, as shown in figure 4.A.1a. In both the solvents, the emission maxima are found to be at 485 nm (Figure 4.A.1b). It seems that the emission spectra do not show any noticeable dependence on polarity of the solvent. The fluorescence quantum yield of ThT in various solvents has been found to be similar and do not show any quantifiable dependence on polarity of the medium and was observed similarly in this case also (absorption corrected emission spectra are shown in figure 4.A.1b) except chloroform and dichloromethane.[16,20] The monotonous increase of ThT fluorescence quantum yield with increase in solvent viscosity was ascribed mainly to the steric restrictions posed to the internal motions within the molecule.[19,20,21] According to the existing excited state relaxation model of ThT, there should not be much difference in ϕ_f of ThT in methanol and chloroform as these two solvents are iso-viscous.[19,20,21]

However, I found a ~30 times higher fluorescence quantum yield of ThT in chloroform ($\phi_f = 146 \times 10^{-4}$) compared to methanol ($\phi_f = 5 \times 10^{-4}$) (see table 4.A.1).

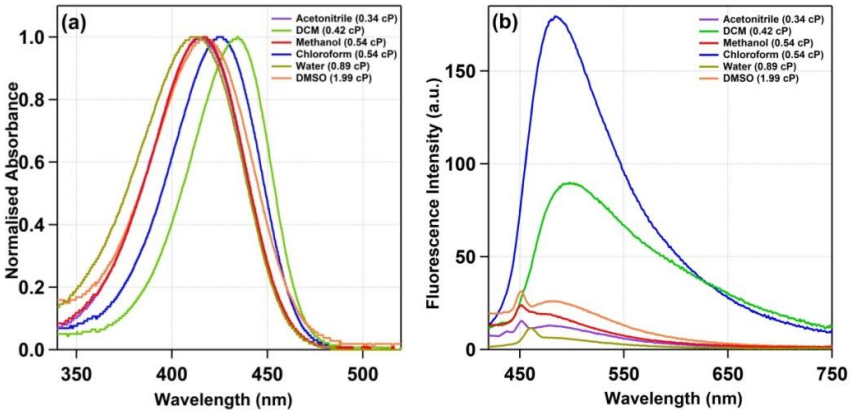

Figure 4.A.1. (a) Absorption and (b) emission spectra of thioflavin-T (ThT) in different solvents at 25˚C. ThT was excited at 400 nm and the fluorescence intensity was corrected for change in absorbance. The signal around 460 nm is because of the solvent Raman band.

Table 4.A.1. Absorption and emission characteristics of of thioflavin-T in different solvents along with the solvent parameters.

Solvent	Viscosity (cP) at 25˚C[a]	Dielectric Constant at 25˚C[b]	Solvation Time (ps)[c]	Absorption Maxima (nm)	Emission Maxima (nm)	Fluorescence Quantum Yield of ThT	Lifetime (ps)
Water	**1.0**	**80.1**	**-**	**412**	**489**	$4 \pm 2 \times 10^{-4}$	**1.0**
Methanol	**0.54**	**32.7**	**4.32**	**415**	**484**	$5 \pm 2 \times 10^{-4}$	**0.90**
Chloroform	**0.54**	**4.81**	**1.32**	**425**	**485**	$146 \pm 15 \times 10^{-4}$	**19.6**
Dichloromethane	**0.41**	**8.93**	**-**	**434**	**490**	$133 \pm 17 \times 10^{-4}$	**-**

[a,b]Data taken from W. M. Hynes *ed.*, CRC Handbook of Chemistry and Physics, 96 edition, CRC Press, 2015-2016.[c]Data taken from Reference S. Gupta, S. Rafiq., P. Sen, J. Phys. Chem. 119 (2015) 3135-3141.

Such a high value of ϕ_f is expected only in highly viscous media like octanol (calculated ϕ_f is 0.0179), wherein the slope of the potential energy curve becomes less steep and the internal motion also becomes restricted, credited exclusively to the viscous nature of the solvation sphere. It should also be noted that despite water having almost twice the viscosity of methanol, the quantum yield is almost same in these two solvents. Such an anomaly in fluorescence quantum yield in chloroform was noticed earlier and has been accredited to the reversible ring opening of the benzothiazole moiety of ThT by Stsiapura *et al.*[21] Ghosh *et al.* forfeited the idea of a photochemical reaction by evoking the concept of triplet state yield of ThT but

they did not comment on the anomaly of ThT in chloroform.[22] I have not observed any perceptible change in the steady-state absorption spectra of ThT in different solvents even after irradiation and comparing with previous literature, I also have discarded the idea of ring opening of benzothiazole moiety.[20,22] Thus in order to know the reason of such an anomaly in observed fluorescence quantum yield under iso-viscous condition for methanol and chloroform, we need to ascertain the potential energy surface more carefully, which has been done in the present work using ultrafast spectroscopy in association with theoretical calculations.

4.A.2.2. Femtosecond Time Resolved Fluorescence Measurements

Femtosecond fluorescence transients of ThT in methanol and chloroform were measured at various wavelengths from 450 nm to 575 nm by exciting the sample at 400 nm, covering the whole emission spectrum. In case of methanol, all the transients, except the last few, were fitted with a bi-exponential function. In case of last 5 transients I have observed a growth part (figure 4.A.2) and are fitted with tri-exponential function. All the measured fluorescence transients have been shown in figure 4.A.2a and the fitting results are tabulated in table 4.A.2. For example, at 450 nm, the observed time constants are 250 fs and 1.2 ps respectively. However, at 575 nm, a distinct rise time of 200 fs was observed followed by two decay time components of 1.3 ps and 3.3 ps. It is to mention that Singh *et al*. used a sum of three exponential functions to fit the fluorescent transients of ThT in acetonitrile with a monotonous increase in average lifetime of ThT with increase in wavelength of detection.[21] This is to note that when I have used a very high concentration of ThT either in methanol or chloroform, I have encountered a residual signal, which lasts for very high time-scale (2 ns, as our time window is 2 ns). However, we have noticed that below 10 μM, the transients are independent on concentration. Because of this I have performed all the experiments at 8 μM of ThT. Under this situation, the contribution from the ThT aggregates is negligible in the observed dynamics.

To dive further into the photophysics of ThT, I have constructed the time resolved emission spectra (TRES) from the transients and the steady state emission spectrum and the experimental points were fitted with the lognormal function.[23,24]

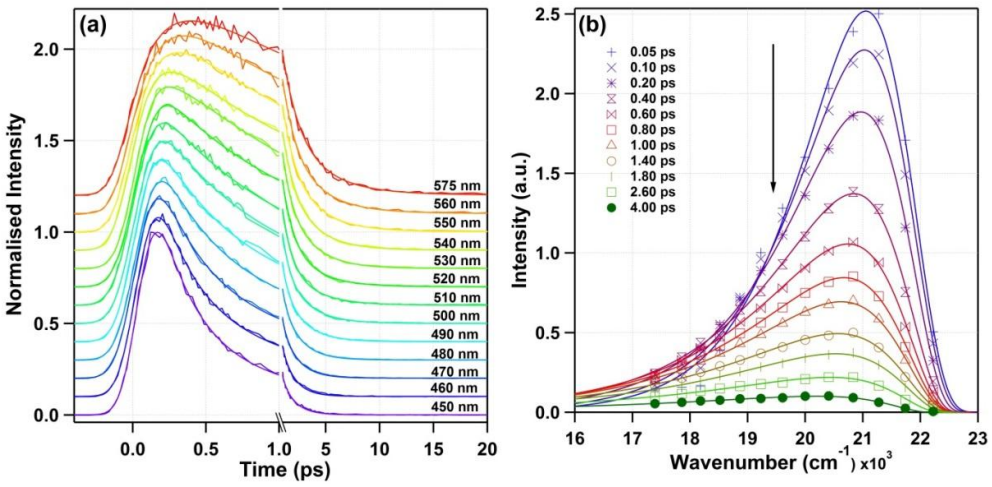

Figure 4.A.2. (a) Fluorescence transients of ThT in methanol at different wavelengths as mentioned in the figure along with the fitting, (b) time resolved emission spectra (TRES) of ThT in methanol at different times from the moment of excitation. The solid lines signify the lognormal fitting of the respective data. Excitation wavelength used is 400 nm.

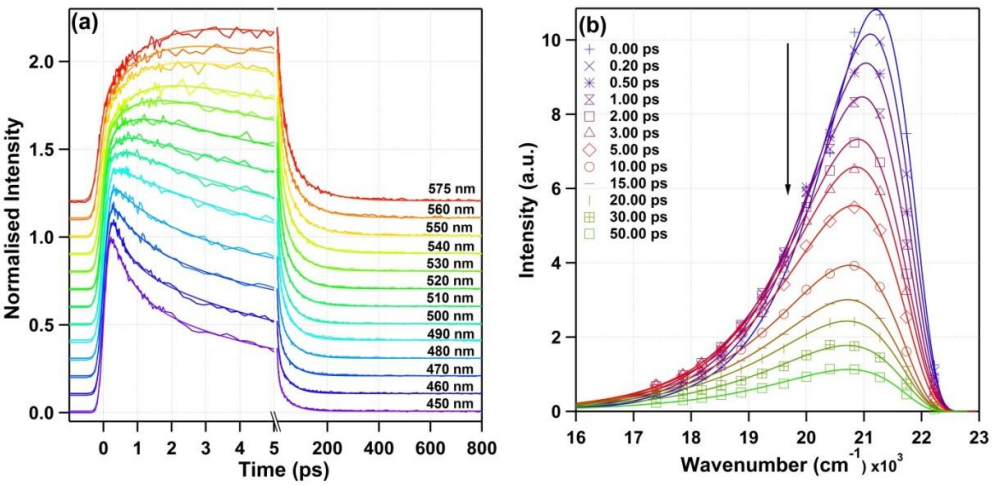

Figure 4.A.3. (a) Fluorescence transients of ThT in chloroform at different wavelengths as mentioned in the figure along with the fitting, (b) time resolved emission spectra (TRES) of ThT in chloroform at different times from the moment of excitation. The solid lines signify the lognormal fitting of the respective data. Excitation wavelength used is 400 nm.

The TRESs are shown in the figure 4.A.2b and a clear time dependent Stokes shift is observed with a broadening of the spectra. The time dependence of the peak frequency and the full width at half maxima (FWHM) of the emission spectra are shown in figures 4.A.4a. A Stokes shift of ~600 cm^{-1} was observed within 2.5 ps of photoexcitation and is found to be single exponential in nature with a time component of 0.9 ps. The change in the width of the spectra also showed a single exponential behaviour with a time constant of ~1.0 ps. The comparable time constants of the dynamic Stokes shift and FWHM indicate that they originate from the same dynamical process. The asymmetric broadening has already been acclaimed due to the rotation around the C-C bond in ThT, which enhances the non-radiative decay channel of the dye.[12,20,21]

The fluorescence transients at different wavelengths in chloroform were fitted by a sum of three exponentials, which are shown in figure 4.A.3a and the fitting results are tabulated in table 4.A.3. In chloroform, the average lifetime varied from ~9 ps to ~100 ps which are much longer compared to the same in methanol, even the viscosity is very similar. The transients from 450 nm to 480 nm showed positive values for all three coefficients of fitting. But from 490 nm to 575 nm a distinct growth have been observed (figure 4.A.3a and table 4.A.3). The timescale of this rise part in chloroform varied from ~100 fs (490 nm) to ~1.3 ps (575 nm). The long rise component signifies the formation of a new state in the excited state of the dye. The time component associated with the rise in fluorescence signal was smaller in methanol, despite having a similar viscosity as that of chloroform. So viscosity may not be the determining factor here. The TRES constructed from the fluorescence transients (figure 4.A.3b) of ThT in chloroform showed broadening and decrease in intensity with time, but at a much slower rate than in methanol. The dynamic Stokes shift in chloroform was about 500 cm^{-1} and was stretched for a longer period of time (~ 25 ps) than in methanol. In case of chloroform the peak frequency vs time plot (figure 4.A.4b) cannot be fitted with a

single exponential time component, rather a bi-exponential one was needed. The two time components obtained from the fitting were 0.6 ps and 6.3 ps, respectively.

Table 4.A.2. Individual fitting parameters of the fluorescence transients of ThT in methanol at different wavelengths along with the global fitting parameters given in the parenthesis. Samples were excited at 400 nm and the transients were recorded at 25˚C.

Wavelength (nm)	a_1	τ_1 (ps)	a_2	τ_2 (ps)	a_3	τ_3 (ps)
450	0.00 (0.70)	0.0 (0.2)	0.75 (0.24)	0.2 (0.8)	0.25 (0.06)	1.2 (2.5)
460	0.00 (0.56)	0.0 (0.2)	0.64 (0.36)	0.2 (0.8)	0.36 (0.08)	1.2 (2.5)
470	0.00 (0.43)	0.0 (0.2)	0.63 (0.47)	0.3 (0.8)	0.37 (0.10)	1.4 (2.5)
480	0.00 (0.28)	0.0 (0.2)	0.58 (0.57)	0.4 (0.8)	0.42 (0.15)	1.6 (2.5)
490	0.00 (0.21)	0.0 (0.2)	0.61 (0.59)	0.5 (0.8)	0.39 (0.20)	1.9 (2.5)
500	0.00 (-0.02)	0.0 (0.2)	0.64 (0.76)	0.7 (0.8)	0.36 (0.26)	2.2 (2.5)
510	0.00 (-0.17)	0.0 (0.2)	0.72 (0.86)	0.9 (0.8)	0.28 (0.31)	2.6 (2.5)
520	0.00 (-0.26)	0.0 (0.2)	0.68 (0.81)	1.0 (0.8)	0.32 (0.45)	2.7 (2.5)
530	-0.61 (-0.41)	0.2 (0.2)	1.01 (0.89)	1.0 (0.8)	0.59 (0.52)	2.7 (2.5)
540	-0.80 (-0.53)	0.2 (0.2)	1.13 (0.82)	1.1 (0.8)	0.68 (0.72)	2.8 (2.5)
550	-1.10 (-1.00)	0.2 (0.2)	1.20 (1.00)	1.1 (0.8)	0.88 (1.00)	2.8 (2.5)
560	-1.43 (-1.43)	0.2 (0.2)	1.51 (1.05)	1.1 (0.8)	0.92 (1.38)	3.0 (2.5)
575	-1.78 (-2.18)	0.2 (0.2)	1.62 (0.91)	1.3 (0.8)	1.16 (2.27)	3.3 (2.5)

Table 4.A.3. Individual fitting parameters of the fluorescence transients of ThT in chloroform at different wavelengths along with the global fitting parameters given in the parenthesis. Samples were excited at 400 nm and the transients were recorded at 25˚C.

Wavelength (nm)	a_1	τ_1 (ps)	a_2	τ_2 (ps)	a_3	τ_3 (ps)
450	0.41 (0.55)	0.6 (1.2)	0.43 (0.32)	5.0 (9.1)	0.17 (0.13)	43.6 (50.6)
460	0.35 (0.46)	0.5 (1.2)	0.45 (0.38)	4.8 (9.1)	0.20 (0.16)	42.1 (50.6)
470	0.28 (0.34)	1.0 (1.2)	0.49 (0.46)	7.3 (9.1)	0.23 (0.21)	49.9 (50.6)
480	0.20 (0.23)	1.1 (1.2)	0.52 (0.49)	8.2 (9.1)	0.28 (0.28)	54.2 (50.6)
490	-0.11 (0.08)	0.1 (1.2)	0.65 (0.56)	7.1 (9.1)	0.46 (0.35)	48.3 (50.6)
500	-0.17 (-0.03)	0.3 (1.2)	0.68 (0.64)	8.2 (9.1)	0.49 (0.39)	47.0 (50.6)
510	-0.29 (-0.15)	0.4 (1.2)	0.80 (0.67)	11.1 (9.1)	0.49 (0.48)	56.4 (50.6)
520	-0.38 (-0.30)	0.5 (1.2)	0.83 (0.71)	12.4 (9.1)	0.55 (0.59)	58.4 (50.6)
530	-0.50 (-0.48)	0.7 (1.2)	0.92 (0.74)	14.0 (9.1)	0.58 (0.74)	63.6 (50.6)
540	-0.67 (-0.68)	0.9 (1.2)	1.00 (0.71)	16.5 (9.1)	0.67 (0.97)	71.6 (50.6)
550	-0.73 (-0.78)	1.0 (1.2)	1.09 (0.66)	19.3 (9.1)	0.64 (1.12)	78.2 (50.6)
560	-0.90 (-1.01)	1.1 (1.2)	1.19 (0.62)	21.2 (9.1)	0.71 (1.39)	83.4 (50.6)
575	-1.09 (-1.37)	1.3 (1.2)	1.39 (0.52)	25.1 (9.1)	0.70 (1.85)	92.4 (50.6)

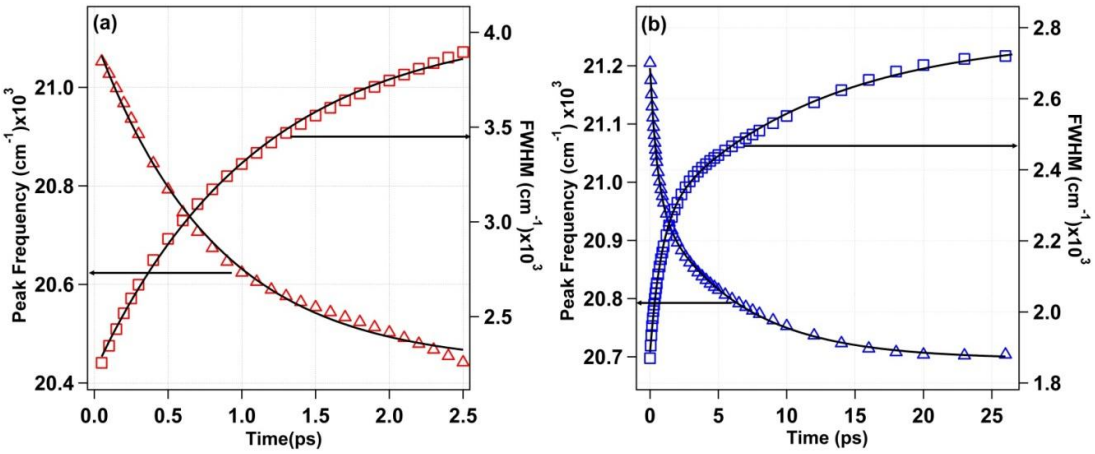

Figure 4.A.4. Plot of peak frequency (open triangles) and full width at the half maxima (open square) of the time resolved spectra of ThT at different times in (a) methanol and (b) chloroform. Solid line indicate its single exponential and bi-exponential fitting respectively.

The width of the spectra at different times also showed a bi-exponential nature (figure 4.A.4b). In this case the time components were ~0.8 ps and 11.7 ps. The first one can be comparable to the fast time component of spectral shift but the slower one differed than the previous. To explore a more generalized idea about the evolution of the excited state dynamics I have fitted the fluorescence up-conversion data using a global fit procedure. For this purpose, I have used a sum of three exponential functions. I observed that in a particular solvent the data could be fitted in using three common lifetime values for all the observed wavelengths. In case of ThT in methanol, the values obtained are 0.2 ps, 0.8 ps and 2.5 ps and in chloroform these are 1.2 ps, 9.1 ps and 50.6 ps respectively. The amplitude of the 0.2 ps and 1.2 ps component, for methanol and chloroform respectively, are found to be quite high at the shorter wavelength side, which become negative at the longer wavelengths. Moreover, the associated amplitudes of the longer two components in both methanol and chloroform were found to be quite low at the shorter wavelength region. The observation of this type of tri-exponential wavelength dependent fluorescence transient clearly indicate the involvement of more than two states in the excited state manifold of ThT.

To rationalize the findings of slow rise time in the fluorescence transients and different dynamics of ThT in methanol and chloroform, I have to differ from the notion of an only barrierless potential energy surface. In both the solvents ThT was excited to a locally excited (LE) state, which is emissive.[20] It was previously reported for ThT that the decay profile of a particular transient have no effect of excitation wavelength, which infer that the contribution from the vibrational relaxation in the relaxation dynamics of ThT is negligible.[20] The general picture of the excited state is that the LE state converted to a TICT state along the torsional coordinate of the dimethylaniline moiety with respect to the benzothiazole ring, which is barrier-less in nature.[12,19,20,21] However, to support my experimental observation, I propose the existence of another state in the excited state manifold of ThT. I also propose that LE to the so-called TICT state could be barrierless, however, LE to the newly proposed state has an intrinsic barrier. This relaxation of the LE state to the so-called TICT state found to be very fast and happens on < 100 fs time scale, whereas, LE to the newly proposed state is slower in nature. A recent study by Ren *et al.* revealed that the LE to TICT relaxation is ultrafast in nature and completes within ~300 fs time scale, which is in accordance to my observation.[26]

The possibility of the contribution of solvent relaxation contributed towards the observed dynamic Stokes shift has been excluded because of the lack of any specific polarity dependence of the steady state emission of ThT. It has been reported by Maskevich *et al.* that though the absorption spectra of ThT shows blue shift with respect to increase in solvent polarity, the emission maxima shows no trend.[16] This has been confirmed by Singh *et al.* in their publication.[20] Moreover the solvation time in methanol and chloroform are 4.3 and 1.3 ps respectively.[25] As the solvation times are probe independent, one should expect a similar time scale of solvation, if at all observed for the present case. The opposite trend in the faster time component in the fluorescence transient (low for methanol and high for chloroform) thus cannot be accounted for the solvent relaxation time. Further, the observed comparable dynamic Stokes shift (600 cm^{-1} in methanol and 500 cm^{-1} in

chloroform) suggests a very weak contribution from solvation relaxation, if at all present.

4.A.2.3. Femtosecond Transient Absorption Spectroscopy

I have also performed transient absorption spectroscopic studies of ThT in methanol and chloroform. In figure 4.A.5 and 4.A.6 represent selected time traces and transient spectra of ThT in methanol and chloroform respectively. The data clearly indicate that the LE state of ThT is long-lived in case of chloroform compared to methanol with its characteristic signature in the stimulated emission region (~500 nm) and excited state absorption region (~750 nm). At longer time, a new excited state absorption peak has formed around 470 nm in both methanol and chloroform and the same is assigned to the TICT-1 state. In case of methanol, a new stimulated emission band is noticed (which is very small in magnitude in case of chloroform) around 730 nm at longer time. The seldom signature of this stimulated emission band in case of chloroform drive me to assign the same for TICT-2 state as the energy barrier between LE and TICT-2 state is higher in chloroform than in methanol. The high energy barrier in case of chloroform prevents the molecules to TICT-2 state and thus the molecule stays longer in LE state. The kinetic data were fitted globally using Glotran software.[27] As the evolution of the ESA band of TICT-1 state must be same as the lifetime of the TICT-1 state and the stimulated emission from the LE state must corroborate lifetime of the LE state obtained in up-conversion study, one can expect that the time components obtained from fluorescence up-conversion study must be echoed in the transient absorption experiments. As expected, the global time components found to be very similar to the time components obtained from the fluorescence upconversion study. During the fitting of the transient absorption data, I observed one extra longer time component, which was not observed in the fluorescence experiment.

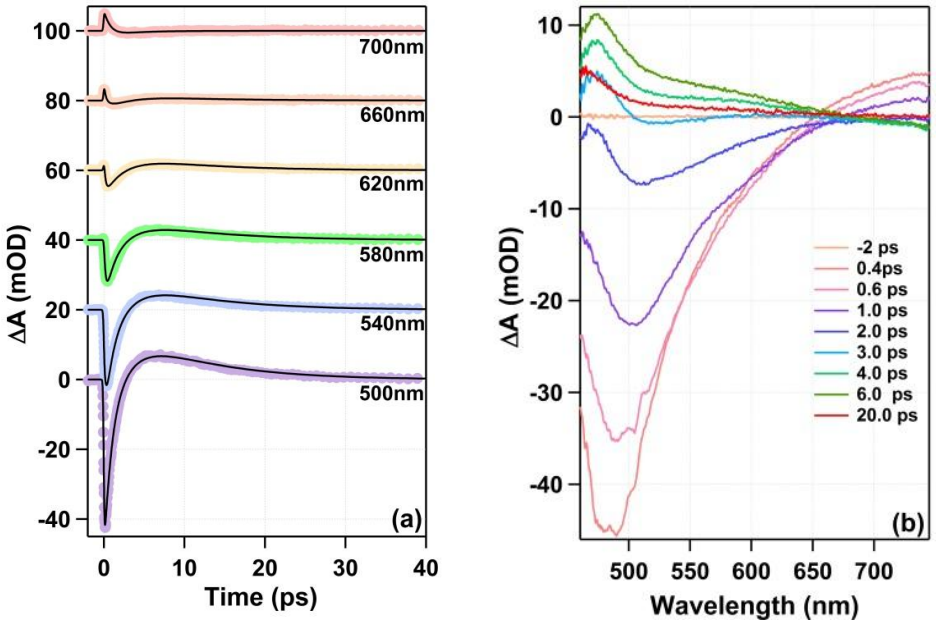

Figure 4.A.5. Transient absorption data of ThT in methanol (a) kinetic traces at selected wavelengths and (b) spectra at different times. Samples were excited at 400 nm and the data were recorded at 25˚C.

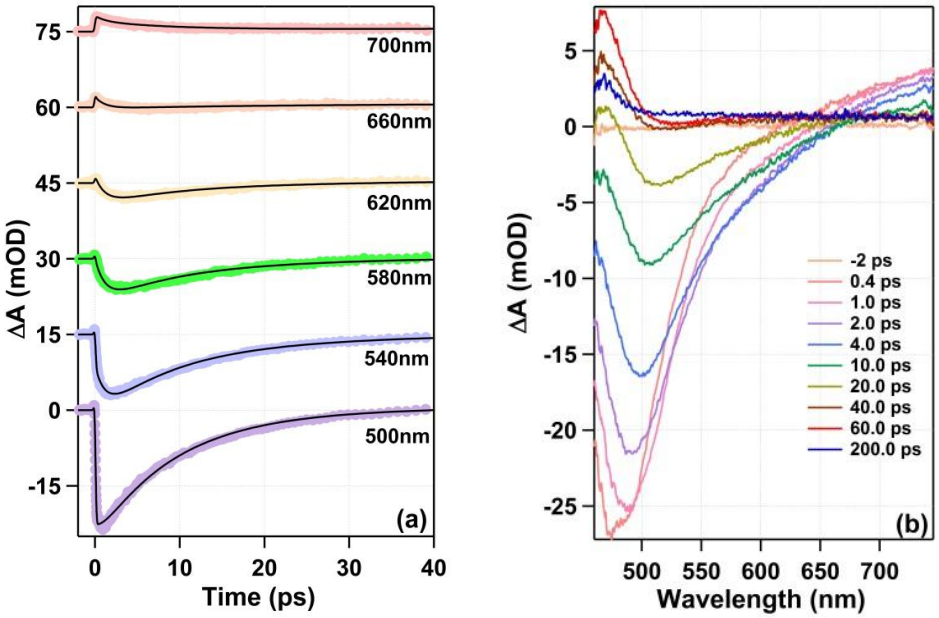

Figure 4.A.6. Transient absorption data of ThT in chloroform (a) kinetic traces at selected wavelengths and (b) spectra at different times. Samples were excited at 400 nm and the data were recorded at 25˚C.

This long time component is assigned to the stable ground state recovery of the molecule from the high energy region, soon after deactivation from the excited state. All the time constants are reported in table 4.A.4.

Table 4.A.4. Global fitting parameters of kinetic traces obtained from fluorescence up-conversion and transient absorption studies of ThT in methanol and chloroform. Samples were excited at 400 nm and the transients were recorded at 25˚C.

Solvent	**Methanol**		**Chloroform**	
Time Constants	Fluorescence upconversion kinetics	Transient Absoprtion kinetics	Fluorescence upconversion kinetics	Transient Absorption kinetics
τ_1 (ps)	0.2	0.3	1.2	1.3
τ_2 (ps)	0.8	1.1	9.1	12.3
τ_3 (ps)	2.5	4.0	50.6	67.3
τ_4 (ps)	-	9.7	-	2000 (fixed)

4.A.2.4. Quantum Mechanical Calculations

To get an idea about the configuration of the states involved in the deactivation process of excited ThT and to scrutinize the existence of the new state as proposed, I have performed time dependent density functional theoretical calculations. The HOMO and LUMO of ThT is shown in figure 4.A.7, which authenticate a prominent charge transfer from the dimethyleanilino moiety to benzothiazole moiety in the LUMO, which present itself as a theoretical evidence of the redistribution of electronic density once the molecule is promoted to higher electronic state. In the ground state, the dimethylanilino group of ThT is pushed off the plane by -37˚, with the dimethylanilino moiety at the plane of the benzene ring. There are two possible large amplitude motion possible in this molecule (see scheme 4.A.1), first the torsional motion of the dimethylanilino moiety with respect to the benzothiazole ring (designated as α) and the second one is the torsional motion of the dimethylamino moiety with respect to the rest part of the molecule (designated as β). TDDFT was used to calculate the energies of 20 electronically excited states corresponding to each 361 geometries of ThT by varying the both the dihedral angles α and β with 10° interval using B3LYP/6-

31+G(d,p) functional. The obtained three-dimensional plot has been shown in figure 4.A.8 along with the contour plots obtained for the ground and excited states, respectively. As expected, I have observed two minimum energy points in the excited state manifold of ThT. The occurrence of point B along the dimethylanilino torsional coordinate has already been discussed extensively in the literature, which earlier proposed to be the solely responsible channel of the deactivation.[12,19,20] However, the existence of point C in the exited state manifold of ThT naturally opens up the possibility of other channel of deactivation and also in turn support our proposition of the existence of other state in the excited state potential energy surface. The nature of this state is also charge transfer in nature (see figure 4.A.9 and 4.A.10) and formed along the torsional coordinate of the dimethylamino moiety. I have designated the B state as the TICT-1 state and C as the TICT-2 state. TICT-1 and TICT-2 states are corresponding to the individual rotation of α and β dihedrals with exact coordinates of α = -87.346°, β = 0.378° (E_{TICT-1} = 56.806 kcal mol^{-1}) and α = -27.346°, β = 90° (E_{TICT-2} = 55.288 kcal mol^{-1}), respectively. The energy landscape from the A point (i.e. LE state) to the TICT-1 state is found to be barrier-less in nature, however, a barrier of ~3 kcal mol^{-1} is observed for the LE to TICT-2 transition, in our TDDFT calculation. It can also be seen from figure 4.A.8 that the global maximum of the ground state potential energy surface is exactly below the TICT-2 state. Thus it is expected that the non-radiative transition is more probable from the TICT-2 to the ground state rather than from the TICT-1 state. Naturally, these calculations do not imply any quantitative basis but the qualitative picture thus obtained satisfies the experimental results. That being said I can get an idea about the pathway that is taken by ThT molecule in its excited state. The actual energies can vary in different solvents but the nature is expected to be retained.

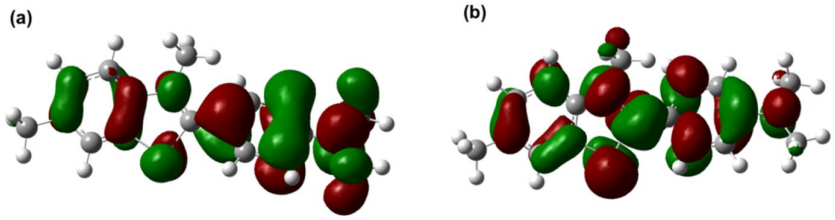

Figure 4.A.7. (a) HOMO and (b) LUMO of ThT calculated by TD-DFT method using B3LYP functional and 6-31+G(d,p) basis set.

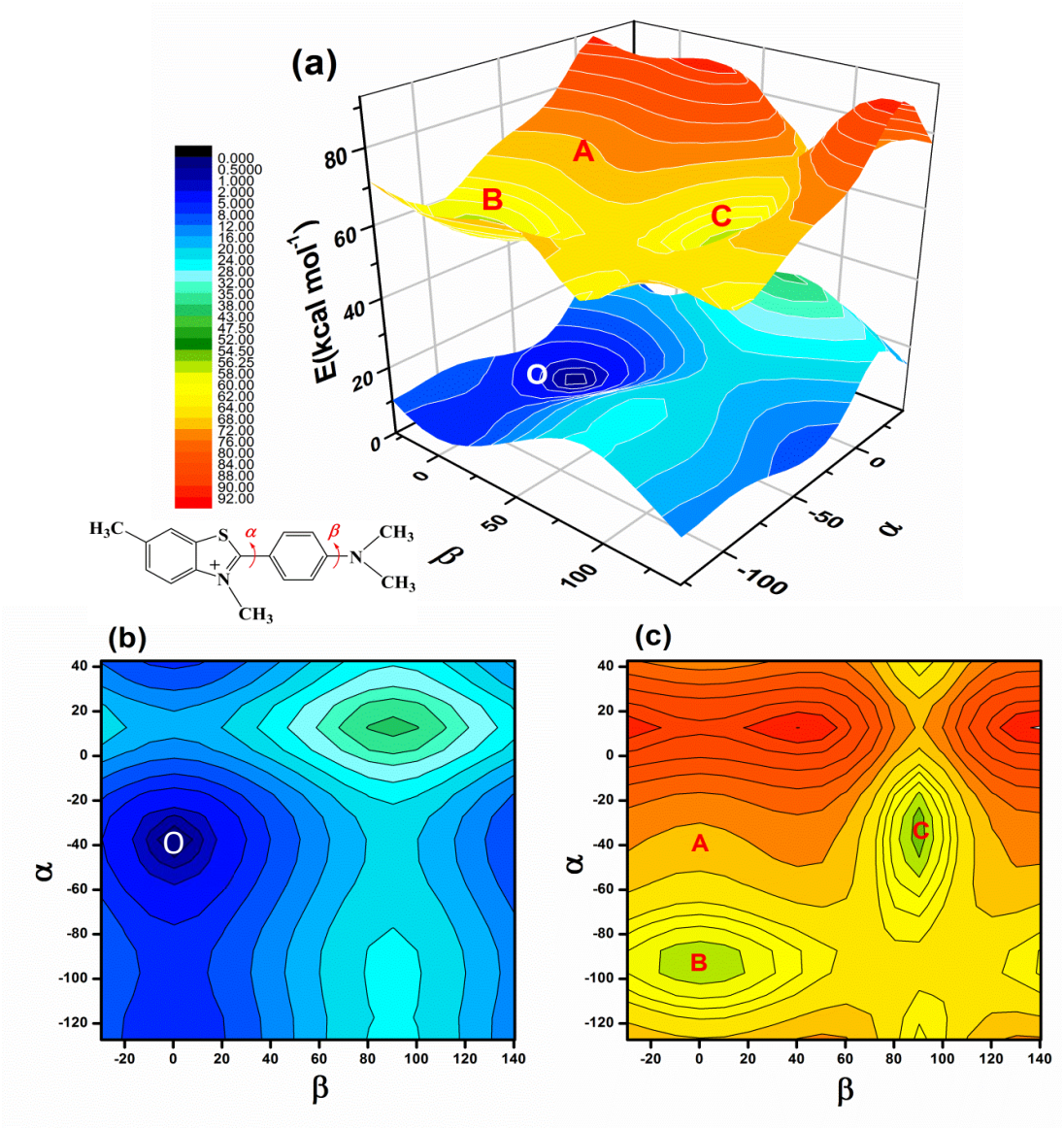

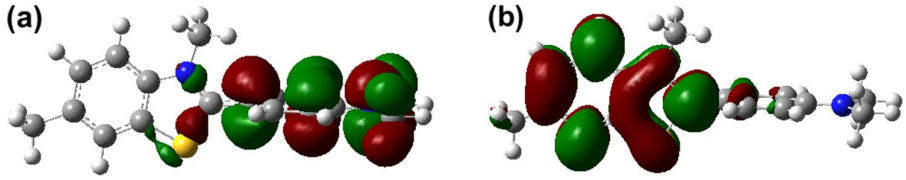

Figure 4.A.9. Twisted intramolecular charge transfer state-1of ThT (a) HOMO (b) LUMO.

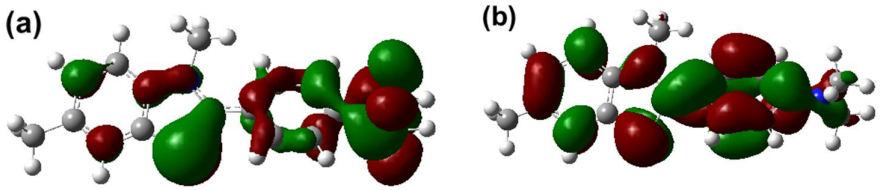

Figure 4.A.10. Twisted intramolecular charge transfer state-2of ThT (a) HOMO (b) LUMO.

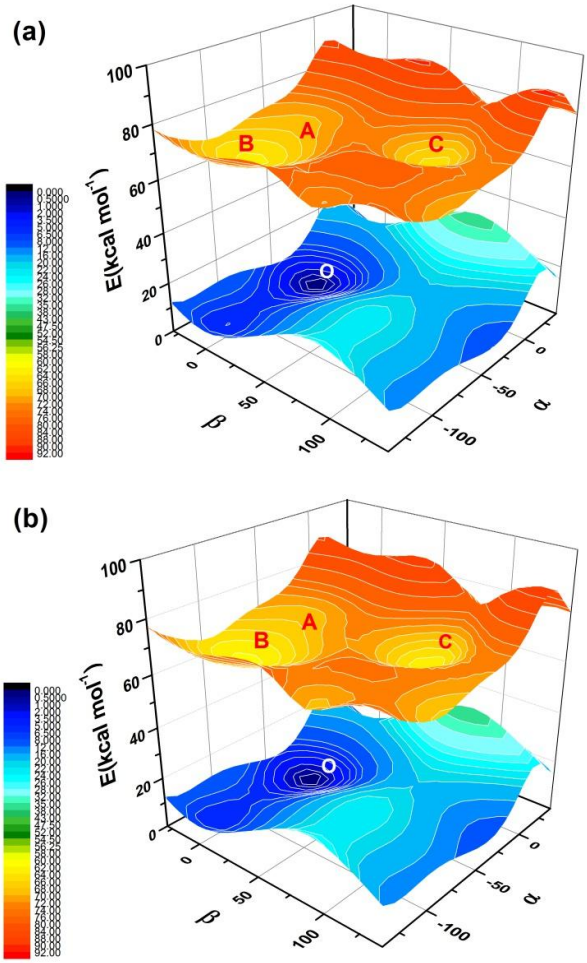

Figure 4.A.11. Ground and excited state potential energy surfaces of ThT (a) in methanol and (b) in chloroform along the dihedral angles α and β coordinates using PCM model.

A similar type of effort has been observed previously to enunciate the mechanism of non-fluorescent nature of thioflavin-T in non-viscous media.[25,26,28] Stsiapura *et al.* have presented a very detailed computational study on ThT and inferred that the rotation of phenyl group with respect to the benzothiazole moiety is the only relaxation channel of the molecule and the excited state potential energy surface is barrier-less in nature. However I would like to point out that although the authors considered both the rotations for calculating the ground state potential energy surface, they have not considered the rotation of dimethylamino group for the construction of the first excited state potential energy surface because of its low contribution to the frontier molecular orbitals. Naturally, they have not observed the presence of the TICT-2 state in their computation. On the other hand, Singh *et al.* actually observed the presence of a barrier in the excited state manifold of ThT along the dimethylamino dihedral angle. However, they have argued that this channel is non-functional because of the presence of energy barrier in the pathway, and only considered the other channel to justify their experimental results. The idea to discard the possibility of the through-barrier relaxation is purely based on the high value of the computed activation energy barrier (0.29 eV) in their case. This is to note that the computed values in such calculation are most of the time over estimated and an experimental determination of such barrier height is necessary. Thus I have performed the temperature dependent study to specify the barrier height in individual solvents. In a recent report by Ren *et al*. a loss of planarity of ThT in the first excited state has been observed. In their simulation, they observed a in-plane geometrical change in the structure of ThT, which indicate the complicated photophysics of ThT.[26] This is to note that in my calculation I have not performed any excited state relaxation and thus the full relaxed excited structure could not be revealed.

To check the effect of solvent on the ground and excited state potential energy surface of ThT, the computation were performed using a PCM model defining the methanol and chloroform respectively. The surfaces obtained are

shown in figure 4.A.11. The existence of a very similar potential energy barrier between LE and TICT-2 state also observed in both the cases as in vacuum. In both the cases the energy of the TICT-2 state is lower than TICT-1 state. The position of the TICT-1 and TICT-2 states are at the same position as was in case of vacuum calculation. However, these kinds of theoretical calculations do not take into account the specific solute-solvent interactions, which may lead to an erroneous estimation of the barrier heights. However, the presence of the barrier is certain and in the next section I determined the height of the barrier in methanol and chloroform experimentally.

I have checked the nature of the three different states (namely, LE, TICT-1 and TICT-2 sates) of ThT in methanol and chloroform by computing the oscillator strength in the above calculation. The computed $S_1 \leftarrow S_0$ oscillator strengths for the LE, TICT-1 and TICT-2 states of ThT in methanol and chloroform are found to be very similar with the values ~1, ~0.08 and ~0.0008, respectively. These values clearly suggest that the LE state is highly fluorescent in nature, however, the both the TICT-1 and TICT-2 states are weakly-fluorescent/non-fluorescent in nature. A very similar observation has been reported previously by Stsiapura *et al.*[19]

4.A.2.5. Temperature Dependent Study

To confirm the presence of an activation barrier in the excited state potential energy surface of ThT, I have performed the temperature dependent steady state emission measurements in chloroform and methanol. These measurements enabled us to calculate the activation energy in the excited state manifold of ThT in either solvent, if at all present. At each temperature the fluorescence spectra were recorded and quantum yields were calculated. I found an increase in the quantum yield of ThT with decrease of temperature. The main theory of such kind of an experiments is discussed before.[38,29-31] Briefly, the Debye-Stokes-Einstein equation relates rate of orientational relaxation (k_{or}) with shear viscosity (η) of the solvent as $k_{or} \propto T/\eta$, where, the k_{or} is responsible for the non-radiative relaxation of ThT, as discussed before. Thus, I can relate the fluorescence quantum yield of ThT with the

viscosity of the medium by assuming that the non-radiative rate (k_{nr}) is comparable to rate of orientational relaxation (k_{or}) and the relation obtained was[32]

$$\frac{\varphi}{1-\varphi} = \frac{k_r}{k_{or}} \propto \eta/T \qquad (4.A.1)$$

If fluorescence quantum yield varies non-linearly with viscosity then we need to introduce a factor for degree of dependence (α) as[32]

$$\frac{\varphi}{1-\varphi} = \frac{k_r}{k_{or}} = C(\eta/T)^{\alpha} \qquad (4.A.2)$$

Here C is the proportionality constant.

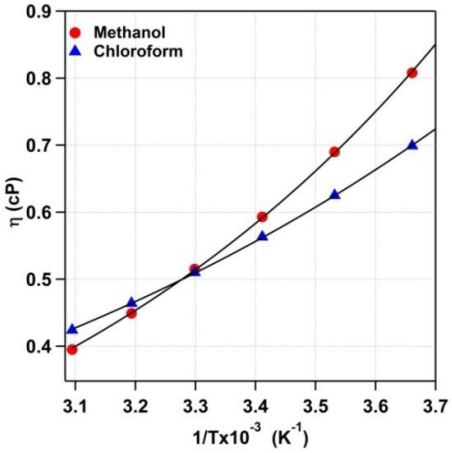

Figure 4.A.12. Plot of shear viscosity with inverse of temperature.

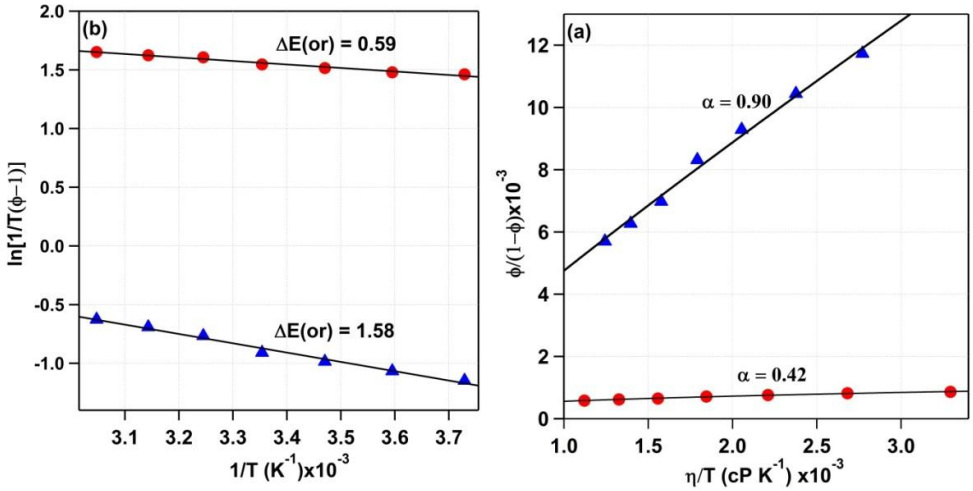

Figure 4.A.13. Plot of (a) φ/(1-φ) vs η/T and (b) ln[1/T(φ-1) vs 1/T of ThT in methanol (red circle) and chloroform (blue triangle). The unit of ΔE(or) is kcal mol^{-1}.

The value of α obtained from our experiments (figure 4.A.13a) were 0.37 and 0.90 for methanol and chloroform respectively. This is to note that the change in the quantum yield of ThT could be a combined effect of presence of an activation barrier on the potential energy surface, as proposed, and the increase in solvent viscosity on decreasing the temperature. In order to envisage the effect of viscosity on the rate of orientational relaxation of ThT, I have calculated the activation energy for viscous flow using Arrhenius-type equation,

$$\eta = \eta_0 e^{\Delta E(\eta)/kT} \qquad (6.A.3)$$

Here $\Delta E(\eta)$ is the activation energy of viscous flow and k is Boltzmann constant. The value $\Delta E(\eta)$ obtained for methanol and chloroform were 2.49 kcal mol^{-1} and 1.74 kcal mol^{-1} respectively (figure 4.A.12). This data implied a larger viscous drag in methanol than in chloroform, and in turn should induce larger fluorescence quantum yield upon decrease in the temperature in case of methanol compared to chloroform. However an opposite observation led us to calculate the actual rate of orientational relaxation by the following equation[32]

$$ln\frac{k_{or}}{k_r} = \ln\left(1/T(1/\varphi - 1)\right) = \ln(c/\eta_0) - \Delta E(or)/RT \qquad (6.A.4)$$

where ΔE(or) is the activation energy of the rate of orientational relaxation along the excited state potential energy surface. The values obtained (figure 4.A.13b) were 0.59 and 1.58 kcal mol^{-1} in methanol and chloroform respectively. The activation energy in methanol was found to be exactly same as that available at room temperature, whereas, the same in chloroform was quite high.

Table 4.A.5. Parameters obtained from temperature dependent study

Solvent	α	E(η) (kcal mol^{-1})	E(or) (kcal mol^{-1})
Methanol	0.37	2.49	0.59
Chloroform	0.90	1.74	1.58

4.A.3. Discussion

Taking into account all the data obtained from the femtosecond time-resolved experiments, TDDFT calculation and temperature dependence on the fluorescence quantum yield of ThT in methanol and chloroform, here a new model for the excited state relaxation dynamics of ThT is proposed and the lifetime components to different states has been assigned. The other two states besides the LE state has been designated as TICT-1 and TICT-2 states, respectively. The LE state can decay either to the TICT-1 state or to the TICT-2 state. I also agree with the general perception that the LE-TICT-1 is extremely fast along the torsional coordinate of dimethylanilino moiety relative to the benzothiazole ring, which is essentially barrierless in nature.[12,19,21] The time constant associated with this process is within our time resolution. I have assigned the 0.2 ps time constant to the lifetime of the LE state in methanol, which appears as a growth component for the TICT-2 state in the same solvent. However, in chloroform, the lifetime of the LE state has been found to be 1.2 ps, which is observed as a growth component at longer wavelengths. The longer time component inherently suggests the existence of barrier in the LE-TICT-2 pathway and the height of the barrier is higher in chloroform than in methanol. The 0.8 ps and 2.5 ps decay components are assigned to the lifetime of TICT-1 and TICT-2 states in methanol, respectively, which become 9.1 ps and 50.6 ps in chloroform. Arguably, the LE population mostly decays to the TICT-1 state, but the TICT-2 channel could be operational depending on the solvent characteristics.

Accepting the barrier-less nature of the LE-TICT-1 transition, I propose that the LE-TICT-2 path has an inherent barrier, which is also supported by the TDDFT calculation. The nature of the newly proposed TICT-2 state is found to be associated with the torsional motion of the dimethylamino moiety from the theoretical calculation. At lowered temperature, the LE-TICT-2 path is not spontaneous and in case of chloroform the LE state emission become higher because of higher activation energy in chloroform compared to methanol. This also

supports the observation of longer rise time in the time resolved emission data in chloroform. Essentially this is the barrier between LE and TICT-2 state that is responsible for the higher quantum yield of ThT in chloroform. For methanol the energy available at room temperature is sufficient to cross this barrier between LE and TICT-2 state, which imparts a low fluorescence quantum yield of ThT in methanol.

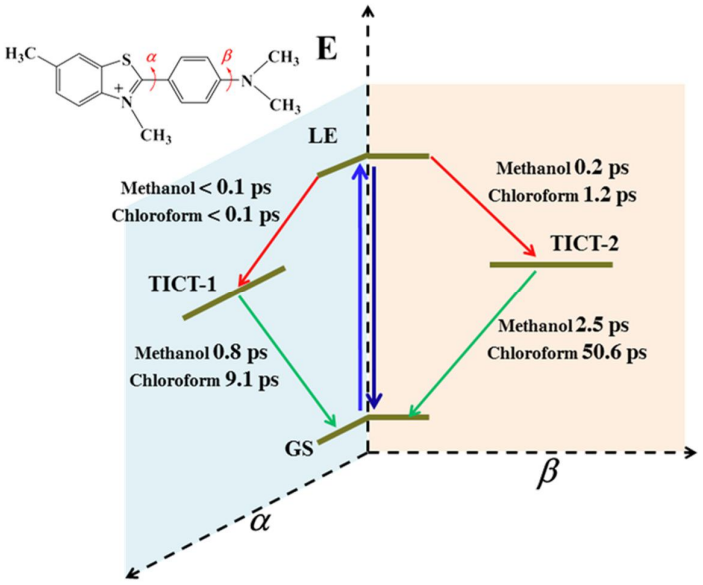

Figure 4.A.14. Schematic representation of excited state relaxation mechanism of ThT in methanol and chloroform.

Overall, ThT upon excitation to the LE state undergoes two different amplitude motions leading to either TICT-1 state or TICT-2 state along the dimethylanilino and dimethylamino torsional coordinate respectively which is shown in figure 4.A.14. LE to TICT-1 is a barrierless process, however, LE to TICT-2 is not and the height of the barrier is solvent dependent. In methanol, the height of the barrier is quite low rendering the overall process a barrierless in nature and thus the fluorescence quantum yield of ThT in methanol is quite low. However in chloroform, the barrier height is quite high, making the ThT molecule live longer in the LE state, exhibiting larger fluorescence quantum yield (about 30 times higher compared to methanol, although the viscosity is very similar).

4.A.4. Conclusion

In this work, I have tried to rationalize the unusual quantum yield of ThT in chloroform compared to methanol (note, both methanol and chloroform have similar viscosity). Our femtosecond fluorescence up-conversion and transient absorption studies showed the involvement of a new TICT emissive state in the excited state manifold of the dye, and has been termed as TICT-2 state, along with the originally proposed TICT-1 state. Upon excitation to the LE state, ThT undergoes two different amplitude motions leading to either TICT-1 state or TICT-2 state along the dimethylanilino and dimethylamino torsional coordinate respectively. Although the LE to TICT-1 pathway is barrier-less in nature, the molecule faces an activation energy barrier when depleting to the TICT-2 state. The height of this activation barrier found to be ~3 times higher in chloroform than in methanol. This barrier has been further proved by temperature dependent study and quantum mechanical calculations.

References

1. Groenning, M. *J. Chem. Biol.* **2010**, *3*, 1–18.
2. Wolfe, L. S.; Calabrese, M. F.; Nath, A.; Blaho, D. V.; Miranker, A. D.; Xiong, Y. *Proc. Natl. Acad. Sci.* **2010**, *107* (39), 16863–16868..
3. Krebs, M. R. H.; Bromley, E. H. C.; Donald, A. M. The Binding of Thioflavin-T to Amyloid Fibrils: Localisation and Implications. *J. Struct. Biol.* **2005**, *149* (1), 30–37.
4. Biancalana, M.; Koide, S. *Biochim. Biophys. Acta* **2010**, *1804*, 1405-1412.
5. Wu, C.; Biancalana, M.; Koide, S.; Shea, J. *J. Mol. Biol.* **2009**, *394*, 627-633.
6. Torres, J. A.; Rimola, A.; Rodriguez, C. R.; Santiago, L. R.; Sodupe, M. *J. Phys. Chem. B* **2013**, *117*, 6674-6680.
7. Wu, C.; Wang, Z., Lei, H.; Duan, Y.; Bowers, M. T.; Shea, J. E. *J. Mol. Biol.* **2008,** *384*, 718-729.
8. Khurana, R.; Coleman, C.; Zanetii, C. I.; Careter, S. A.; Krishna, V.; Grover, R. K.; Roy, R.; Singh, S. *J. Struct. Biol.* **2005**, *151*, 229-238.
9. Robbins, K. J.; Liu, G.; Selmani, V.; Lazo, N. D. *Langmuir* **2012**, *28*, 16490-16495.
10. Babenko, V.; Dzwolak, W. *Chem. Comm.*, **2011**, *47*, 10686.
11. Mohanty, J.; Barooah, N.; Dhamodharan, V.; Harikrishna, S.; Pradeepkumar, P. L.; Bhasikuttan, A. C. *J. Am. Chem. Soc*. **2013**, *135*, 367-376.
12. Amdursky, N.; Erez, Y.; Huppert, D. *Acc. Chem. Res.* **2012,** *45*, 1548-1557.
13. Zhou, F.; Shao, J.; Ynag, Y.; Zhao, J.; Guo, H.; Li, X.; Ji, S.; Zhang, Z. *Eur. J. Org. Chem.* **2011**, 4773-4787.
14. Advanced Fluorescence Reporters in Chemistry and Biology I Springer Series on Fluorescence Volume 8, 2010, pp 267-308.
15. Voropai, E. S.; Samtsov, M. P.; Kaplevskii, K. N.; Maskevich, A. A.; Stepuro, V. L.; Povarova, O. I.; Kuzentsova, I. M.; Turoverov, K. K.; Flink, A. L.; Uverskii, V. N. *J. Appl. Spectrosc.* **2003,** *70*, 868-874.
16. Maskevich, A. A.; Stsiapura, V. I., Kuzmitsky, V. A.; Kuznetsova, I. M.; Povarova, O. I.; Uversky, V. N.; Turoverov, K. K. *J. Proteome Res.* **2007**, *6*, 1392-1401.
17. Naik, L. R.; Naik, A. B.; Pal, H. *J. Photochem. Photobiol. A* **2009**, *204*, 161-167.
18. Singh, P. K.; Kumbhakar, M.; Pal, H.; Nath, S. *J. Phys. Chem. B* **2010,** *114*, 5920-5927.

19. Stsiapura, V. I.; Maskevich, A. A.; Kuzmitsky, V. A.; Uversky, V. N.; Kuznetsova, I. M.; Turoverov, K. K. *J. Phys. Chem. B* **2008**, *112*, 15893-15902.
20. Singh, P. K.; Kumbhakar, M.; Pal, H.; Nath, S. *J. Phys. Chem. B* **2010**, *114*, 2541-2546.
21. Stsiapura, V. I.; Maskevich, A. A.; Tikhomirov, S. A.; Buganov, O. V. *J. Phys. Chem. A* **2010,** *114*, 8345-8350.
22. Ghosh, R.; Palit, D. Ultrafast Bond Twisting Dynamics of Thioflavin-T: Spectroscopy of the Twisted Intramolecular Charge-Transfer State. *ChemPhysChem* **2014,** *15*, 4126-4131.
23. Rafiq, S.; Rajbongshi, B.K.; Nair, N. N.; Sen, P.; Ramanathan, G. *J. Phys. Chem. A* **2011**, *115*, 13733-13742.
24. Maroncelli, M.; Fleming, G.R. *J. Chem. Phys*. **1987,** *86*, 6221-6239.
25. Gupta, S.; Rafiq, S.; Sen, P. *J. Phys. Chem. B* **2015**, *119*, 3135–3141.
26. Ren, H.; Fingerhut, B. P.; Mukamel, S. *J. Phys. Chem. A* **2013**,*117*, 6096-6104.
27. Snellenburg. J. J; Laptenok, S. P.; Seger, R.; Mullen, K. M.; vanStokkum, I. H. M. *J. Stat. Softw.* **2012,** *49*, 1-22.
28. Stsiapura, V.I.; Maskevich, A.A.; Kuzmitsky, V.A.; Turoverov, K.K.; Kuznetsova, I.M. **2007**, *111*, 4829–4835.
29. Rocker, C.; Heilemann, A.; Fromherz, P. *J. Phys. Chem.* **1996**, *100*, 12172-12177.
30. Waldeck, D. H.; Fleming, G. R. *J. Phys. Chem.* **1981**, *85*, 2614-2617.
31. Loutty, R. O.; Arnold, B. A. *J. Phys. Chem.* **1982,** *86*, 4205-4211.
32. Rafiq, S.; Sen, P. *J. Chem. Phys*. **2013**, *139*, 124302-1-124302-8.

This page intentionally left blank

Chapter 4

Part B

Ultrafast Excited State Deactivation Channel of Thioflavin T Adsorbed on SDS Micelle: A Combined Femtosecond Fluorescence and Transient Absorption Study

Puspal Mukherjee, Aritra Das and Pratik Sen *J. Photochem. Photobiol. A Chem.* **2017**, *348*, 287–294.

4.B.1. Introduction

Thioflavin T (ThT) has been used for a long time as a sensor and marker for *β*-amyloid structure in proteins and G-quadraplex DNA for its remarkable enhancement of fluorescent quantum yield in the bound form.[1-11] In last couple of years, ThT has been extensively used in fluorescent bio-imaging of apoptotic cell, recognizing duplex motifs in bimodular aptamer, strand displacement amplification technique in biosensing and in recognition of RNA G-quadruplex.[6-10] Although the mechanism of ThT binding to amyloid fibrils and so called short wavelength excitation and emission are not fully understood till date, the dye and its neutral derivatives have been used extensively for imaging amyloid aggregates both *in vivo* and *in vitro*, even in brain.[1-5] Primary reason for this widespread application of ThT lies in the fact that in a restricted environment the green fluorescence of the dye can be as high as ~1000 times brighter than in a non-restricted environment such as in aqueous solutions.[12-17] Being a molecular rotor, ThT undergoes a large amplitude motion in its excited electronic state rendering its excited state lifetime extremely small in low viscous media. Dzwolak *et al.* have shown that when ThT binds to insulin fibrils, it experienced an intramolecular twisting in the ground state itself, manifesting a strong Cotton effect around 450 nm.[11] In the bound form, i.e. in the restricted environment, the restriction on the large amplitude motion is imposed and the fluorescence intensity and lifetime increased immensely.[12-17] Therefore, ThT can also be used as a ruler for viscosity of surrounding environment because viscous drag creates a hindrance on rotation of molecular fragments, which changes the fluorescence quantum yield of ThT.[15,18-22] For example, Singh *et al.* used ThT in two tris(pentafluoroethyl) trifluorophosphate (FAP) ionic liquids (IL) to show that ILs can offer unique microenvironment.[23] Although they have observed the long time behavior of ThT depends on ILs viscosity, the short time behavior is found to be independent of bulk viscosity.[23]. In another work they have showed that the micro-viscosity felt by ThT in ILs can be different from the bulk viscosity.[24] ThT has been used by Chatterjee and Seth to elucidates the micro-viscosity of non-aqueous reverse micelles and dioxane-water

binary solvent mixture.[25] They claimed that glycerol containing reverse micelles offer a unique increase followed by decrease in viscosity, which is not observed for any other solvents.[25] Moreover using dioxane-water mixture, they have tried to show that rotation of ThT is affected by the polarity of the medium.[25] However, Friedhoff *et al.* have previously claimed that fluorescence intensity of ThT does not have a simple variation with solvent dielectric constant and the change in emission maxima is also negligible.[26] All of these understanding along with many previous ones are based on a barrierless two state electronic excited state potential energy surface of ThT.

Here, I have studied ThT adsorbed on sodium dodecyl sulfate (SDS) micelle. As ThT is positively charged and the surfactant head groups of SDS are negatively charged, ThT is expected to remain in the Stern layer of the micelle. This phenomenon should affect the deactivation channels of the dye. I have shown that dynamics of ThT on miceller interface gets retarded compared in pure water in such a manner that it solidifies the idea of a complicated excited state potential energy surface rather than a simple two state model along the twisted coordinate of dimethylanilino moiety.

4.B.2. Results

4.B.2.1. Steady State Spectroscopy

On addition of SDS in a ThT solution in water a red shift in the absorption spectra of ThT was observed (Figure. 4.B.1a). The maxima shifted from 412 nm in water to 429 nm in 40 mM SDS without any significant broadening of the absorption spectra. On the contrary, the emission spectra did not show any significant peak shift but the intensity increased by a large amount (Figure. 4.B.1b). I have compared the absorption and emission spectra of ThT in pure water and in 40 mM SDS to elucidate the point, which confirms the interaction of ThT with SDS. The absence of any perceivable broadening of the absorption spectra of ThT in SDS micelle lead me to believe that ThT is not distributed throughout the heterogeneous milellar environment (Stern layer to the core of the micelle) and I

believe the ThT stayed only at the Stern layer due to columbic attraction between the negatively charged surfactant head groups and positively charged dye.

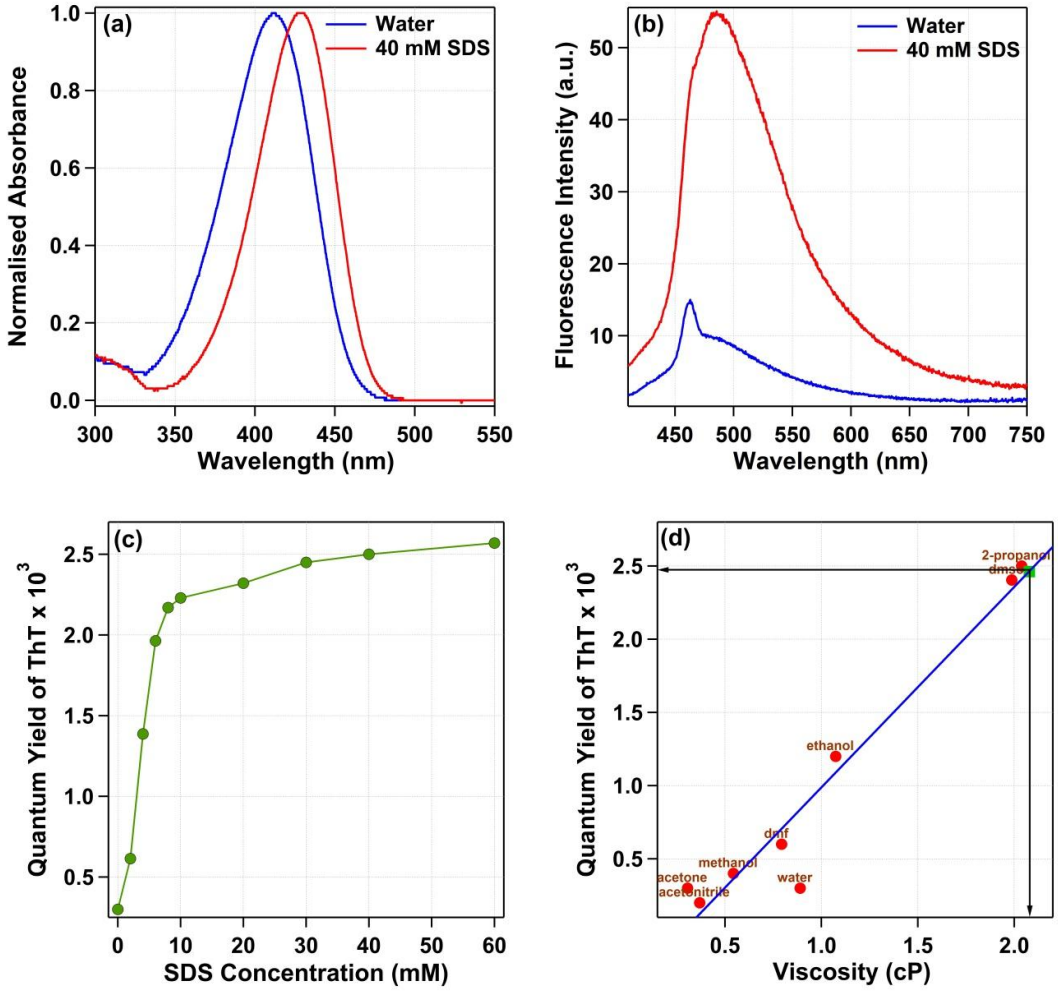

Figure 4.B.1. Effect of SDS micelle on the steady state spectra of ThT. (a) Absorption (b) Fluorescence (c) Variation of quantum yield of ThT with increasing concentration of SDS in water. (d) Comparison of quantum yield of ThT in 40 mM SDS with that in pure solvents (data taken from reference 17)

In figure 4.B.1c I have given the increase in the quantum yield of ThT with enhancement of SDS concentration in water. It is clear that after the critical micelle concentration (CMC) of SDS (~8 mM) the quantum yield attained saturation. In this context we would like to mention the previous work by Kumar *et al.*, where they demonstrated the change in integrated fluorescence intensity of ThT in water with addition of SDS upto a concentration of 10 mM.[27] However, they have

performed their experiment in pH 8.5 buffer solution and probably because of that they achieved saturation before CMC. I, on the other hand, have used neutral water for preparation of the solutions. Moreover as the quantum yield of ThT is extremely low (e.g. in water it is 0.0003), the emission spectra is overshadowed by Raman response from the solvents. Hence, I have taken ThT in water as our reference for quantum yield measurement and observed ~8 fold increase in the quantum yield. In figure 4.B.1d we have plotted the quantum yield values of ThT in different solvents.[17] For comparison purpose, I have assumed a linear dependence of quantum yield upon viscosity of the medium. Here to note that, I have excluded the chlorinated solvents such as chloroform and dichloromethane, as ThT have unusually high quantum yields in such solvents compared to other solvents of similar viscosities, which was elaborately examined in the previous chapter. The position of quantum yield of ThT in 40 mM SDS indicated a viscosity value of 2.1 cP. From this study it can be concluded that on the SDS miceller surface the non-emissive states of ThT are forming inefficiently. Thus it should enable us to study the dual relaxation channel more easily than studying it in water.

4.B.2.2. Femtosecond time-resolved fluorescence measurements

I have recorded fluorescent transients of ThT in 40 mM SDS at 16 different wavelengths ranging from 450 nm 575 nm. All the transients were fitted with a sum of three exponential functions (Figure 4.B.2a) and the fitted parameters are given in table 4.B.1. The average lifetime gradually increased from 2.5 ps at 450 nm to 19.4 ps at 575 nm. Individual three exponential fitting implies that the LE state is decaying through at least two channels. If the LE state only decayed through its radiative channel and TICT1, I would have obtained not more than two exponential time component, considering the more or less homogeneous environment of ThT in the Stern layer of the micelles. Moreover, I have observed a rise part in the florescence transients upto 600 fs for the last three wavelengths i.e. 550 nm, 560 nm and 575 nm (Figure. 4.B.2a and Table 4.B.1). This observation is similar with the previous study of ThT in chloroform and methanol. Observation of

a rise part in the fluorescence transient means formation of a new state involving a finite delay time. Here, the possibility of solvation of ThT in the Stern layer of SDS micelle is not accounted as ThT does not show any solvatochromic properties.[28] From the time resolved fluorescence decay I have constructed the time resolved emission spectra as shown in figure 4.B.2b.[29] In the TRES, the intensity of fluorescence decays to ~10% of its original value within 14 ps.

Table 4.B.1. Fitting parameters of fluorescent transients of ThT in 40 mM SDS at different wavelengths obtained from femtosecond fluorescence up-conversion spectroscopy.

Wavelength (nm)	τ_1 (ps)	a_1	τ_2 (ps)	a_2	τ_3 (ps)	a_3	τ_{avg} (ps)
450	0.27	0.6967	1.53	0.54	12.88	0.2073	2.55
455	0.25	0.6276	1.80	0.5882	15.72	0.1933	3.02
460	0.28	0.5826	2.04	0.555	15.89	0.2395	3.70
465	0.31	0.4594	2.23	0.5697	16.00	0.263	4.35
470	0.35	0.3764	2.35	0.5382	16.38	0.3056	5.25
475	0.38	0.4265	2.68	0.513	17.68	0.2823	5.34
480	0.44	0.4026	3.09	0.4926	17.83	0.3096	5.99
490	0.47	0.257	3.23	0.5249	19.30	0.38	7.88
500	0.45	0.168	3.38	0.5515	19.63	0.3856	8.60
510	0.53	0.1051	3.44	0.5087	19.29	0.444	9.80
520	0.40	0.062044	3.54	0.51882	20.28	0.47874	10.92
530	0.47	0.05514	4.63	0.53416	22.02	0.4345	11.79
540	0.05	-0.0372	4.89	0.52181	23.22	0.48554	14.25
550	0.29	-0.02032	5.43	0.5186	24.27	0.50748	15.04
560	0.32	-0.12397	4.47	0.41731	22.11	0.63565	17.09
575	0.63	-0.13654	6.83	0.4289	24.08	0.60246	19.39

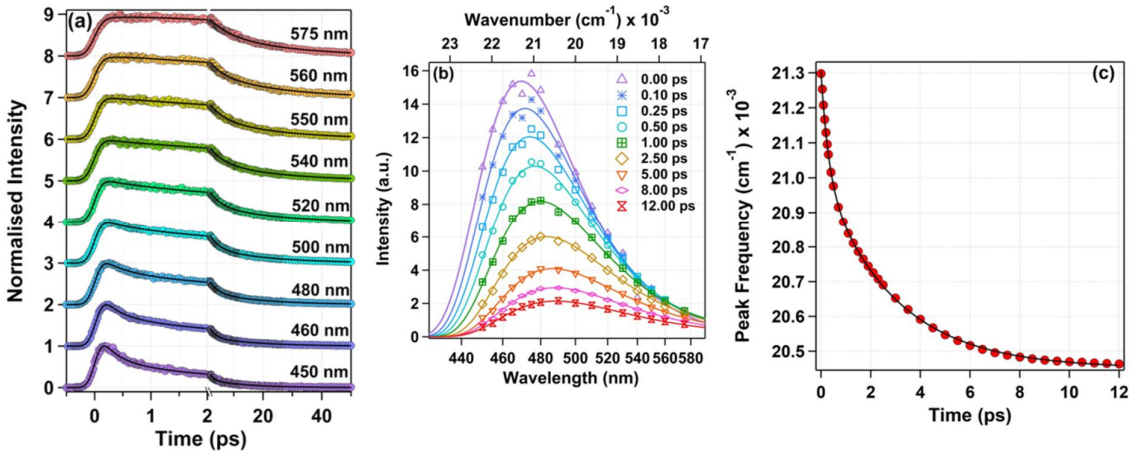

Figure 4.B.2. Time resolved fluorescence studies of ThT in SDS micelle in femtosecond time domain. (a) Kinetic traces of fluorescence decay at different wavelengths. (b) Time resolved emission spectra (TRES). (c) variation of emission maxima with time for ThT in 40 mM SDS. Solid lines indicate fitting.)

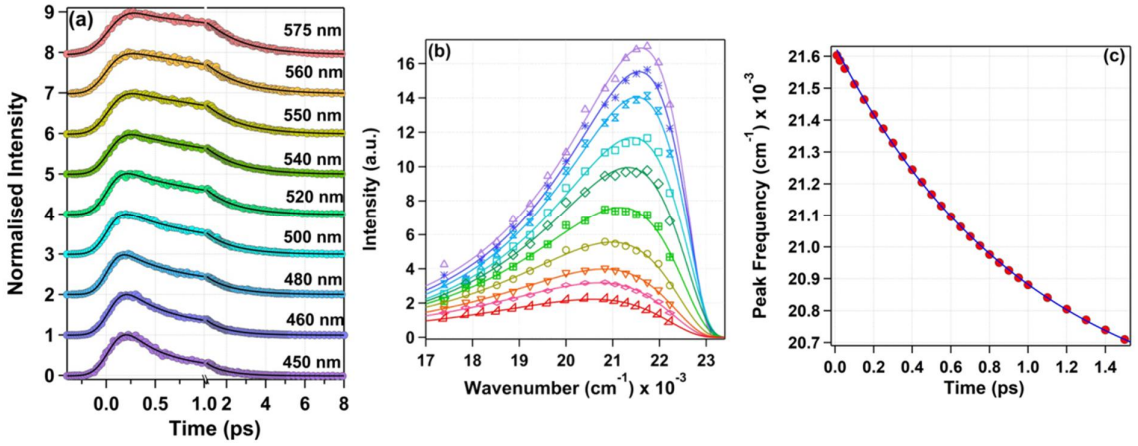

Figure 4.B.3. (a) Kinetic traces of fluorescence at different wavelengths, (b) time resolved emission spectra (TRES) and (c) variation of emission maxima of TRES with time for ThT in water. Solid lines indicate the fitting.

Here a comparison with dynamics of ThT in water can be presented. Dynamics of ThT in water has been reported previously using fluorescence up-conversion spectroscopy and broadband transient absorption spectroscopy.[19.21] In both cases the authors used a single rotation channel in the excited state to describe the photophysics, but there are some ambiguity among the two reports. For the purpose of comparison I have performed the experiments again in our setup (figure 4.B.3). Although a two-exponential function was sufficient to fit the fluorescence

transients from 450 nm to 530 nm, a sum of three exponential functions was needed to fit the 540 nm – 575 nm data, out of which the first one came out as a rise part with a maximum value of ~200 fs. Average lifetime of ThT in water varied from ~0.6 ps to ~1.3 ps, which are much less than the same in SDS. Thus it is confirmed that with formation of SDS micelles in water, ThT molecules no longer stays in the bulk water but moves to the interface of micelle and water where the amplitude motion of ThT governing its lifetime is significantly affected. According to the proposition in the previous chapter, with slowing down of the rotation we should be able to observe the dual relaxation pathway of ThT which is reflected here.

In water, both the decays (LE →TICT1 and LE →TICT2) are ultrafast and due to our instrumental time resolution we can distinguish them. However, when the Stern layer of SDS micelle hinders the rotation of dimethylamino and dimethylanilino group, owing to its restricted environment, a clear three-exponential nature of fluorescent transients was observed. To make this idea clear, in figure 4.B.2c and figure 4.B.3c the variation of peak positions of TRES are plotted against time for both in 40 mM SDS and in water. It can be clearly seen that in case of SDS about 900 cm^{-1} Stokes shift was observed which follows a biexponential decay behavior with two time constants as 0.3 ps and 2.9 ps. In case of water the total observed Stokes shift of 750 cm^{-1} follows a single exponential decay with a time constant of ~1 ps. In our previous study, the variation of time resolved emission maxima of ThT in methanol was also found to be single exponential with a time constant of 0.9 ps and the same in chloroform was 0.6 ps and 6.3 ps. So, water behaves quite similar to methanol, which is expected. So I can confirm the potential energy barrier between LE → TICT2 have similar magnitude in water and methanol. Therefore, at room temperature, LE → TICT2 channel is operating presumably experiencing no barrier, which makes the process faster. In SDS, however, two situations are arising. The rotation is hindered and the barrier is more than that in water. So the barrierless decay of LE → TICT1 slows down due to slow rotation, which increases its timescale. The LE → TICT2

transition experiences slower rotation as well as an increased barrier height, which increased its time scale a lot. To get a generalized idea about the time scales of rotations we fitted the all the 16 wavelengths using global fitting method, and got three time constants (Table 4.B.2). When this fitting is performed, a rise component has been observed in 540 nm – 575 nm confirming the delayed formation of TICT2 state. This means that ThT spends more time in the LE state. But before assigning the lifetime of the three states, I want to discuss the broadband femtosecond transient absorption study, which will confirm the dynamics of ThT in SDS micelle.

4.B.2.3. Femtosecond broadband transient absorption spectroscopy

Previously femtosecond broadband transient absorption spectroscopy has been employed to study the dynamics of ThT in polar protic solvents (water, ethanol, 2-propanol and butanol) by Stiapura *et al.*, polar aprotic solvents (acetonitrile, dimethyl formamide, dimethyl sulfoxide and propylene carbonate) by Ghosh *et al.* and in methanol and chloroform in previous chapter.[21,30] In our setup, I can detect the stimulated emission (SE) band around 500 nm and the corresponding LE excited state absorption band (ESA) around 700 nm. The TICT1 state of ThT showed an ESA band around 480 nm at later delay time. However unlike Ghosh *et al.*, I cannot observe the ground state bleaching (GSB) of ThT, which is around 400 nm.[30] Here I want to mention that Ghosh *et al.* observed a long lived ESA band, which they assigned to the triplet state of ThT and they have assigned the timescale of rise part of SE band in acetonitrile to the vibrational relaxation of Franck-Condon state (FC) to the LE state.[30] In figure 4.B.4a I have presented the difference spectra obtained at various times for ThT in 40 mM SDS in our TA setup. A broad SE band around 480 nm was obtained, which formed rapidly after excitation. With progress of time, this band showed bathochromic shift and its intensity decreased. After 40 ps, the SE band was almost diminished in intensity and has been shifted to ~506 nm. Associated with this negative SE band, I can also observe the decay of ESA signal around 720 nm. However, the ESA

signal of TICT1 state, which appeared around 470 nm did not reach a positive value within the lifetime of ThT.

Table 4.B.2. Global fitting parameters obtained for ThT in 40 mM SDS and in water by analyzing the fluorescence up-conversion and broadband femtosecond transient absorption data.

	Fluorescence up-conversion		Broadband Transient Absorption	
	ThT in SDS	ThT in water	ThT in SDS	ThT in water
τ_1 (ps)	0.50	0.15	0.50	0.15
τ_2 (ps)	3.40	0.80	3.10	0.85
τ_3 (ps)	19.20	5.70	15.70	4.40

This signal was very clear in water (figure 4.B.5a). The absence of positive ESA signal from TICT1 state signifies the inefficient formation of the same from the LE state. Thus the sluggish rotation of dimethylanilino moiety, which is responsible for the major population decay, is confirmed under the effect of SDS micelle. The entire data was fitted in a global fitting procedure using GLOTRAN software and presented them in figure 4.B.4b.[31]. A sum of three exponential functions convoluted with a Gaussian instrument response function was necessary to fit the data and the obtained time constants are tabulated in table 4.B.2. The three time constants are very similar to the same obtained from up-conversion studies. Similarly I have fitted the transient absorption spectra obtained for ThT in water in the same global fitting manner with a sum of three exponential functions. The time constants obtained are also reported in table 4.B.2. Comparing the two data, I can conclude that there is ~4 times increase of all the three time constants in SDS compared to water. So the lifetime of all the states are increased by 4 times, which is concluded from both up-conversion and transient absorption studies.

4.B.3. Discussions

From quantum yield measurements, I have observed 8 times increase in fluorescence quantum yield of ThT from water to 40 mM SDS, which corresponded to slightly more than 2 times increase in viscosity considering a linear behavior. However, in fluorescence up-conversion study I clearly observed

three exponential decays for all the transients, which indicates the involvement of three distinct states in the photophysics of ThT.

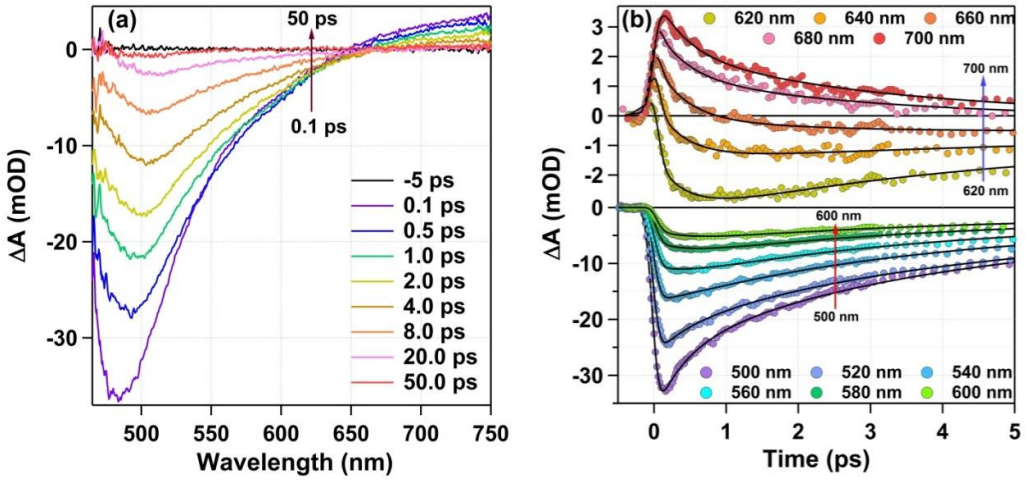

Figure 4.B.4. Broadband femtosecond transient absorption study of ThT in SDS micelle. (a) Transient absorption spectra at different times. (b) Kinetics at different wavelengths for ThT in 40 mM SDS. Solid lines indicate fitting.

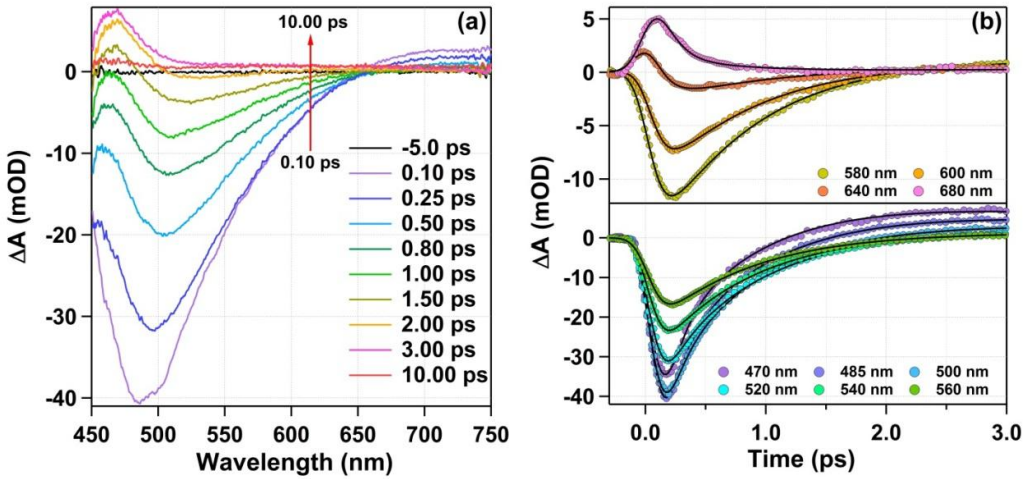

Figure 4.B.5. (a) Transient absorption spectra at different times and (b) kinetics at different wavelengths for ThT in water. Solid black lines indicate fitting.

The bi-exponential nature of the emission maxima vs time plot also indicated two distinct relaxation channels. One can argue that the multi-exponential nature of the data can be originated from the solvation dynamics. In a recent publication by Stsiapura *et al.*, the identical timescale of dynamic solvent response and LE state

lifetime was hinted.[32] In this system, ThT definitely remains on the Stern layer of SDS micelle if not inside it. The ultrafast solvation time on SDS micelle is known to be 1.48 ps.[33] The lifetime of the LE state, which is responsible for the majority of fluorescence decay is found to be 0.5 ps in our study. Therefore any dynamical solvation effect in the excited state should be insignificant. Perhaps both the relaxation channels can be controlled by viscosity alone. When comparing the quantum yield data with that of the pure solvents, I observed two solvents namely dimethylsulphoxide (DMSO) and 2-propanol in the vicinity of ThT in 40 mM SDS. Between them, DMSO should be a good choice for comparison as the dielectric constant of DMSO (~47) is very close to the same of Stern layer of SDS micelle (~48) both of which are higher than that of 2-propanol (~20).[32,34]. When Ghosh *et al.* studied ThT in DMSO by transient absorption study, they found three lifetime components (0.45, 2.8 and 9.0 ps).[30] I have allotted the lifetimes of LE, TICT1 and TICT2 states as 0.50 ps, 3.1 ps and 15.7 ps respectively from the broadband transient absorption spectroscopy. Clearly, the first two states (LE and TICT1) for ThT in both DMSO and 40 mM SDS micelle have close similarities. Ghosh et al. found the first time component to be independent of solvent viscosity for polar aprotic solvents but the second lifetime component follows the trend of solvent viscosity. Thus they assigned the first component to vibrational relaxation an idea with which I differ.[30] I think, following the dielectric constant values, that the Stern layer of SDS micelle behaves quite like an aprotic solvent and all of them have similar intrinsic potential energy barrier between LE → TICT2 state. The existence of this potential energy barrier has been established in details using time resolved studies along with temperature dependent study and quantum mechanical calculations for ThT in methanol and chloroform in the previous chapter. In a recent publication, Rybicka *et al*. also discussed the possibility of dual relaxation channels of ThT.[35] Thus the LE → TICT2 process dictates the lifetime of LE state and due to presence of the potential energy barrier, this process is not solely controlled by medium viscosity. LE → TICT1 transition however is completely viscosity controlled and therefore showed similar values to DMSO. The third

lifetime component (lifetime of TICT2) showed the mismatch may be due to difference between the potential energy of TICT2 state in DMSO and SDS micelle. So basically, once excited, the LE state get populated quickly and from there most of the population decayed by the rotation of dimethylanilino moiety with respect to benzothiazole fragment, forming the TICT1 state. The barrier between LE-TICT2 prevented a fast population migration to TICT2 state, which increased the LE state lifetime. The whole proposition has been schematically represented in scheme 4.B.1. I can establish the viscosity dependence of LE → TICT1 process using a simple model incorporating the torque generated by viscous drag upon rotation of dimethylanilino molecular fragment with respect to benzothiazole moiety of ThT in SDS and in water. This model was used by Huppert and co-workers in their work.[15,36]

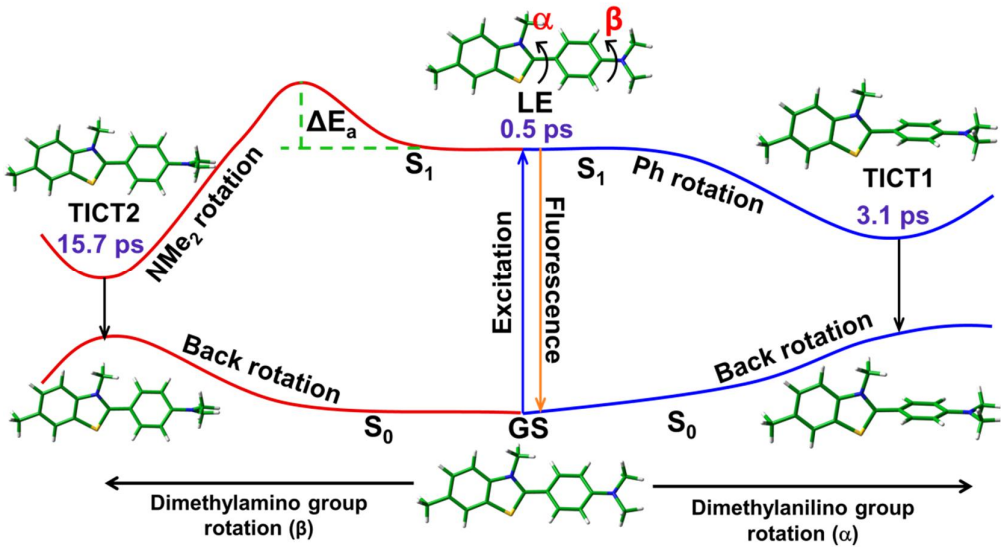

Scheme 4.B.1. Deactivation scheme of ThT adsorbed on SDS micelle.

From the computed potential energy surface in the previous publications we can see that the rotation of phenyl group from -37˚ to -90˚ takes the molecule from LE → TICT1 state with a ~200 meV/1600 cm^{-1} change in energy. [15,36] Although this energy gap would change based on the dielectric property of the medium, a rough estimate can be obtained with this value. The generated torque (t) is given by

$$t = \frac{\partial U}{\partial \theta} \qquad (4.B.1)$$

Here, $\frac{\partial U}{\partial \theta}$ is the derivative of potential energy with respect to rotation angle. Torque multiplied by angular mobility (μ) can give us angular rotation velocity (ω)

$$\omega = \mu \times t \quad (4.B.2)$$

Angular momentum is defined as

$$\mu = \frac{D_r}{k_B T} \quad (4.B.3)$$

where D_r is rotational diffusion coefficient, k_B is Boltzmann constant and T is temperature. The rotational diffusion is given by

$$D_r = \frac{k_B T}{2\eta V} \quad (4.B.4)$$

Finally, the rotational relaxation time is defined by

$$\tau_{rot} = \frac{\Delta\theta}{\omega} = \frac{2\eta V}{t} \quad (4.B.5)$$

Considering the volume of phenyl group as 20 $Å^3$ and the viscosity value of ~2.1 cP as obtained from figure 4.B.1d (steady state quantum yield study) I obtained the value of τ_{rot} = 2.625 ps. The same calculation in water yields τ_{rot} = 1.0 ps . So almost three times increase in the τ_{rot} from water to SDS justifies the increase of lifetime of LE and TICT1 state by three times. The dimethylamino group being much smaller than the phenyl group will face a much less viscous drag and so its rotation is expected to be less dependent on the viscosity. Now, as proposed, the potential energy barrier between LE → TICT2 state for ThT in SDS micelle must have changed in height compared to water, which enforce a lower excited state population of the TICT2 state. Moreover the rotation of dimethylanilino group was slowed down due of the restricted environment offered by the micellar interface. Therefore both the timescales of LE → TICT1 and LE → TICT2 rotations have increased compared to water. In this approach, the unusual origin of multiexponential decays of ThT can be addressed.[30,32]

4.B.4. Conclusion

In this work, I have demonstrated the effect of SDS micelle on the photophysics of ThT. Adsorption of this positively charged dye on the negatively charged SDS micelle increased the quantum yield of the dye by 8 times compared

to water. Fluorescence up-conversion and broadband femtosecond transient absorption study revealed the existence of locally excited state followed by two twisted intramolecular charge transfer states (TICT1 and TICT2). The transition of LE → TICT1 state is barrierless and majorly controlled by the medium viscosity, however the LE → TICT2 transition proposed to possess an intrinsic potential energy barrier.

References

1. Alavez, S.; Vantipalli, M.C.; Zucker, D.J.S.; Klang, I.M.; Lithgow, G.J. *Nature*. **2011,** *472*, 226–229.
2. Freire, S.; De Araujo, M.H.; Al-Soufi, W.; Novo, M. *Dye. Pigment.* **2014,** *110* 97–105.
3. Nesterov, E.E.; Skoch, J.; Hyman, B.T.; Klunk, W.E.; Bacskai, B.J.; Swager, T.M. *Angew. Chemie -Int. Ed.* **2005**, *44*, 5452–5456.
4. Wendler, D. S. *J. Clin. Ethics* **2013**, *24*, 387–394.
5. Xue, C.; Lin, T. Y.; Chang, D.; Guo, Z. *R. Soc. Open Sci.* **2017**, *4*, 160696.
6. Liu, Z.; Luo, X.; Li, Z.; Huang, Y.; Nie, Z.; Wang, H.-H.; Yao, S. *Anal. Chem.* **2017**, *89*, 1892–1899.
7. Deng, M.; Zhang, L.; Jiang, Y.; Liu, M. *Angew. Chemie - Int. Ed*. **2016**, *55*, 15062–15066.
8. Li, Y.; Xu, S.; Wu, X.; Xu, Q.; Zhao, Y.; Lou, X.; Yang, X. *Anal. Bioanal. Chem.* **2016**, *408*, 8025–8036.
9. Du, Y. C.; Zhu, L. N.; Kong, D. M. *Biosens. Bioelectron.* **2016**, *86*, 811–817.
10. Xu, S.; Li, Q.; Xiang, J.; Yang, Q.; Sun, H.; Guan, A.; Wang, L.; Liu, Y.; Yu, L.; Shi, Y.; et al. *Sci. Rep.* **2016**, *6*, 24793.
11. Dzwolak, W.; Pecul, M. *FEBS Lett.* **2005**, *579*, 6601–6603.
12. Groenning, M. *J. Chem. Biol.* **2010**, *3*, 1–18.
13. Hawe, A.; Sutter, M.; Jiskoot, W. *Pharm. Res.* **2008**, *25*, 1487–1499.
14. Biancalana, M.; Koide, S. *Biochim. Biophys. Acta - Proteins Proteomics* **2010**, *1804*, 1405–1412.
15. Amdursky, N.; Erez, Y.; Huppert, D. *Acc. Chem. Res.* **2012**, *45*, 1548–1557.
16. Wolfe, L. S.; Calabrese, M. F.; Nath, A.; Blaho, D. V.; Miranker, A. D.; Xiong, Y. *Proc. Natl. Acad. Sci.* **2010**, *107*, 16863–16868.
17. Maskevich, A. A.; Stsiapura, V. I.; Kuzmitsky, V. A.; Kuznetsova, I. M.; Povarova, O. I.; Uversky, V. N.; Turoverov, K. K. *J. Proteome Res.* **2007**, *6*, 1392–1401.
18. Singh, P. K.; Kumbhakar, M.; Pal, H.; Nath, S. *J. Phys. Chem. B* **2010**, *114*, 5920–5927.
19. Singh, P. K.; Kumbhakar, M.; Pal, H.; Nath, S. *J. Phys. Chem. B* **2009**, *113*, 8532–8538.
20. Singh, P. K.; Kumbhakar, M.; Pal, H.; Nath, S. *J. Phys. Chem. B* **2010**, *114*, 2541–2546.
21. Stsiapura, V. I.; Maskevich, A. A.; Tikhomirov, S. A.; Buganov, O. V. *J. Phys. Chem. A* **2010**, *114*, 8345–8350.

22. Stsiapura, V. I.; Maskevich, A. A.; Kuzmitsky, V. A.; Uversky, V. N.; Kuznetsova, I. M.; Turoverov, K. K. *J. Phys. Chem. B* **2008**, *112* (49), 15893–15902.
23. Singh, P. K.; Mora, A. K.; Nath, S. *J. Phys. Chem. B* **2015**, *119*, 14252–14260.
24. Singh, P. K.; Mora, A. K.; Nath, S. *Chem. Phys. Lett.* **2016**, *644*, 296–301.
25. Chatterjee, A.; Seth, D*Photochem. Photobiol. Sci.* **2013**, *12*, 369–383.
26. Bergen, M. Von; Friedhoff, P.; Schneider, a; Kampera, T.; Biernat, J.; Mandelkow, E. M.; Mandelkow, E. *Mol. Biol. Cell* **1998**, *9*, 394A–394A.
27. Kumar, S.; Singh, A. K.; Krishnamoorthy, G.; Swaminathan, R. Thioflavin T *J. Fluoresc.* **2008**, *18*, 1199–1205.
28. Sarkar, N.; Datta, A.; Das, S.; Bhattacharyya, K. *J. Phys. Chem.* **1996**, *100*, 15483–15486.
29. Maroncelli, M.; Fleming, G. R. *J. Chem. Phys.* **1987**, *86*, 6221–6239.
30. Ghosh, R.; Palit, D. K. *ChemPhysChem* **2014**, *15*, 4126–4131.
31. Snellenburg, J. J.; Laptenok, S. P.; Seger, R.; Mullen, K. M.; Stokkum, I. H. M. van. *J. Stat. Softw.* **2012**, *49* (3).
32. Stsiapura, V. I.; Kurhuzenkau, S. A.; Kuzmitsky, V. A.; Bouganov, O. V.; Tikhomirov, S. A. *J. Phys. Chem. A* **2016**, *120*, 5481–5496.
33. Choudhury, P. K. Mondal, V. K. Sharma, S. Mitra, V. G. Sakai, R. Mukhopadhyay, S. K. Pal, J. Phys. Chem. B **2015**, *119*, 10849–10857.
34. Warr, G. G.; Evans, D. F. *Langmuir* **1988,** *4*, 217–224.
35. Rybicka, A.; Longhi, G.; Castiglioni, E.; Abbate, S.; Dzwolak, W.; Babenko, V. et al., *ChemPhysChem.* **2016**, *17*, 2931–2937.
36. Amdursky, N.; Gepshtein, R.; Erez, Y.; Huppert, D. *J. Phys. Chem. A* **2011**, *115*, 2540–2548.

This page intentionally left blank

Chapter 5

Solvent Relaxation Accompanied Ultrafast Excited State Proton Transfer Dynamics Revealed in a Salicylideneaniline Derivative

Puspal Mukherjee, Aritra Das, Md. Serajul Hq. Faizi and Pratik Sen *Submitted in Chemistry Select*

In this chapter the dynamics of a new excited state proton transfer probe has been studied using femtosecond fluorescence up-conversion and broadband transient absorption spectroscopy along with density functional theory calculations. The study was conducted in cyclohexane, methanol and SDS micelle. As the molecule is insoluble in water, SDS micelle was used to explore the dynamics in presence of water. A solvation component was present in polar solvents in the fluorescence transients of the keto form. Therefore the proton transfer timescale was extracted by modeling the formation of keto tautomer in the excited state and it was found that the time component was similar in all three medium. However, in non-polar solvent cyclohexane, vibrational relaxation was extracted which became very fast to observe in polar medium.

5.1. Introduction

Excited state intramolecular proton transfer (ESIPT) process or formation of the tautomer (enol to keto) in the electronically excited state of a molecule was first discovered by Weller in 1950's in *o*-salicylic acid.[1-3] The process is characterized by dual emission, from the excited *enol* and *keto* form of the molecule and in most of the cases the proton migration takes places from a hydroxyl or amine group to a electronegative oxygen or nitrogen atom.[2-4] It is also associated by a large Stokes shift (6000-10000 cm^{-1}) of the fluorescence spectrum.[2-5] Dual emission property of ESIPT molecules attracted several applications including the white light emission for application in luminescence devices, sensing, sunscreen lotion, etc.[6-17] The staggering amount of applications of ESIPT is beyond the scope of discussion here, however, the following examples may illustrate the importance of studying new ESIPT molecules.

The process, ESIPT, has been observed in derivatives of large class of molecules such as flavone, anthraquinone, quinolones, di and tri azoles, etc.[6,18-25] In these molecules, the conversion of enol to keto form can vary depending on the medium and timescale of proton transfer process in the excited state. The ESIPT process generally occurs in sub-picosecond time scale. For example, Glassbeek and co-workers measured the timescale of proton transfer process in the popular ESIPT probe 2-(2'-hydroxyphenyl)benzoxazole as 150 fs using fluorescence up-conversion spectroscopy.[26] Zewail and co-workers studied 2-(2'-hydroxyphenyl)-4-methyloxazole (HPMO) in non-polar 2-methylpentane and found that ESIPT occurs in less than 300 fs timescale, which slowed down appreciably when incorporated within the β-cyclodextrin.[5] In case of salicylideneaniline (SA), the ESIPT process is as fast as 50 fs.[27] Femtosecond time resolved fluorescence measurements have also been used by Simkovitch and Huppert to measure a time scale of 70 fs for ESIPT process in quercetin.[28] But probably the fastest ESIPT have been observed in case of 2-(2'-hydroxyphenyl)benzoxazole (HBT) and 10-hydroxybenzo[h]quinolone (HBQ) few years ago.[29] Lee *et al.* with the help of

nonlinear fluorescence up-conversion setup with instrument response function as low as 40 fs have observed that ESIPT is occurring with a timescale of 12-18 fs for HBT and 62 fs for HBQ.[29] They have assigned ballistic proton wave packet motion and structural deformation as the key process for this ultrafast nature of ESIPT for HBT and HBQ, respectively.[29] Takeuchi and Tahara studied emission from 7-azaindole dimer using fluorescence up-conversion spectroscopy and revealed that the proton transfer occurred from the lower excited state of the dimer.[30]

ESIPT processes are often associated with intramolecular charge transfer.[31-34] For example, Kim *et al.* have observed that in a benzoxazole derivative ESIPT process is followed by intramolecular charge transfer (ICT).[31] In the excited state of the molecule the enol form did not show any dynamic Stokes shift, which confirmed that ESIPT occurred prior to ICT as the ICT process is solvent dependent and in polar solvent it follows solvation.[31] On the other hand, Alarcos *et al.* have studied amino-2-(2-hydroxyphenyl)benzoxazole and its methyl derivative in different solvent to show that in this molecule ICT occurs prior to ESIPT.[32] Long-lived ICT components followed by ESIPT has been reported in *p*-N,N-dimethylaminosalicylic acid by Kim *et al*.[34] In all these cases and many more, occurrence of charge transfer phenomenon leads to dielectric stabilization i.e. the polar solvents will stabilize the charge transfer state more than non-polar solvents, which is reflected from the nature of emission of the enol and/or keto state depending upon the order of appearance of ESIPT and ICT. Thus, specific solvation effect coupled to ESIPT is possible. In this context two works must be highlighted. Rumble *et al.* recently studied 4′-N,N-diethylamino-3-hydroxyflavone, a dual fluorescence emitting molecule, using femtosecond kerr-gated emission spectroscopy.[35] To investigate the solvation effect they have studied the molecule in propylene carbonate - acetonitrile mixture, which have variable solvation time at different composition but the polarity remains almost same.[35] They have used a ESIPT-solvation coupling model, previously proposed by Kimura *et al.*,[36] and established that the timescale of ESIPT process changes

inversely with the solvation time of the mixture.[35] Polar protic solvents can also directly take part in the proton transfer process, which has been previously explored by Douhal and co-workers in the nanocavity of cyclodextrin.[5] Ghosh *et al.* have studied the effect of hydrogen bonding solvents on the ESIPT of 4′-N,N-dimethylamino-3-hydroxyflavone and concluded that H-bonding of solvents plays a vital role in the activation barrier crossing of the reaction.[37] Moreover they have observed slower ESIPT of the molecule in micelle, which is related to slower solvation time in the system.[37]

Among the works cited above, analytical modeling has been undertaken by some groups to understand the ESIPT dynamics in a better way. However, it seems that the proper kinetic modeling of the process is still undone and with that goal set in mind I have initiated this work. Here, I have synthesized a new Schiff base molecule, (E)-2,4-di-tert-butyl-6-(((4(phenylamino)phenyl)imino)methyl)phenol (BPIMP, scheme 5.1), which undergoes ultrafast ESIPT from phenolic group to imine nitrogen. Schiff bases are easy to synthesis and there are previous reports where Schiff base molecules have been used as ESIPT probes.[27] The extended conjugated structure of the molecule leads to yellowish green keto emission, which can be further explored in devices. Here I have explored the mechanism of ESIPT process in BPIMP and demonstrated the effect of solvation on the ESIPT process by studying the molecule in cyclohexane, methanol and sodium dodecyl sulfate micelle, and finally using density functional theory (DFT) calculations came up with a simple kinetic model, which explains the experimental data quite satisfactorily.

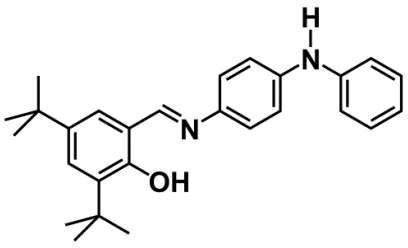

Scheme 5.1. Structure of BPIMP ((E)-2,4-di-tert-butyl-6-(((4(phenylamino) phenyl)imino)methyl)phenol)

5.2. Results

5.2.1. Steady State Spectroscopy

I have recorded the steady state absorption and emission spectra of BPIMP in cyclohexane, methanol and 40 mM SDS in water solution. The normalized spectra are shown in figure 5.1 and the wavelength maxima are listed in table 5.1. The absorption maximum of the molecule shows a gradual red shift with increase in the polarity of the medium. Here, it should be noted that within the micelle there is major amount of water penetration, which means BPIMP experienced polarity due to surrounding water molecules in the SDS micelle. In all the cases, only a single peak was observed in the absorption spectra indicating that the keto form of the compound is mostly absent in the ground state and the stable enol form prevails (supported from NMR data also, see experimental section). From the emission spectra in all the three cases, it is clear that BPIMP showed dual emission behavior, typical of ESIPT molecule, and the enol emission is much weaker than the keto emission. The emission maxima of the enol and keto forms are tabulated in table 5.1. It is to be noted that the enol peak is not responsive towards change in solvent but the keto peak is. In all the three cases, I observed a Stokes shift in the range of 8500 to 9500 cm^{-1}, which further supports the ESIPT process. In figure 5.1 I have shown the emission spectra of BPIMP with λ_{ex} = 360 nm, which is on the blue side of absorption maxima to avoid any masking of the enol emission peak by solvent Raman response. One of the easiest ways to check the origin of the large Stokes shifted peak is to check the excitation spectra of the molecule, which I have reported in the figure 5.2. As can be seen in the figure that the excitation spectra overlaps quite nicely with the absorption spectra of BPIMP signifying that the dual nature of BPIMP emission originated from a common ground state, which in turn concretes the idea of ESIPT process. The large difference in the intensity of the enol to keto emission suggests that in the excited state the enol form is not stable and mostly underwent proton transfer at an ultrafast rate. Therefore, I did the following femtosecond studies to explore its kinetics.

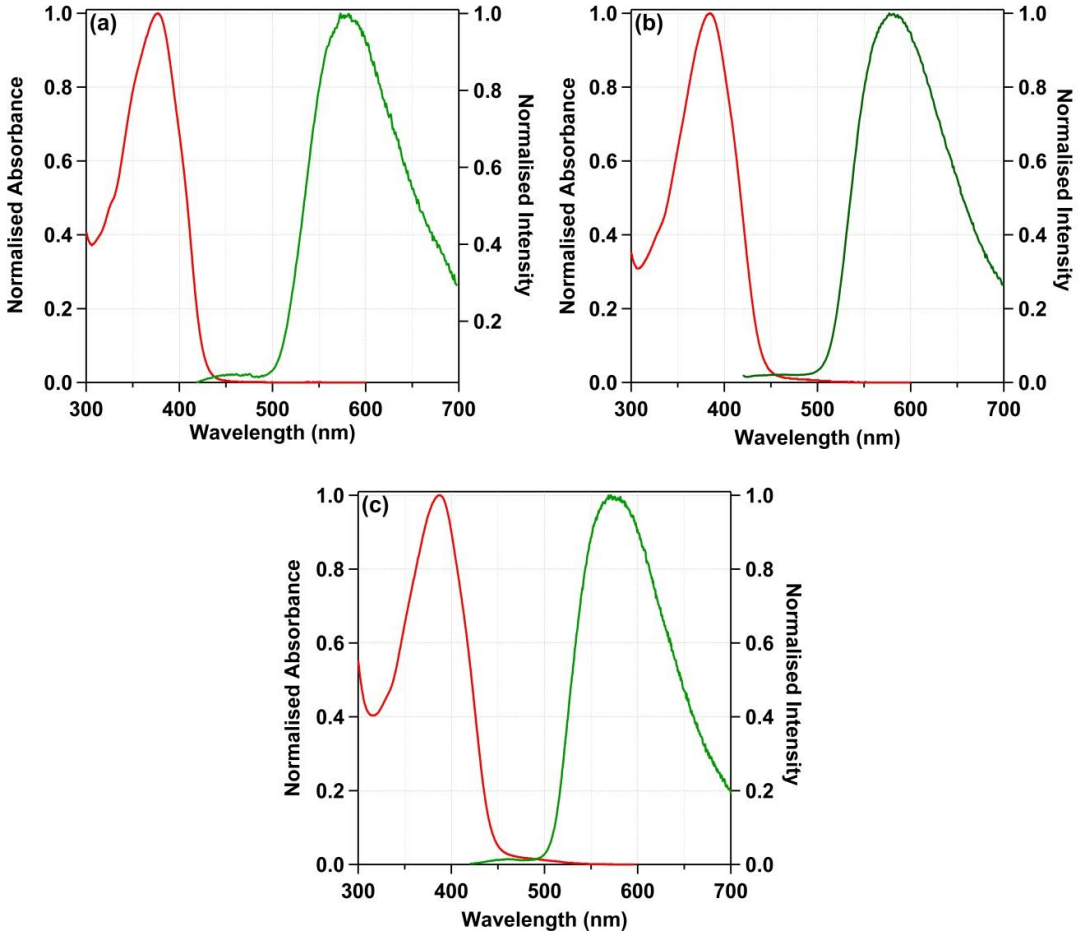

Figure 5.1. Steady state absorption and emission spectra of BPIMP in (a) cyclohexane (b) methanol and (c) 40 mM SDS in water.

Table 5.1. Absorption and emission chracteristics of BPIMP in different media

	λ_{max}^{abs}(nm)	λ_{max}^{em}(nm) (enol)	λ_{max}^{em}(nm) (keto)
Cyclohexane	376.8	462.0	582.0
Methanol	384.6	462.0	578.0
SDS Micelle	387.0	461.8	576.0

5.2.2. Femtosecond fluorescence up-conversion study

Exploration of dynamics of ESIPT reactions require time resolved fluorescence study and I found that femtosecond time-resolved up-conversion technique was necessary to resolve the problem.

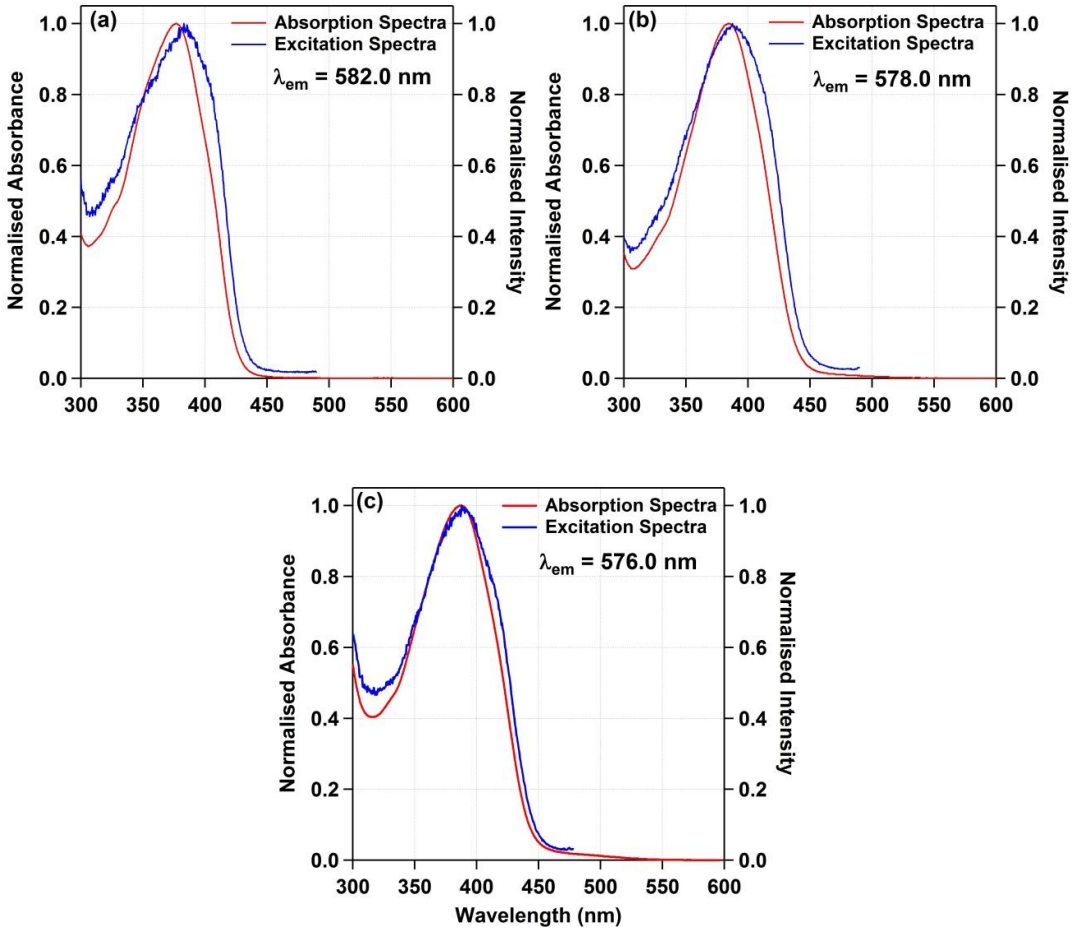

Figure 5.2. Normalised absorption and excitation spectra of BPIMP in (a) cyclohexane (b) methanol (c) SDS micelle.

I have excited all the samples using 400 nm pump beam and recorded the fluorescence transients at different wavelengths covering the emission spectra of the molecule. As evident from the steady state spectra, in all the three media, the intensity of the enol emission is very weak and therefore I could not go beyond 420 nm in the blue side of the emission spectra as it was below the time resolution of our setup. Nonetheless, I recorded fluorescent lifetime decays at 28 different wavelengths spanning over 420 nm to 690 nm and observed that the wavelengths at the blue side of the spectrum have much faster decay than the wavelengths at the red side. I found that in methanol and in 40 mM SDS, the fluorescence transients from 420 nm – 480 nm can be fitted using a sum of two exponential functions, whereas in case of cyclohexane same function was used to fit the fluorescence

transients upto 500 nm. The average lifetime of BPIMP in methanol and SDS micelle varied from 0.1 ps to 0.6 ps in this wavelength region, which corresponds to the enol emission. In cyclohexane, the lifetime of the enol form was found to vary between 0.08 ps – 0.3 ps, over 420 nm to 500 nm. The deactivation of the excited enol-form could either be by its natural lifetime or by the ESIPT process and the lifetime variation suggest that the processes occurred in sub-picosecond time scale. For the fluorescence transients recorded at rest of the wavelengths, I required a sum of three exponential functions to fit. As an example, I have given the fitting parameters obtained for BPIMP in SDS micelle at six different wavelengths in table 5.2.

Table 5.2. Lifetime parameters obtained from the fitting of fluorescence transients of BPIMP at various wavelengths in 40 mM SDS in water. The normalized coefficients are given in the parenthesis.

Wavelength (nm)	τ_1 (ps) (a_1)[a]	τ_2 (ps) (a_2) [a]	τ_3 (ps) (a_3) [a]	τ_{avg} (ps) [a]
450	0.1 (0.95)	0.3 (0.05)	-	0.11
500	0.1 (0.95)	1.2 (0.04)	65.3 (0.01)	0.80
550	0.1 (0.46)	1.9 (0.13)	90.3 (0.41)	37.30
600	0.3 (0.18)	15.5 (0.13)	99.6 (0.69)	70.80
650	0.1 (-0.10)	13.3 (0.33)	95.5 (0.77)	77.90
690	0.6 (-0.05)	14.3 (0.28)	99.5 (0.77)	80.60

a ±10%

It was found that the enol form has extremely short lifetime but the keto-form has much longer lifetime, which explains the intensity ratio in steady state spectra. The fast decay component at 460 nm has the same time constant (0.1 ps) as of the growth part of 650 nm, which gives us an idea that ESIPT occurs in femtosecond time scale. However, the rise part of extreme red side of the spectrum i.e. at 690 nm has a 0.65 ps time constant associated with it. To make a comparison of these transients I have shown the time resolved fluorescence data at four different wavelengths for all three media in figure 5.3. If proton transfer is the only process

happening in the excited state, then I would have observed same kind of rise part but the increase of rise part in polar solvent signifies that there must be charge stabilization/solvation happening in the keto from of BPIMP. More proof of this aspect will be discussed later.

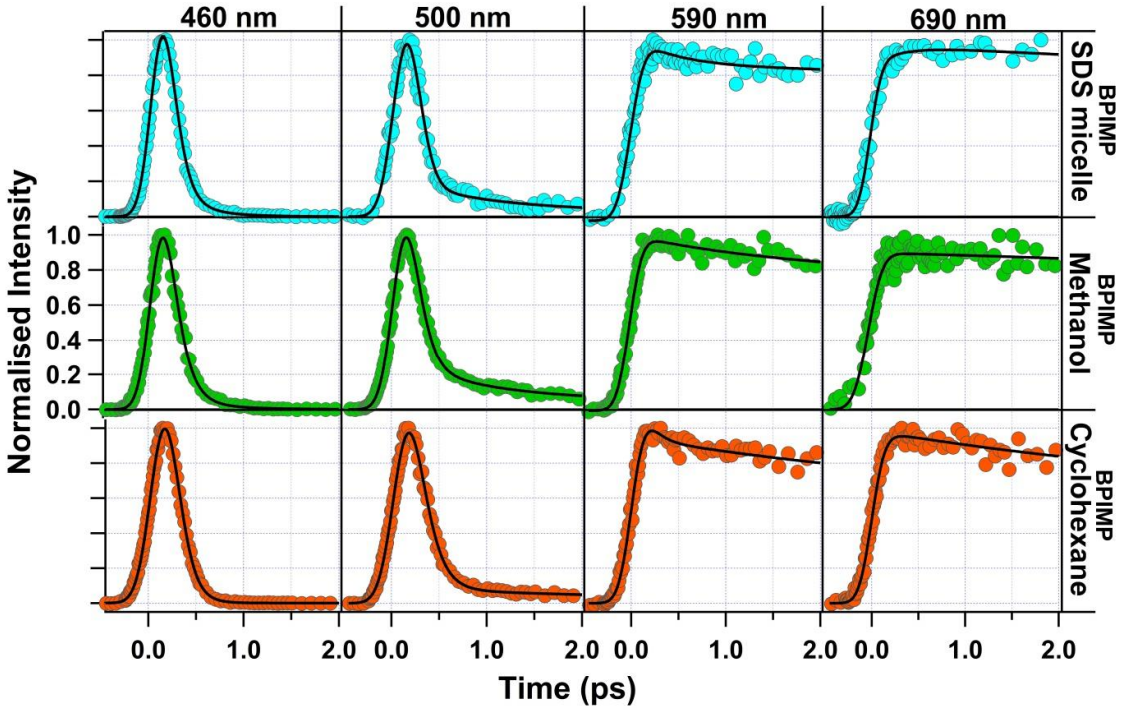

Figure 5.3. Fluorescence transients recorded at different wavelengths for BPIMP in cyclohexane, methanol and in 40 mM SDS in water. The black solid lines indicate fitting.

To achieve an overall idea about the kinetics of the process, I have constructed the time resolved emission spectra from the fluorescence transients. Here, the area normalized time resolved emission spectra (TRANES) is more useful as the proton transfer time scale can be extracted from the concurrent reduction and escalation of enol and keto peak, respectively.[38] The area normalized time resolved emission of BPIMP consists of two distinct peaks, originate from each of the tautomer forms. Therefore, a sum of two lognormal functions was needed to fit the data as given below.

$$L(\nu,t) = \sum_{i=1}^{2} g_i \exp\left\{-\ln(2)\left(\frac{\ln\left(1+\frac{2b_i(\nu-\nu_i^p)}{\Delta_i}\right)}{b_i}\right)^2\right\} \qquad (5.1)$$

Here, $L(\nu, t)$ is the time resolved emission spectra at a given time, g_i is the peak height, b_i is the asymmetry parameter, ν_i^p is the peak frequency, and Δ_i is the bandwidth parameter related to full width half maxima (Γ) as follows

$$\Gamma = \Delta\left(\frac{\sinh(b)}{b}\right) \tag{5.2}$$

In figure 5.4, TRANES of BPIMP in cyclohexane, methanol and SDS micelle have been shown. In all the three cases a clear isoemissive point is visible in the early times; however, methanol and SDS differ from cyclohexane in one aspect. For BPIMP in cyclohexane, the emission maxima of enol and keto forms were around 21740 cm^{-1} and 17400 cm^{-1}, respectively and the isoemissive point is located around 19750 cm^{-1} or 506 nm, which did not shift with the progress in time. After 1.0 ps, the enol peak at the right side of figure 5.4a diminished, which signified the completion of the proton transfer process and no significant peak shift has been observed for the keto form in cyclohexane. In methanol, the position of the isoemissive point is around 19900 cm^{-1} from 0 to 0.60 ps. After 0.6 ps, the intensity of the enol form almost diminished and only the keto emission remained. The emission maxima of the keto form in methanol showed a constant shift towards lower wavenumber or higher wavelength as evident from figure 5.4b. After 10 ps the TRANES more or less overlapped with the steady state spectra of the molecule, which was also observed for BPIMP in 40 mM SDS. In this case, the isoemissive point is around 19485 cm^{-1} and the emission maxima of the enol form is about 21720 cm^{-1}, which did not shift much with time. However the keto emission showed bathochromic shift. In both the polar medium, the decrease of intensity of enol emission is faster than in cyclohexane and there is a distinct red shift of the keto spectra in polar solvents due to the solvation. Thus I can conclude that in BPIMP the ultrafast excited state proton transfer is followed by solvation of the keto form in the excited state. The information gathered from TRANES can be used to estimate the rate of proton transfer, which I have discussed later. In the

next section the photophysics of the molecule is explained through femtosecond broadband transient absorption spectroscopy.

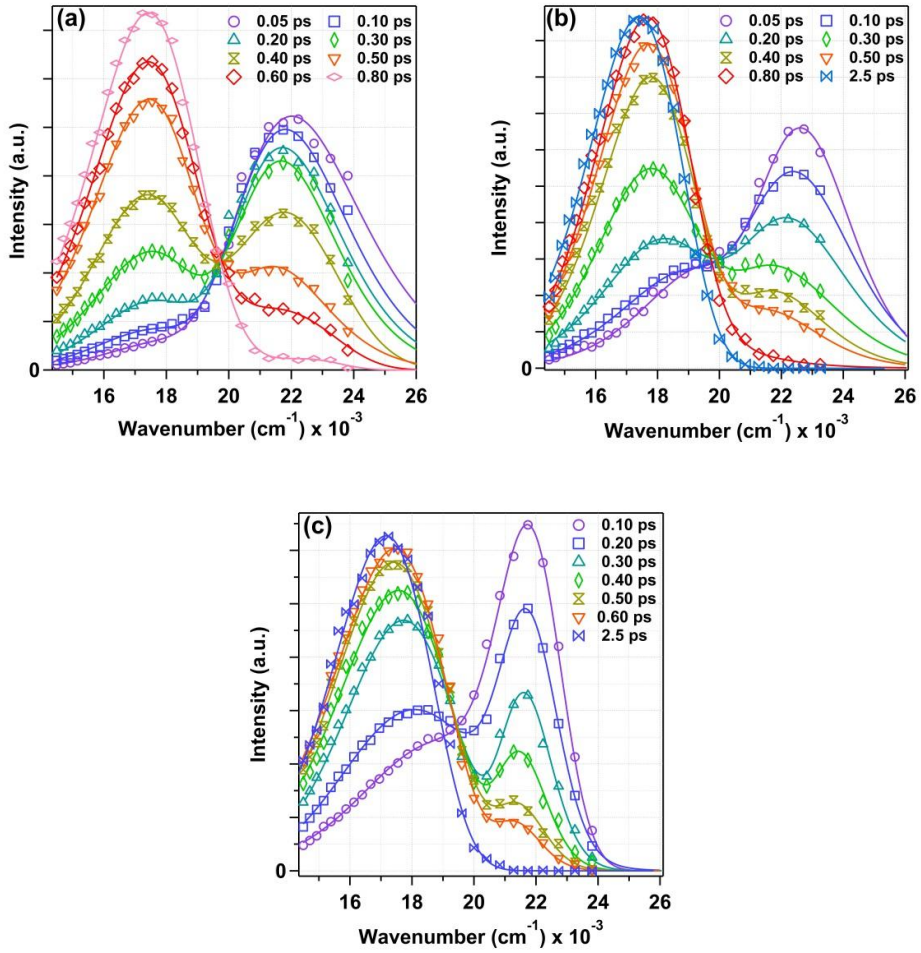

Figure 5.4. Time resolved area normalized emission spectra of BPIMP in (a) cyclohexane (b) methanol and (c) 40 mM SDS in water.

5.2.3. Femtosecond broadband transient absorption study

In our femtosecond broadband transient absorption spectroscopy I have excited BPIMP using 400 nm light and recorded the transient spectra over 460 – 750 nm at different times. In figure 5.5 and in figure 5.6 and 5.7, some of these spectra are shown in 40 mM SDS, methanol and cyclohexane, respectively. Clearly an excited state absorption (ESA) band and a stimulated emission (SE) band are observed in all the three sets of data. For example, BPIMP in 40 mM SDS (figure 5.5a) showed a strong positive ESA signal around 485 nm at early times, which shifted to longer wavelength (around 505 nm) at later times. The same signal was

centered at 490 nm in methanol at early times and at 502 nm at the later times. In cyclohexane it was centered at 480 nm, which does not shifts with time. The negative SE band in SDS was centered at 620 nm, which became broad as time progress. A comparison with the steady state emission spectra confirmed that the SE signal originated from the keto BPIMP. Unfortunately, the weak SE band of the enol form overlapped with the strong ESA signal of the molecule and therefore could not be detected even at early times. The same SE band is situated at 620 nm and 635 nm in methanol and cyclohexane, respectively. Another distinct feature obtained was the presence of an isosbestic point in the transient absorption spectra. The position of the said characteristics was at 560 nm and 570 nm for methanol and both for cyclohexane and SDS micelle, respectively. Thus to access the information about the lifetimes of the associated processes, I have fitted the whole kinetic data employing global fitting procedure using the Glotaran software.[39] Here, it is necessary to mention that in all the three cases, I observed a small residual positive signal, which did not decay within our observation window of 2 ns. I have to reject the idea of photodegradation as the steady state absorption spectra of BPIMP before and after exposer to laser radiation remained same and there were no residual signal in the fluorescence up-conversion data. Therefore the signal probably originated from triplet conversion or ground state keto-enol tautomerism process. Either way, while fitting the data I needed an extra-long lifetime component in each case. Thus I fitted the data with sum of four exponential functions convoluted with a Gaussian instrument response function. The lifetime values obtained are reported in table 5.3. Clearly, the overall fluorescence lifetime of the molecule is longest in SDS micelle and shortest in cyclohexane. The fast lifetime component was found to be well matched with the rise part observed in fluorescence transient. The second component was 3 times smaller in cyclohexane than in methanol or in SDS micelle. Probably this signifies the dielectric stability offered by the polar solvents, which is absent in non-polar solvent and makes the intrinsic lifetime component longer. The third lifetime

component reflected the intrinsic lifetime of the keto form, which is naturally highest in SDS micelle because of the confinement.

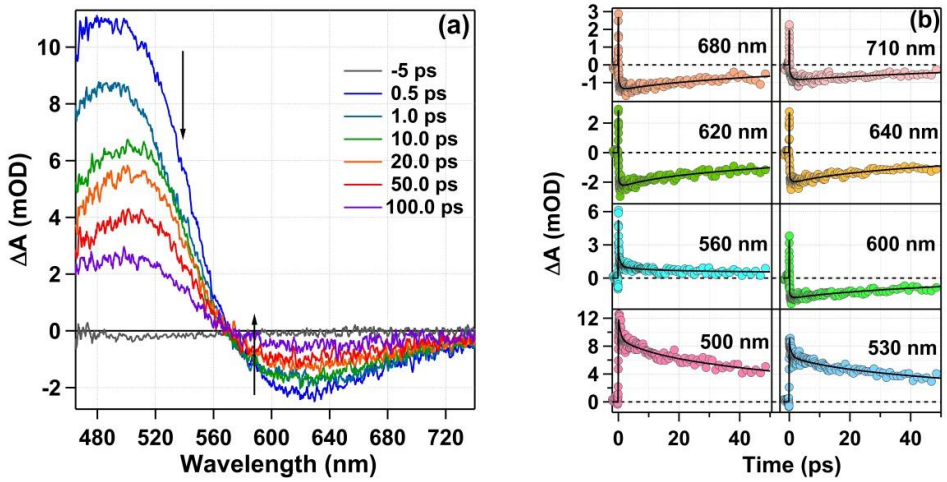

Figure 5.5. Broadband transient absorption result of BPIMP in 40 mM SDS in water. (a) Spectra at different times and (b) kinetics at different wavelengths.

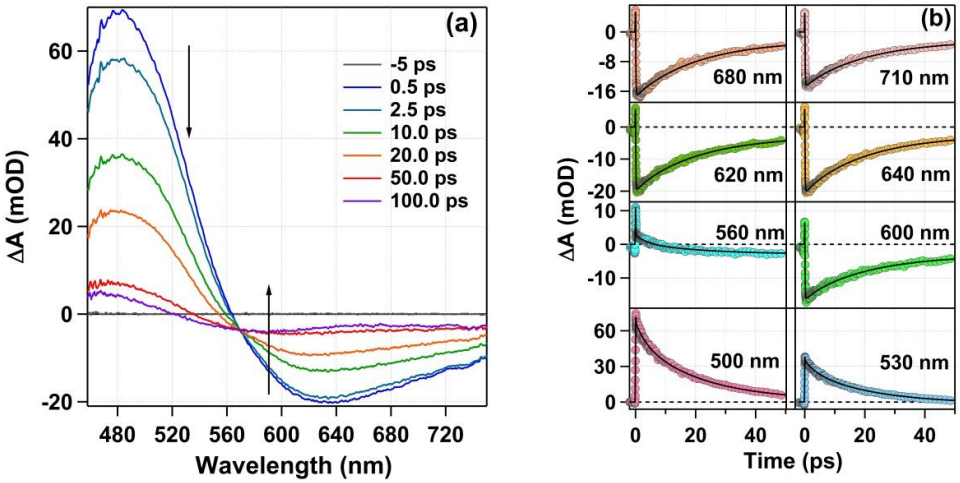

Figure 5.6. Broadband transient absorption spectroscopic data of BPIMP in cyclohexane. (a) Spectra at different times and (b) kinetics at different wavelengths.

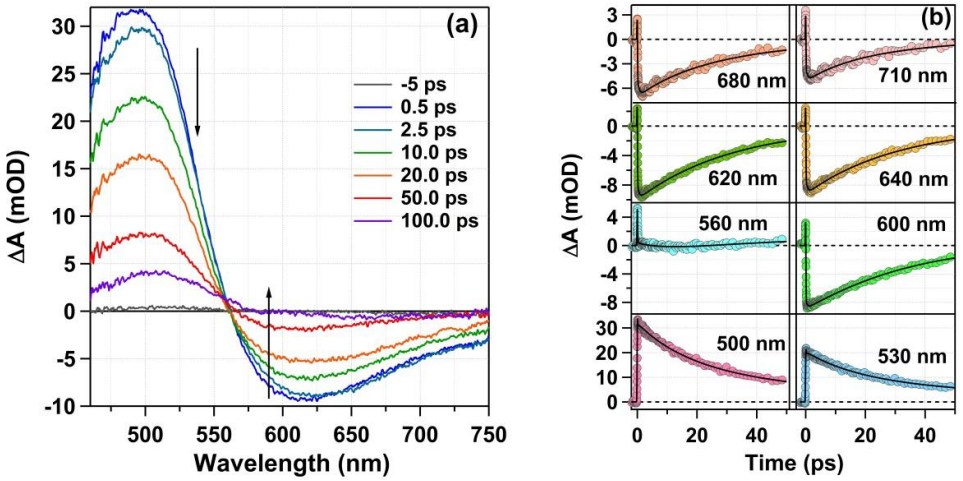

Figure 5.7. Broadband transient absorption spectroscopic data of BPIMP in methanol. (a) Spectra at different times and (b) kinetics at different wavelengths.

Table 5.3. Lifetime parameters obtained from the global fitting of the broadband transient absorption data in different media.

	τ_1 (ps)[a]	τ_2 (ps)[a]	τ_3 (ps)[a]	τ_4 (ps)
Cyclohexane	0.15	3.6	21.3	20000 (fixed)
Methanol	0.50	11.2	32.0	20000 (fixed)
SDS micelle	0.75	10.0	86.0	20000 (fixed)

a ±10%

5.3. Computational Study

Density functional theory calculations were performed using Gaussian 09 package.[40] For my calculations I have used Becke, three-parameter, Lee-Yang-Parr (B3LYP) exchange correlation functional and 6-311++g(d,p) basis set. First, the enol form of BPIMP was optimized in vacuum and the ground state optimized structure has been shown in figure 5.8a. The structural optimization was confirmed by absence of any imaginary frequency in the vibrational modes.[40] In figure 5.8a it can be seen that the –OH group is oriented towards the imine N atom of the Schiff base. In the ground state, the OH bond distance is 0.99 Å and the distance of H and N is 1.7 Å. The optimized enol form was used to calculate the vertical transition energy of the system. I have used the TD-DFT formalism using the same basis set to find the transition energy, which is 3.108 eV or 399 nm for $S_0 \rightarrow S_1$ transition

with oscillator strength of 0.83. The calculation matched well with the observed UV-Visible absorption spectra of BMIPM. The transition of the electron associated with the $S_0 \rightarrow S_1$ is from HOMO to LUMO and I have presented the images of HOMO and LUMO of the enol form in figure 5.8b and 5.8c, respectively. Significant charge transfer from the imine side to the phenol ring was observed from HOMO to LUMO. I have also optimized BPIMP in methanol and cyclohexane applying the polarizable continuum model (PCM) using the integral equation formalism variant (IEFPCM).[40] Both the optimized structures are given in the figure 5.9 and there is insignificant difference among the three optimized structures. Henceforth, I have done my computations in vacuum. In the optimized keto form, shown in figure 5.8d, the N-H bond distance is 1.04 Å and distance of C=O and H is 1.68 Å. I have observed that the enol form is 15.06 kJ/mol more stable than the keto form in the ground state. The HOMO and LUMO of the keto form are also shown in figure 5.8e and 5.8f, respectively.

To get the idea about the potential energy surface along the proton transfer coordinate first I subjected the optimized enol form to a potential energy scan along the O-H-N bond. The idea is, as the O-H bond lengthens the N-H bond will form, that leads to the formation of the keto form. For this purpose, potential energy scan was performed over O-H bond length from 0.83 Å to 2 Å. At each step of this scan, BPIMP geometry was relaxed or optimized except for the O-H bond length. For each of the optimized structure, TD-DFT has been applied to calculate the vertical transition energies and consequently the first excited state (S_1) potential energy surface was constructed. Taking the minimum in the ground state corresponding to the enol form, which I have taken as the zero energy value; both the ground and first excited state potential energy surface have been shown in figure 5.10. However, the vertical transition energies do not correctly represent the actual electronic excited state of enol-BPIMP. Actually, the vertical Franck-Condon (FC) state will relax to a more stable form before it emits or undergoes the proton transfer process. This is apparent from the Stokes shift observed between

the absorption and emission maxima of the enol-BPIMP. Moreover, the keto geometry predicted from the vertical energy calculations from the ground state scan may not be most stable form. So it became necessary to optimize the structures in the excited state to find out the most stable enol and keto geometry in the excited state. Such calculations are computationally very costly and when two different from of same molecule exists in the excited state, the convergence of optimization for each of them is hugely time consuming with large basis sets.

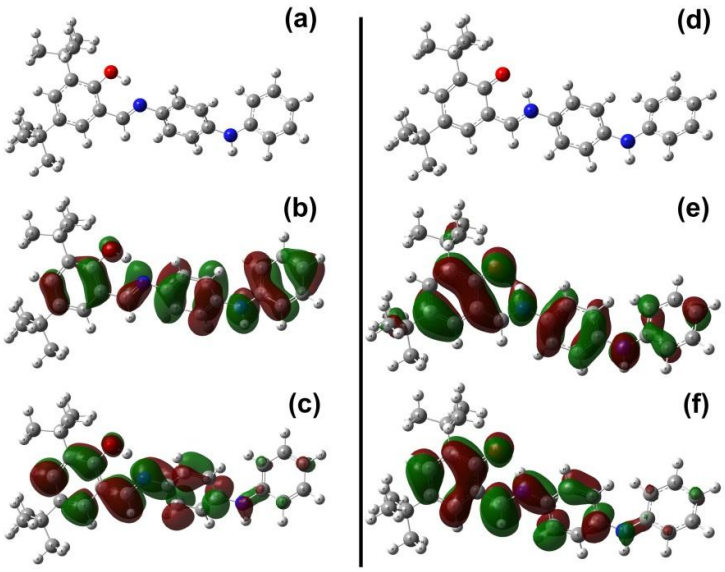

Figure 5.8. Ground state optimized structure of the (a) enol form and (d) keto form of BPIMP; frontier molecular orbital of HOMO of the (b) enol form and (e) keto form of BPIMP; frontier molecular orbital of LUMO of the (c) enol form and (f) keto form of BPIMP; obtained from the DFT calculations.

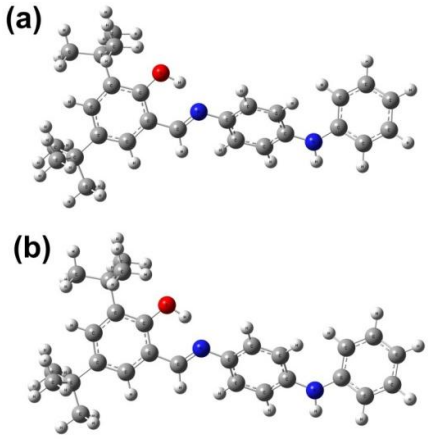

Figure 5.9. Ground state optimized structure of BPIMP in (a) cyclohexane and (b) methanol.

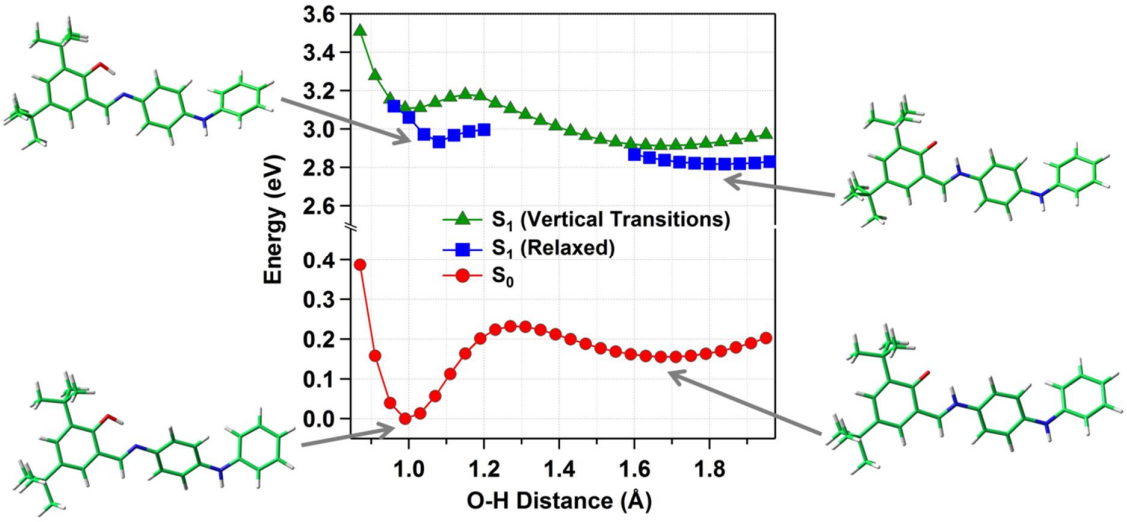

Figure 5.10. Relaxed potential energy surface scan of BPIMP against O–H distance coordinate in the ground state and their corresponding vertical excitations. The ground state energy of the enol form has been set to zero.

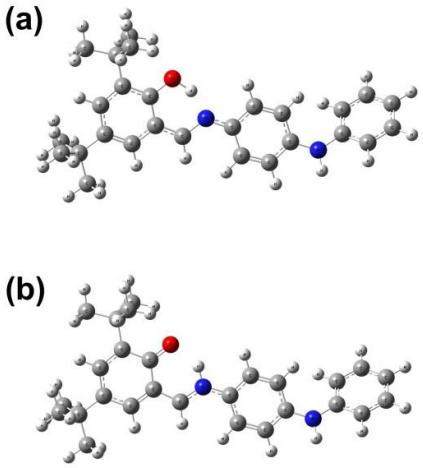

Figure 5.11. Excited state optimized structure of the (a) enol form and (d) keto form of BPIMP.

Therefore I have performed the excited state optimizations in the following manner. For ESIPT process, the keto form is more stable than the enol form in the excited state. So I took the ground state optimized keto BPIMP structure and optimized it in the excited state by TD-DFT method using the same functional and basis set. As expected the excited state optimized structure was found to be ~0.1 eV more stable than the structure predicted from vertical transition calculations and

moreover the O – H distance lengthened by ~0.15 Å in the excited state optimization compared to that in the ground state optimization. Performing a relaxed excited scan starting from this geometry, as done for the ground state, is again computationally costly. Thus to get an idea about the relaxed excited state I scanned few points in the vicinity of both the enol and the keto structures. Similar to the ground state scan, in this case too, I fixed only the O-H distance and let all other geometrical parameters optimized at each point. In this way I can reach a structure very close to the actual optimized enol form in the excited state, which was then used to find the actual optimized enol form in the excited state. The obtained energy values are also shown in figure 5.10. Interestingly unlike ground state, the most stable enol-BPIMP geometry has a O-H bond length 1.08 Å. To confirm this, I performed an excited state optimization for the most stable ground state enol form, which matches closely to the excited state geometry determined from the keto side. Excited state optimized geometries for both the keto and enol forms has been represented in figure 5.11. To check whether the structures at the peaks of the two barriers are the transition states, I ran frequency calculations in these two geometries. In both the cases, I have identified one negative frequency, which immediately confirms the idea of the transition state (TS).

5.4. Discussion

The experimental study gave us confirmation about the proton transfer process followed by dielectric stabilization of the keto form in polar medium and the computational study elucidated the existence of a small barrier in the excited state. However a proton transfer timescale has not been assigned in any of these cases. The reason is the mismatch of fast decay of the fluorescence transients of the enol form with the comparatively slower rise part of the keto form. If they matched exactly then I could have easily assigned this as the timescale of the proton transfer. Moreover, since the computational study indicated that there could be barrier present is the excited state manifold of the system, it become necessary to explore the actual time scale of the reaction. At this stage I want to highlight that I

have checked for primary kinetic isotope effect (KIE) by measuring the steady state emission spectra of BPIMP in methanol and methanol-OD and the result is shown in figure 5.12. The intensity ratio of enol to keto emission of BPIMP in CH_3OD was found to be 1.4 times less than the same in CH_3OH, which means there is almost no "tunneling through barrier" mechanism operating here. So it left me to examine the evolution of the keto emission from TRANES. However, the intensity of a certain wavelength cannot be compared at different times because the solvation is also present along with the ESIPT process. The area normalization in TRANES ensures that we are observing only the excited state processes and must consists of the enol emission and the keto emission having the effect of solvation. Essentially it means that the keto emission will shift to the lower energy as time progress. Therefore if I can calculate the area of the keto emission in TRANES then its time evolution shall give us the required ESIPT rate. As mentioned before, I have used a sum of two lognormal functions, each one for enol and keto emission, to fit the TRANES data. Therefore I obtained the fitting parameters of the lognormal function of the keto BPIMP and can calculate the area of the same using the following relation.[35]

$$A = \sqrt{\frac{\pi}{4ln2}}.g.\Delta.exp\left(\frac{b^2}{4ln2}\right) \tag{5.3}$$

In the above equation, A is the area of the lognormal peak and the other parameters bear the same meanings as stated for equation 6.1. Accordingly I calculated the area of the keto form following the fitting of the TRANES at different times and plotted the same in figure 5.13. Here, I should mention that the area of the enol emission can also be retrieved to calculate the time scale but it is of no use in determining the mechanism of ESIPT as in all cases it will show a single exponential decay. So I focused on the increment in area of emission of the keto form instead of the decay of the same parameter for enol form. Now, for BPIMP in methanol and 40 mM SDS the time evolution of the keto form area can be fitted using a single exponential function, which essentially means a single step (enol →

keto) mechanism is operating, but not for in the cyclohexane. To justify the time evolution of the keto emission in cyclohexane, I have proposed a two-step process as

$$E_{FC}^{*} \overset{k_1}{\rightarrow} E^{*} \overset{k_2}{\rightarrow} K^{*} \tag{5.4}$$

Here, E_{FC}^{*} represent the vertically excited enol form; K^{*} represent the keto-BPIMP formed in the excited state and for time being let E^{*} represent an intermediate state, k_1 and k_2 are the two rate constants. Equation 5.4 is a classic example of consecutive reaction and the kinetic equations can be found in any text book of kinetics and I can naturally write the kinetic equations as[41]

$$\frac{d[E_{FC}^{*}]}{dt} = -k_1[E_{FC}^{*}] \tag{5.5}$$

$$\frac{d[E^{*}]}{dt} = k_1[E_{FC}^{*}] - k_2[E^{*}] \tag{5.6}$$

$$\frac{d[K^{*}]}{dt} = k_2[E^{*}] \tag{5.7}$$

Moreover, as I am considering TRANES data, the population created by the laser excitation ($[E_{FC}^{*}]_0$) will be the total population at any time and that follows

$$[E_{FC}^{*}]_0 = [E_{FC}^{*}] + [E^{*}] + [K^{*}] \tag{5.8}$$

Solving the above four equations I get

$$[E_{FC}^{*}] = [E_{FC}^{*}]_0 e^{-k_1 t} \tag{5.9}$$

$$[E^{*}] = \frac{k_1[E_{FC}^{*}]_0}{k_2 - k_1}(e^{-k_1 t} - e^{-k_2 t}) \tag{5.10}$$

$$[K^{*}] = [E_{FC}^{*}]_0 \left(1 - \frac{k_2}{k_2 - k_1} e^{-k_1 t} - \frac{k_1}{k_1 - k_2} e^{-k_2 t}\right) \tag{5.11}$$

For $k_1 \gg k_2$, equation 5.11 transforms to

$$[K^{*}] = [E_{FC}^{*}]_0 (1 - e^{-k_2 t}) \tag{5.12}$$

which is nothing but the single step model of proton transfer and essentially will give a single exponential fit.

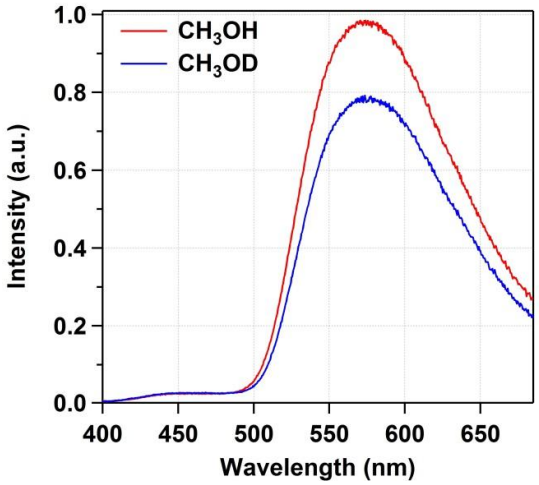

Figure 5.12. Steady state emission spectra of BPIMP in methanol and methanol-OD.

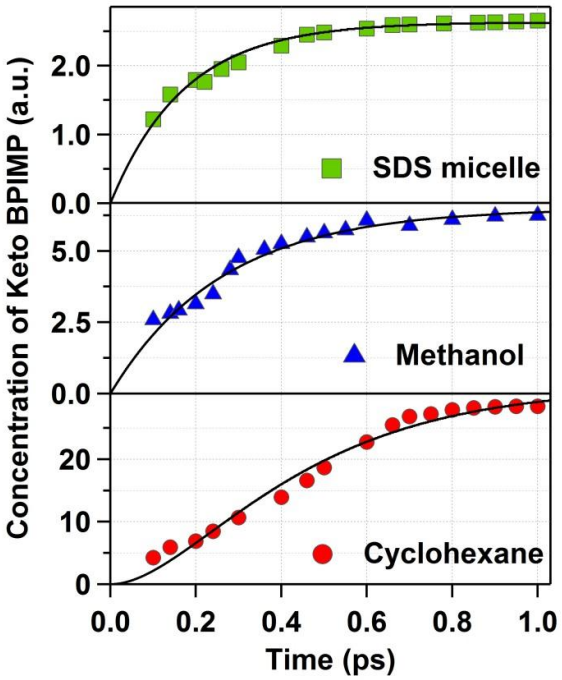

Figure 5.13. Evolution of the area of the keto emission with time calculated using equation 5.3.

I have fitted the cyclohexane data with equation 5.11 and obtained a good fit with more or less same values for k_1 and k_2 i.e. 4.35×10^{12} s^{-1} (time constant 0.23 ps). However when I tried to fit the data for methanol and SDS micelle with equation

5.11, I obtained a very high value for k_1, which is impossible to achieve with the time resolution of our instrument. So I used equation 5.12 to fit the data and the rate constants obtained were 3.85 × 10^{12} s^{-1} (0.26 ps) and 5.0 × 10^{12} s^{-1} (0.20 ps) for methanol and SDS micelle, respectively. I have listed the time constants in all media in table 4. Thus I have estimated the rate constants in all the three media and it is quite clear that the proton transfer rate was fastest in SDS micelle followed by methanol.

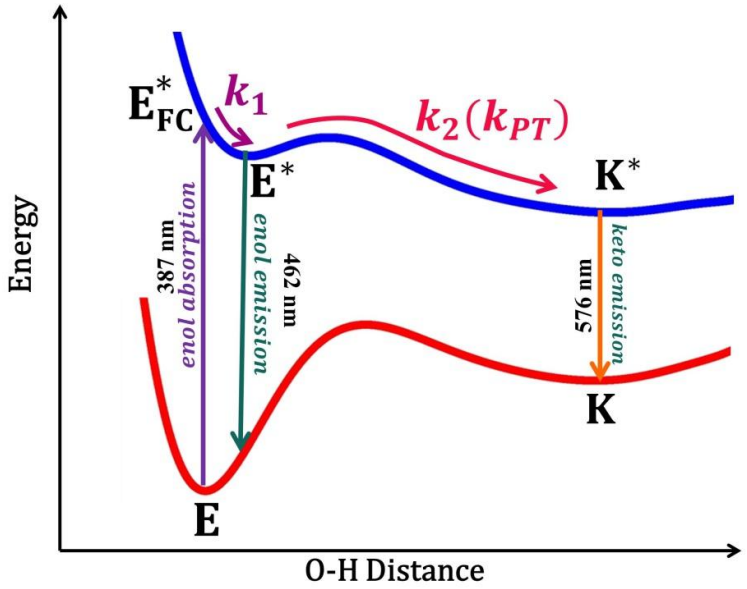

Scheme 5.2. Excited state deactivation scheme of BPIMP.

The rate constant k_1 is assigned to the initial relaxation of vertically excited enol-BPIMP (Franck-Condon (FC) state) to the excited state stable enol configuration which is shown in scheme 5.2. Generally this process is vibrational relaxation and previous studies suggested that the intermolecular vibrational relaxation (IVR) can become very fast in presence of an hydrogen bond accepting or donating solvent.[42] So in non-polar cyclohexane the IVR process is in femtosecond time domain whereas in methanol and SDS micelle it became lot faster which I cannot detect in the time resolution of our setup. From the DFT calculations also I got similar structural relaxation of the enol-BPIMP from the vertically excited state to a minimum before proton transfer took place.

Thus in scheme 5.2, I designated E^*_{FC} to the FC state of enol-BPIMP and $E^*$to be the most stable form of enol-BPIMP in the excited state and K^* as the stable keto-BPIMP in the excited state. Rate constant k_2 represents the kinetics of barrier crossing from E^* to K^* in all the three cases.

Table 4. Time constants obtained from fitting of area of keto emission.

Solvent	τ_1 (ps)	τ_2 (ps)
Cyclohexane	0.23	0.23
Methanol	-	0.26
SDS micelle	-	0.20

5.5. Conclusion

In conclusion, I have synthesized a new Schiff base compound, which showed ESIPT reaction. I examined the compound in cyclohexane, methanol and in SDS micelle using femtosecond fluorescence up-conversion and broadband transient absorption spectroscopy. I found that in methanol and in SDS micelle the molecule exhibits a 0.6 ps rise component in fluorescence transients, which is larger than in cyclohexane. This lead me to believe that a significant dielectric relaxation is operational for the keto tautomer. DFT calculations hint towards the existence of a small barrier (~0.07 eV) in the excited state. A kinetic model was used to find that the ESIPT is a single step process in methanol and SDS micelle, happening at a timescale of ~0.25 ps, whereas in cyclohexane the indication of the two rate cosntants (~0.2 ps each). This two rate constants were assigned to the relaxation of enol-BPIMP in the excited state and formation of keto-BPIMP from the enol form.

References

1. Goodman, J.; Brus, L. E. *J. Am. Chem. Soc*. **1978**, *100* (24), 7472–7474.
2. *Principles of Fluorescence Spectroscopy*; Lakowicz, J. R., Ed.; Springer US: Boston, MA, 2006.
3. Kwon, J. E.; Park, S. Y. *Adv*. *Mater*. **2011**, *23*, 3615–3642.
4. Wu, Y.; Peng, X.; Fan, J.; Gao, S.; Tian, M.; Zhao, J.; Sun, S. *J*. *Org*. *Chem.* **2007**, *72*, 62–70.
5. Douhal, A.; Fiebig, T.; Chachisvilis, M.; Zewail, A. H. *J. Phys. Chem. A* **1998**, *102*, 1657–1660.
6. Liu, H.; Cheng, X.; Zhang, H.; Wang, Y.; Zhang, H.; Yamaguchi, S. *Chem. Commun*. **2017**, *53* (55), 7832–7835.
7. Shono, H.; Ohkawa, T.; Tomoda, H.; Mutai, T.; Araki, K. *ACS Appl. Mater. Interfaces* **2011**, *3* (3), 654–657.
8. Mutai, T.; Tomoda, H.; Ohkawa, T.; Yabe, Y.; Araki, K. *Angew. Chemie Int. Ed*. **2008**, *47* (49), 9522–9524.
9. Liang, F.; Wang, L.; Ma, D.; Jing, X.; Wang, F. *Appl. Phys. Lett.* **2002**, *81* (1), 4–6.
10. Sun, W.; Li, S.; Hu, R.; Qian, Y.; Wang, S.; Yang, G. *J. Phys. Chem. A* **2009**, *113*, 5888–5895.
11. Yan, D.; Evans, D. G. *Mater. Horiz.* **2014**, *1* (1), 46–57.
12. Sinha, S.; Chowdhury, B.; Ghosh, P. *Inorg*. *Chem.* **2016**, *55* (18), 9212–9220.
13. Balakrishnan, C.; Neelakantan, M. A.; Banerjee, S. A *Sensors Actuators, B Chem.* **2017**, *253*, 1012–1025.
14. Chen, L.; Ye, J.-W.; Wang, H.-P.; Pan, M.; Yin, S.-Y.; Wei, Z.-W.; Zhang, L.-Y.; Wu, K.; Fan, Y.-N.; Su, C.-Y. *Nat. Commun.* **2017**, *8*, 15985.
15. Lin, H.; Chang, X.; Yan, D.; Fang, W.-H.; Cui, G. *Chem. Sci.* **2017**, *8*, 2086–2090.
16. Enchev, V.; Angelov, I.; Mantareva, V.; Markova, N. *J. Fluoresc*. **2015**, *25*, 1601–1614.
17. Klymchenko, A. S.; Duportail, G.; Mély, Y.; Demchenko, A. P. *Proc*. *Natl. Acad. Sci. U. S. A.* **2003**, *100*, 11219–11224.
18. Santos, F. S.; Ramasamy, E.; Ramamurthy, V.; Rodembusch, F. S. *Photochem. Photobiol. Sci.* **2014**, *1*, 992–996.
19. Sengupta, P. K.; Kasha, M. *Chem. Phys. Lett.* **1979**, *68* (2), 382–385.
20. Klymchenko, A. S.; Demchenko, A. P. *J. Am. Chem. Soc*. **2002**, *124*, 12372–12379.

21. Smith, T. P.; Zaklika, K. A.; Thakur, K.; Walker, G. C.; Tominaga, K.; Barbara, P. F. *J. Phys. Chem.* **1991**, *95*, 10465–10475.
22. Nagaoka, S. I.; Endo, H.; Ohara, K.; Nagashima, U. *J. Phys. Chem. B* **2015**, *119*, 2525–2532.
23. Stasyuk, A. J.; Banasiewicz, M.; Cyrański, M. K.; Gryko, D. T. *J. Org. Chem.* **2012**, *77*, 5552–5558.
24. Zamotaiev, O. M.; Shvadchak, V.; Sych, T. P.; Melnychuk, N. A.; Yushchenko, D.; Mely, Y.; Pivovarenko, V. G. *Methods Appl. Fluoresc.* **2016**, *4*, 34004.
25. Lins, G. O. W.; Campo, L. F.; Rodembusch, F. S.; Stefani, V. *Dye. Pigment.* **2010**, *84*, 114–120.
26. Wang, H.; Zhang, H.; Abou-Zied, O. .; Yu, C.; Romesberg, F. .; Glasbeek, M. *Chem. Phys. Lett.* **2003**, *367*, 599–608.
27. Ziółek, M.; Kubicki, J.; Maciejewski, A.; Naskręcki, R.; Grabowska, A. *Phys. Chem. Chem. Phys.* **2004**, *6*, 4682–4689.
28. Simkovitch, R.; Huppert, D. *J. Phys. Chem. B* **2015**, *119*, 10244–10251.
29. Lee, J.; Kim, C. H.; Joo, T. *J. Phys. Chem. A* **2013**, *117*, 1400–1405.
30. Takeuchi, S.; Tahara, T. *J. Phys. Chem. A* **1998**, *102*, 7740–7753.
31. Kim, C. H.; Park, J.; Seo, J.; Park, S. Y.; Joo, T. *J. Phys. Chem. A* **2010**, *114*, 5618–5629.
32. Alarcos, N.; Gutierrez, M.; Liras, M.; Sanchez, F.; Douhal, A. *Phys. Chem. Chem. Phys*. **2015**, *17*, 16257–16269.
33. Ghosh, R.; Palit, D. K. *Photochem. Photobiol. Sci.* **2013**, *12*, 987.
34. Kim, Y.; Yoon, M.; Kim, D. *J. Photochem. Photobiol. A Chem.* **2001**, *138*, 167–175.
35. Rumble, C. A.; Breffke, J.; Maroncelli, M. *J. Phys. Chem. B* **2017**, *121*, 630–637.
36. Suda, K.; Terazima, M.; Sato, H.; Kimura, Y. *J. Phys. Chem. B* **2013**, *117*, 12567–12582.
37. Ghosh, D.; Batuta, S.; Das, S.; Begum, N. A.; Mandal, D. *J. Phys. Chem. B* **2015**, *119*, 5650–5661.
38. Maroncelli, M.; Fleming, G. R. *J. Chem. Phys.* **1987**, *86*, 6221–6239.
39. Snellenburg, J. J.; Laptenok, S. P.; Seger; R.; Mullen, K. M.; vanStokkum, I. H. M. *J. Stat. Softw.* **2012**, *49*, 1-22.
40. Frisch, M. J. et al. Gaussian 09, Revision E.01; Gaussian, Inc. Wallingford CT, **2009.**
41. Upadhyay, S. K. *Chemical Kinetics and Reaction Dynamics*; Springer Netherlands: Dordrecht, **2006**.

42. Whitnell, R. M.; Wilson, K. R.;. Hynes, J. T *J. Phys. Chem.* **1990**, *94*, 8625–8628.

This page intentionally left blank

Chapter 6

Solvation Dynamics in SDS Micelle Revisited with Femtosecond Time Resolution to Reveal the Probe and Concentration Dependence

Puspal Mukherjee, Aritra Das and Pratik Sen, *Submitted in Chem. Phys. Lett.*

6.1. Introduction

Solvation dynamics in the micellar environment has been an interesting topic of research for last three decades because of its similarities with the biological environments, and among all the micelles anionic sodium dodecyl sulfate (SDS) micelle was studied more frequently.[1-4]. In this chapter, I have studied solvation dynamics in SDS micelles in water and therefore here I am presenting a comprehensive overview of the previous research on the topic. Of course there are several similar studies performed in neutral (e.g. TX-100), cationic (e.g. CTAB) and other anionic (e.g. AOT) micelles and reverse micelles along with many other confined environments, which are beyond the scope of discussion here.[5-10] Solvation dynamics is explored by the time variation of the well-known solvent response function as given below.

$$C(t) = \frac{\nu(t)-\nu(\infty)}{\nu(0)-\nu(\infty)} \quad (6.1)$$

In the above equation $\nu(t)$, $\nu(0)$ and $\nu(\infty)$ are the peak frequencies of time resolved emission spectra (TRES) of the solvatochromic molecule at time t, 0 and ∞, respectively. For a molecule with high excited state dipole moment compared to the ground state, the $\nu(\infty)$ is appeared at the lower energy than $\nu(0)$. The theory of solvation dynamics has been discussed in many popular review articles and the readers are referred to those for further understanding on this topic.[1,4,5,6]

Coming back to the specific system of SDS micelle, the first ever observation was done by Sarkar et al. using coumarin 480 dye.[11] They observed that in 32 mM SDS the time variation of $C(t)$ is biexponential in nature having two time constants 180 ps and 2140 ps accompanied by 445 cm^{-1} shift with an average solvation time of 690 ps.[11] Pal et al. studied the solvation dynamic in 100 mM SDS using 4-(dicyanomethylene)-2-methyl-6-(4-dimethylaminostyryl)-4H-pyran (DCM) dye with a time resolution of 80 ps and found 450 cm^{-1} shift in $C(t)$ with time constants of 160 ps and 2900 ps.[12] The average solvation time calculated was 1400 ps in this case.[12] Later the same dye was studied by Mandal et al. in

femtosecond time domain in TX-100 and CTAB micelle but not in SDS micelle.[13] Another solvatochromic dye 4-aminopthalimide (4-AP) has been used by Datta et al. in 160 mM SDS to observe a shift of 1043 cm^{-1} with a single time constant of 82 ps.[14]. However, use of 4-AP to determine solvation dynamics has an intrinsic problem of specific solvation.[15,16]. In theory, nonspecific solvation time is accompanied by less significant change in the shape of time resolved emission spectra (TRES). In case of 4-AP, polar protic solvents induces a change in the shape of TRES due to specific hydrogen bonding interactions with solvent molecules as pointed out by Dobek.[15,16]. Moreover, the origin of emission in case of 4-AP can be from S_1 or S_2 state depending on the nature of environment, which make 4-AP a complicated molecule to be used as solvatochromic probe to study solvation dynamics.[15,16]. Tamoto et al. have studied solvation dynamics in 16 mM SDS using picosecond streak camera technique.[17]. They observed biexponential decay of $C(t)$ with 140 ps and 2140 ps time components.[17]. Mitra et al. studied temperature dependent solvation dynamics of DCM in 50 mM SDS micelle and observed that with increase in temperature the solvation dynamics becomes faster as expected from activation energy barrier crossing model.[18]. Ghosh et al. reported the time components of $C(t)$ in 80 mM SDS to be 1.5 ps and 180 ps using coumarin 480 as probe molecule.[19]. Hara et al. described the effect of pressure on solvation time of coumarin 153 in 40 mM SDS to be proportional.[20]. Coumarin 307 has also been used to study the solvation dynamics in 60 mM SDS micelle using broadband transient absorption spectroscopy by Dhenadhayalan et al. and they observed a 230 ps time constant of solvent relaxation.[21]. Choudhury et al., in a recent study, examined the coupling between structural fluctuation and solvation dynamics in 300 mM SDS micelle.[22]. In that paper, they reported 1.48 ps and 27 ps time constant of solvation in the time window of 150 ps.[22]. A very interesting fact about curcumin in micelle was revealed by Adhikary et al.[23]. They demonstrated that the molecule has an ultrafast femtosecond time component of solvation followed by a picosecond component in 100 mM SDS micelle.[23]. They also showed the slow time component was affected by deuteration, which indicated the

presence of an intramolecular proton transfer mechanism.[23]. Shirota et al. studied coumarin 480 and 153 in different concentration of SDS micelle (16.2 to 810 mM) with picosecond time resolution.[24]. They have reported a biexponential nature of both solvation time and reorientation time with shorter and longer timescales, which have no significant changes with concentration change.[24]. However, the aggregation number of surfactant in SDS micelle does increase with increase in concentration as pointed out by many scientists using several types of experimental techniques.[25-28]

The above discussion laid out the fact that the solvation dynamics in SDS micelle have been studied in a large variety of fluorescent probes and SDS concentrations and it appear that the nature of solvatochromic molecule and concentration of surfactant may play a role in the solvent relaxation in SDS micelle. It was expected and also discussed by several researchers that the solvation dynamics must have probe dependence because of the micro-heterogeneous environment within the micelle.[1,4]. The systematic study of solvation dynamics by Castner, Jr. and co-workers in non-ionic triblock co-polymer micelles using C153, C480 and C343 dyes showed that indeed solvation dynamics is probe location dependent as the three coumarins reside in the three distinct region of the micelle.[29,30]. They have also characterized the hydrophilicity of the dyes based on the partition coefficient in ocatanol-water system and showed that C153 being most hydrophobic takes up the least water penetrated region of the micelle while C343 resides at the bulk water interface and C480 in the middle.[29,30]. Recently, Kumpulainen et al. used femtosecond broadband fluorescence up-conversion spectroscopy to study solvation dynamics of six couamrin dyes and 4-AP in polar solvents and concluded that even solvation dynamics of bulk solvent depend on character of the probe.[31]. Moreover, a change in concentration of SDS is accompanied by changes in aggregation number, which alter the nature of Stern layer of the micelle.[1,11] Thus it is expected to affect the solvation dynamics too.

The experimental studies performed on SDS micelle so far have mostly used ~100 picosecond time resolution. However, several theoretical studies indicated the presence of sub-picosecond to few picosecond time components in the solvent relaxation of water at the micelle interface.[32-36] Even with a sub-picosecond time resolution it would probably be very hard to observe the libration and damped oscillation time scales, however the short component of overall orientation and translation dynamics can be observed.[32-36] Therefore I feel that solvation dynamics in SDS micelle over femtosecond to nanosecond time scale combining both fluorescence up-conversion and time correlated single photon counting technique need to be studied to get the overall picture of the problem, which have not been done till now. Moreover, the exact probe and surfactant concentration dependence of individual time components and average solvation time is not clear because experiments were not performed under the same conditions. Probes differing in hydrophobicity and charge criteria will make them occupy different parts of the micellar system. The hydrogen bonding structure of water controls the solvation time and water in different parts of micellar structure have different hydrogen bond networks. Thus the heterogeneity in the rigidity of water structure in the micelle can be explored by the probes used here provided I can track all the components of solvation.

6.2. Result and Discussion

To study the probe dependence of the solvation dynamics in SDS micelle I have used four solvatochromic probes namely, C460, C480, C153 and DCM (scheme 6.1). These four dyes have very different absorption and emission, which I have shown in figure 6.1, and the corresponding maxima are reported in table 1. The CMC value of SDS micelle is ~8 mM and I have chosen 40 mM SDS for studying the probe dependence. To study the solvation dynamics from femtosecond to nanosecond time domain, I have used femtosecond fluorescence up-conversion and TCSPC technique and conveniently matched the two data.

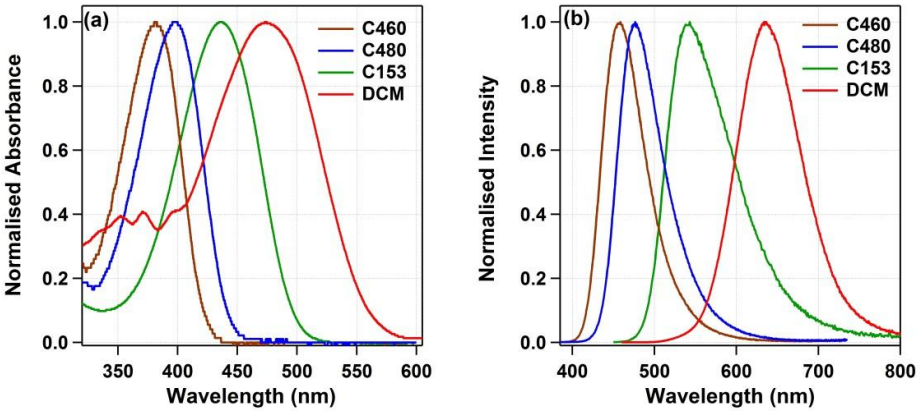

Figure 6.1. Steady State (a) absorption and (b) emission spectra of different fluorescent solvatochromic probes used in this study in 40mM SDS micelle.

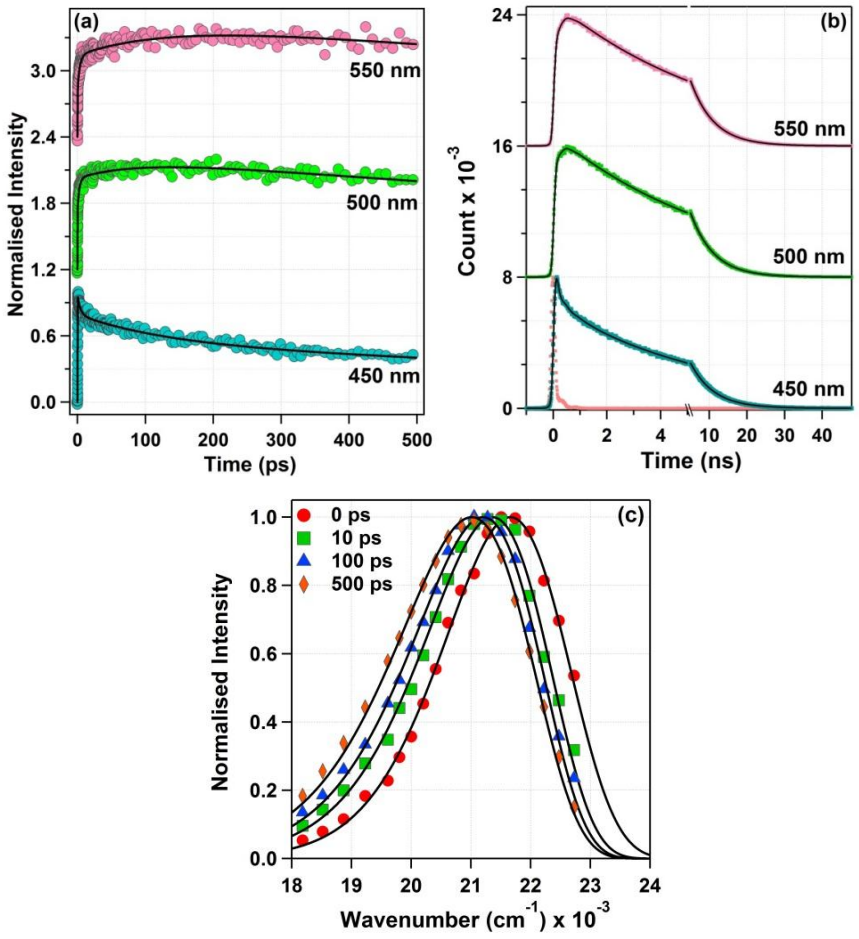

Figure 6.2. Fluorescence transients of C480 in 40 mM SDS in (a) fluorescence up-conversion and (b) TCSPC setup. (c) TRES constructed from the fluorescence decay at different times. The black solid lines in each graph represents fitting lines.

Here I present in details the experiments and analysis of C480 data in 40 mM SDS micelle and for rest of the systems I followed the same procedure. Fluorescence intensity decays at 19 different wavelengths from 440 nm to 550 nm over the entire emission spectra of C480 in 40 mM SDS were recorded in up-conversion setup exciting the sample at 390 nm and three of those are shown in figure 6.2a. The lifetime of the dye is over 6 ns in SDS and the fluorescence transients did not decayed completely within the maximum delay time of our setup i.e. 2 ns. So the fluorescence intensity decays at same wavelengths were also recorded in the TCSPC setup with a time window of 50 ns exciting the samples at 375 nm using picosecond diode laser, which are shown in figure 6.2b. The transients obtained from both techniques were fitted using a sum of three exponential functions. In case of up-conversion data, transients from 440 nm to 455 nm showed three decay components with the ultrafast component varying from 3.1 ps to 7.1 ps. For the fluorescence transients from 460 nm to 470 nm one rise component was observed with time constant ranging from 0.3 ps to 1.3 ps. For rest of the wavelengths (475 nm – 550 nm), two rise components were present in the fitting. The fast rise component varied from 0.5 ps to 3.4 ps and the slower rise component varied from 5 ps to 170 ps. The rise component signified solvation of the excited state of the dye. In TCSPC measurement, I obtained only one rise component in the higher wavelength region with maximum time constant of 180 ps, which is justifiable from the up-conversion data. From each of the data set, I have constructed the time resolved emission spectra (TRES) adopting the procedure described by Maroncelli and Fleming.[38]. Each of the TRESs was fitted by a single lognormal function $L(\nu)$ described below.

$$L(\nu) = g_0 exp\left\{-\ln 2\left(\frac{\ln\left(1+\frac{2b(\nu-\nu_p)}{\Delta}\right)}{b}\right)^2\right\} \tag{6.2}$$

In the above function g_0, b, ν_p and Δ are the peak height, asymmetry parameter, peak frequency and width parameter, respectively. The intensity

normalized TRES are shown in figure 6.2c and it is important to mention here that I have overlapped the TRES obtained from up-conversion and TCSPC experiments at 80 ps time and they overlapped quite satisfactorily as shown in figure 6.3. Therefore in figure 6.2c, the first two TRES are from up-conversion experiment and the last two are from TCSPC experiment. The maxima of the TRESs are plotted against time in figure 6.4a. The peak frequency variation in figure 6.4a consists of up-conversion data upto 80 ps and after that data obtained from TCSPC study. I achieved perfect convergence of the peak frequency data (figure 6.4a), which was expected and very important. The total peak frequency variation can be adequately fitted with a sum of four exponential functions. However, the frictionless component of solvation cannot be found in those fitting. Maroncelli and co-works used an extra 30 fs time component to extract the libration part of the solvation dynamics in pure solvents.[39]. Following their work, I have fixed an extra 0.1 ps time component in the fitting. This component originates from the libration and damped rotation of the water molecules and should be normally observed in the fitting. However, water molecules in proximity of the interface show a motion in < 0.1 ps timescale.[1,4,7] Therefore it is hard to identify them in my experimental time resolution and from the fitting parameters listed in table 6.1, we can see that the contribution of this 0.1 ps time component is ~2% in case of C480. If the time resolution of the instrument was shorter, then the contribution of this ultrashort component would have been larger. The longer time components (130 ps and 1030 ps) of solvation of C480 in 40 mM SDS micelle can be traced back to the earlier reports but the ultrafast components of 1.2 ps and 4.0 ps were clearly obtained from up-conversion experiment and they were not previously known.[11]. The total shift obtained in case of C480 in 40 mM SDS is 730 cm^{-1} however it is worth mentioning that TCSPC experiment could reveal only ~450 cm^{-1} shift in the time resolved emission spectra, because of large IRF. The nature of variation of emission maxima against time readily can yield the solvation time, yet following the tradition I have constructed normalized solvent response function according to equation 6.1, which is shown in figure 6.4b.

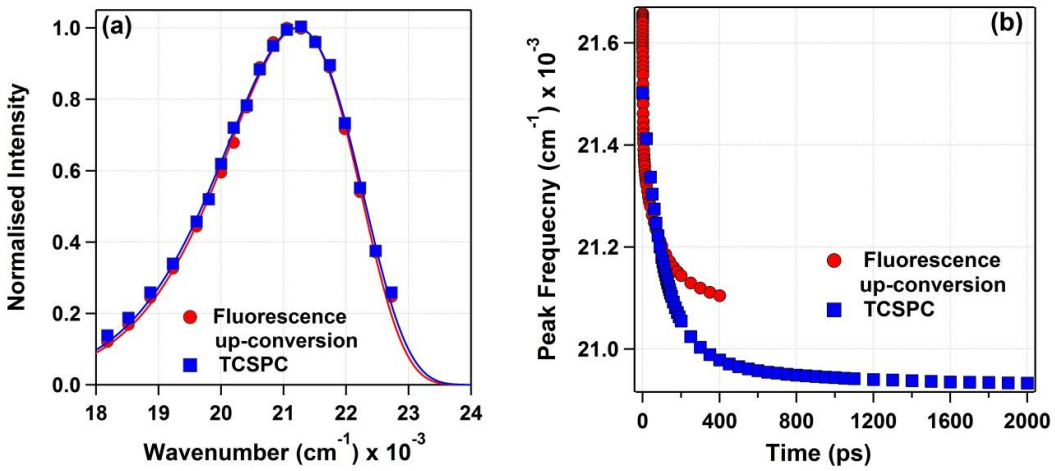

Figure 6.3. (a) Time resolved emission spectra at 80ps for C480 in 40mM SDS solution constructed from fluorescence intensity decays (b) variation of peak frequency of time resolved emission spectra against time obtained using two different techniques i.e. femtosecond fluorescence up-conversion and TCSPC.

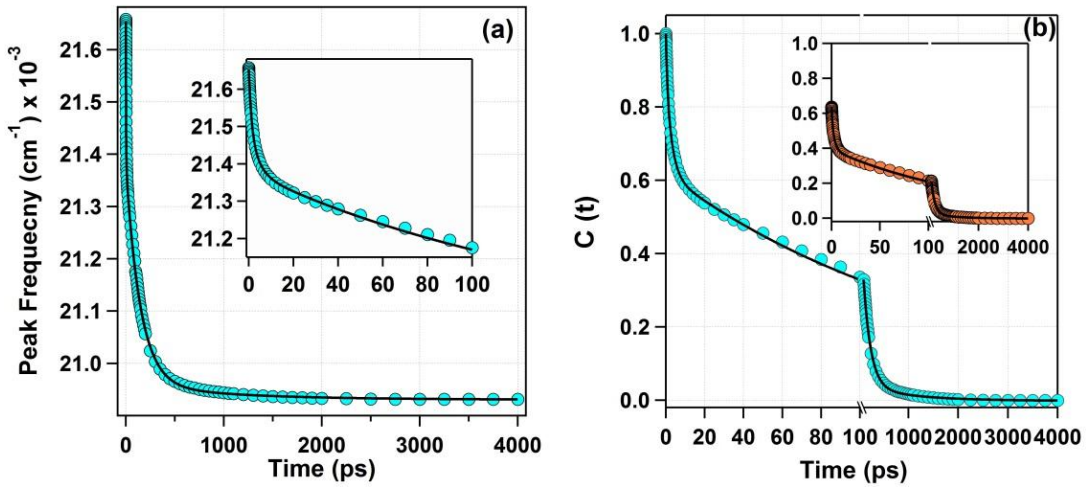

Figure 6.4. (a) Variation of maxima of TRES with time and (b) solvent response function constructed from peak frequency data for C480 in 40 mM SDS. Inset showing solvent response function corrected for time zero spectrum calculated using Fee-Maroncelli method described in ref. 39. The black solid lines in each case represent fitting lines.

Although I have obtained a very fast solvation time in our experiment but still a significant part of solvation can be missed because of the 250 fs IRF of our up-conversion setup.[40,41]. Therefore, I have used the Fee-Maroncelli procedure to estimate the time zero spectrum.[40,41].

Table 6.1. Steady state absorption and emission maxima, parameters obtained from fitting peak frequency vs time for different solvatochromic probes in 40 mM SDS, total Stokes shift calculated from Fee-Maroncelli procedure (ref 40), theoretically corrected average lifetime data for different solvatochromic probes in 40 mM SDS.

Dye	[SDS] mM	λ_{max}^{abs} nm	λ_{max}^{em} nm	a_1	τ_1 ps	a_2	τ_2 ps	a_3	τ_3 ps	a_4	τ_4 ps	a_5	τ_5 ps	$< \tau_s >$ ps	$\Delta\nu_{expt}$ cm^{-1}	$\Delta\nu_{theo}$ cm^{-1}	% miss	$< \tau_s >$ ps corr
C460	40	381.6	457.0	5	0.1	379	1.6	213	10.9	171	190	-	-	46	768	1219	37.0	29
C153	40	436.2	541.0	10	0.1	280	2.3	381	87.0	42	1650	-	-	145	711	1205	41.0	86
DCM	40	475.0	635.5	58	0.1	593	0.8	510	3.0	148	105	160	1550	180	1470	1964	25.1	135
C480	10	398.2	477.0	8	0.1	226	1.3	168	7.1	260	140	55	670	104	717	1115	36	67
	20	398.0	477.0	8	0.1	208	1.9	83	4.8	430	110	42	790	116	771	1105	30	81
	40	398.0	476.0	9	0.1	145	1.2	123	4.0	412	130	41	1030	132	730	1140	36.0	85
	200	397.6	476.0	10	0.1	263	1.1	129	7.8	372	190	23	1880	144	797	1208	34	95

In this procedure, the absorption and emission spectra of the probe is measured in a non-polar solvent (in my case cyclohexane) and the Stokes shift is calculated, which then plugged into the system under study to estimate the time zero spectrum as shown below.

$$\nu_{em}^{p}(0) = \nu_{abs}^{p} - \left[\nu_{abs}^{np} - \nu_{em}^{np}\right] \quad (6.3)$$

In the above equation, $\nu_{em}^{p}(0)$ is the emission maximum at zero time in polar solvent, ν_{abs}^{p} is the absorption maxima in polar solvent, ν_{abs}^{np} and ν_{em}^{np} are the absorption and emission maxima in non-polar solvent.[40, 41] The absorption and emission maxima of C480 measured in cyclohexane were 362 nm (27624 cm^{-1}) and 407 nm (24570 cm^{-1}) respectively. In 40 mM SDS, the absorption maximum of C480 is 398 nm (25125 cm^{-1}), which is the ν_{abs}^{p} for the present case. Using equation 6.3, the theoretical time zero spectrum maximum of C480 in 40 mM SDS is calculated to be 22072 cm^{-1}, which implies total dynamics Stokes shift should be 1140 cm^{-1}. The procedure adopted here uses the Stokes shift in a non-polar media but it does not account for the effect of interface i.e. the Stokes shift in the non-polar medium does not contain the interfacial effect. Thus an inherent error is carried on by the estimations made according to equation 6.3, which has been discussed earlier by Biswas and co-workers.[42]. However I have observed only 730 cm^{-1} shift in our femtosecond-nanosecond combined experiment. Thus I have missed about 36% of solvation in 40 mM SDS using C480 as the probe molecule. Incorporation of the missed solvation in the solvent response has been shown in inset of figure 6.4b. If I assume that the missed ultrafast component will be in the order of our IRF then I can estimate the maximum solvation time of C480 in 40 mM SDS by multiplying the experimental average solvation time (132 ps) by percentage of solvation observed and it was found to be 85 ps.

Now, if we change the nature of the solvatochromic probe then based on its hydrophobicity, the probe location within the micelle should change and as the water penetration in different micellar region is different, I should see a change in

the solvation time.[29,30] Therefore I have performed the same study with C153, DCM and C460 in 40mM SDS. In each case, I recorded fluorescence intensity decays at multiple wavelengths in both fluorescence up-conversion and TCSPC setups and constructed TRES using the same procedure described above.

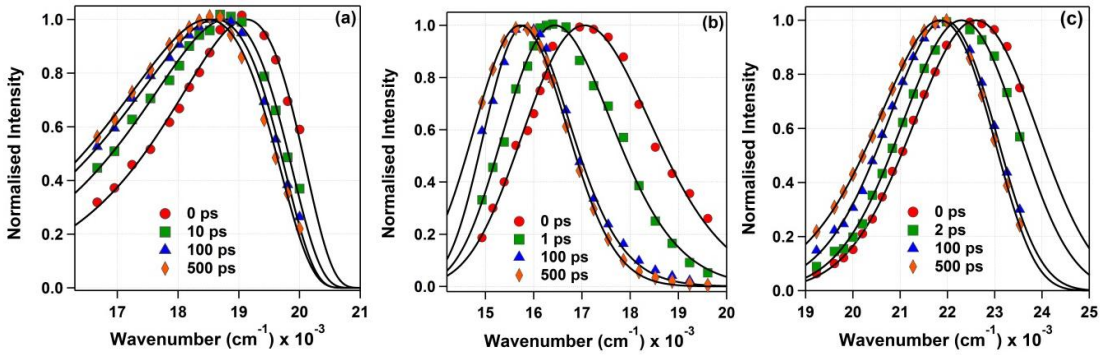

Figure 6.5. Time resolved emission spectra of (a) C153 (b) DCM and (c) C460 in 40mM SDS.

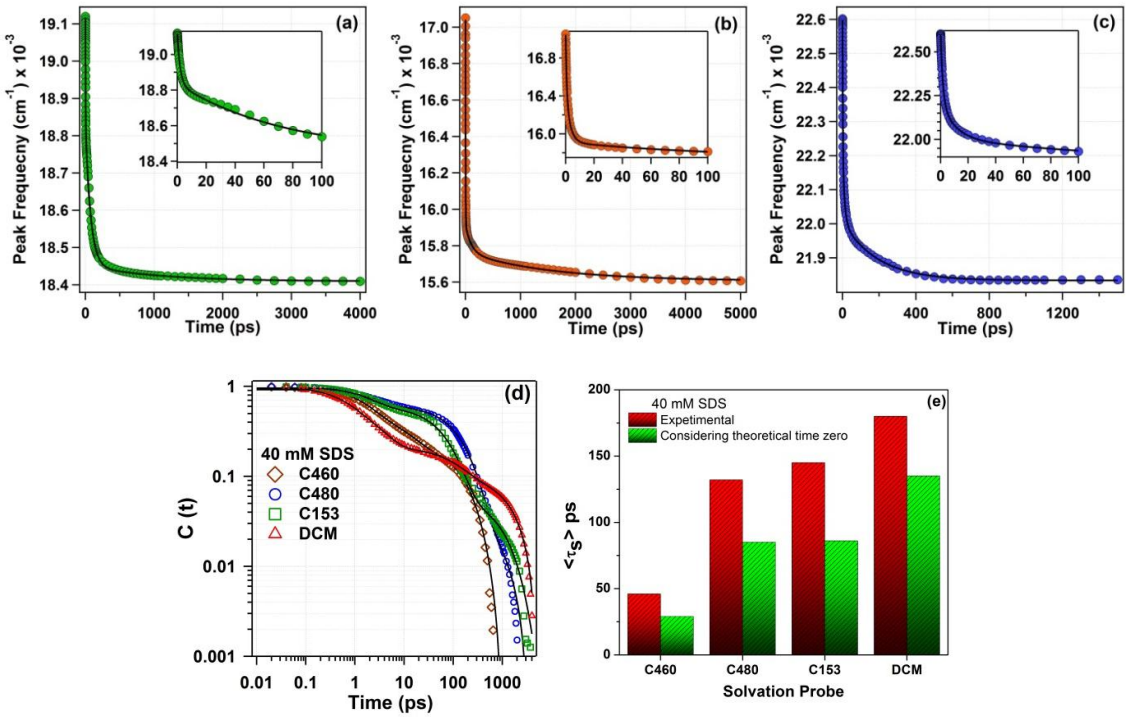

Figure 6.6. Variation of maxima of TRES with time for (a) C153 (b) DCM (c) C460 in 40 mM SDS. (d) Comparison of solvent response functions of different dyes in 40 mM SDS. (e) Variation of average solvation time of different probes in 40 mM SDS micelle.

The TRES are shown in figure 6.5 and the emission maxima variation with time is shown in figure 6.6a, 6.6b, and 6.6c for C153, DCM and C460, respectively. In case of C153 and C460 the peak frequency variation was fitted with a sum of four exponential functions whereas for DCM a sum of five exponential functions was needed reserving the first component for 0.1 ps like in the case of C480. All the fitting parameters are reported in table 6.1. For coumarins the contribution of the ultrashort component was ~2% and the same for DCM was ~5%. To compare the solvation dynamics experienced by the four solvatochromic probes in 40 mM SDS solution, I have plotted the solvent response function C(t) for all the 4 molecules in figure 6.6d. The comparison revealed that in case of DCM, the ultrafast component of solvation is 0.7 ps, which is faster among all the dyes. Moreover DCM showed a total dynamic Stokes shift of 1470 cm^{-1}, which is significantly high compared to other 3 dyes. However, in terms of total solvation, the fastest response was shown by C460. C480 showed slower solvation in the early time but average solvation time was less compared to both C153 and DCM dye. I have also employed Fee-Maroncelli procedure to these dyes, which are reported in table 6.1 and figure 6.7. The overall solvation missed was highest in case of C153 and least in the case of DCM. The trend of solvation time clearly follows their solubility in water. C460 solubility in water is highest among these four dyes and it is expected to remain near bulk water molecules, which is at the Stern layer of the micelle. From the previous report by Castner and co-workers we have the information that C153 remains more buried in a micelle compared to C480 because of their difference in hydrophobicity. DCM has been reported to be completely insoluble in water.[12, 29, 30]. So we can expect it to be distributed closer to micellar core. Translational, orientational and diffusional dynamics of water molecules close to the interface will be faster compared to the water molecules incarcerated within the miceller core. Interestingly, the early part of solvation is very similar in all the cases as evident from Table 6.1, but the longer parts are different because of the access of different kinds of water molecules by different probes. Considering C460 and DCM have similar fluorescence lifetimes but completely different solvation times,

it seems that the location of the probes is the only explanation. Although, an extensive search of the involvement of molecular photophysics of the probe may reveal more details, however we generally consider that the change in peak frequency of TRES of these well-known solvatochromic probes originate due to solvation. To put it into perspective, I have represented the average solvation time of each probe in figure 6.6e. Thus I conclude that the solvation time in a particular concentration of SDS micelle is highly dependent on the location of the probe molecule.

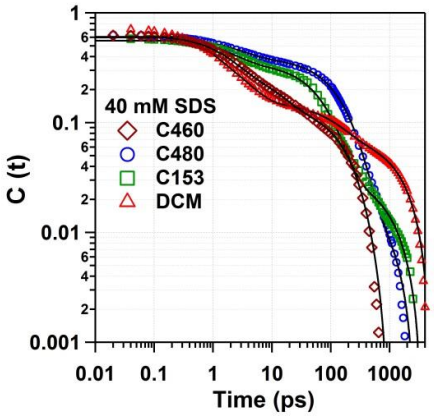

Figure 6.7. Solvent response function of different fluorescent probes used in the study in 40mM SDS micelle incorporating theoretically estimated time zero spectra calculated according to ref 39.

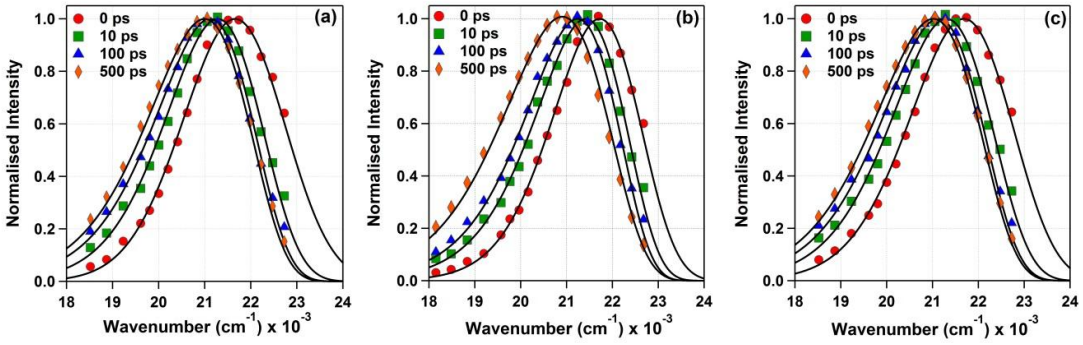

Figure 6.8. Time resolved emission spectra of C480 in (a) 10mM (b) 20mM and (c) 200mM SDS in water.

To investigate further, I have studied the SDS concentration dependent solvation dynamic using C480. I have performed similar experiment in 10, 20 and 200 mM SDS. First of all, the absorption and emission spectra of C480 measured

in 10, 20 40 and 200 mM SDS did not show any difference as evident from the data given in table 6.1. Thus there is no sudden change of excited state dynamics of C480 with change in SDS concentration, which is very much expected result. However there are subtle changes, which can only be seen through femtosecond experiments. I followed the procedure described in detail for C480 in 40 mM SDS in all other three cases. The fluorescence transients in up-conversion and TCSPC instrument were recorded at multiple wavelengths and were used to construct the TRES in each case, which I have represented in the figure 6.8. The peak frequency vs time of TRESs in each case are represented in figure 6.9a, 6.9b, 6.9c and each of the variation was fitted using a sum of five exponential functions with a 0.1 ps component. The parameters obtained are reported in table 6.1, which reflects a very interesting trend. Although the time constants are very close to one another, there is a steady increase of longest component with increase in concentration of SDS. The ultrafast component is quite similar in all the cases but the comparison is difficult as the relative amplitudes are different. So the average lifetime was calculated and it showed a steady increasing trend from 104 ps in 10 mM to 144 ps in 200 mM SDS. I applied Fee-Maroncelli procedure in all these cases (table 6.1 and figure 6.10) to find that the solvation missed in all the 4 cases were same. To give a visual comparison between the solvent response function I have plotted the same for 10 mM and 40 mM SDS in a figure 6.9d and it shows that the difference lies within the first 100 ps time. So only TCSPC experiments with ~100 ps time resolution is not expected to find the difference in solvation dynamics. As I have done the experiments from fs to ns time domain, I was able to find the difference in ultrafast component as well as the merging of fluorescence up-conversion and TCSPC data resolve the difference in longer time component. From the present study, it is clear that there is a slowing down of solvation dynamics however it is not easy to find the reason behind it and if we consult earlier literature we can see that there is not much significant change in orientation relaxation time either.[24].

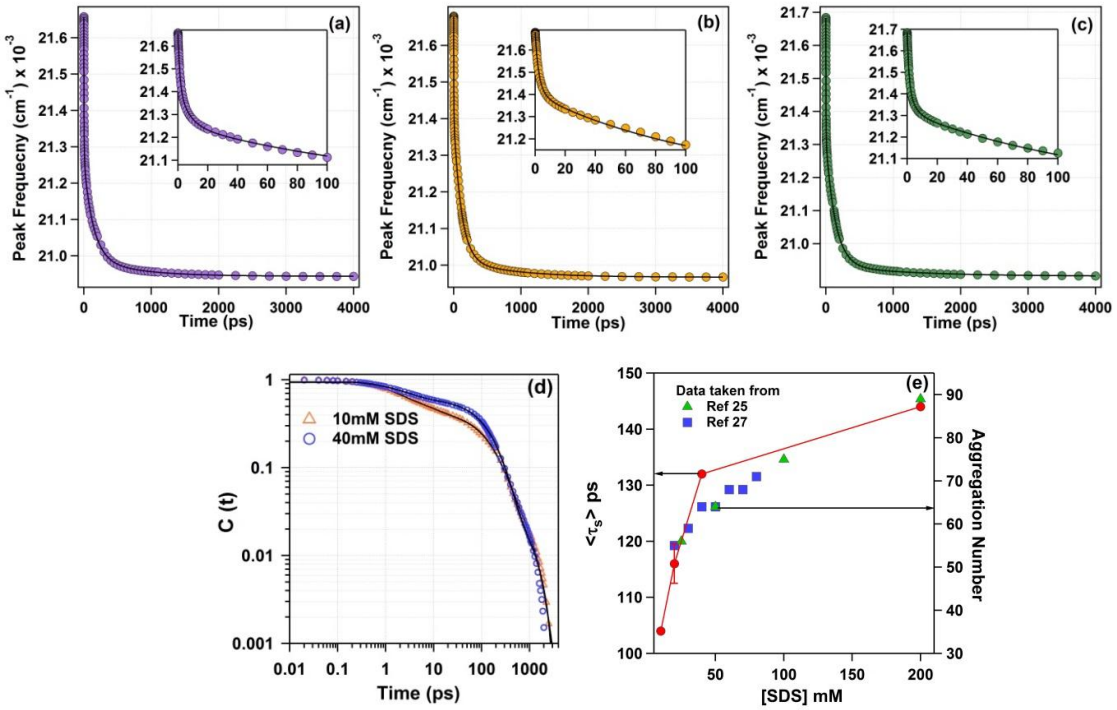

Figure 6.9. Variation of maxima of TRES with time for C480 in different concentrations of SDS in water (a) 10 mM (b) 20 mM (c) 200 mM. (d) Comparison of solvent response functions of C480 in 10 mM and 40 mM SDS. (e) Variation of average solvation time of C480 with SDS concentration along with the aggregation number of SDS micelle.

Interestingly, the increase in aggregation number of SDS micelle with increase in SDS concentration is found to agree well with the variation of the solvation time, which is shown in figure 6.9e.[25-28] We know that a micelle cannot remain truly spherical with increase in aggregation number/concentration and the shape will distort from spherical to elliptical to accommodate increasing number of alkyl chains.[43] For a surfactant with single alkyl chain like SDS, increasing concentration would mean decrease of surface area per molecule and that would affect the dynamics of water penetrating the micelle.[43]. If I assume that the distribution of C480 inside SDS micelle did not change when i increase the concentration, distortion of shape of SDS micelle from spherical to ellipsoid will decrease the surface area per molecule leading to the incarceration of water molecules, which in turn slowed down their orientational and translational dynamics.

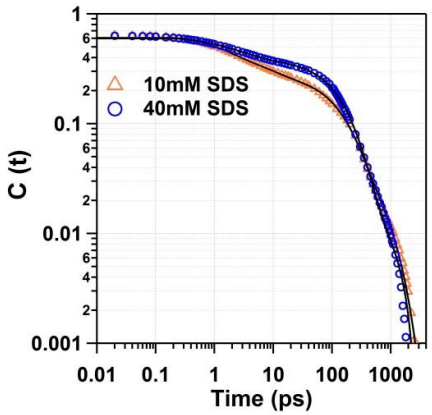

Figure 6.10. Solvent response function of C480 in 10mM and 40mM SDS micelle incorporating theoretically estimated time zero spectra calculated according to ref 39.

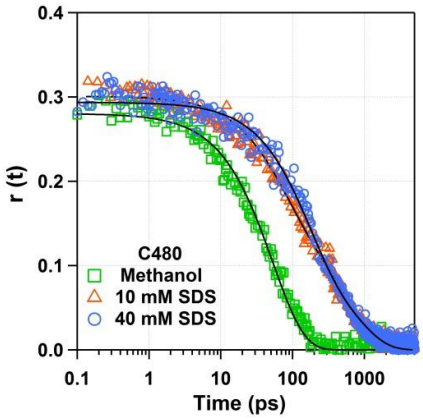

Figure 6.11. Fluorescence anisotropy decay of C480 in methanol, 10mM and 40mM SDS solution measured at 465 nm. The black solid lines indicate fitting.

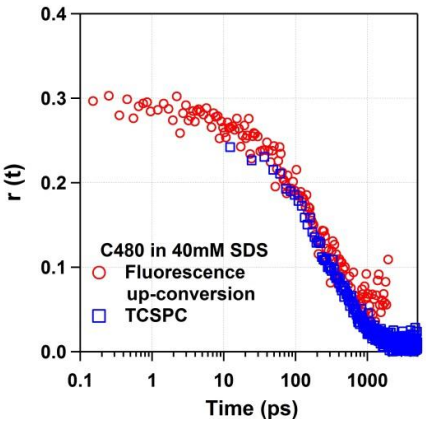

Figure 6.12. Fluorescence anisotropy decay of C480 in 40mM SDS micelle obtained from two different techniques i.e. femtosecond fluorescence up-conversion and TCSPC.

Thus with increase in SDS concentration I observed increase in solvation time and so in figure 6.9e, the overall trend of solvation time and aggregation number followed the same trend. It should be noted that the distortions for micelle containing branched alkyl chain are different and therefore micelles formed by other surfactants may not show this variation.[43]. But for SDS micelle in water at least upto 200 mM concentration of SDS, increasing surfactant concentration shall slow down the solvent response.

The notion of distribution of C480 inside the micelle can be readily checked by measuring fluorescence anisotropy of the probe. For this purpose, I have measured the anisotropy of C480 in all the four concentrations SDS micelle and C153 in 40 mM SDS micelle. Fluorescence intensity decays were collected at the blue side of the emission maxima i.e. at 465 nm for C480 and 530 nm for C153. This is to note here that anisotropy decay of both those probes was measured in methanol to compare with reported data.[38]. In methanol, the anisotropy decays were finished within the time window of the fluorescence up-conversion setup as evident from figure 6.11. However, the same in SDS micelle required the use of TCSPC measurements to obtain the long component rotational decay. In figure 6.11, the total anisotropy decay of C480 has been shown for 10 and 40 mM SDS joining the fluorescence up-conversion and TCSPC data around 200 ps. Individual data obtained from the two measurement techniques for C480 in 40 mM SDS has been shown in figure 6.12. The time components obtained from all the anisotropy decay are reported in table 6.2. As expected, the bulk solvent has only one single rotational time component but in micelle one short and another long component were obtained. Interestingly, for C480 in all different SDS micelle of varying concentrations, the time components are very much comparable and the average rotational time is well within the experiment errors. This shows that the rotation of the probe was not affected, which confirms that the location of C480 within the micelle does not change with change in concentration of SDS. Moreover

comparison with the data obtained from C153 signifies that C153 is situated at a different location within the SDS micelle compared to C480.

Table 6.2. Rotational diffusion time constants obtained from fitting fluorescence anisotropy data of C480 and C153 in methanol and SDS in water.

Dye	Medium	a_1	τ_1 ps	a_2	τ_2 ps	$< \tau_s >$ ps
C480	Methanol	0.28	52	-	-	52
	10 mM SDS	0.14	104	0.158	530	330
	20 mM SDS	0.144	135	0.167	520	342
	40 mM SDS	0.138	117	0.153	538	338
	200 mM SDS	0.115	108	0.184	513	357
C153	Methanol	0.33	45	-	-	45
	40 mM SDS	0.17	150	0.184	667	418

6.3. Conclusion

This femtosecond to nanosecond solvation dynamics study summarizes the probe and concentration dependence of solvation dynamics in SDS micelle. Using four solvatochromic molecules I established that in 40 mM SDS the solvent response highly depends on the nature of the probe molecule. Among them, DCM showed the largest average solvation time (180 ps) followed by C153 (145 ps), C480 (132 ps) and C460 (46 ps). The only possible explanation of this phenomenon is the location of the probe within the SDS micelle. Further a surfactant concentration dependence study of the solvation dynamics of C480 in SDS micelle showed a steady increase of solvation time with increase in SDS concentration. Explanation of this behavior was found in the variation of aggregation number of SDS micelle as a function of its concentration. Furthermore, I studied the anisotropy of C480 and C153 in SDS micelle to find that the rotational diffusion of C153 is slower compared to C480 which confirmed that C153 is more buried compared to C480. The change in concentration of SDS micelle did not changed the average rotational diffusion time of C480 signifying no large change in distribution of the dye with variation in SDS concentration.

References

1. Nandi, N.; Bhattacharyya, K.; Bagchi, B. *Chem. Rev*. **2000**, *100* (6), 2013–2045.
2. Tulumello, D. V.; Deber, C. M. SDS *Biochemistry* **2009**, *48* (51), 12096–12103.
3. Mahiuddin, S.; Zech, O.; Raith, S.; Touraud, D.; Kunz, W. *Langmuir* **2009**, *25* (21), 12516–12521.
4. Bhattacharyya, K. *Acc. Chem. Res.* **2003**, *36* (2), 95–101.
5. Sen, P.; Mukherjee, S.; Halder, A.; Dutta, P.; Bhattacharyya, K.. *Res. Chem. Intermed*. **2005**, *31* (1–3), 135–144.
6. Sarkar, N.; Das, K.; Datta, A.; Das, S.; Bhattacharyya, K. *J. Phys. Chem.* **1996**, *100* (25), 10523–10527.
7. Faeder, J.; Ladanyi, B. M. *J. Phys. Chem. B* **2005**, *109* (14), 6732–6740.
8. Shirota, H.; Horie, K. *J. Phys. Chem. B* **1999**, *103* (9), 1437–1443.
9. Sen, P.; Roy, D.; Mondal, S. K.; Sahu, K.; Ghosh, S.; Bhattacharyya, K. *J. Phys. Chem. A* **2005**, *109* (43), 9716–9722.
10. Sen, S.; Sukul, D.; Dutta, P.; Bhattacharyya, K. *J. Phys. Chem. A* **2001**, *105* (47), 10635–10639.
11. Sarkar, N.; Datta, A.; Das, S.; Bhattacharyya, K. *J. Phys. Chem.* **1996**, *100* (38), 15483–15486.
12. Pal, S. K.; Sukul, D.; Mandal, D.; Sen, S.; Bhattacharyya, K. *Chem. Phys. Lett.* **2000**, *327* (1–2), 91–96.
13. Mandal, D.; Sen, S.; Bhattacharyya, K.; Tahara, T. *Chem. Phys. Lett.* **2002**, *359* (1–2), 77–82.
14. Datta, A.; Mandal, D.; Pal, S. K.; Das, S.; Bhattacharyya, K. *J. Mol. Liq.* **1998**, *77* (1–3), 121–129.
15. Maciejewski, A.; Kubicki, J.; Dobek, K. *J. Phys. Chem. B* **2003**, *107* (50), 13986–13999.
16. Maciejewski, A.; Kubicki, J.; Dobek, K. *J. Phys. Chem. B* **2005**, *109* (19), 9422–9431.
17. Tamoto, Y.; Segawa, H.; Shirota, H. *Langmuir* **2005**, *21* (9), 3757–3764.
18. Mitra, R. K.; Sinha, S. S.; Pal, S. K. *J. Phys. Chem. B* **2007**, *111* (26), 7577–7583.
19. Ghosh, S.; Mondal, S. K.; Sahu, K.; Bhattacharyya, K. *J. Chem. Phys.* **2007**, *126* (20), 204708.
20. Hara, K.; Baden, N.; Kajimoto, O. *J. Phys. Condens. Matter* **2004**, *16* (14), S1207–S1214.

21. Dhenadhayalan, N.; Selvaraju, C.; Ramamurthy, P. *J. Phys. Chem. B* **2011**, *115* (37), 10892–10902.
22. Choudhury, S.; Mondal, P. K.; Sharma, V. K.; Mitra, S.; Sakai, V. G.; Mukhopadhyay, R.; Pal, S. K. *J. Phys. Chem. B* **2015**, *119* (34), 10849–10857.
23. Adhikary, R.; Carlson, P. J.; Kee, T. W.; Petrich, J. W. *J. Phys. Chem. B* **2010**, *114* (8), 2997–3004.
24. Shirota, H.; Tamoto, Y.; Segawa, H. *J. Phys. Chem. A* **2004**, *108* (16), 3244–3252.
25. Bales, B. L.; Almgren, M. *J. Phys. Chem.* **1995**, *99* (41), 15153–15162.
26. Gehlen, M. H.; De Schryver, F. C. *J. Phys. Chem.* **1993**, *97* (43), 11242–11248.
27. Quina, F. H.; Nassar, P. M.; Bonilha, J. B. S.; Bales, B. L. *J. Phys. Chem.* **1995**, *99* (46), 17028–17031.
28. Bales, B. L.; Stenland, C. *J. Phys. Chem.* **1993**, *97* (13), 3418–3433.
29. Grant, C. D.; DeRitter, M. R.; Steege, K. E.; Fadeeva, T. A.; Castner, E. W. *Langmuir* **2005**, *21* (5), 1745–1752.
30. Grant, C. D.; Steege, K. E.; Bunagan, M. R.; Castner, E. W. *J. Phys. Chem. B* **2005**, *109* (47), 22273–22284.
31. Kumpulainen, T.; Rosspeintner, A.; Vauthey, E. *Phys. Chem. Chem. Phys.* **2017**, *19* (13), 8815–8825.
32. Pal, S. K.; Peon, J.; Bagchi, B.; Zewail, A. H. *J. Phys. Chem. B* **2002**, *106* (48), 12376–12395.
33. Bhattacharyya, K.; Bagchi, B. *J. Chem. Sci.* **2007**, *119* (2), 113–121.
34. Balasubramanian, S.; Bagchi, B. *J. Phys. Chem. B* **2002**, *106*, 3668–3672.
35. Maroncelli, M.; Kumar, V. P.; Papazyan, A. *J. Phys. Chem.* **1993**, *97*, 13–17.
36. Horng, M.-L.; Gardecki, J. A.; Maroncelli, M. *J. Phys. Chem. A* **1997**, *101* (6), 1030–1047.
37. Mukherjee, P.; Das, A.; Sengupta, A.; Sen, P. *J. Phys. Chem. B* **2017**, *121* (7), 1610–1622.
38. Maroncelli, M.; Fleming, G. R *J. Chem. Phys.* **1987**, *86* (11), 6221–6239.
39. Horng, M. L.; Gardecki, J. A.; Papazyan, A.; Maroncelli, M. *J. Phys. Chem.* **1995,** *99*, 17311-17337.
40. Fee, R. S.; Maroncelli, M. *Chem. Phys.* **1994**, *183* (2–3), 235–247.
41. Sen, P.; Satoh, T.; Bhattacharyya, K.; Tominaga, K. *Chem. Phys. Lett.* **2005**, *411*, 339–344.
42. Guchhait, B.; Biswas, R.; Ghorai, P. K. **2013,** *117*, 3345-3361.
43. Tanford, C. *J. Phys. Chem.* **1972**, *76* (21), 3020–3024.

This page intentionally left blank

List of Publications

1. Ultrafast Electron Transfer from Upper Excited State of Encapsulated Azulenes to Acceptors across an Organic Molecular Wall.

   Mohan Raj, Mintu Porel, **Puspal Mukherjee**, Xiuyuan Ma, Rajib Choudhury, Elena Galoppini, Pratik Sen, V. Ramamurthy. *J. Phys. Chem C* **2017**, *121*, 20205–20216.

2. Ultrafast Excited State Deactivation Channel of Thioflavin T Adsorbed on SDS Micelle: A Combined Femtosecond Fluorescence and Transient Absorption Study.

   Puspal Mukherjee, Aritra Das, Pratik Sen. *J. Photochem. Photobiol. A Chem.* **2017**, *348*, 287–294.

3. Multi-mode Hydrogen Storage in Nanocontainers.

   Suboohi Shervani; **Puspal Mukherjee**; Anshul Gupta; Gargi Mishra; kavya Illath; Ajith Kumar; Sri Sivakumar; Pratik Sen; Kantesh Balani, Anandh Subramaniam. *Int. J. Hydrogen Energy*., **2017,** *42*, 24256-24262.

4. Dynamical response in methanol–chloroform binary solvent mixture over fs–μs time regime.

   Shradhey Gupta, **Puspal Mukherjee**, Bhaswati Sengupta, Pratik Sen. *Phys. Chem. Liq.* **2017**, **DOI** :- 10.1080/00319104.2017.1346649

5. Decoupling the diffusion from bimolecular photoinduced electron transfer reaction: A Combined Ultrafast Spectroscopic and Kinetic Analysis

   Puspal Mukherjee, Pratik Sen. *Phys. Chem. Chem. Phys.*, **2017**,*19*, 11220-11229.

6. Bi-Molecular Photo-Induced Electron Transfer in Static Quenching Regime: Illustration of Marcus Inversion in Micelle.

   Puspal Mukherjee, Aritra Das, Arunava Sengupta, Pratik Sen. *J. Phys. Chem. B*, **2017**, *121*, 1610–1622.

7. Mixed Solvent Chemistry through Synergistic Solvation: Structure, Property and Function of t-Butanol – Dichloromethane Binary Solvent Mixture.
   Shradhey Gupta, Keshaba Nanda Parida, **Puspal Mukherjee**, Pratik Sen. *J. Sol. Chem*. **2017**, *46*, 461-465.
8. Dual relaxation channel in thioflavin-T: An ultrafast spectroscopic study.
   Puspal Mukherjee, Shahnawaz Rafiq, Pratik Sen. *J. Photochem. Photobiol. A Chem.* **2016**, *328*, 136–147.
9. Ramping of pH Across the Water-Pool of a Reverse Micelle.
   Puspal Mukherjee, Shradhey Gupta, Shahnawaz Rafiq, Rajeev Yadav, Vipin Kumar Jain, Jayraj Raval, and Pratik Sen. *Langmuir*, **2016**, *32*, 1693–1699.
10. A chemosensor for Al^{3+} ions in aqueous ethanol media: photophysical and live cell imaging studies.
    Nabanita Chatterjee, Shubhra Bikash Maity, Asmita Samadder, **Puspal Mukherjee**, Anisur Rahman Khuda-Bukhsh, Parimal K. Bharadwaj. *RSC Adv.*, **2016**, *6*, 17995-18001.
11. Real Time Quantification of Ultrafast Photoinduced Bimolecular Electron Transfer Rate: Direct Probing of the Transient Intermediate.
    Puspal Mukherjee, Somnath Biswas, Pratik Sen. *J. Phys. Chem. B*, **2015**, *119*, 11253–11261.
12. Graphene: a self-reducing template for synthesis of graphene–nanoparticles hybrids.
    M. Manolata Devi, Sumit Ranjan Sahu, **Puspal Mukherjee**, Pratik Sen, Krishanu Biswas. *RSC Adv.*, **2015**, *5*, 62284-62289.
13. Graphene–Metal Nanoparticle Hybrids: Electronic Interaction Between Graphene and Nanoparticles.
    M. Manolata Devi, S. R. Sahu, **Puspal Mukherjee**, Pratik Sen, Krishanu Biswas. *Trans Indian Inst. Met.* **2016**, *69*, 839–844.

14. Femtosecond dynamics of photoinduced cis-trans isomerizationof ethyl-3-(1H-indole-3-yl) acrylate.

    Bhaswati Sengupta, **Puspal Mukherjee**, Saikat Das, Shahnawaz Rafiq, Shradhey Gupta,Dattatraya H. Dethe, Pratik Sen. *Chem. Phys. Lett.* **2015**, *638*, 31–37.

15. Optical Property Characterization of Novel Graphene-X (X=Ag, Au and Cu) Nanoparticle Hybrids.

    Sumit Ranjan Sahu, Mayanglambam Manolata Devi, **Puspal Mukherjee**, Pratik Sen, Krishanu Biswas. *Journal of Nanomaterials*, **2013**, Article ID 232409, 9 pages,

16. Förster resonance energy transfer between pyrene and bovine serum albumin: Effect of the hydrophobic pockets of cyclodextrins.

    Arnab Maity, **Puspal Mukherjee**, Tarasankar Das, Prasun Ghosh, Pradipta Purkayastha. *Spectrochimica Acta Part A* **2012**, *92*, 382– 387.

Submitted Manuscripts

1. Solvent Relaxation Accompanied Ultrafast Excited State Proton Transfer Dynamics Revealed in a Salicylideneaniline Derivative.

   Puspal Mukherjee, Aritra Das, Md. Serajul Haque Faizi and Pratik Sen. *Submitted in ChemistrySelect*.

2. Solvation Dynamics in SDS Micelle Revisited with Femtosecond Time Resolution to Reveal the Probe and Concentration Dependence.

   Puspal Mukherjee, Aritra Das and Pratik Sen. *Submitted in Chem. Phys. Lett*.

Manuscripts under preparation

1. Ultrafast twisting dynamics of green fluorescence protein chromophore in micelle: surfactant charge and probe location dependence. A femtosecond time resolved fluorescence study.

Puspal Mukherjee and Pratik Sen. *Manuscript under preparation*.

2. Intriguing Increase of Polarity in Water- N,N-Dimethylformamide Binary Solvent Mixture: A Molecular Level Investigation.

   Puspal Mukherjee, Aritra Das, Nishith Maity and Pratik Sen. *Manuscript under preparation.*

3. Effect of *o,m,p*- electron donating substitution on the photophysics of fluorenone. A combined ultrafast spectroscopy and DFT study.

   Puspal Mukherjee, Arindam Mukhopadhyay, J.N. Moorthy and Pratik Sen. *Manuscript under preparation*

4. Spectroscopic Investigation of ZnO Nanoparticles Size and Shape Controlled by Ethanol-Benzyl Alcohol Binary Solvent Mixture.

   Shradhey Gupta, **Puspal Mukherjee**, Bhaswati Sengupta and Pratik Sen. Manuscript under preparation.

5. Spectroscopic Investigation of DMF/Chloroform Binary Solvent Mixture.

   Puspal Mukherjee, Sayoni Roy and Pratik Sen. Manuscript under preparation.

6. Molecular level interactions in water-methanol binary solvent mixture investigated by multiple spectroscopic methods.

   Puspal Mukherjee, Shradhey Gupta and Pratik Sen. Manuscript under preparation.